



Transport and structural properties
of aqueous solutions of organic solvents

Carlos E. Nieto Draghi
Tarragona, 2003.

Transport and structural properties
of aqueous solutions of organic solvents

TRANSPORT AND STRUCTURAL PROPERTIES OF AQUEOUS SOLUTIONS OF ORGANIC SOLVENTS

Memòria presentada per optar al títol de
Doctor per la Universitat Rovira i Virgili

CARLOS EDUARDO NIETO DRAGHI

Departament d'Enginyeria Química
Escola Tècnica Superior d'Enginyeria Química
Universitat Rovira i Virgili
Av. Països Catalans 26
43007 Tarragona

Tesi dirigida per el Dr. Josep Bonet i Avalos

Membres del Tribunal de Tesi:

President: Dr. Bjørn Hafskjold

Secretari: Dr. Allan Mackie

Vocals:

Dra. Elvira Guàrdia

Dr. Carles Bo Jané

Dra. Dolors Salvatierra

Suplents:

Dr. Jefferson W. Tester, Dr. Jörg Baschnagel.

Evaluadors externs (European Label):

Dr. Simone Wiegand, Dr. Bertrand Guillot.

Universitat Rovira i Virgili

Tarragona, 2003

El sota signant, Dr. Josep Bonet i Àvalos

FA CONSTAR

Que la tesi doctoral que porta per títol

TRANSPORT AND STRUCTURAL PROPERTIES OF AQUEOUS SOLUTIONS
OF ORGANIC SOLVENTS

i que presenta el Sr. Carlos Eduardo Nieto Draghi per optar al grau de Doctor per la Universitat Rovira i Virgili, ha estat realitzada sota la meva direcció i que tots els resultats presentats i la seva anàlisi són fruit de la investigació realitzada per l'esmentat doctorand.

I perquè se'n prengui coneixement i tingui els efectes que correspongui, signo aquest certificat.

Josep Bonet i Àvalos
Professor Titular
Dep. d'Enginyeria Química
Universitat Rovira i Virgili

Tarragona, 9 de setembre del 2003

A mis padres, a Pachi y a los Diegos

A Ester

Quisiera expresar mi agradecimiento a todas aquellas personas que participaron directa o indirectamente en la realización de esta tesis doctoral.

En primer lugar quisiera agradecer al Dr. Josep Bonet por haber aceptado dirigir esta tesis. Aún hoy recuerdo su entrada en mi despacho con un manajo de artículos sobre agua supercrítica. El destino ha querido que aprenda una que otra cosa sobre el agua..., nunca más me atreveré a decir..."esta claro como el agua...". Gracias por todo su tiempo y esfuerzo en enseñarme muchas cosas.

También quisiera agradecer al Dr. Bjorn Hafskjold, Dr. Allan Mackie, Dra. Elvira Guàrdia, Dra. Dolors Salvatierra, Dr. Carles Bo, Dr. Jefferson Tester y al Dr. Joerg Bashnagel por haber aceptado formar parte del tribunal de esta tesis.

A la Dra. Simone Wiegand y al Dr. Bertrand Guillot por aceptar ser los evaluadores externos de este trabajo. Es encomiable tener que leer una tesis doctoral en dos semanas y poder hacer un informe objetivo en tan poco tiempo.

Quisiera agradecer especialmente al Dr. Bernard Rousseau por haberme acogido en París y haberme enseñado muchas cosas sin las cuales esta tesis no hubiera podido ser terminada.

Al Dr. Joan Padró y a la Dra. Elvira Guàrdia por las fructíferas discusiones que fueron de gran ayuda a la hora de interpretar y discutir muchos de los resultados.

También quiero agradecer, dentro del departamento de Ingeniería Química de la Universitat Rovira i Virgili, al Dr. Allan Mackie y a la Dra. Dolors Salvatierra por su ayuda en muchas discusiones.

Por supuesto a mis compañeros de despacho y penurias, al Olivieri, al Pep, Zaid, Carmelo y Henry. A los viejos amigos de la peña, el Roger, la Montse, la Gloria, el Alvarito, la Gabriela, el Maxi, el Albert, la Magda, la Maru, la Paula y el Joseli. Muy especialmente a mi amiga Susanita por compartir esos pesados veranos de trabajo y los momentos buenos y malos de estos 4 años.

A mi querida familia por el gran apoyo independientemente de los miles de kilómetros que nos separan, el estar aquí se los debo a todos ellos por igual.

A la Nena por su apoyo incondicional, gracias por aguantar mis achaques y angustias.

Por último, quisiera agradecer al Gobierno Español *Ministerio de Educación Ciencia y Tecnología* (proyectos No. PPQ2000-2888-E, PPQ 2001-0671), a la *Generalitat de Catalunya* (proyectos ACI2000-13, ACI2001-39 y ACI2002-37), a la Universitat Rovira i Virgili (proyecto No. 2000PIR-21) y por la beca predoctoral. Finalmente quisiera agradecer al *Ministerio de Educación Cultura y Deporte* por la beca de posgrado para la Formación de Profesorado Universitario (FPU AP2000-2391) sin la cual este trabajo no hubiera podido realizarse.

Contents

List of Figures	xiii
List of Tables	xxi
Introduction	xxiii
1. LIQUID THEORY	1
1 Structural and collective behavior of a system of N particles	1
1.1 Decomposition of $g(\mathbf{r})$ in terms of spherical harmonics	4
1.2 Orientational order parameter	7
1.3 Translational order parameter	8
2 Dynamic behavior and transport properties of fluids	8
2.1 Self-diffusion	9
2.2 Maxwell-Stefan mutual diffusion coefficient	11
2.3 Shear Viscosity η	13
2.4 Thermal conductivity λ	14
2.4.1 Soret coefficient	18
3 Water: Important considerations	20
3.1 Water structure	21
3.2 The concept of hydrogen bonding	23
4 Molecular Dynamics	24
5 Ensembles	25
5.1 Micro-canonical NVE	25
5.2 Canonical NVT	27
5.3 NPT	28
6 Algorithm	30
6.1 Short and long range intermolecular potentials and forces	32
6.2 Intermolecular potential models	35
6.2.1 Water models	35
6.3 Hydrogen bond definition in MD Simulations	39
7 MD Code: Mdmix	40

2.	STRUCTURAL AND DYNAMICAL PROPERTIES OF PURE WATER	43
1	Introduction	43
2	Fundamentals: Oxygen-oxygen coordination number	46
3	Water Models and Computational details	46
4	First Part: Comparison of the behavior of the four models of water	48
4.1	Self-diffusion coefficient	48
4.2	Structure and Hydrogen Bonding	50
4.2.1	Site-site radial distribution function	51
4.2.2	HB analysis	55
4.2.3	Order parameter	57
4.2.4	Spherical harmonic projections and 3D representation of $g_{ab}(r)$	58
5	Second Part: Order transition in pure water	65
6	Conclusions	67
3.	TRANSPORT PROPERTIES OF AQUEOUS SOLUTIONS	71
1	Introduction	71
2	Fundamentals: Hydrogen bond lifetimes	74
3	Computational details	74
4	Results and Discussion	79
4.1	Shear viscosity	79
4.2	Thermal conductivity	88
5	Conclusions	93
4.	SORET EFFECT IN ASSOCIATING FLUIDS	97
1	Introduction	97
2	Computational details	100
3	Results and Discussion	102
3.1	Lattice model of a mixture of particles	105
4	Conclusions	111
5.	DYNAMICAL AND STRUCTURAL PROPERTIES OF BENZENE IN SUPERCRITICAL WATER	115
1	Introduction	115
2	Fundamentals	117
2.1	Dielectric response of a mixture of dipolar and quadrupolar interactions	117
2.2	Tetrahedral structure of water around benzene molecules	121
3	Computational details	123

<i>Contents</i>	xi
4 Results and discussion	126
5 Conclusions	141
6. CONCLUSIONS AND PERSPECTIVES	145
Appendices	148
Spherical Harmonics expansion of the RDF	149
Quaternion formalism for rotational dynamics	151
Error function and complementary error function	153
Adaptation of the DEC model parameters for the use of reaction field methodology	155
NEMD algorithm to generate heat flux	157
Correlations	161
1 Correlation for Self-diffusion coefficient of water	161
2 Average number of Hydrogen bond in function of Temperature	161
Physical properties	163
1 Properties of the different models to simulate water	163
Resumen de la Tesis	177
Publication list	183

List of Figures

1.1	g_{OO} comparison of old (Soper et al., 1997) and new (Soper, 2000) NDS with the most recent X-Ray experiments (Hura et al., 2000) for water at 298 K and $\rho = 0.995 \text{ g/cm}^3$.	5
1.2	Local polar system of coordinates centered at the oxygen atom, and oriented in the direction of the permanent dipole vector of the molecule.	6
1.3	Schematic representation of half of the simulation box using the non-equilibrium PeX algorithm. Particles in blue have less kinetic energy than red particles.	17
1.4	In this figure it is possible to see a schematic representation of a water molecule. Here O and H are, respectively, the oxygen and the hydrogen atoms, and “e” represents the position of the lone pair electrons of the oxygen atom (Chapling, 2003).	22
1.5	Water structure showing the electron density distribution (high densities around the oxygen atoms have been omitted for clarity)(Chapling, 2003).	22
1.6	In this figure it is possible to see a water dimmer showing the partial charges(Chapling, 2003).	23
1.7	Clusters, hydrogen bonded pentamer (Chapling, 2003).	24
1.8	Different type of model for water: the types a, b and c are all planar whereas type d is almost tetrahedral. The values of the symbols in each model correspond to those in Table 1.1 (Chapling, 2003)	36
1.9	Geometry of the spatial oriented definition of hydrogen-bonded molecules.	39
1.10	General methodology to extract information from MD simulation.	41

2.1	Phase diagram of pure water showing the different types of Ice structures(Chapling, 2003)	44
2.2	Comparison of the temperature evolution of the self-diffusion coefficient of the four models studied with experiments(Krynicky et al., 1980) and theoretical correlation(Svishchev and Zassetsky, 2000) from state 1 to 11 ($\rho = 0.995 \text{ g/cm}^3$). The correlation has been obtained up to 510 K, and it is extrapolated up to 1300 K.	48
2.3	Temperature dependence of the number of neighboring molecules in the first coordination shell at constant density for the models studied ($\rho = 0.995 \text{ g/cm}^3$).	49
2.4	Density evolution of the self-diffusion coefficient at 673 K supercritical isotherm. Comparison of experimental data (Lamb et al., 1981) with the simulation results of four models studied.	50
2.5	Comparison of the site-site distribution function of the four models with <i>NDS</i> (Soper, 2000) and <i>ALS</i> (Hura et al., 2000) (<i>ALS</i> data only for O-O) experiments at state 2 (298 K and $\rho = 0.995 \text{ g/cm}^3$). a) Oxygen-oxygen, b) oxygen-hydrogen and c) hydrogen-hydrogen pair distribution functions.	51
2.6	Comparison of the site-site distribution function of the four models with <i>NDS</i> (Soper, 2000) experiments at state 11 (673 K and $\rho = 0.66 \text{ g/cm}^3$). a) Oxygen-oxygen, b) oxygen-hydrogen and c) hydrogen-hydrogen pair distribution functions. Sharp inner peaks in the experimental data in plots <i>b</i> and <i>c</i> correspond to intra-molecular oxygen-hydrogen and hydrogen-hydrogen interactions.	52
2.7	Comparison of the temperature evolution of the average number of hydrogen bond per molecule for the four models studied using the geometric definition with the theoretical correlation (Suresh and Naik, 2000) at constant density ($\rho = 0.995 \text{ g/cm}^3$).	53
2.8	Density evolution of the average number of hydrogen bond per molecule at the supercritical 673 K isotherm. Experimental data com from reference (Matubayasi et al., 1997). The correlation is extra-poled at different densities at this temperature reference (Suresh and Naik, 2000).	54
2.9	Temperature dependence of the two order parameter q and q' at constant density ($\rho = 0.995 \text{ g/cm}^3$).	55
2.10	Density dependence of the two order parameter q and q' on the supercritical isotherm (T=673 K).	56

2.11	Relation between the self-diffusion coefficient and the q at constant density for the models studied ($\rho = 0.995 \text{ g/cm}^3$).	58
2.12	Relation between the self-diffusion coefficient and the $\langle N_{HB} \rangle$ at constant density for the models studied ($\rho = 0.995 \text{ g/cm}^3$).	59
2.13	3D oxygen-oxygen pair distribution function for the TIP4P, TIP5P, SPC/E and DEC (from top to bottom) at 434 K, 424 K, 447 K and 510 K respectively and the same orientational order parameter $q \approx 0.5$, at $\rho = 0.995 \text{ g/cm}^3$.	60
2.14	3D oxygen-hydrogen pair distribution function for the TIP4P, TIP5P, SPC/E and DEC (from top to bottom) at 434 K, 424 K, 447 K and 510 K respectively and the same orientational order parameter $q \approx 0.5$, at $\rho = 0.995 \text{ g/cm}^3$.	61
2.15	Comparison of oxygen-oxygen radial distribution function projected with spherical harmonics for the four models at the same temperature (T=298 K, at $\rho = 0.995 \text{ g/cm}^3$). (---)TIP4P, (---)TIP5P, (---)DEC and (---)SPC/E.	62
2.16	Comparison of oxygen-hydrogen radial distribution function projected with spherical harmonics for the four models at the same temperature (T=298 K, at $\rho = 0.995 \text{ g/cm}^3$). (---)TIP4P, (---)TIP5P, (---)DEC and (---)SPC/E.	63
2.17	Comparison of the two order parameters for pure water (SPC/E model), at different densities and temperatures, a) translational order parameter and b) orientational order parameter.	64
2.18	Temperature evolution of the $g_{OO}(r)$ at $\rho = 0.995 \text{ g/cm}^3$, from 275 K to 1250 K. The second peak lies between a and b only below T=447 K. At higher temperatures the second peak is shifted to larger radial distances, laying between lines b and c . Each $g_{OO}(r)$ are shifted by a factor of 1 from bottom to top.	65
2.19	Loci of the maximum (squares) and minimum (circles) of the translational order parameter for pure water.	66
2.20	Mobility of pure water (FPC/E model), at different densities and temperatures.	67
3.1	Comparison of the experimental density of the mixture of water+DMSO (Cowie and Toporowski, 1961) at 298 K and 1 atm with that obtained with the simulations at same conditions using the SPC/E (Berendsen et al., 1987) model for water and two models of DMSO, for instance, the P2 model (Luzar and Chandler, 1993) and the Liu <i>et al.</i> (Liu et al., 1995) model.	75

- | | | |
|------|---|----|
| 3.2 | Shear viscosity of mixture of water+DMSO at 298 K and 1 atm. Experimental values are from ref.(Cowie and Toporowski, 1961). | 79 |
| 3.3 | Shear viscosity of mixture of water+acetone. Our simulations were done at constant density at 298 K (<i>NVT</i>) and only two points were computed at constant pressure at 298 K and 1 atm (<i>NPT</i>). Our results are compared with the values obtained by Wheeler <i>et al.</i> (Wheeler and Rowley, 1998). Experimental values for the viscosity are from ref.(Noda <i>et al.</i> , 1982). | 80 |
| 3.4 | Comparison of the experimental density of the mixture of water+acetone (Griffiths, 1952) at 298 K and 1 atm with that obtained with the simulations at same condition using the SPC/E (Berendsen <i>et al.</i> , 1987) model for water and the model of Wheeler <i>et al.</i> (Wheeler and Rowley, 1998) for acetone. | 81 |
| 3.5 | Variation of the tetrahedral order parameter q in function of the water concentration in the system at 298 K. Lines are only guides for the eyes. | 83 |
| 3.6 | Variation of $\langle N_{HB} \rangle$ in function of the water concentration in the system water+Methanol at 298 K. | 84 |
| 3.7 | Variation of $\langle N_{HB} \rangle$ in function of the water concentration in the system water+DMSO at 298 K. | 85 |
| 3.8 | Variation of $\langle N_{HB} \rangle$ in function of the water concentration in the system water+Acetone at 298 K. | 86 |
| 3.9 | Variation of the life-times of continuous H-bond (τ_{HB}^c) with the molar fraction of water at 298 K, for a) Water-water and b) water-solute hydrogen bonds. | 87 |
| 3.10 | Variation of the life-times of intermittent H-bond (τ_{HB}^i) in function of the molar fraction of water at 298 K, for a) water-water and b) water-solute hydrogen bonds. | 88 |
| 3.11 | Comparison of experimental data of thermal conductivity (Qun-Fang <i>et al.</i> , 1997) of water+ethanol at 298.15 K and 1 atm with simulations employing the TIP4P (Jorgensen <i>et al.</i> , 1983) model of water and the OPLS (Jorgensen <i>et al.</i> , 1984) model of ethanol. | 89 |
| 3.12 | Comparison of thermal conductivity predicted with correlations (GOWProp-v5.1, 2002) of water+methanol at 313.15 K and 1 atm with simulations employing the TIP4P (Jorgensen <i>et al.</i> , 1983) model of water and the OPLS (Jorgensen <i>et al.</i> , 1984) model of methanol. | 90 |

- 3.13 Comparison of thermal conductivity predicted with the correlation of Li (Li, 1976) (thermal conductivity estimated for DMSO using the correlation of Bridgman (Bridgman, 1923)) of mixture of water+DMSO at 298 K and 1 atm with simulations employing the SPC/E (Berendsen et al., 1987) model for water and the P2 (Luzar and Chandler, 1993) model of DMSO. 91
- 3.14 Comparison of the thermal conductivity predicted with the correlation of Li (Li, 1976) (and the experimental values of λ for acetone and water taken from ref. (Qun-Fang et al., 1997)) for the mixture of water+acetone at 298 K and 1 atm with our simulations employing the SPC/E (Berendsen et al., 1987) model of water and the model of Wheeler (Wheeler and Rowley, 1998) for acetone. 92
- 4.1 Comparison of the thermal diffusion factor α for the mixture water+methanol at 313 K and 1 atm with the experimental data of (Tichacek et al., 1955). 101
- 4.2 Comparison of the thermal diffusion factor α for the mixture water+ethanol at 298 K and 1 atm with the experimental data of Bou-Ali (Bou-Ali, 1999), Kolodner (Kolodner et al., 1988) and Zhang (Zhang et al., 1996). 102
- 4.3 Prediction of the thermal diffusion factor α for the mixture water+DMSO at 298 K and 1 atm. 103
- 4.4 Prediction of the thermal diffusion factor α for the mixture water+acetone at 298 K and 1 atm. 104
- 4.5 Schematic representation of two particles chosen to be interchanged in the lattice. a) The state A before the switch process and b) the state B after the switch process. 106
- 4.6 Schematic representation of the lattice simulation of an equimolar mixture of 5000 particles computed with Non-equilibrium MC. 108
- 4.7 Thermal diffusion factor α for the mixture of particles in function of the molar fraction of one component varying the cross interactions. The pure component interactions are $\epsilon_{11} = -2000$ and $\epsilon_{22} = -1000$, the mixture interactions are computed through $\epsilon_{12} = c_1(\epsilon_{11} \cdot \epsilon_{22})^{1/2}$. 109
- 4.8 Excess enthalpy of mixing for the systems water+methanol and water+ethanol at 298 K and 1 atm. Experiments come from reference (Ness, 1989, Raddzio and Tomaszewicz, 1986) 110

- 4.9 Thermal diffusion factor α for the mixture of particles in function of the molar fraction of one component varying the relation of the strength interaction between pure components. Here $\epsilon_{11} = -2000$ and $\epsilon_{12} = -3000$. 111
- 5.1 Representation of the dipole moment vector μ of the water molecule (a), a vector normal to the plane of the benzene molecules \mathbf{Q} (b) and a schematic representation of a possible HB between water and the center of the electron cloud of the benzene molecule (c). 121
- 5.2 Phase diagram for water-benzene mixtures. The thick solid lines: one -phase critical curve and liquid-liquid-gas three phase curve; c.p is the critical points and the diamond symbols are the different thermodynamic states presented in table 5.2. Experimental data taken from the literature (Alwani and G. M. Schneider, 1967, Tsionopoulos and Wilson, 1983). 123
- 5.3 Snapshot of the mixture Water+Benzene at $x_B = 0.21$, at 573 K and 329 bar for two AUA models of benzene. Without point charged (left) and with the inclusion of point charges (right)124
- 5.4 Density variation of the self-diffusion coefficient of water in the mixture water+benzene at the supercritical isotherm (T=673 K). Additionally, the self-diffusion of water at 573 K and 329 bar is included at three concentrations. The experimental data (Lamb et al., 1981) of self-diffusion of pure water (continuous line) is presented for comparison. 125
- 5.5 Density variation of the Self-diffusion coefficient of benzene in the mixture water+benzene at the supercritical isotherm (T=673 K). Additionally, the self-diffusion of benzene at 573 K and 329 bar is included at three concentrations. 126
- 5.6 Density variation of the Maxwell-Stefan mutual diffusion coefficient of the mixture water+benzene at the supercritical isotherm (T=673 K). Additionally, the mutual-diffusion of the mixture at 573 K and 329 bar is included at three concentrations127
- 5.7 Density variation of the shear viscosity coefficient of the mixture water+benzene at the supercritical isotherm (T=673 K). Additionally, the viscosity at 573 K and 329 bar is included at three concentrations. Here we also include the experimental data of Lamb (Lamb et al., 1981) for pure water. 128
- 5.8 Variation of the local tetrahedral order parameter q of the mixture water+benzene at 673 K. Additionally, the same parameter at 573 K and 329 bar is included at three concentrations. 129

- 5.9 Radial variation of the local tetrahedral order parameter q of the mixture water+benzene at three concentrations. From top to bottom, a) 573 K and 329 bar, b) 673 K and $\rho = 0.3 \text{ g/cm}^3$, c) 673 K and $\rho = 0.66 \text{ g/cm}^3$ and d) 673 K and $\rho = 0.995 \text{ g/cm}^3$ 130
- 5.10 Variation of the coordination number of water molecules in the first solvation shell around benzene molecules with the density and composition of benzene in the supercritical isotherm of 673 K, and at 573 K and 324 bar. 131
- 5.11 Center of mass to center of mass radial distribution function between benzene and water molecules at $x_B \rightarrow 0$ (continuous line), $x_B = 0.1$ (dashed line) and $x_B = 0.21$ (dotted line). From top to bottom, a) 573 K and 329 bar, b) 673 K and $\rho = 0.3 \text{ g/cm}^3$, c) 673 K and $\rho = 0.66 \text{ g/cm}^3$ and d) 673 K and $\rho = 0.995 \text{ g/cm}^3$. 133
- 5.12 Density variation of the average number of hydrogen bonds $\langle N_{HB} \rangle$ of the mixture water+benzene at the supercritical isotherm (T=673 K). Additionally, $\langle N_{HB} \rangle$ at 573 K and 329 bar is included at three concentrations. Full symbols are w-w HB and empty symbols are benzene-water HB. 134
- 5.13 Density variation of life times of continuous HB for the mixture water+benzene at the supercritical isotherm (T=673 K). Additionally, τ_{HB}^c at 573 K and 329 bar is included at three concentrations. Full symbols are w-w HB and empty symbols are water-benzene HB. 135
- 5.14 Density variation of life times of intermittent HB for the mixture water+benzene at the supercritical isotherm (T=673 K). Additionally, τ_{HB}^i at 573 K and 329 bar is included at three concentrations. Full symbols are w-w HB and empty symbols are water-benzene HB. 136
- 5.15 Normalized time-correlation function of the dipole moment vector of water molecules for $x_B \rightarrow 0$ (line), $x_B = 0.1$ (dashed line) and $x_B = 0.21$ (dashed dotted line) at a) 573 K and 329 bar, b) 673 K and $\rho = 0.3 \text{ g/cm}^3$, c) 673 K and $\rho = 0.66 \text{ g/cm}^3$ and d) 673 K and $\rho = 0.995 \text{ g/cm}^3$. 137
- 5.16 Density variation of decay time of the dipole vector τ_μ (full symbols) of water molecules and the decay time of quadrupolar vector τ_Q (empty symbols) of benzene molecules for the mixture water+benzene at the supercritical isotherm (T=673 K). Additionally, both quantities are included at 573 K and 329 bar at three concentrations. 138

- 5.17 Density variation of the dielectric constant $\epsilon(0)$ (in F/m) of the mixture water+benzene at the supercritical isotherm (T=673 K). Additionally, $\epsilon(0)$ is included at 573 K and 329 bar at three concentrations. Simulation results of Skaf *et al.* (Skaf and Laria, 2000) (cross symbols) and the experimental data of Uemata (Uematsu and Franck, 1980) (plus symbols) of pure water at 650 k are also included for comparison. 139
- 5.18 Radial variation of the product of the dipole vector of water molecules $\mu_i \cdot \mu_j$ in the mixture at for $x_B \rightarrow 0$ (line), $x_B = 0.1$ (dashed line) and $x_B = 0.21$ (dashed dotted line) for (from top to bottom) a) 573 K and 329 bar, b) 673 K and $\rho = 0.3 \text{ g/cm}^3$, c) 673 K and $\rho = 0.66 \text{ g/cm}^3$ and d) 673 K and $\rho = 0.995 \text{ g/cm}^3$. 140

List of Tables

1.1	Molecular parameter of the most common water models (Chapling, 2003).	37
1.2	Potential parameters of DEC (Guillot and Guissani, 2001).	38
2.1	Simulated thermodynamic states for the comparison analysis	46
2.2	Simulated thermodynamic states for the order analysis, for each state different densities has been considered	47
2.3	Comparison of the remarkable details of the models studied and the experimental data. Information is listed as $r(\text{\AA})$, $g_{OO}(r)$.	53
2.4	Average number of hydrogen bond per molecule computed by means of the geometrical criterion (sec II.D) for the four models studied here at $\rho = 0.995 \text{ g/cm}^3$	55
3.1	Simulated thermodynamic states for the comparison analysis. All data at 298 K and 1 atm (water+methanol system at 313.15 K). (References for the experimental density: water+methanol (GOWProp-v5.1, 2002), water+ethanol (Bou-Ali, 1999), water+DMSO (Cowie and Toporowski, 1961) and water+acetone (Griffiths, 1952))	77
3.2	Potential parameters of the models employed. For more details about the models see ref.(Borin and Skaf, 1999) and ref. (Berendsen et al., 1987).	78
5.1	Potential parameters of the models employed. For more details about the models see the cited reference.	122
5.2	Simulated thermodynamic states for the benzene+water mixture.	123

Introduction

Molecular Modeling Techniques have been used to predict physical properties of systems of industrial interest almost since the computers birth. Computer simulations have been used as a source of relevant data where extreme conditions of temperature and pressure makes it impossible the use of the traditional phenomenological equations of states, which are unable to reproduce the real behavior of the fluids under these conditions. Extreme conditions are also hard to carry out experimentally because very expensive and sophisticate equipment is required to achieve high temperatures and pressures, for instance. In all these cases, molecular simulation appears as a promising alternative way to determine properties, which are relevant for prediction and design (wor, 1999). Consequently, molecular modeling techniques have been played an important role in the development of theories and in a general understanding of the behavior of the different states of the matter (Barrat and Hansen, 2003). Molecular modeling requires a set of models that are representations of real atoms and molecules. These models are the core of an appropriate microscopic description of any fluid (Allen and Tildesley, 1989).

Particularly, the Molecular Dynamics (MD) simulation technique is used to obtain equilibrium as well as transport properties of physical systems (Hansen and McDonald, 1991). This technique is based on the principle that atoms and molecules obey the laws of classical mechanics (Goldstein, 1996) and their motion can be simulated in a computer. The main difference between the results obtained by this technique and those derived from phenomenological equations of state and empirical correlations is that, in the former, the parameters are molecular in nature and do not depend on the thermodynamic conditions of the system, while, in the latter, the parameter, often lack of physical meaning and depend usually on thermodynamic conditions such as temperature or pressure. In this way MD is analogous to real experiments because, after some interval of

time, *measures* of physical macroscopic properties are obtained from averages involving velocities and positions of the particles.

The study of systems with biological and industrial applications gives rise to a great effort to provide accurate molecular models of compounds that can be used in the simulations. Additionally, the continuous increment of the computing power also motivates the application of molecular modeling techniques to real systems, particularly, in the biological ones (DNA, 2001), where water molecules play an important role as solvent. Even though the water molecule can be considered as *simple*, the collective behavior of water is far from being simple. Water is a fascinating fluid with several peculiar properties at different thermodynamic conditions (Chapling, 2003). Most of its anomalous behavior at ambient and sub cooled conditions can be understood by the presence of hydrogen bonds, producing three dimensional networks of connected molecules (Franks, 2000, NIST, 2001). Water expands on cooling at ambient pressure, and below 4°C; it exhibits a line of Temperature of Maximum Density (TDM) in liquid phase when changing the temperature (Heide, 1984, Mishima and Stanley, 1984). At lower temperatures (below the freezing temperature of water 0°C) water crystallize in such a way that the ice is less dense than the liquid phase, and the relationship between its dynamics and structure are by far non-trivial (Stanley et al., 2002b, Netz et al., 2002b, Netz et al., 2002a, Scala et al., 2000a, Starr et al., 2000). Additionally, mixtures of water with other compounds present a complex behavior, especially if such species are capable of share hydrogen bonds with water molecules (Matsumoto and Gubbins, 1990, Saiz et al., 1999, Slusher, 2000, Sesé and Palomar, 2001). Many physical properties of aqueous solutions present a non ideal behavior, like large negative excess enthalpy of mixing (Ness, 1989, Raddzio and Tomaszkiwicz, 1986), high vaporization energy, enhancement of the shear viscosity (Ferrario et al., 1990, Wheeler and Rowley, 1998, Venables and Schmuttenmaer, 2000), minimum in thermal conductivity (Li, 1976), change in the sign of the Soret coefficient (Kolodner et al., 1988, de Gans et al., 2003a, de Gans et al., 2003b), etc. In some of these cases the comprehension of the nature of the processes involved from a microscopic point of view, is still lacking.

Water at supercritical conditions has gained a considerable amount of interest among the scientific community and in industry, due to its particular properties at these conditions (Chialvo and Cummings, 1996b, Shaw et al., 1991, Katrizky et al., 1996). One of the main interests to study supercritical water (SCW) is that, according to the experimental data available, it exists a relaxation in the structure of the hydrogen bond network responsible for a substantial reduction of the dielectric constant of water (Skaf and Laria, 2000, Yao and Okada, 1998, Jedlovsky et al., 1998). This fact allows SCW to solve non-polar substances and precipitate the most common ions, contrary to what sub-critical water does.

Moreover, due to the fact that the density of water can be tuned from gas-like to liquid-like by just adjusting the pressure, SCW can be employed as a powerful solvating agent for separation purposes and as a medium for chemical reactions. The variation of density has a direct influence in the viscosity and diffusion of the molecules (Haar et al., 1984), being this fact of particular interest for diffusion controlled reactions. Supercritical extraction, wet oxidations of waste organic materials, waste water treatment in pharmaceutical industries, and processed water in power plant generation are some examples of industrial applications of SCW (Modell et al., 1982, Thomason et al., 1990, Thomason and Modell, 1984, Tester et al., 1991, Killilea et al., 1992).

The peculiar behavior observed in pure water and its mixtures with other substances at different thermodynamic conditions, and the knowledge and understanding of the properties of these systems are the motivations of this work. We have employed Molecular Dynamics Simulations to study the intrinsic relationship existing between the structure and the dynamics of pure water, and the influence that mixtures with other organic solvents (such as alcohols, ketones, sulfoxides and benzene) may have on the properties of these solutions. Consequently, we have first studied the relationship existing between the structural and dynamical properties of pure water at sub and supercritical conditions, as predicted by different molecular models of water, commonly used in the literature (van der Spoel et al., 1998, Mahoney and Jorgensen, 2000, Berendsen et al., 1987, Guillot and Guissani, 2001). We have made a direct connection between the local tetrahedral structure of water (Errington and Debenedetti, 2001, Chau and Hardwick, 1998), created by the presence of hydrogen bonds, and the self-diffusion coefficient at liquid-like densities. In addition, we have paid special attention to the analysis of the transition of the structural order of water molecules from medium densities to very high density. We have found some indications of an order transition in the three dimensional structure of water at certain conditions of temperature (above ~ 345 K) and densities (between 0.9 to 1.3 g/cm³). The analysis presented in this part of the work, through the comparison of different models of water, is also in the line of providing a set of useful tools for the development of more accurate models of water.

The strong hydrogen bond interaction observed in pure water plays a central role in aqueous solutions. Particularly, when the solute is also an associating fluid, able to form hydrogen bonds, the solution is usually a non-ideal. We have studied several properties of aqueous mixtures of associating fluids, such as methanol, ethanol, acetone and dimethyl sulfoxide (DMSO). We have selected these substances because their properties are well known, and because they are also employed as organic solvents in many industrial applications. We observe that the presence of each type of solute perturb the local structure of water in a different manner, being the magnitude of the effect related to the associating

character (being donor or acceptor of hydrogen bonds) of the solute. The loss of the tetrahedral order in the water, due to the presence of the solute (through crossed hydrogen bonds), produces an increase of the local rigidity of the water molecules, with respect to *more symmetrical* less rigid structures existing in pure water. In other words, the breaking of the tetrahedral symmetry of the environment, gives rise to the formation of chain-like structures with long-range correlation of hydrogen-bonded water molecules that is responsible for the high viscosity of the mixture. This fact has been corroborated by the observed increment in the lifetimes of hydrogen bonds between water molecules. We have also computed the thermal conductivity of the different mixtures, obtaining very good agreement between our simulation results and the available experimental data.

One of the properties that we have analyzed for these binary mixtures is the Ludwig-Soret effect (Ludwig, 1856, Soret, 1879a), which is a macroscopic cross effect where a diffusion process is caused by the presence of a temperature gradient in a multicomponent system. The degree of the separation observed and the sign of the separation (the direction of the migration of each specie) is quantified by the Soret coefficient or the thermal diffusion factor. In most cases, where fluids without association are considered, this coefficient is positive in the whole range of compositions. This means that the heaviest component will tend to accumulate in the cold region, and the opposite occurs for the lightest component (Prigogine et al., 1950a). The value of the Soret coefficient depends mostly on the differences in the molar masses and molar volumes of the constituents for ideal mixtures (Simon et al., 1998, Simon et al., 1999, Bedrov and Smith, 2000). However, in the case of associating fluids, the value of this coefficient may have a change in its sign at some particular composition. In this case the lighter component will migrate to the cold side of the system (Tichacek et al., 1955). This effect has been studied for more than hundred years and several theories have been proposed (Kempers, 2001, Haase et al., 1971, Dougherty and Drickamer, 1955). It seems that, in the case of associating fluids, this phenomenon still lacks of a clear physical explanation. In view of this situation, we have computed the thermal diffusion factor for aqueous solutions of the same species mentioned before, aiming at providing some qualitative picture that would contribute to a better understanding of this process. Our simulations reproduce even quantitatively the change in the sign of the Soret coefficient experimentally observed (Tichacek et al., 1955, Bou-Ali, 1999, Kolodner et al., 1988, Zhang et al., 1996), and to the best of our knowledge, this is the first time that such achievement is reached for a mixture of molecular fluid employing molecular dynamic simulations. Additionally, we have devised a simple lattice model to support the hypothesis that the change in the sign of the Soret coefficient will appear in all cases in which the energy

of the crossed interaction between different species is more negative than the interaction energies between pure components. In addition, we have confirmed this fact with Molecular dynamics simulations of Lennard-Jones particles with crossed interactions enhanced and, again, a change in the sign of the Soret effect was observed. This particular behavior is commonly observed in other mixtures also containing associating fluids (Leppla and Wiegand, 2003, de Gans et al., 2003a, de Gans et al., 2003b).

The final part of this work is devoted to the computation of structural, transport and dielectric properties of benzene in water at supercritical conditions. We have selected the benzene because it is the simplest aromatic compound, and because the results obtained can be of interest in the study of some of the industrial processes such as supercritical water oxidation. We have employed a new Anisotropic United Atom (AUA) model of benzene (Contreras, 2002, Nieto-Draghi et al., 2003a) that reproduce the quadrupolar moment of this molecule through the inclusion of point charges. We have demonstrated that, in order to solvate this molecules in supercritical water, this kind of interactions should be included. We have computed self-diffusion coefficient and Maxwell-Stefan coefficients, and shear viscosity for the mixture at supercritical conditions. A strong density and composition dependence of the properties is observed. Experimental data shows the presence of aggregates between water and benzene molecules (Furataka and Ikawa, 1998a). This fact suggests the presence of some degree of hydrogen bonding between the electron cloud of the benzenic ring and the hydrogen atom of water molecules (Furataka and Ikawa, 2000). Our simulations are in qualitative agreement with this fact since we found that, at medium densities (0.6 g/cm^3 and 673 K), almost half of the benzene molecules present one hydrogen bond with water molecules. In addition, we observe that these bonds are longer lived than the corresponding hydrogen bonds between water molecules. Similarly, we obtain an important reduction of the dielectric constant of the mixture with the increment of the amount of benzene molecules, at least at medium and high densities. The knowledge of the behavior of the dielectric constant of the system in supercritical water is of great interest, particularly if one considers some chemical reactions involving electrolytes (Marrone et al., 1998).

The present manuscript is organized in the following way. In chapter 1 we present a general description of liquid theory, where the basic information required for the comprehension and the analysis of the different properties studied are presented. In addition, the methodologies employed and the descriptions of the concepts related to the molecular dynamics technique in different ensemble averages are also included in this chapter. The analysis done on the relationship between the structure and the dynamical behavior of pure water at different thermodynamic conditions, and the comparison of the different water

models is given in chapter 2. Chapter 3 is devoted to the study of transport properties of aqueous solutions of organic associating fluids such as methanol, ethanol, acetone and dimethyl sulfoxide. For clarity reasons we have dedicated chapter 4 exclusively to the analysis of the Soret coefficient of water with the same organic solvents presented in chapter 3. In chapter 5 we present the results obtained for the dielectric and transport properties of mixtures of benzene in supercritical water with the new model of benzene. Finally, we close the present work with the concluding remarks and perspectives for future investigations (chapter 6).

Chapter 1

LIQUID THEORY

The main objective of this chapter is to review the elements of liquid theory, as well as the fundamentals that support the implementation of computer simulations, specifically the Molecular Dynamics (MD) simulation, employed in this work. Concepts about thermodynamics and transport properties of liquids are briefly discussed, exclusively concerning classical liquids. This means that the mean distance between the molecules, $1/\rho^{1/3}$, should be greater than the de Broglie wavelength Λ , defined as

$$\Lambda \equiv \left(\frac{2\pi\hbar^2}{k_B T m} \right)^{1/2} \quad (1.1)$$

where $\hbar = h/2\pi$, k_B being the Boltzmann constant, T the absolute temperature, h the Planck constant and m , the mass of the particle. Thus, no quantum effects are considered in this work.

1. Structural and collective behavior of a system of N particles

The description of the structure of a molecular fluid should be done in terms of particle density and distribution functions. Thus, the radial pair distribution function, $g(\mathbf{r})$, measures how atoms organize themselves around each other, i.e. it gives information about the local structure of a given system (Haile, 1997). Let us define the n -particle distribution function $g_N^{(n)}(\mathbf{r})$, which is defined in term of the corresponding particle density by

$$g_N^{(n)}(\mathbf{r}) = \rho_N^{(n)}(\mathbf{r}_1, \dots, \mathbf{r}_n) / \prod_{i=1}^n \rho_N^{(1)}(\mathbf{r}_i) \quad (1.2)$$

where

$$g_N^{(n)} = \left\langle \sum_i \sum_{j \neq i} \sum_{k \neq i, j} \dots \sum \delta(\mathbf{r}_1 - \mathbf{r}_i) \delta(\mathbf{r}_2 - \mathbf{r}_j) \dots \delta(\mathbf{r}_n - \mathbf{r}_l) \right\rangle \quad (1.3)$$

the brackets stand for an ensemble average. For homogeneous systems, by

$$\rho^n g_N^{(n)}(\mathbf{r}^N) = \rho_N^{(n)}(\mathbf{r}^n) \quad (1.4)$$

where $\mathbf{r}^n = \{\mathbf{r}_1 \dots \mathbf{r}_n\}$.

The particle distribution function measures the extent to which the structure of the fluid deviates from complete randomness. If the system is isotropic as well as homogeneous, the pair distribution function $g_N^{(2)}(\mathbf{r}_1, \mathbf{r}_2)$ is a function only of the separation $r_{12} = |\mathbf{r}_1 - \mathbf{r}_2|$; it is then usually called the *radial distribution function* (RDF) and written simply as $g(r)$.

$g(r)$ is related to the probability that an atomic center lies in a spherical shell of radius r and thickness Δr with the shell centered on another atom.

The radial distribution function indicates how the presence of one atom influences the position of neighboring atoms. In general, for separations less than about one atomic diameter, $g(r) = 0$. In fluids, one atom should have no influence on the position of another atom at large distances; thus $g(r) \rightarrow 1$ as $r \rightarrow \infty$.

For molecular fluids, the structure of the molecules introduces the orientations as relevant variables in the description (Hansen and McDonald, 1991). The expression for the pair distribution function however resembles closely that obtained for atomic fluids, and it is defined as,

$$g(R_{12}, \Omega_1, \Omega_2) = \left(\frac{\Omega}{\rho} \right)^2 \rho^{(2)}(R_{12}, \Omega_1, \Omega_2) \quad (1.5)$$

in this definition, R_{12} is usually the separation between the centers of mass of each molecule, Ω_1 and Ω_2 are, respectively, angles describing the orientation

of each molecule. This molecular distribution function is a complex object due to its multidimensional character, difficult to be directly related with physical quantities of interest. The reader is addressed to the literature for details (Hansen and McDonald, 1991).

Due to this disadvantage, it is more convenient to analyze the structure of molecular fluids in terms of site-site distribution functions referred to the positions of pairs of atoms on each molecule. Usually this procedure is particularly appropriate in cases where the intermolecular potential is cast in a site-site form. If the position of a site a on the molecule i is denoted by \mathbf{r}_{ia} , and that of a site b on molecule j ($j \neq i$) by \mathbf{r}_{jb} , then the site-site distribution function, g_{ab} , is defined in a manner similar to (1.4), according to

$$\rho^2 g_{ab}(\mathbf{r}) = \left\langle \sum_{i \neq j}^N \sum \delta(\mathbf{r}_{ia}) \delta(\mathbf{r}_{jb} - \mathbf{r}) \right\rangle \quad (1.6)$$

The site-site distribution function is, of course, of interest in a wider context than that of interaction-site models, and has a simple physical interpretation. In a molecular simulation it is relatively easy to compute a set of these functions, and of course, they are also directly related to the structure factors measured in X-ray diffraction (Hura et al., 2000), neutron-scattering (Tassaing and Bellissent-Funel, 2000), as well as neutron diffraction (Soper et al., 1997) experiments. Other techniques, like nuclear magnetic resonance (NMR) (Lamb et al., 1981), infrared adsorption (IR) (Franck and Roth, 1992), Raman scattering (Carey and Korenowski, 1998), or inelastic neutron scattering (Ricci et al., 1998) are useful in the determination of the structure of fluids. In the case of water, information of the degree of hydrogen bond at different thermodynamic conditions can be inferred from these measurements.

For the case of neutron scattering the information of the atom-atom distribution functions is obtained indirectly from the measured structure factor $S^N(\mathbf{k})$. This structure factor is defined according to

$$\left(\sum_a b_a \right)^2 S_N^{intra}(k) = \sum_a b_a^2 + \sum_{a \neq b} \sum b_a b_b \frac{\sin(kl_{ab})}{kl_{ab}} \quad (1.7)$$

$$\begin{aligned} \left(\sum_a b_a \right)^2 S_N^{inter}(k) &= \rho \sum_a \sum_b b_a b_b \int dr \exp(-ik \cdot \mathbf{r}) [g_{ab}(r) - 1] \\ &= \sum_a \sum_a b_a b_b [S_{ab}(k) - 1] \end{aligned} \quad (1.8)$$

where the sums run over all nuclei in a molecule, b_a is the coherent neutron scattering length of a nucleus a , and l_{ab} is the separation of nuclei a and b . After removal of the intra molecular term, the Fourier transform of $S_{inter}^N(k)$ yields a weighted sum of atomic pair distribution functions, in the form

$$g_N(r) = \frac{\sum_a \sum_b b_a b_b g_{ab}(r)}{\left(\sum_a b_a\right)^2} \quad (1.9)$$

Isotopic substitution makes it possible to vary the weights with which the different $g_{ab}(r)$ contribute to $g^N(r)$ and, hence, in favorable cases, to determine some (or all) individual atom-atom distribution functions in the molecular fluid.

A formula similar to eq. (1.9) also applies to X-ray scattering. The only difference being that nuclear scattering lengths are replaced by the atomic form factors in this case.

In neutron diffraction experiments of water (Badyal et al., 2000), usually a mixture of deuterated and hydrogenated water is used, this technique is the so-called *neutron diffraction of isotopic substitutions* (NDIS). The determination of the spatial distribution functions involves three experiments at different isotopic compositions, each of which gives the structural information as a linear combination of the site-site structure factors. Because the k-space data must be inverted to real space to determine different g_{ab} , the resulting correlation may have some uncertainties (truncation, elimination of intra molecular contributions, etc) (Chialvo and Cummings, 1996a). Recent studies comparing results of this method and X-ray however find very good agreement between both results (Badyal et al., 2000). In Figure 1.1 it is possible to appreciate the evolution of the quality of the experimental oxygen-oxygen radial distribution function in pure water. Old and new NDS is compared with the most recent X-Ray experiments (ALS Advanced Light Source data).

1.1 Decomposition of $g(r)$ in terms of spherical harmonics

In a system composed of molecules in which different sites ¹ can be identified, the site-site pair distribution function is an important tool to study the structure of fluids. Of particular importance is the angular averaged site-site pair distribution function, which is a function only of inter-sites distances. Its magnitude, for specific sites, can be derived by inverse Fourier transform of the structure factor

¹different atoms, which are responsible for the overall complexity of the intermolecular potential

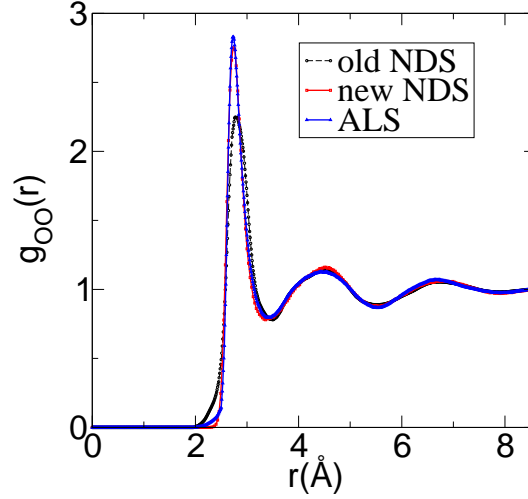


Figure 1.1. g_{OO} comparison of old (Soper et al., 1997) and new (Soper, 2000) NDS with the most recent X-Ray experiments (Hura et al., 2000) for water at 298 K and $\rho = 0.995 \text{ g/cm}^3$.

obtained from neutron and X-rays diffraction scattering (Soper, 2000, Hura et al., 2000). For spherically symmetric particles, the pair distribution function is isotropic. However, in molecules such as water, the particular geometry of the potential effectively introduces anisotropy in the local structure. A possible way to describe such an anisotropy is to expand the complete $g_{ab}(\mathbf{r})$ in a basis set of angular dependence of the spherical harmonics. One then writes

$$g_{ab}(\mathbf{r}) = \sum_{l,m} g_{ab}^{lm}(r) \cdot \mathbf{Y}_l^m(\theta, \phi) \quad (1.10)$$

From now on, the different $g_{ab}^{lm}(r)$ in eq. 1.10 will be referred to as components of $g_{ab}(\mathbf{r})$ in the base of spherical harmonics. These spherical harmonics, $\mathbf{Y}_l^m(\theta, \phi)$, are defined as

$$\mathbf{Y}_l^m(\theta, \phi) \equiv (-1)^m \sqrt{\frac{2l+1}{4\pi} \cdot \frac{(l-m)!}{(l+m)!}} \cdot \mathbf{P}_l^m(\cos \theta) \cdot e^{im\phi} \quad (1.11)$$

where $\mathbf{P}_l^m(\cos \theta)$ are associated Legendre functions (Arfken, 1981). The spherical harmonics are functions of the conventional angles in a polar coordi-

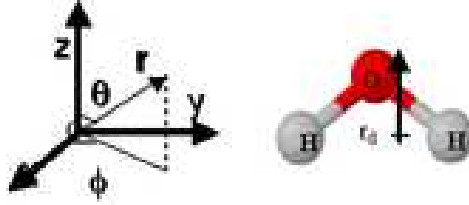


Figure 1.2. Local polar system of coordinates centered at the oxygen atom, and oriented in the direction of the permanent dipole vector of the molecule.

nate system. In the case of water molecules we have chosen the coordinates to be located at the center of the oxygen atom of the water molecule. The z-axis is pointing in the direction of the dipolar moment, and the y-axis is parallel to the line joining the two hydrogen atoms (see Figure 1.2). The components of the site-site pair distribution functions are thus defined as

$$g_{ab}^{lm}(r) = \int d\Omega g_{ab}(\mathbf{r}) \cdot \mathbf{Y}_l^{m*}(\theta, \phi) \quad (1.12)$$

where the integration is extended over all the solid angle Ω , and the asterisk stands for the complex conjugate. The periodicity of the angular distribution is related to the index l and m . In particular, $g_{ab}^{00}(r)$ is proportional to the radial distribution function, i.e, the angular average of $g_{ab}(\mathbf{r})$, while $g_{ab}^{32}(r)$ indicates, in the case of the oxygen-oxygen distribution function, how likely it is to find oxygen atoms of water molecules simultaneously in an almost tetrahedral arrangement at a distance r . To obtain component $g_{ab}^{lm}(r)$ from molecular simulations, we compute

$$g_{ab}^{lm}(r) \equiv \left\langle \frac{1}{N} \sum_{i=1}^N \left[4\pi \sum_{j=1}^{N_j} \frac{\mathbf{Y}_l^{m*}(\theta, \phi)}{V(r)} \right] \right\rangle \quad (1.13)$$

where (θ, ϕ) are the angular coordinates of site b , found at a distance r from site a on molecule i (see Figure 1.2). $V(r)$ is the volume of the spherical shell where the molecule j is located (in fact, to numerically evaluate $g_{ab}^{lm}(r)$ a discretization of space in the radial direction has to be introduced, as it is customary in the numerical calculation of pair distribution functions (Hansen and McDonald, 1991)). Furthermore, it is possible to reconstruct a three dimensional picture of the structure of the system from the set of functions $g_{ab}^{lm}(r)$, according to eq.

1.10. A truncation of the series in eq. 1.10, at given values of l and m , results in a smoothing out of the three-dimensional site-site particle distribution. After truncation, $g_{ab}(\mathbf{r})$ can be negative, this is an artifact caused by the truncation, with no physical meaning. In this work, we have considered values of l from 0 to 4, with m being all the even values ranging from $-l$ to l . Odd values of m give zero contributions, due to the symmetry of the water molecule. Such a choice ignores angular variations with a periodicity smaller than $\pi/2$ but it is enough to identify molecules in a tetrahedral arrangement, for instance. More details on the selected spherical harmonics are given in Appendix A.

1.2 Orientational order parameter

The ability of any fluid to produce tetrahedral arrangements can be described by the orientational parameter q , which is defined according to (Errington and Debenedetti, 2001, Chau and Hardwick, 1998)

$$q = 1 - \frac{3}{8} \sum_{j=1}^3 \sum_{k=j+1}^4 \left(\cos(\Psi_{jk}) + \frac{1}{3} \right)^2 \quad (1.14)$$

where ψ_{jk} is the angle formed by the lines joining the oxygen atom of a given molecule with that of each of the four nearest neighboring molecules. In this work water molecules have been selected to be the center of reference to compute the orientational parameter. Additionally, if aqueous solutions are analyzed, the neighboring oxygen of the molecules employed in the calculus of this coefficient could be indistinctly that of the solute or the water. Although the numerical value of this parameter ranges from -3 to 1 , it is expected that, for physical reasons, q would effectively range from 0 , in a random distribution of molecules (ideal gas), to 1 , in a perfect tetrahedral arrangement. It is important to realize that the value of this order parameter is not subject to the choice of any particular local coordinate system in the reference molecule (see the reference (Tanaka, 1999) where an order parameter was employed to study order correlations in metals). Therefore it has a finite value even for a spherical fluid, as in a fluid of Lennard-Jones molecules, due to the excluded volume correlations in the particles of the first shell of neighbors if the system is dense. The physical implications of the existence of local tetrahedral arrangement in a spherical fluid are discussed in ref. (Tanaka, 1999, Frank, 1952, Kleman and Sadoc, 1979, Nelson, 1983).

In this work we are also interested in the formation of tetrahedral structures hydrogen bonded, thus having a well-defined orientation with respect to the

dipolar moment of the reference molecule. We thus introduce a new parameter q' defined as

$$q' \equiv \rho \int_0^{r_{OO}^{min}} |g_{OO}^{32}(r)| r^2 dr \quad (1.15)$$

where ρ is the oxygen number density, $g_{OO}^{32}(r)$ is the spherical harmonic projection of the oxygen-oxygen pair distribution function and r_{OO}^{min} is the first minimum of $g_{OO}(r)$ at the same conditions. This parameter measures the formation of a tetrahedral structure in a given orientation with respect to the reference molecule. Consequently, this parameter is zero for a spherical fluid.

1.3 Translational order parameter

Together with the orientational order parameter, the so-called translational order parameter t measures the tendency of pairs of molecules to adopt preferential separations thus, translational order. This parameter is defined as (Errington and Debenedetti, 2001)

$$t \equiv \frac{1}{\xi_c} \int_0^{\xi_c} |g(\xi) - 1| d\xi \quad (1.16)$$

where ξ_c , the cut-off value, is 2.843 as in the original reference (Errington and Debenedetti, 2001). Typically, in a ideal gas $g(r) \rightarrow 1$ and t vanishes. In a crystal, on the other hand, there is long-range translational order, and $g(r) \neq 1$ over long distances. Hence t is large.

2. Dynamic behavior and transport properties of fluids

This part of the chapter is dedicated to analyze the dynamics of a system of particles. The collective behavior of species in fluids should be described in terms of matter fluxes, which can be given either in terms of molar fluxes or in terms of mass fluxes. These fluxes are related to the advection and diffusive process.

Diffusion is the process whereby matter is transported due to thermal agitation, in absence of macroscopic overall mass or molar flow. Although different definitions of the diffusive flux can be introduced (de Groot and Mazur, 1984), the macroscopic diffusive flow is defined here with respect to the so-called barycentric velocity, given by

$$\rho \mathbf{v} = \sum_i \rho_i \mathbf{v}_i \quad (1.17)$$

where $\rho = \sum_i \rho_i$ is the total density, ρ_i being the mass density of the i^{th} species, and \mathbf{v}_i is the velocity of each species. Thus, the diffusive mass flux is defined by

$$\mathbf{J}_i = \rho_i \cdot (\mathbf{v}_i - \mathbf{v}) \quad (1.18)$$

The diffusive flow in an isothermal binary mixture is phenomenologically given by the Fick's law

$$\mathbf{J}_1 = -c_T D_{12} \nabla x_1 = -\mathbf{J}_2 \quad (1.19)$$

where D_{12} is referred to as the diffusion coefficient and is of dynamic nature. Notice that diffusion is an irreversible process that exists only in mixtures.

2.1 Self-diffusion

Even though, it is possible to define self-diffusion as a process in which a mentally *tagged* particle diffuses embedded in a bulk of particles identical to the tagged one. If one can identify and follow the tagged particle, it diffuses due to thermal agitation. In this case, one can identify the diffusion coefficient as a quantity related to the mean square displacement of the erratic motion of the *tagged* particle, according to the well-known relation due to Einstein (Frenkel and Smith, 1996)

$$D = \lim_{t \rightarrow \infty} \frac{1}{6t} \langle |\mathbf{r}(t) - \mathbf{r}(0)|^2 \rangle \quad (1.20)$$

where $\mathbf{r}(t)$ is the vector position of one particle at time t , $\mathbf{r}(0)$ is the position at $t = 0$, and D is the self-diffusion coefficient. This equation is a direct consequence of the Fick's Law (Frenkel and Smith, 1996).

Additionally, it is possible to also determine the self-diffusion coefficient analyzing the relaxation of the velocity-velocity auto-correlation function of a tagged particle in a system in thermal equilibrium. This is one of the known

Green-Kubo relations, which give D from the time integral of the velocity auto-correlation function (VACF). Such a relation between a transport coefficient and an integral over a time-correlation function is called *Green-Kubo relation*. Definitions for more complex *Green-Kubo* relationships are also possible (Hansen and McDonald, 1991, Zhou and Miller, 1996, de ven Lucassen et al., 1998) aiming at determining other transport coefficient, such as: Thermal conductivity, viscosity coefficient, dielectric constant, etc. Even though, in this work, mean square displacement has been employed to compute self-diffusion coefficient, both, in pure systems as well as in mixtures.

Experimentally the self-diffusion coefficient can be measured by several techniques, but the most common are Proton NMR (Lamb et al., 1981) and quasi-elastic incoherent neutron scattering (Tassaing and Bellissent-Funel, 2000). In the second case one measures the quasi-elastic and inelastic incoherent neutron scattering of the sample. Then this data is used to fit a theoretical equation that involve the dynamical structure factor (also called the Debye-Waller factor),

$$S(Q, \omega) = \exp\left(\frac{-Q^2 \langle u^2 \rangle}{3}\right) T(Q, \omega) \otimes R(Q, \omega) \quad (1.21)$$

where Q is the momentum transfer, u^2 is the mean square amplitude of the molecular vibrations. $R(Q, \omega)$ accounts for the hindered rotation and $T(Q, \omega)$ represents the contribution from the translational motion of the molecules. Assuming that the translational and rotational degrees of freedom are decoupled it is possible to analyze only the translational part, therefore, the dynamical structure factor S is reduced to the expression

$$S(Q, \omega) = \exp\left(\frac{-Q^2 \langle u^2 \rangle}{3}\right) T(Q, \omega) \quad (1.22)$$

where $T(Q, \omega)$ can be expressed in terms of the half-width of the translational line of the molecule $\Gamma(Q)$

$$T(Q, \omega) = \frac{1}{\pi} \frac{\Gamma(Q)}{\{\omega^2 + [\Gamma(Q)]^2\}} \quad (1.23)$$

and this factor $\Gamma(Q)$ is related with the translational diffusion coefficient (self-diffusion coefficient) through a random jump diffusion model,

$$\Gamma(Q) = \frac{DQ^2}{1 + DQ^2\tau_0} \quad (1.24)$$

here τ_0 is the residence time between jumps. Finally, the mean square displacement (MSD) of the molecules can be expressed as $6D\tau_0$ that is the same quantity computed in a Molecular Dynamic simulation (expression between angular parentheses in eq. (1.20)). In resume, the experimental accessible quantity is the quasi-elastic incoherent neutron scattering spectra $I(Q,\omega)$ which is related with the $S(Q,\omega)$ through this equation

$$I(Q,\omega) = S(Q,\omega) \otimes R(\omega) + I_{background} \quad (1.25)$$

where $R(\omega)$ is the energy resolution function of the instrument and $I_{background}$ denotes the contribution coming from the background due to fast rotational motion. From eq. (1.25) you have $S(Q,\omega)$ and using eq. (1.22) to eq. (1.24) it is possible to determine the self-diffusion coefficient. More details about experimental determination of this transport property can be found in (Krynicky et al., 1980, Lamb et al., 1981) and (Tassaing and Bellissent-Funel, 2000).

2.2 Maxwell-Stefan mutual diffusion coefficient

The diffusion coefficient presented in eq.(1.19), or, the normally called Fick's D coefficient, is the most commonly used in different engineer processes. It is, therefore, important to have predictions of this coefficient in cases where experimental measurements are unavailable. Microscopic relations to compute D in binary and ternary systems had been developed by Zhou and Miller (Zhou and Miller, 1996). In this case the coefficient can be computed using time correlation functions through the Green-Kubo formalism. The expression to compute D in the case of binary mixtures is,

$$D_{12} = \frac{x_2 Q}{3n_1} \left(\frac{M_1 x_1 + M_2 x_2}{M_2 x_2} \right)^2 \int_0^\infty \left\langle \sum_{i=1}^{n_1} \mathbf{v}_1^i(t) \cdot \sum_{j=1}^{n_1} \mathbf{v}_1^j(0) \right\rangle dt \quad (1.26)$$

where x_1, x_2, M_1 and M_2 are the molar fractions and masses of species 1 and 2 respectively, n_1 is the number of molecules of species 1. Additionally, \mathbf{v}_1 is the center of mass velocity of particles of specie 1. The thermodynamic factor Q , may be expressed in terms of radial distribution functions of the molecules in a binary system (Zhou and Miller, 1996),

$$Q = \frac{1}{1 + x_1 x_2 \rho (\Gamma_{11} + \Gamma_{22} + \Gamma_{12})} \quad (1.27)$$

where ρ is the density of the system, and each $\Gamma_{\alpha\beta}$ is defined as

$$\Gamma_{\alpha\beta} = 4\pi \int_0^\infty r^2 [g_{\alpha\beta}(r) - 1] dr \quad (1.28)$$

The thermodynamic factor Q is in addition directly related to chemical potential derivatives of each species in the mixture,

$$Q = \frac{x_1}{k_B T} \left(\frac{\partial \mu_1}{\partial x_1} \right)_{T,P} \quad (1.29)$$

However, the computation of the thermodynamic factor Q is not easily accessible in computer simulation, due to the fact that radial distribution functions present some degree of uncertainties, as it was mentioned before. For this reason, the computation of the Maxwell-Stefan mutual diffusion coefficient presents an advantage with respect of the normal Fick's diffusion coefficient. For instance, comparing eq. (1.19) with the Maxwell-Stefan equation one has (Taylor and Krishna, 1993),

$$\mathbf{J}_1 = -c_T \bar{D}_{12} \cdot Q \cdot \nabla x_1 \quad (1.30)$$

Diffusion coefficient in binary liquid mixtures can be strong functions of composition. In this respect non-ideal solutions originate also a non-monotonous behavior of the thermodynamic factor Q . Consequently, in view of eq. (1.19) and eq. (1.30), these two coefficients are related as follow (Taylor and Krishna, 1993)

$$\bar{D}_{12} = \frac{D_{12}}{Q} \quad (1.31)$$

Then, the Maxwell-Stefan diffusion coefficient can be calculated in computer simulation from eq. (1.26) using the relation given in eq. (1.31), and it is partially free of the strong influence of the composition of the system.

2.3 Shear Viscosity η

The macroscopic local densities associated with the conserved variables are the particle number density $\rho(\mathbf{r}, t)$, the momentum density $\mathbf{p}(\mathbf{r}, t)$ and the total energy density $e(\mathbf{r}, t)$. The local velocity field $\mathbf{v}(\mathbf{r}, t)$ is defined via the relation (Hansen and McDonald, 1991)

$$\mathbf{p}(\mathbf{r}, t) = \rho(\mathbf{r}, t)\mathbf{v}(\mathbf{r}, t) \quad (1.32)$$

where $\rho(\mathbf{r}, t)$ is the mass density. Focusing in the transport of momentum, the conservation law for the local density is the Newton's Law in a control volume,

$$\frac{d}{dt} \int_V dV \mathbf{p}(\mathbf{r}, t) = \int_V dV \nabla \cdot \bar{\bar{\sigma}} \quad (1.33)$$

where $\bar{\bar{\sigma}}$ is the momentum current, or the *stress tensor*. The elements of the stress tensor in Newtonian fluids are given phenomenologically by

$$\begin{aligned} \sigma_{\alpha\beta}(\mathbf{r}, t) = & \delta_{\alpha\beta}P(\mathbf{r}, t) - \eta \left(\frac{\partial v_\alpha(\mathbf{r}, t)}{\partial r_\beta} + \frac{\partial v_\beta(\mathbf{r}, t)}{\partial r_\alpha} \right) \\ & + \delta_{\alpha\beta} \left(\frac{2}{3}\eta - \zeta \right) \nabla \cdot \mathbf{v}(\mathbf{r}, t) \end{aligned} \quad (1.34)$$

where $P(\mathbf{r}, t)$ is the hydrostatic pressure, η is the shear viscosity and ζ is the bulk viscosity. The subscripts α, β stand for the different Cartesian coordinates.

The shear viscosity of any fluid can be microscopically calculated from the simulations. Due to the long time decay of the pressure tensor time correlation function in some aqueous systems (specially those of associating fluids, which will be discussed later), the computation of the viscosity through a Green-Kubo expression (Hansen and McDonald, 1991) (using time integrals of the pressure tensor) is very inefficient in systems where molecules has electrical charges, due to the high fluctuation and long tails presented in the pressure tensor correlation function of the system. However, the use of the Einstein relation (Smith and van Gunsteren, 1993) permits to overcome the effect of these long temporal queues in the Green-Kubo calculations and obtain precise values of the viscosity with a reasonable computational effort. Consequently, the Einstein relation is employed as described by Smith *et. al.* (Smith and

van Gunsteren, 1993) but, contrary to the original work, where only the off-diagonal elements of the pressure tensor were employed, here we use all of the elements of the stress tensor (according to ref. (Dysthe et al., 1999a)) to improve convergence and statistics. Thus, the viscosity coefficient is given by the expression (Petrvic, 2000)

$$\eta = \frac{1}{20} \frac{V}{k_B T} \lim_{t \rightarrow \infty} \frac{d}{dt} \left[\sum_{\alpha} \langle \Delta P_{\alpha\alpha}^T(t) \rangle^2 + 2 \sum_{\alpha > \beta} \langle \Delta P_{\alpha\beta}(t) \rangle^2 \right] \quad (1.35)$$

Here, α and β are indexes running over the three Cartesian coordinates, V is the volume, T is the temperature, and $\Delta P_{\alpha\beta}(t)$ denotes the *displacement* of the elements of the pressure tensor $P_{\alpha\beta}$ (notice that, following eq. (1.34), $P_{\alpha\beta} = -\sigma_{\alpha\beta}$), which is defined as

$$\Delta P_{\alpha\beta}(t) = \int_0^t \frac{1}{2} (P_{\alpha\beta}(\tau) + P_{\beta\alpha}(\tau)) d\tau \quad (1.36)$$

and,

$$\Delta P_{\alpha\alpha}^T(t) = \int_0^t (P_{\alpha\alpha}(\tau) - \frac{1}{3} \sum_{\beta} P_{\beta\beta}(\tau)) d\tau \quad (1.37)$$

The microscopic expression for the elements of the pressure tensor $P_{\alpha\beta}$ appearing in the integrand of eq. (1.36) and eq. (1.37) is given by

$$P_{\alpha\beta}(t) = \frac{1}{V} \left(\sum_i \frac{p_{\alpha i}(t) p_{\beta i}(t)}{m_i} + \sum_{i < j} \sum f_{\alpha ij}(t) r_{\beta ij}(t) \right) \quad (1.38)$$

In eq. (1.38), $p_{\alpha i}$ is the α -component of the momentum of particle i , $f_{\alpha ij}$ is the α -component of the force exerted on particle i by particle j , and $r_{\beta ij}$ is the β -component of the particle-particle vector, $\mathbf{r}_{ij} \equiv \mathbf{r}_j - \mathbf{r}_i$. The viscosity is obtained from the slope of eq.(1.35), always after some initial time, were the displacement is not a linear function of the time.

2.4 Thermal conductivity λ

Heat conduction can be considered as a process where the energy is propagated through *lattice waves*, induced by atomic motion, without macroscopic

motion. This diffusion process is phenomenologically described by the *Fourier's Law*, which, in a pure system reads,

$$\mathbf{J}_q \equiv -\lambda \nabla T \quad (1.39)$$

where \mathbf{J}_q is the heat flux (energy per unit of area), ∇T is the temperature gradient and λ the thermal conductivity. This latter property, which is referred to as a *transport coefficient*, provides an indication of the rate at which energy is transferred by the diffusion process described. Thermal conductivity depends on the physical structure of the matter (atomic and molecular) and the physical state of the matter (solid, liquid, etc). This coefficient can be experimentally measured with high accuracy, and many empirical equations have been developed to estimate this property in solids, liquids and gases. In liquid mixtures some correlations are very good to predict the behavior of common solutions (Li, 1976) but, however, this kind of correlations are unable to predict non-ideal behaviors such as maximum and minimum of the thermal conductivity at particular compositions.

Then, from a microscopic point of view, the computation of the thermal conductivity can be achieved from molecular simulations, and different techniques can be employed. For instance, a Green-Kubo expression can be employed to calculate this property in systems in thermal equilibrium (Hansen and McDonald, 1991)

$$\lambda = \frac{1}{3k_B V T^2} \int_0^\infty \langle \mathbf{J}_e(0) \cdot \mathbf{J}_e(\tau) \rangle d\tau \quad (1.40)$$

This formula requires a microscopic expression of the energy current \mathbf{J}_e , (in general, for mixtures) (Vogelsang et al., 1987),

$$\begin{aligned} \mathbf{J}_e = & \sum_{\alpha=1}^{n_{esp}} \sum_{j=1}^{N_\alpha} \frac{1}{2} m_\alpha |\mathbf{v}_{j\alpha}|^2 \mathbf{v}_{j\alpha} \\ & - \frac{1}{2} \sum_{\alpha=1}^{n_{esp}} \sum_{\beta=1}^{n_{esp}} \sum_{j=1}^{N_\alpha} \sum_{k=1}^{N_\beta} \left(\mathbf{r}_{j\alpha k\beta} \frac{\partial U(r_{j\alpha k\beta})}{\partial \mathbf{r}_{j\alpha k\beta}} - U(\mathbf{r}_{j\alpha k\beta}) \bar{\mathbf{i}} \right) \mathbf{v}_{j\alpha} \\ & - \sum_{\alpha=1}^{n_{esp}} h_\alpha \sum_{j=1}^{N_\alpha} \mathbf{v}_{j\alpha} \end{aligned} \quad (1.41)$$

The subscripts α, β stands for the different kinds of molecules and j, k count the number of particles. N_α and N_β are the number of particles of kind α , i.e., β . The heat current \mathbf{J}_e is composed of a kinetic part, a *potential* part, and a term containing the partial enthalpies (last term on eq. (1.41)). $\mathbf{v}_{j\alpha}$ denotes the center of mass velocity of a particle j of kind α , h_α denotes the partial enthalpy per particle of species α , $U(r_{j\alpha k\beta})$ is the interaction potential (Vogelsang et al., 1987). However, in this microscopic expression of the heat current (eq.(1.41)), which is required in the Green-Kubo expression (eq.(1.40)), there is a contribution due to the partial molar enthalpies of the different species (Hoheisel, 1999). These quantities are difficult to obtain in simulations with fixed number of particles, like those used in this work. Thus, its determination would require a separate set of simulations if the partial molar enthalpies for the different substances were not known a priori. Only in the case of ideal mixtures, the contribution arisen from the partial molar enthalpies can be disregarded in the Green-Kubo formalism (Dysthe et al., 1999b). In the case of very non-ideal solutions, like water solutions, this simplification is not valid. For this reason in this work we have adopted a non-equilibrium scheme, where the direct imposition of a thermal gradient and the computation of the resulting heat flow permits the determination of the thermal conductivity from their ratio. Then, thermal conductivity can be computed through a constant temperature PeX (momentum exchange algorithm) non-equilibrium molecular dynamic simulation (Muller-Plathe, 1997, Bedrov and Smith, 2000) (see ref. (Nieto-Draghi and Avalos, 2003) and appendix E).

In this scheme, the total momentum and energy of the system are held constant. Moreover, the simulation box has periodic boundary conditions in the three dimensions of space. In the z -direction, one considers two slabs of a given thickness, large enough to contain many particles in average but much smaller than the length of the box in the z -direction. To maintain a temperature gradient, the faster particle in the so-called *cold* slab is selected with frequency ν to exchange its momentum with the slowest particle in the *hot* slab. Thus, the energy transfer induced by this exchange of momentum is added to the value of the accumulated energy transferred between the two slabs (see Figure 1.3). Thus, the heat flow density at steady state is thus given by the relation

$$\langle J_z(t) \rangle = \frac{1}{2At} \sum_{transfers(t), i} \frac{m_i}{2} (\mathbf{v}_{ci}^2 - \mathbf{v}_{hi}^2) \quad (1.42)$$

In this expression, A is the crosssectional area. Furthermore, $\langle J_z(t) \rangle$ is the heat flux density in the z direction (i.e. the direction of the imposed temperature gradient). On the right hand side of eq. (1.42), \mathbf{v}_{ci} and \mathbf{v}_{hi} stand, respectively, for the velocities of the particles of the i^{th} species that participate in the exchange

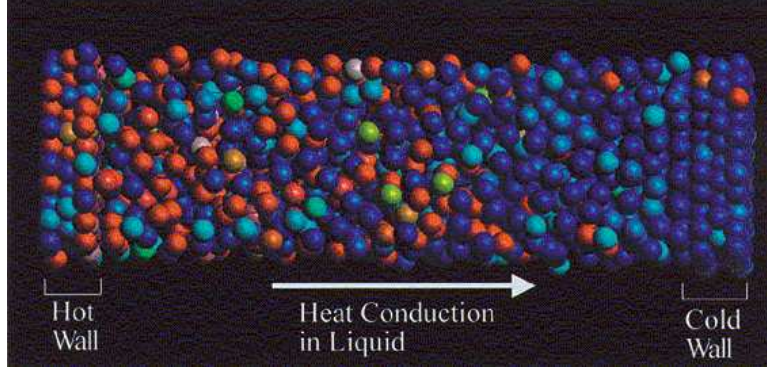


Figure 1.3. Schematic representation of half of the simulation box using the non-equilibrium PeX algorithm. Particles in blue have less kinetic energy than red particles.

procedure, from the cold c and hot h slabs (Bedrov and Smith, 2000). The sum is done over all the transfers occurred after an initial time, t thus being the time interval since this origin. With this special configuration, heat is delivered from the center to the right and left cold slabs. Thus, the heat flux is half of the energy *pumped* by the algorithm per unit of time. Moreover, eq. (1.42) is a trivial generalization of the original method (Muller-Plathe, 1997) for the case of mixtures. Thus, we have to point out that; the momentum exchange is done only between particles of the same species, and simultaneously for all species. Hence, it is required that the number of particles in both slabs is sufficiently large, on one hand, to be sure that it is always possible to find particles of each species to exchange their energy. On the other hand, it is also desirable that the collisions inside the slabs properly thermalize the velocity distribution before a new exchange is done. These requirements are fulfilled in our case, in which liquid densities are considered. Once the thermal gradient is stabilized and the process is stationary, the thermal conductivity can be obtained from the relation

$$\lambda = \frac{\langle J_z(t) \rangle}{\langle dT/dz \rangle} \quad (1.43)$$

where $\langle dT/dz \rangle$ is the resulting temperature gradient in the z direction (Bedrov and Smith, 2000). Notice, however, that in this relation crossed effects due to the presence of induced concentration gradients (Soret effect) are absorbed into the definition of λ , which, in this way, is directly accessible from both simulations and experiments (Evans, 1997). Other definitions can be used (de Groot and Mazur, 1984) which explicitly separate the direct effect of the temperature gradient from the induced by that concentration gradient, whose contribution

to the heat transport usually is much smaller than the direct effect. These contributions may be important if the temperature gradient imposes large gradients in composition along the box, which is not the case under the conditions of our simulations. Eq.(1.43) allows the computation of the thermal conductivity in away similar to what is done in traditional experimental techniques through the *Fourier's law* (eq.1.39).

2.4.1 Soret coefficient

When a temperature gradient is applied to a liquid mixture not only causes a heat flux but also gives rise to a diffusion current of the constituent components. The resulting separation of the components causes a concentration gradient parallel with respect to the temperature gradient. This cross-effect between temperature and concentration is well known in irreversible thermodynamics as *thermal diffusion* or Ludwig-Soret-effect. Even though this effect has been known for long time, and some theories have been proposed (Kempers, 2001, Dougherty and Drickamer, 1955) for ideal mixtures and gases, there is still no simple satisfactory theory to explain the effect in liquids, solids and polymers. The theory of Kempers *et al* (Kempers, 2001) has been successfully tested in mixtures of hydrocarbons (light normal paraffins, heavy normal paraffins, branched paraffins, naphthenes, monocyclic aromatics, etc), but non-ideal mixtures such as aqueous solutions with associating fluids such as alcohols, ketones, sulfoxides, etc, are still matter of study. This lack of knowledge in the behavior of such mixtures motivates the study of this property through molecular dynamics simulations, where, it is possible to have a microscopic picture of the process.

From a macroscopic point of view and following the framework of irreversible thermodynamics, the coupling between the different fluxes (mass and heat) are described according Onsager's linear relationships (de Groot and Mazur, 1984),

$$\begin{aligned} \mathbf{J}_k &= \sum_{j=1}^N L_{kj} \mathbf{X}_j + L_{kq} \mathbf{X}_q, \\ \mathbf{J}_q &= \sum_{j=1}^N L_{qj} \mathbf{X}_j + L_{qq} \mathbf{X}_q, \end{aligned} \tag{1.44}$$

with \mathbf{J}_k being the flux of component k with respect to the center of mass of the system and \mathbf{J}_q being the heat flux. The \mathbf{X}_α are thermodynamic forces,

that (for the specific case of binary mixtures) are defined as $\mathbf{X}_q = -(\nabla T/T)$ and $\mathbf{X}_j = -\nabla_T(\mu_1 - \mu_2)$ (here the gradient is formally done at constant temperature). The $L_{\alpha\beta}$ are the Onsager coefficients with $\alpha = (k, q)$ and N is the number of species in the mixture. Using an appropriate frame of reference, the Onsager coefficients can be related to the macroscopic coefficients λ and S_T (the thermal conductivity and the Soret coefficient) respectively for a binary mixture according to (MacGowan and Evans, 1986b, Evans and MacGowan, 1987),

$$S_T = \frac{L_{1q}}{\rho T D_{12}} \quad (1.45)$$

$$\lambda = \frac{1}{T^2} \left[L_{qq} - \frac{L_{1q}^2}{L_{11}} \right]$$

where ρ is the system density, D_{12} is the mutual diffusion. The first expression in eq. (1.45) can be employed to compute the Soret coefficient but it lacks of practicality due to the difficulty inherent to the measurement of the Onsager coefficients. In essence, the base of the experiments is the same as that employed in the computation of the thermal conductivity, the main difference lay in the devices employed to detect the concentration gradient in the system. Usually, the Soret coefficient has been measured through optical techniques, traditionally with refraction indexes of the fluid (Tichacek et al., 1955, Kolodner et al., 1988) and more recently by X-Ray microscopy (Rondot et al., 2002), where the technique permits a rapid acquisition (a few seconds) of a quantitative elemental map of the species in the system. In this respect, molecular simulation permits the precise knowledge of the positions of the molecules in the system and due to this advantage this coefficient can be analyzed more in detail from a microscopic point of view. Similarly to other coefficients, a Green-Kubo expression can be employed to determine the *thermal diffusion* coefficient (Vogelsang and Hoheisel, 1988),

$$D^T = \frac{1}{3Vk_B T} \int_0^\infty \langle \mathbf{J}_e(0) \cdot \mathbf{J}_m(t) \rangle dt \quad (1.46)$$

The heat flux \mathbf{J}_e is the same defined in eq.(1.41) and the mass flux \mathbf{J}_m of one specie is,

$$\mathbf{J}_m = m_1 \sum_{j=1}^{N_1} \mathbf{v}_{j1} \quad (1.47)$$

where m_1 and \mathbf{v}_{ji} are the mass and the velocity of specie 1 in the system. The Soret coefficient is then computed with (Vogelsang et al., 1987),

$$S_T = -\frac{D^T}{w_1 w_2 \rho T D_{12}} \quad (1.48)$$

being w_1 and w_2 the mass fractions of the constituents and ρ the mass density of the system. As it was commented before in the computation of the thermal conductivity, the heat flux employed in eq.(1.46) requires the use of \mathbf{J}_e (eq.(1.41)) where the partial molar enthalpies are required. The selection of an appropriate simulation technique avoids the computation of partial molar enthalpies of each species in the system. Thus, non-equilibrium techniques have been proven to be more efficient to compute the Soret coefficient in molecular simulations (Bedrov and Smith, 2000) and do not require these properties. Then, applying the same constant temperature PeX (momentum exchange algorithm) technique one has,

$$S_T = -\frac{1}{x_1(1-x_1)} \left(\frac{\partial x_1}{\partial z} \right) \left(\frac{\partial T}{\partial z} \right)^{-1} \quad (1.49)$$

where x_1 is the molar fraction of species 1 (in a binary system), the gradients $(\partial x_1 / \partial z)$ and $(\partial T / \partial z)$ can be obtained fitting to a straight line the concentration and temperature profiles rising from the simulation. The advantage of this technique is that it is similar to what is done in normal experiments, where the sample is inside a box where a thermal gradient is imposed through one direction (the z direction in the case of simulation) of the box.

3. Water: Important considerations

Due to the fact that the main objective of this work is to study the dynamical and thermodynamical behavior of pure water and aqueous solutions, the knowledge of some of the peculiar characteristics of this substance are very important to understand the information presented in the rest of the chapters. Water (H_2O) is one of the most common molecules in the Universe. Due to its importance it has been very well studied, both theoretically and experimentally, and a number of model structures aiming at simulating its behavior have

been proposed. Liquid water is unique with a number of particular properties (Chapling, 2003).

- 1 High boiling point at ambient conditions, 100.0°C when compared with similar hydrogenated compound (HF, H_2S , NH_3 , etc) (Franks, 2000, NIST, 2001)
- 2 High Critical Temperature 373.99°C (Franks, 2000, NIST, 2001)
- 3 Maximum in the density as a function of the temperature 0.999972 g/cm^3 at 3.984°C and 1 bar (Franks, 2000, NIST, 2001)
- 4 Its self-diffusion increase when the fluid is compressed at high density (Stanley et al., 2002b, Netz et al., 2002b, Netz et al., 2002a, Scala et al., 2000a, Starr et al., 2000)
- 5 Simulation results suggest the presents a second critical point and a complex supercooled region (Stanley et al., 2002a, Franzese et al., 2001d, Mishima and Stanley, 1998, Bluhm et al., 2002, Scala et al., 2000b, Franzese et al., 2001a)
- 6 Divergence of the isochoric heat capacity near the critical point (Polikhronidi et al., 2001)

The capability of forming complex 3D networks in solid and liquid states, as well as the strong long-range interactions between the molecules may explain some of these anomalous properties. The presences of these collective, long-range interactions between water models can be understand analyzing the structure of the water molecule.

3.1 Water structure

Water has the molecular formula H_2O but the hydrogen atoms are constantly exchanged between molecules due to protonation/de-protonation processes. Water molecules are symmetric with respect to two planes and rotation axis, as shown in Figure 1.4.

The water molecule is often described simply as having four, approximately tetrahedrally arranged, sp^3 -hybridized electron pairs, two of which are associated with hydrogen atoms leaving the two remaining lone pairs. In a perfect tetrahedral arrangement the bond-bond, bond-lone pair and lone pair-lone pair angles would all be 109.47° and such tetrahedral bonding patterns are found in condensed phases such as hexagonal ice (Chapling, 2003). *Ab initio* calculations on isolated molecules, however, do not confirm the presence of significant directed electron density where lone pairs are expected. Some 5-point

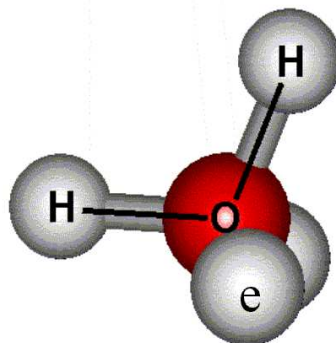


Figure 1.4. In this figure it is possible to see a schematic representation of a water molecule. Here O and H are, respectively, the oxygen and the hydrogen atoms, and “e” represents the position of the lone pair electrons of the oxygen atom (Chapling, 2003).

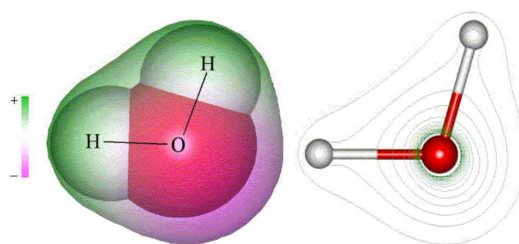


Figure 1.5. Water structure showing the electron density distribution (high densities around the oxygen atoms have been omitted for clarity)(Chapling, 2003).

molecular-models (that will be discussed more in detail in the intermolecular models section) explicitly include those lone pairs electrons, but of course this specific geometry is based on the hypothesis that this lone pair electrons exist (probabilistically speaking) in that particular geometry (Chapling, 2003).

Although the lone pairs of electrons do not appear to give distinct directed electron density in isolated molecules, there are minima in the electrostatic potential at approximately the expected positions given in Figure 1.5. Hydrogen atoms are attached to the oxygen through covalent bonds. In covalent bonds electrons are shared between atoms, but in the case of water the sharing is not equal. The oxygen atom attracts the electrons more strongly than the hydrogen. This gives water asymmetrical distribution of charge (DNA, 2001). This charge distribution can be seen in Figure 1.5,

3.2 The concept of hydrogen bonding

The positive regions in one of the water will attract the negative charged regions in other waters. This electrostatic interaction between two or more molecules is called the hydrogen bond. In Figure 1.6 its possible to see two water molecules hydrogen-bonded.

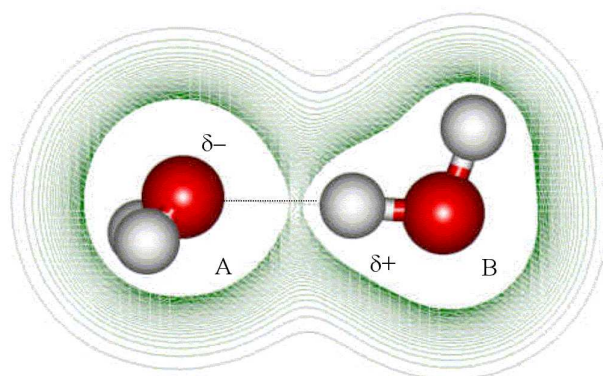


Figure 1.6. In this figure it is possible to see a water dimer showing the partial charges (Chapling, 2003).

Typically this hydrogen bonding occurs where the partially positively charged hydrogen atom is close to partially negatively charged oxygen. This process can also be found in other systems, like Fluorine atoms in HF_2^- and between water and the smaller halide ions F^- , Cl^- and Br^- (e.g. $\text{HO-H} \cdots \text{Br}^-$, (Mayanovic et al., 2001)), and, to a much smaller extent, to I^- (Kropman and Bakker, 2001), and in all associating fluids (alcohols, ketones, sulfoxides, etc).

Hydrogen bonds are much weaker than covalent bonds. In water the hydrogen atom is covalently attached to the oxygen of a water molecule (about 470 kJ/mol) but has an additional attraction (about 23.3 kJ/mol (Isaacs et al., 2000)) to a neighboring oxygen atom of another water molecule (Isaacs et al., 2000).

When a large number of hydrogen bonds act cooperatively they will make a strong contributory effect, on thermodynamic, structural as well as dynamic properties of physical relevance. This many-body effect is reflected in the formation of clusters, of several number of water molecules in different configurations (Chapling, 2003). In figure 1.7 a pentamer cluster can be seen.

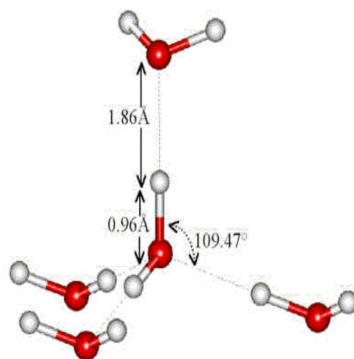


Figure 1.7. Clusters, hydrogen bonded pentamer (Chapling, 2003).

4. Molecular Dynamics

In this section a description of the tools required to carry out Molecular Dynamic simulations are discussed. Details of the algorithms used to integrate the Newton's equations of motion are presented, in addition to the mathematical description of the treatment of short and long-range intermolecular potentials and forces.

Molecular Dynamic Simulations for transport and equilibrium properties of liquids are customary based on the principle that particles' behavior obeys the classical mechanics; it means that neither quantum nor relativistic effects are considered. This approximation leads to an important simplification, namely that the contribution to thermodynamic properties that arise from thermal motion can be separated from those due to interactions between particles (Hansen and McDonald, 1991). The separation of potential and kinetic term suggests a simple means of characterizing the liquid state (or any other one). Thus a precise and coherent dynamical description of a system of particles, and, of course, a mathematical representation of this dynamics for computer implementations is required. The dynamics of a system of particles can be described through Newton's equation of motion.

The dynamics of a system of particles is described by Newton's equations of motion, which are written as set of two first order differential equations for convenience

$$\dot{\mathbf{r}}_i = \frac{\mathbf{p}_i}{m_i} \quad (1.50)$$

$$\dot{\mathbf{p}}_i = \mathbf{F}_i$$

where \mathbf{r}_i is the position, $\mathbf{p}_i \equiv m_i \mathbf{v}_i$ is the momentum and \mathbf{F}_i is the resultant of all the forces acting on *ith* particle.

Hamiltonian mechanics is equivalent. Such a description is based on the Hamiltonian

$$H(\mathbf{r}^N, \mathbf{p}^N) = \sum_i \frac{\mathbf{p}_i^2}{2m_i} + U(\mathbf{r}^N) = E \quad (1.51)$$

where $\mathbf{r}^N = \{\mathbf{r}_1, \mathbf{r}_2 \cdots \mathbf{r}_N\}$ and $\mathbf{p}^N = \{\mathbf{p}_1, \mathbf{p}_2 \cdots \mathbf{p}_N\}$

The Hamiltonian is the total energy if no time-dependent external forces act on the system. With this formulation, the equations of motion take the form

$$\begin{aligned} \dot{\mathbf{r}}_i &= \frac{\partial H}{\partial \mathbf{p}_i} \\ \dot{\mathbf{p}}_i &= \frac{\partial H}{\partial \mathbf{r}_i} \end{aligned} \quad (1.52)$$

understanding that \mathbf{r}^N is an ensemble of independent (generalized) coordinates.

5. Ensembles

In this section we will focus the attention in the different possible ensembles that are relevant for the application of the Molecular Dynamics (MD). As it was mentioned in the previous section, MD is a scheme to study the natural time evolution of a classical system of N particles in volume V (Frenkel and Smith, 1996). Hence, the natural accessible quantity in any MD simulation is the total energy E , which is held constant (see the Hamiltonian formulation expressed in eq. (1.51)). Assuming that the time averages are equivalent to ensemble averages, the (time) averages obtained in conventional MD simulations are equivalent to ensemble averages in the micro-canonical (constant NVE) ensemble.

5.1 Micro-canonical NVE

The NVE ensemble is the natural ensemble of a simple MD simulation since the total energy is preserved by the equations of motion under conservative

forces. Here, the total volume V and the total number of molecules of the system N and the total energy E are held constant. The micro-canonical ensemble is defined if the average of any thermodynamic function U , is given by

$$U(N, V, E) \equiv [N! \Omega(N, V, E)]^{-1} \int_V d\mathbf{r}^N \int d\mathbf{p}^N \times \delta[H(\mathbf{r}^N, \mathbf{p}^N) - E] U(\mathbf{r}^N, \mathbf{p}^N) \quad (1.53)$$

where

$$\Omega(N, V, E) \equiv (N! h^{3N})^{-1} \int_V d\mathbf{r}^N \int d\mathbf{p}^N \delta[H(\mathbf{r}^N, \mathbf{p}^N) - E] \quad (1.54)$$

is the micro-canonical ensemble partition function. Here δ is the Dirac function, H is the Hamiltonian of the system. The total energy of the system can be computed using eq. (1.51), where the $U(\mathbf{r}^N)$ represents the potential energy of the molecules (which will be discussed in detail in section 4.5), and the K term represent the total kinetic energy (i.e for a rigid molecule) (Marrion, 1992),

$$K = \frac{1}{2} \sum_{j=1}^N m_j |\mathbf{v}_j|^2 + \frac{1}{2} \sum_{j=1}^N m_j (\boldsymbol{\omega}_j \times \mathbf{r}_j)^2 \quad (1.55)$$

where m_j is the mass, $\boldsymbol{\omega}_j$ the angular velocity and \mathbf{r}_j the center of mass position of the molecule. The first term of eq.(1.55) is the translational part of the kinetic energy, while the second term is the rotational part of the kinetic energy. These two terms are equal in average due to the equipartition theorem. The temperature of the system can be then computed as,

$$T = \frac{2 \langle K \rangle}{k_B N_d} \quad (1.56)$$

Here $\langle K \rangle$ represent a time average, that is equivalent to an ensemble average of the kinetic energy, and N_d is the total degrees of freedom of the molecules. Consequently, in any NVE simulation while the total energy of the system remains constant, the temperature of the system fluctuates during the simulation. In this respect, no changes should be done in the velocities and positions of the molecules if we are interested to do a simulation in the micro-canonical ensemble.

5.2 Canonical NVT

From a statistical mechanical point of view, a system of particles are in the canonical ensemble if we can impose a temperature to the system by bringing it into thermal contact with a large heat bath. Here any thermodynamic function A of the system ($A(N, V, T)$) is defined as,

$$A(N, V, T) \equiv [N!Q(N, V, T)]^{-1} \int_V d\mathbf{r}^N \int d\mathbf{p}^N \times \exp\left(-\frac{H(\mathbf{r}^N, \mathbf{p}^N)}{k_B T}\right) A(\mathbf{r}^N, \mathbf{p}^N) \quad (1.57)$$

where

$$Q(N, V, T) \equiv (N!h^{3N})^{-1} \int_V d\mathbf{r}^N \int d\mathbf{p}^N \exp\left(-\frac{H(\mathbf{r}^N, \mathbf{p}^N)}{k_B T}\right) \quad (1.58)$$

where Q is the canonical partition function. Under this conditions, the probability to find the system in a given energy state is given by the Boltzmann distribution of the velocities of the molecules (Frenkel and Smith, 1996),

$$\mathcal{P}(p) = \left(\frac{1}{k_B T 2\pi m}\right)^{(3/2)} e^{\left[\frac{-p^2}{k_B T 2m}\right]} \quad (1.59)$$

where p is the momentum of the particles. Then, the temperature of the system can be computed through eq.(1.56). However, the condition of constant temperature is not equivalent to the condition that the kinetic energy per particle is constant. In fact, in a canonical ensemble of a finite system, the instantaneous kinetic energy per particle or the instantaneous kinetic temperature fluctuates.

There are several manners to maintain constant the temperature of the system; some of them preserve a canonical distribution of the velocities of the molecules (Nosé-Hoover thermostat (Nosé, 1984a, Nosé, 1984b)) while others kept constant the kinetic energy of the system (Andersen, 1980) (also called iso-kinetic MD schemes and velocity-scaling schemes (Berendsen et al., 1984)). In the second group one does not simulate a true constant-temperature ensemble, but in practice, the difference between iso-kinetic and canonical schemes is often negligible (Frenkel and Smith, 1996).

Then, the easiest way to maintain constant the temperature of the system is using the temperature rescaling procedure,

$$f_{rescale} = \sqrt{\frac{T_{req}}{T}} \quad (1.60)$$

here T_{req} is the desired temperature and T is the actual temperature. Once the factor $f_{rescale}$ is obtained, the velocities of the molecules in the system can be rescaled,

$$\mathbf{v}_j^{new} = \mathbf{v}_j^{old} f_{rescale} \quad (1.61)$$

If this procedure is applied with a certain coupling constant τ_T , big enough, to the thermal bath then the trajectories of the molecules are also weakly disturbed. This is the principle of the weak coupling bath (Berendsen et al., 1984)

5.3 NPT

In the isobaric-isothermal ensemble the pressure P , the temperature T and the total number of particles N in the system are held constants, while the total volume V of the system fluctuates around an equilibrium value. Here any thermodynamic function F of the system ($F(N, P, T)$) is defined as,

$$F(N, P, T) \equiv [N! \Delta(N, P, T)]^{-1} \int_0^\infty dV \int_V d\mathbf{r}^N \int d\mathbf{p}^N \\ \times \exp\left(-\frac{PV + H(\mathbf{r}^N, \mathbf{p}^N)}{k_B T}\right) F(\mathbf{r}^N, \mathbf{p}^N; V) \quad (1.62)$$

where

$$\Delta(N, P, T) \equiv (N! h^{3N})^{-1} \int_0^\infty dV \int_V d\mathbf{r}^N \int d\mathbf{p}^N \\ \times \exp\left(-\frac{[PV + H(\mathbf{r}^N, \mathbf{p}^N)]}{k_B T}\right) \quad (1.63)$$

here P is the pressure of the system. There are several methods to maintain constant both, the temperature and the pressure of the system. Some of them

combined a canonical distribution of the velocities of the molecules (Nosé-Hoover thermostat (Nosé, 1984a, Nosé, 1984b)) with a barostat coupled to a hypothetical piston that fluctuates to maintain the average pressure of the system constant (Andersen, 1980), these methods are time reversible and preserve the phase space volume. The so called *pseudo NPT* methods, on the contrary, are neither canonical nor reversible, but they are much easier to be implement in molecular dynamics codes. Additionally, ensemble averages computed with them are equal to those computed with the canonical methods (Berendsen et al., 1984). To implement this type of barostat, the pressure of the system is defined according to,

$$VP(t) = \frac{1}{3} \sum_{\alpha=x,y,z} P_{\alpha\alpha}(t) \quad (1.64)$$

where $P_{\alpha\alpha}$ are the diagonal elements of the pressure tensor defined in the eq.(1.38). Then, the pressure of the system is kept constant changing the total volume of the system using the isothermal compressibility β ,

$$\frac{dP}{dt} = -\frac{1}{\beta V} \frac{dV}{dt} \quad (1.65)$$

and dP/dt can be approximate to,

$$\left(\frac{dP}{dt}\right)_{bath} = \frac{P_0 - P(t)}{\tau_P} \quad (1.66)$$

Here τ_P is the coupling constant of the pressure, and P_0 is the desired pressure. Then, using eq.(1.65) and eq.(1.66) the volume of the system can be rescaled according to a factor,

$$\mu = 1 - \frac{\beta\Delta t}{3\tau_P}(P_0 - P(t)) \quad (1.67)$$

and, hence, the volume is rescaled according to,

$$V_{new} = \mu V_{old} \quad (1.68)$$

Finally, the thermalization of the system is adjusted using the velocity rescaling procedure described in eq.(1.60) and eq.(1.61). The position of the center of mass of the molecules are rescaled according to,

$$\mathbf{r}_{com}^{new} = \mathbf{r}_{com}^{old} (\mu)^{1/3} \quad (1.69)$$

with vectors taken from the center of the simulation box. The choice of appropriate values of the coupling constants τ_T and τ_P are very important. In general $\tau_P > \tau_T > 0.01$ ps are required to preserve the philosophy of the weak coupling to the thermal and barostat bath (Berendsen et al., 1984).

6. Algorithm

In essence any MD program has the same structure and some of the steps are commonly known. The typical steps can be the following (Frenkel and Smith, 1996):

- 1 Introduce the parameters that specifies the conditions of the system (initial temperature, number of particles, density, time step).
- 2 Initialize the system (select the initial positions and velocities)
- 3 Compute the forces on all the particles:
 - This is one of the cornerstones of any MD simulation. According to the intermolecular interaction between particles chosen, the results can agree or not with the experimental data.
- 4 Integrate Newton's equation of motion according to the calculated forces. This step and the previous one are the Core of the simulation. They are repeated until one has computed the time evolution of the system for the desired interval of time.
- 5 After completion of the central loop, we compute and print the averages of the measured quantities, and stop.

To achieve step 4 in this procedure we need to integrate the Newton's equation of motion. It is highly desirable to have an appropriate integrator that preserves the Hamiltonian properties of the system. The so-called Verlet (Frenkel and Smith, 1996) algorithm was used in this work to integrate translational part of the equation of motion in the NVE ensemble, while the *Leap-Frog* algorithm was employed for the same purposes in the case of the NVT and NPT ensembles.

One of the most important aspects of the first algorithm is that the volume of an ensemble of phase space point is preserved. Thus, it is a suitable algorithm to perform constant energy simulations. The second one is not time reversible, but it has the advantage that the NVT and NPT ensembles are simple to be implemented. Furthermore, in NVT and NPT simulations there is no real need to preserve the phase-space volume, due to the coupling with the bath.

To derive an reversible algorithm of the type of Verlet is convenient to start with a Taylor expansion of the position of each particle for small time step Δt from a given time t ,

$$\mathbf{r}(t + \Delta t) \approx 2\mathbf{r}(t) - \mathbf{r}(t - \Delta t) + \frac{\mathbf{F}(\mathbf{r}(t))|_{t=t}}{m} \Delta t^2 \quad (1.70)$$

where \mathbf{F} is the interparticle force. From eq. (1.70), it is then possible to compute the velocity of each particle through equation

$$v(t) = \frac{\mathbf{r}(t + \Delta t) - \mathbf{r}(t - \Delta t)}{2\Delta t} + O(\Delta t^2) \quad (1.71)$$

with the same degree of accuracy of eq. (1.70), $(\Delta t)^2$.

The rotational part of the equation of motion can be solved through time derivatives of the Euler angles, however this methodology presents some important drawbacks (Allen and Tildesley, 1989). Consequently, a stable implicit version (Svanberg, 1997) of the Quaternion (Evans, 1997) formalism was employed in this work in order to handle the rotational degrees of freedom of the molecules (a short description and its relation with the solid rotation is given in Appendix B). In addition, Quaternions are suitable for rigid geometries and are simpler and less computationally expensive than the RATTLE algorithm (Andersen, 1983).

The *Leap-Frog* algorithm employed for NVT and NPT ensemble is described as follows,

$$\mathbf{v}(t + \Delta t) = \mathbf{v}(t - \Delta t) + \frac{\mathbf{F}(\mathbf{r}(t))}{m} \quad (1.72)$$

$$\mathbf{v}'(t + \Delta t) = \mathbf{v}(t + \Delta t) f_{rescale} \quad (1.73)$$

Here $f_{rescale}$ is computed with eq.(1.60). Although $f_{rescale}$ is based on temperature at $t - \Delta t$, its value can be used to scale the velocity at $t + \frac{1}{2}\Delta t$

because of the slow variation of $f_{rescale}$. The positions of the center of mass of the molecules can be computed with,

$$\mathbf{r}(t + \Delta t) = \mathbf{r}(t) + \mathbf{v}'(t + \Delta t)\Delta t \quad (1.74)$$

$$\mathbf{r}'(t + \Delta t) = \mathbf{r}(t + \Delta t)(\mu)^{1/3} \quad (1.75)$$

$$V(t + \Delta t) = V(t)\mu \quad (1.76)$$

The rescaling factor μ of the positions and volume is computed through eq.(1.67). If the coupling constants τ_T and τ_P are larger than the total simulation time, the simulation is reduced to a NVE ensemble.

6.1 Short and long range intermolecular potentials and forces

One of the cornerstones of the molecular simulation is the representation of the interaction between molecules and atoms. This representation is carried out through the intermolecular potential and most of the models employed in the literature are based in the *United Atom* concept. This means that some group of atoms in a molecule are treated together as an entity. For example, the methane molecule CH_4 is represented as one interaction site instead of treating separately hydrogen and carbon atoms. One of the most common functional forms is to describe the interactions of electrons in internal orbitals by means of Lennard-Jones sites

$$U_{LJ}(r) = 4\varepsilon \left[\left(\frac{\sigma}{r} \right)^{12} - \left(\frac{\sigma}{r} \right)^6 \right] \quad (1.77)$$

where, r is the distance between two particles, σ is the collision diameter, which is the separation of the particles such that $U_{LJ}(r)=0$, and ε , the depth of the potential well at the minimum of $U_{LJ}(r)$. The Lennard-Jones potential is usually truncated at a distance r_c , or cut-off, because beyond this distance the intermolecular potential is assumed to be very small.

This type of potential is enough for non-polar atoms and molecules. On the other hand, molecules that present partial charges or dipoles should be treated in a different manner due to the long-range character of the electrostatic

interactions. Hence, an electrostatic or coulombic pair wise additive term should be added to account for these interactions,

$$U_{coul}(r^{ab}) = \frac{1}{4\pi\epsilon_0} \sum \frac{q_a q_b}{r_{ab}} \quad (1.78)$$

where ϵ_0 is the permittivity of the vacuum, q_a and q_b are point charges being r_{ab} is the distance between these sites in different molecules.

The Lennard-Jones interaction eq. (1.77) accounts for the size of the molecules. Effectively, it is repulsive at short distances but, at intermediate distance, it is significantly attractive but non-directional, and competes with the directional electrostatic interactions, eq.(1.78). In the simulations carried out in this work some molecules have electrostatic interactions and, due to the periodic boundary conditions employed (to mimic an infinite system), it is necessary to treat the long-range forces in a special way, due to the interactions between particles in different images of the box. There are two main techniques to treat long-range electrostatics interactions, the *Lattice sum* technique or Ewald summation and the *Reaction Field* technique. We have chosen the *Reaction Field* (RF) (Neuman, 1986a) technique in order to manage these long-range interactions in a system with periodic boundary conditions. The main idea of this methodology is that interactions between close neighbors are calculated with a spherical cut-off convention, while the region outside the truncation sphere is treated interacting with a dielectric continuum (Hansen and McDonald, 1991). This technique keeps the computational effort in the computation of the long-range coulombic interactions to a minimum (Neuman, 1986b), as compared with the Ewald-type sum (Allen and Tildesley, 1989). Thus, applying this methodology, the coulombic interaction eq. (1.78) is modified as follows

$$U_{RF}(r^{ab}) = \frac{1}{4\pi\epsilon_0} \sum \frac{q_a q_b}{r_{ab}} \left[1 + \frac{\epsilon_{RF} - 1}{2\epsilon_{RF} + 1} \frac{r_{ab}^3}{r_c^3} \right] \quad (1.79)$$

here r_c is the cut-off radius out of which the electrostatic interaction is truncated, and ϵ_{RF} is the reaction field dielectric permittivity of the continuum, the rest of the parameters being the same as that in eq. (1.78).

Hence, the force necessary to carry out a MD simulation can be obtained from the intermolecular potential expression given in eq. (1.77) and eq. (1.79), for the case of RF, the final expression is

$$\mathbf{F}_{RF}(r^{ab}) = \frac{1}{4\pi\epsilon_0} \sum \frac{q_a q_b}{r_{ab}} \left[\frac{1}{r_{ab}^2} - \frac{\epsilon_{RF} - 1}{2\epsilon_{RF} + 1} \frac{2r_{ab}}{r_c^3} \right] \mathbf{r}_{ij} \quad (r_{ab} < r_c) \quad (1.80)$$

Additionally, long-range corrections should be applied to the Lennard-Jones part of the potential energy and the total pressure of the system, to correct the effect of the simulation cut-off truncation (van der Spoel et al., 1998) at a distance r_c . Additionally, when simulations are performed in the NPT ensemble, long range corrections for the pressure and energy are important, so, these new terms should be added to eq.(1.64) and eq.(1.51), respectively. The corrections for the energy and pressure for polyatomic molecules in a mixture are defined as (Petrvic, 2000),

$$U_{LJ}^{lr} = -\frac{8\pi}{V} \sum_{i=1}^{N_{type}} N_i \sum_{j=1}^{N_{type}} N_j \frac{\epsilon_{ij} \sigma_{ij}^6}{3r_c^3} \left(1 - \frac{\sigma_{ij}^6}{3r_c^6} \right) \quad (1.81)$$

$$VP^{lr} = -\frac{16\pi}{V} \sum_{i=1}^{N_{type}} N_i \sum_{j=1}^{N_{type}} N_j \frac{\epsilon_{ij} \sigma_{ij}^6}{3r_c^3} \left(1 - \frac{2\sigma_{ij}^6}{3r_c^6} \right) \quad (1.82)$$

where indexes i and j round all interaction sites N_{types} in the system, σ_{ij} and ϵ_{ij} are the same parameters as in eq.(1.77), r_c is the cut-off employed in eq.(1.77) and eq.(1.79).

If we are dealing with mixtures, the cross interactions between atoms of different types requires a mixing rule. Two of the most common rules employed in simulations are the Lorentz-Berthelot and the Jorgensen (Jorgensen et al., 1984) mixing rule. The Lorentz-Berthelot is defined as,

$$\epsilon_{ij} = \sqrt{\epsilon_i \epsilon_j} \quad (1.83)$$

$$\sigma_{ij} = \frac{1}{2}(\sigma_i + \sigma_j) \quad (1.84)$$

where i, j are interaction sites. If site $i = j$, the collision diameter and the potential depth remains unaffected. The mixing rule of Jorgensen (Jorgensen et al., 1984) is,

$$\epsilon_{ij} = \sqrt{\epsilon_i \epsilon_j} \quad (1.85)$$

$$\sigma_{ij} = \sqrt{\sigma_i \sigma_j} \quad (1.86)$$

here all crossed interactions are geometrical averages. The use of one or other mixing rules depends on the intermolecular potentials. The set of Optimized Potentials for Liquid Systems (*OPLS*) developed by Jorgensen *et al* (Jorgensen *et al.*, 1984) requires the use of the Jorgensen rules, for instance.

The use of the *Reaction Field* methodology, to treat electrostatic interactions, presents the inconvenience of a small drift in the total energy of the system due to the truncation of the torque of the molecules in the computation of the force (Neuman, 1986b, Mahoney and Jorgensen, 2000). Then a velocity rescaling every certain number of steps is required to overcome this problem, even though, the overall dynamics of the system is not affected by the rescaling.

Several authors have found a good agreement between different equilibrium and transport properties as calculated using either RF or Ewald summation. Also, the effect of varying the cut-off distance and the reaction field permittivity of the continuum has been studied (van der Spoel *et al.*, 1998, Nyman and Linse, 2000), founding that most properties of interest are independent of the choice of the value of ϵ_{RF} . In fact, any value between 10 and ∞ shows an appropriate accuracy in the calculations. Even though, in another analysis (Hunenberger and van Gunsteren, 1998) it has been found some discrepancies between different calculated properties, when different types of RF are applied to simulate polar molecules (like water) in comparison with the Ewald summation. The disagreement has been found in the dielectric constant. In the case of the transport and structural properties studied in this work, the values found are equivalent within the statistical error with other works employing Ewald summation technique (Tironi *et al.*, 1997).

6.2 Intermolecular potential models

The development of accurate models for the interaction potentials is the key to have a reliable description of the thermodynamic and transport behavior of any system through molecular dynamics simulations. In this work, we are mostly interested in aqueous solutions, which requires a detail analysis of the possible options of water models present in the literature.

6.2.1 Water models

In general each water model is developed to give an accurate description with a given set of physical properties, ranging from structural properties (site-site radial distribution functions, etc.) to thermodynamic aspects such as the

experimental internal energy or critical parameters, etc. Obviously, the more fitting parameters are introduced in the model (and some require over 50), the better the fit is (Chapling, 2003). In order to give an idea of the diversity of models, some of the more successful are given in Table 1.1 and its geometry, in Figure 1.8.

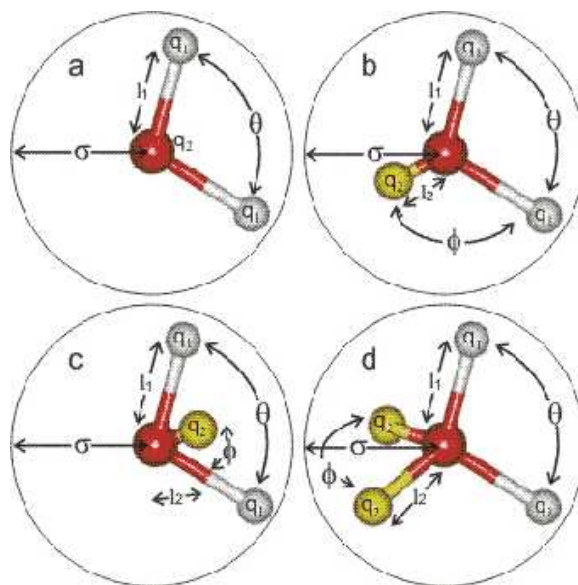


Figure 1.8. Different type of model for water: the types a, b and c are all planar whereas type d is almost tetrahedral. The values of the symbols in each model correspond to those in Table 1.1 (Chapling, 2003)

The DEC model (diffuse electron charge) recently presented by Guillot et al. (Guillot and Guissani, 2001) introduces several changes with respect to other rigid non-polarizable models. Basically, the point charges are replaced in this model by point charges embedded in a cloud of diffuse charge density. Such a structure allow for a better description of electrostatic interaction at short distances, that are ignored by the single point charge approach of models such as SPC/E, TIP4P or even the recent TIP5P, some of them also analyzed in this work. Thus, the electrostatic interactions between the different contributions in the DEC are given by eq. (1.87) to eq. (1.92). In addition, the typical Lennard-Jones interactions are here replaced by the terms given in eq. (1.91) and eq. (1.92).

Table 1.1. Molecular parameter of the most common water models (Chapling, 2003).

Model	Type	σ Å	ϵ (kJ/mol)	l_1 Å	l_2 Å	q_1	q_2	θ°	ϕ°
SPC	a	3.166	0.650	1.0000	-	+0.410	-0.8200	109.47	-
SPC/E	a	3.166	0.650	1.0000	-	+0.4238	-0.8476	109.47	-
TIP3P	a	3.15061	0.6364	0.9572	-	+0.4170	-0.8340	104.52	-
DEC	a	3.166	0.6565 ¹	1.0000	-	²	²	109.47	-
PPC ^{3,4}	b	3.23400	0.6000	0.9430	0.06	+0.5170	-1.0340	106.00	127.00
TIP4P	c	3.15365	0.6480	0.9572	0.15	+0.5200	-1.0400	104.52	52.26
TIP4P/RF	c	3.15365	⁵	0.9572	0.15	+0.5213	-1.0426	104.52	52.26
TIP4P-FQ	c	3.15365	0.6480	0.9572	0.15	+0.63 ³	-1.26 ³	104.52	52.26
SWFLEX AI ⁴	c	Four terms used		0.968 ³	0.14 ^{3,6}	+0.6213	+1.2459	102.7 ³	51.35 ³
TIP5P	d	3.12000	0.6694	0.9572	0.70	+0.2410	-0.2410	104.52	109.47

$$u_{qq} = \frac{1}{2} \sum_{i,j} \frac{q_i q_j}{r_{ij}} \quad (1.87)$$

$$u_{q^d q^d} = \frac{1}{2} \sum_{i,j} \frac{q_i^d q_j^d}{r_{ij}} \cdot \text{erf} \left(\frac{r_{ij}}{2\xi} \right) \quad (1.88)$$

$$u_{qq^d} = \sum_{i,j} \frac{q_i q_j^d}{r_{ij}} \cdot \text{erf} \left(\frac{r_{ij}}{\sqrt{2}\xi} \right) \quad (1.89)$$

$$u_{q^d q} = \sum_{i,j} \frac{q_i^d q_j}{r_{ij}} \cdot \text{erf} \left(\frac{r_{ij}}{\sqrt{2}\xi} \right) \quad (1.90)$$

$$u_{rep} = A_{rep} \frac{\text{erfc}(z)}{z} \left(z = \frac{r_{oo}}{2\xi_r} \right) \quad (1.91)$$

$$u_{disp} = -\frac{C_6}{r_{oo}^6} \quad (1.92)$$

where r_{ij} is the distance between the O and the H atoms in different molecules, 1 and 2, erf and erfc are, respectively, the error and error-complementary functions (see Appendix C), r_{oo} is the distance between oxygen atoms. This implies

that eq. (1.91) and eq. (1.92) only describe interactions between O-O sites of the molecules. The rest of the parameters of this model not shown in Table 1.1 are listed in Table 1.2.

Table 1.2. Potential parameters of DEC (Guillot and Guissani, 2001).

$q_O(e)$	-0.888
$q_O^d(e)$	0.226
$q_H(e)$	-0.444
$q_H^d(e)$	-0.113
$\xi(\text{\AA})$	1.5
$\xi_r(\text{\AA})$	0.615
$A_{rep}(\text{kJ/mol})$	22484.40
$C_6(\text{kJ/mol})$	2545.44

The *Reaction Field* expressions for the intermolecular potentials and forces for this model (eq. (1.87) to eq. (1.90)) are described in detail in the Appendix D (eq. (D.7) through eq. (D.12)).

Polarizable versions of some non-polarizable models, using, for instance, flexible bonding (e.g. SWFLEX-AI), induced dipoles, energy optimization (e.g. the TIP4P-FQ version of TIP4P) or movable charge (e.g. SWFLEX-AI), all of which generally give better fit to specific experimental data. However, an increase in the sophistication is accompanied by a parallel increase in the computational effort required in the simulations. Such polarizable models generally perform better than the simpler models away from the ambient conditions, under which they have been adjusted (Chapling, 2003). A résumé table describing the physical properties of some of the models mentioned here can be seen in Appendix G.

In chapter 2 four models have been chosen (TIP4P, TIP5P, SPC/E and DEC) to analyze the structural and dynamical behavior of water. Two of them, the well-known TIP4P (van der Spoel et al., 1998), and the SPC/E (Berendsen et al., 1987), have been extensively analyzed so that their thermodynamics and transport properties are described in the literature. The other couples of models were recently presented, and are the TIP5P (Mahoney and Jorgensen, 2000) and DEC (Guillot and Guissani, 2001) (from *Diffuse Electron Charge*). The TIP5P model was developed to reproduce the mentioned Temperature of Maximum Density (*TMD*) line, improving its predecessor, the ST2 model (Stillinger and Rahman, 1974). TIP5P model reproduces well the local structure of water at ambient conditions when compared with NDS (Soper, 2000) and X-Ray (Hura et al., 2000) experimental data. Moreover, this model was also employed in the

computation of the time of crystallization of pure water (Yamada et al., 2002). The DEC model introduces several changes with respect to other rigid non-polarizable models. Basically, the point charges are replaced by point charges embedded in a cloud of diffuse charge densities. Such a structure allows the model to give a better descriptions of electrostatic interactions at short distances, aiming at mimicking the internal proton chemical shift (Matubayasi et al., 1997) occurring when two molecules are hydrogen bonded (Chau and Hardwick, 1998). The comparison of these four models, together with the tools presented to analyze the local structure of water, will help us to shed some light on the predictive capabilities of each model in the range of thermodynamic conditions studied. For the case of mixtures, the SPC/E and TIP4P models have been chosen, because previous works demonstrate that these models are adequate to reproduce transport as well as thermodynamic properties in mixtures (Borin and Skaf, 1999, Skaf, 1999).

6.3 Hydrogen bond definition in MD Simulations

Even though a qualitative picture of the hydrogen bonding interaction is possible, there is no unequivocal way to formally define, in a precise context, such an interaction. Therefore, what we call a hydrogen-bonded pair (O-H) is subject to the criteria chosen for discriminate between bonded and non-bonded pairs. We have chosen a geometrical criterion because it is the most commonly used in molecular simulation and has a simple implementation. In this case, three conditions should be satisfied in order to consider two molecules as being hydrogen bonded (see Figure 1.9 for more clarity):

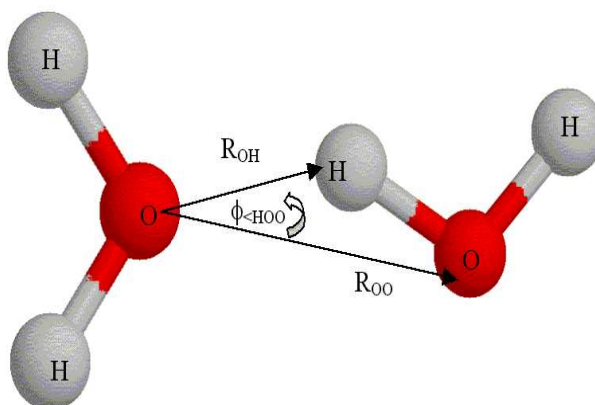


Figure 1.9. Geometry of the spatial oriented definition of hydrogen-bonded molecules.

- 1 The distance R_{OO} between the oxygen atoms of both molecules is smaller than a given R_{OO}^c ;
- 2 The distance R_{OH} between the oxygen of the *acceptor* molecule and the hydrogen of the *donor* is less than a given R_{OH}^c ;
- 3 The bond angle $\phi_{<HOO}$ between the O-O direction and the molecular O-H direction of the *donor*, where H is the hydrogen that forms the bond and O is the oxygen atom, has to be less than a given ϕ^c .
 - The cut-off value of R_{OO}^c is exactly the same as in the energetic definition. The cut-off R_{OH}^c is usually taken as the first minimum of the radial distribution function $g_{OH}(r)$, and is generally taken as 2.4 Å for all thermodynamic conditions. Finally, the angular constrain should be determined from a bond-angle distribution, and some authors present 30° as an acceptable value (Martí et al., 1996). A sketch of this definition is given in Figure 1.9.

7. MD Code: Mdmix

Now we have the whole information required to understand the general structure of a Molecular Dynamic program. In general once the simulation is carried out using the proposed algorithm (Verlet, Leap-Frog, quaternions), and potential parameters for the different models, any calculations can be done in order to extract useful information about the system. In Figure 1.10 is showed the methodology to carry out these computations.

The *Mdmix* program was developed in FOTRAN 77 to carry out Molecular Dynamics simulations in different ensembles for multicomponent systems. The most important characteristics of the code are:

- Molecular dynamics simulation in different ensembles:
 - Micro-canonical ensemble *NVE*
 - Constant temperature *NVT*, through weak coupling bath (Berendsen et al., 1984)
 - Constant temperature and pressure *NPT*, through weak coupling a thermal bath and barostat
- Equilibrium and non-equilibrium schemes (modified *PeX* momentum exchange algorithm to simulate heat flux (Appendix E).
- Capability to handle binary mixtures of rigid non-polarizable molecules

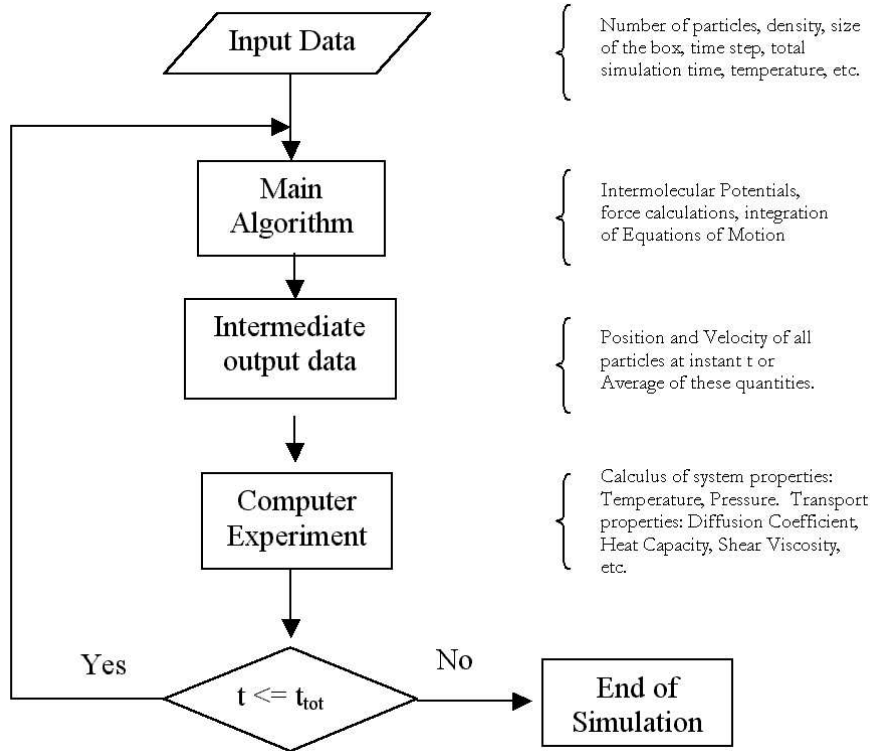


Figure 1.10. General methodology to extract information from MD simulation.

- Long-range electrostatic interactions treated through *Reaction Field* methodology
- Determination of structural and thermodynamical properties:
 - Average thermodynamic properties of the system (Temperature, pressure, translational and rotational kinetic energy, potential energy)
 - Angular average site-site radial distribution function ($g_{ab}(r)$) and pair distribution functions projected with spherical harmonics
 - Translational and orientational order parameters of water and aqueous solutions
 - Average number of hydrogen bonds
- Dynamical and transport properties:
 - Self-diffusion coefficient (D)
 - Maxwell Stefan mutual diffusion coefficient (\bar{D}_{12})

- Shear viscosity coefficient (η)
- Thermal conductivity coefficient (λ)
- Soret coefficient (S_T) and thermal diffusion factor (α_T)
- Hydrogen bond lifetime autocorrelation function ($C_{HB}(t)$)
- Dielectric constant (μ) and dipole moment relaxation time (τ_D)
- Reorientational autocorrelation function of the dipole moment of water ($C_\mu(t)$)

Notes

1. Modified from its original value of 0.65 kJ/mol for the use of reaction field methodology
2. diffuse electron density
3. Average values
4. Polarizable models
5. optimized for the use of reaction field with two parameters $C_6=2.5543 \times 10^{-3}$ kJ.nm⁶/mol and $C_{12}=2.45 \times 10^{-6}$ kJ.nm¹²/mol in the Lenard-Jones interaction
6. charge = -2.48856

Chapter 2

STRUCTURAL AND DYNAMICAL PROPERTIES OF PURE WATER

1. Introduction

Water is one of the most common fluids in nature, and plays an important role in biological systems as well as in many industrial applications. Even though the molecule could be considered as simple, the collective behavior of water is far from being simple and has many non-ideal properties. Water expands on cooling, for instance, at ambient pressure and below 4°C, exhibiting a line of Temperature of Maximum Density TMD in the liquid phase. Many experimental and theoretical studies describe a very complex scenario of water at super cooled states (Heide, 1984, Mishima and Stanley, 1984). The peculiar macroscopic behavior of water is also encountered in supercritical region, where water can solvate non-polar substances and precipitate common ions, contrary to what is observed under ambient conditions. This change in the solubility properties is explained as caused by a relaxation of the three dimensional structure of a hydrogen bond network (Yao and Okada, 1998). Such high pressure and high temperature conditions are of particular interest due to their relevance in many industrial processes, including supercritical water oxidation, supercritical extraction, etc.

In this chapter, we focus our attention on an analysis of dynamic and structural properties predicted by different *rigid, non-polarizable* models for pure water systems, with special emphasis on the comparison between models recently appeared in the literature with others commonly used. Such class of models is of particular interest due to its simplicity, which permits the study of properties that require an intensive use of computer time, as in collective dynamic properties, non-affordable with models of major complexity. Additionally, we pay

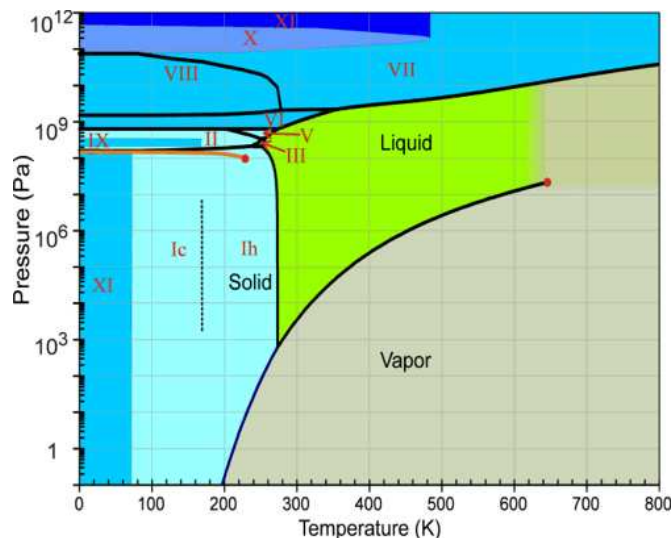


Figure 2.1. Phase diagram of pure water showing the different types of Ice structures(Chapling, 2003)

attention on the analysis of the transition of the structural order of water from medium densities (0.8 g/cm^3) up to very high densities (1.3 g/cm^3).

In the first part of this chapter, two main regions of the phase diagram have been studied, *i.e.* the dense isochore of 0.995 g/cm^3 in a wide range of temperatures (starting from 275 K up to 1250 K), and the super-critical isotherm at 673 K (densities varying from 0.1 to 0.995 g/cm^3). Under these conditions the influence of T and density on the variation of the local structure of the system, and its influence on the dynamical behavior of water molecules has been analyzed through the comparison of the four models, TIP4P, TIP5P, SPC/E and DEC (already discussed in chapter 1). In particular, the temperature dependence of the self-diffusion coefficient is related to a change in the activation energy due to a variation in the local environment of the first solvation shell of water molecules. Additionally, a first analysis of different structural properties of the system has been also undertaken as, for instance, the orientational order parameter q (Errington and Debenedetti, 2001, Chau and Hardwick, 1998), which measures the tendency of the system to adopt tetrahedral arrangements around a given molecule, as well as a set of components of the site-site radial distributions functions, projected on a base of spherical harmonics.

In Figure 2.1 a schematic representation of the phase diagram of water in the super cooled region can be seen. In this phase diagram, several zones (I to XI) have been identified as to have different Ice structures, for instance, the

glassy water, low-density amorphous ice (LDA) and high-density amorphous ice (HDA) (this phenomenon is called poly-amorphism). Additionally, a hypothetical second critical point has been suggested to exist in this region (the point at the end of the line between liquid and vapor in Figure 2.1, $T_c' \approx 220$ K, $P_c' \approx 100$ MPa and $\rho \approx 1$ g/cm³). This second critical point has been reported only in simulations (Poole et al., 1992) because, in this region, the *liquid* phase is not accessible experimentally due to the fact that super cooled water freezes spontaneously below the homogeneous nucleation temperature T_H (temperatures below 235 K) (see references (Mishima and Stanley, 1998, Bluhm et al., 2002, Scala et al., 2000b) for more information about the different Ice structures and phase transitions). This complex behavior has been explained through three different hypothesis, the first one related to the stability limit hypothesis (Speedy, 1982), the percolation hypothesis, which treats water as a locally structured transient gel comprised of monomers held together by hydrogen bonds (Stanley and Teixeira, 1980), and the liquid-liquid phase transition hypothesis recently arisen from molecular dynamics studies (Poole et al., 1992, Franzese et al., 2001d, Franzese et al., 2001a, Franzese et al., 2001b, Franzese et al., 2001c, Stanley et al., 2002a), where a coexistence between low-density liquid (LDL) phase at low pressure and a high-density liquid (HDL) takes place.

On the other hand, at higher temperatures (above ambient temperatures) the three-dimensional network of water molecules hydrogen bonded starts to be broken under the influence of temperature (Jedlovsky et al., 1998). Hence, a particular point, where the percolating network, or more precisely, the infinite cluster of molecules hydrogen bonded is destroyed, exists at different densities. Moreover, the set of different anomalous behaviors of water are consequence of the presence of this percolating network, thus, no anomalous properties can be found in clusters of finite size. Such a crossover in the behavior could be described through an appropriate order parameter, however, there is no a straightforward choice for this order parameter. In any case, one can be expected that this parameter should has some characteristics, for instance, must be 1 at low temperatures when all molecules are hydrogen bonded and collapses to 0 when a percolating network in finite cluster cannot exist. Such a behavior has analogies with the second order phase transition between normal and super fluid helium. If an unequivocal definition of the hydrogen bond network can be established, a line similar to the d-line of the transition described could then be done. Strictly speaking, this order parameter can only be achieved through a detailed cluster analysis. Even though, the translational as well as the orientational order parameter t and q discussed in chapter 1 can give some information about this local structure. Consequently, the second part of this chapter is devoted to the analysis of these two order parameters from sub-critical up to supercritical conditions. Particularly, we have studied a similar

Table 2.1. Simulated thermodynamic states for the comparison analysis

State	ρ (g/cm^3)	T (K)
1	0.995	275
2	0.995	298
3	0.995	447
4	0.995	673
5	0.995	950
6	0.995	1250
7	0.1	673
8	0.2	673
9	0.3	673
10	0.5	673
11	0.66	673

temperature range considered in the first part (T ranging from 275 K up to 1250 K), but a wider range of densities has been explored, starting from $0.8 g/cm^3$ up to a very dense region at $1.3 g/cm^3$. The idea behind this exhaustive analysis is to explore the possibility of a transition of the form order \rightarrow disorder when temperature and density are increased from sub to supercritical conditions.

2. Fundamentals: Oxygen-oxygen coordination number

Although the concept of hydrogen bond was discussed on chapter 1 we want to add the concept of the oxygen-oxygen coordination number C_{OO}^{min} , that counts the number of oxygen atoms presents in the first solvation shell, and is given by (Jedlovsky et al., 1998)

$$C_{OO}^{min} = 4\pi\rho \int_0^{r_{OO}^{min}} g_{OO}(r) r^2 dr \quad (2.1)$$

where r_{OO}^{min} corresponds to the first minimum of the oxygen-oxygen radial distribution function defined in eq. (1.6). This tool can be important to discriminate transitions on the structure of nearest neighbors in fluid water. The different tools employed in this chapter were defined in Chapter 1.

3. Water Models and Computational details

As it was mentioned in chapter 1, four different water models have been selected for the study, TIP4P (van der Spoel et al., 1998), TIP5P (Mahoney

Table 2.2. Simulated thermodynamic states for the order analysis, for each state different densities has been considered

State	T (K)	ρ (g/cm^3)					
12	275	0.8	0.9	0.995	1.1	1.2	1.3
13	298	0.8	0.9	0.995	1.1	1.2	1.3
14	324	0.8	0.9	0.995	1.1	1.2	1.3
15	385	0.8	0.9	0.995	1.1	1.2	1.3
16	447	0.8	0.9	0.995	1.1	1.2	1.3
17	560	0.8	0.9	0.995	1.1	1.2	1.3
18	673	0.8	0.9	0.995	1.1	1.2	1.3
19	950	0.8	0.9	0.995	1.1	1.2	1.3
20	1250	0.8	0.9	0.995	1.1	1.2	1.3

and Jorgensen, 2000), SPC/E (Berendsen et al., 1987) and DEC (Guillot and Guissani, 2001). As far as the DEC model is concerned, we have included the appropriate modification of the expressions for the potential to properly account for the reaction field methodology (see Appendix D). The SPC/E model has been employed for the second analysis due to its simplicity (this model has only 3 point charges which is appropriate for the long simulations required in the case of dense systems), additionally, this model has also been employed on analysis of the order parameters of water at sub cooled conditions (Errington and Debenedetti, 2001). We have performed several classical Molecular Dynamics simulations of the water models with 256 molecules at different thermodynamic conditions in the canonical ensemble (NVT) employing the weak coupling method with $\tau_T = 1$ ps. In the first part of the analysis we investigate two main regions of the phase diagram, which are summarized in Table 2.1. The simulated conditions of the second part of the chapter are described in Table 2.2.

All simulations were performed with periodic boundary conditions, and Reaction Field methodology (Neuman, 1986b), to account for the long-range interactions, with $\epsilon_{RF} = \infty$. The reaction field cut-off length was 8.5 Å, and a Verlet nearest neighbor list technique (Allen and Tildesley, 1989) with cut-off radius of 9.1 Å was also used. The time step was 0.8 fs in all cases, the run periods being of 800 ps after an equilibration time of 16 ps for the first set of simulations, and 2 ns for the run lengths on the second part. Velocities and positions were stored every 10 time steps. Average values for the diffusion constant were computed using 4 independent runs using the center of mass mean square displacement (Frenkel and Smith, 1996). All radial distribution functions were computed during the simulations and after the equilibration period. All sets of radial distribution functions were calculated storing histograms every 10 time

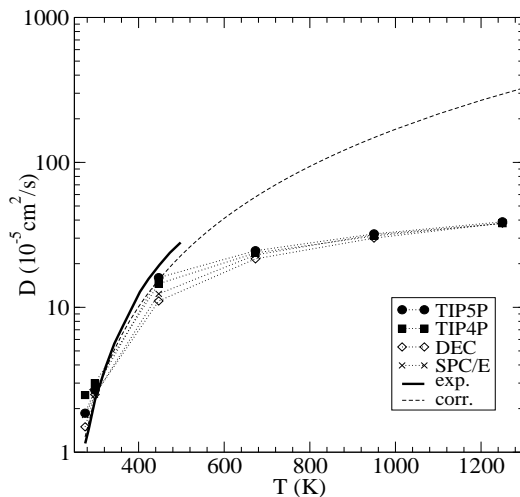


Figure 2.2. Comparison of the temperature evolution of the self-diffusion coefficient of the four models studied with experiments (Krynicky et al., 1980) and theoretical correlation (Svishchev and Zassetsky, 2000) from state 1 to 11 ($\rho = 0.995 \text{ g/cm}^3$). The correlation has been obtained up to 510 K, and it is extrapolated up to 1300 K.

steps with a resolution of $7.4 \times 10^{-3} \text{ \AA}$, corresponding to divisions of 1000 spherical shells.

4. First Part: Comparison of the behavior of the four models of water

In this section, the dynamic behavior of the models studied are first presented and compared with the available experimental data. Then, different structural information concerning the projected and normal radial distribution functions, together with the different order parameters introduced, are compared. The relationship between this structural information and the self-diffusion coefficient is also discussed.

4.1 Self-diffusion coefficient

We present in Figure 2.2 the temperature dependence of the self-diffusion coefficient at constant density ($\rho = 0.995 \text{ g/cm}^3$) for the four models studied. Simulated data are compared with the experimental data of Krynicky (Krynicky et al., 1980) and the correlation obtained by Svishchev et al. (from simulation data with the polarizable model PPC) (Svishchev and Zassetsky, 2000). At 298

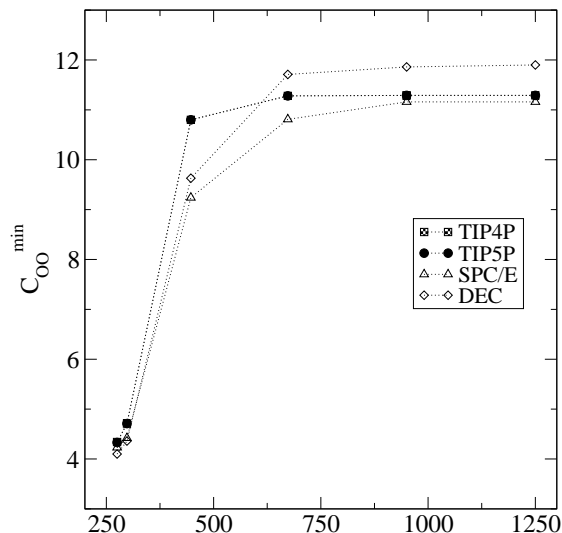


Figure 2.3. Temperature dependence of the number of neighboring molecules in the first coordination shell at constant density for the models studied ($\rho = 0.995 \text{ g/cm}^3$).

K, all models agree within a 17%. This is due to the fact that all force fields were adjusted in this region of the phase diagram. The models have however a different slope of D versus T . TIP5P gives the best agreement with experiments. In this region D is sensitive to the details of the model and some discrepancies appear between the models at temperatures lower (275 K) and higher (447 K) than 298 K. On the contrary, in the region between 500 and 1250 K, the self-diffusion data obtained by the different models converge with increasing temperature. At such high temperatures, collisions become more and more important and the interactions are mostly controlled by the repulsive part of the force field. In Figure 2.3 we present the temperature dependence of the coordination number, as defined in eq. (2.1). It is clear that all models predict a structural transition between tetrahedral towards dodecahedral arrangements as temperature increases. In addition, recent observations (Jedlovsky et al., 1998) report that the percolating network on HB is believed to disappear around 450 K. This could explain the abrupt change in the activation energy of the self-diffusion process observed for all models in this range of temperature. Experimental data at such high temperature and pressure could shed some light on the reality of such a behavior of the diffusion coefficient, under high temperature and density conditions, as predicted by the models analyzed here.

In Figure 2.4, we plot the self-diffusion coefficient versus density at the supercritical temperature of 673 K. At high densities, the agreement between experimental (Lamb et al., 1981) and simulated data is good (between 2-5%

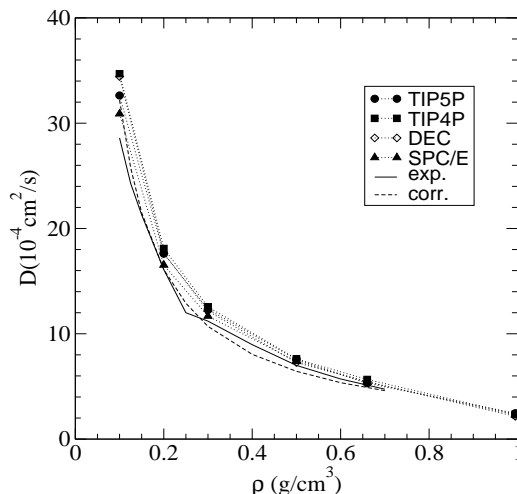


Figure 2.4. Density evolution of the self-diffusion coefficient at 673 K supercritical isotherm. Comparison of experimental data (Lamb et al., 1981) with the simulation results of four models studied.

at $\rho = 0.65 \text{ g/cm}^3$). The highest disagreement ($\approx 15\%$) is observed at low density, and can be attributed to the lack of polarizability of the models. This fact is in agreement with reference (Skaf and Laria, 2000) where an underestimation of the experimental Debye relaxation time was observed for the SPC/E model at low density at supercritical states.

4.2 Structure and Hydrogen Bonding

In this subsection we initiate our discussion by analyzing the different site-site radial distribution functions, which can be compared with data corresponding to NDS and ALS experimental techniques. Secondly, we present the spherical harmonics components of the site-site pair distribution function obtained by the models analyzed here and at different conditions. We have selected for comparison plots at given temperature (298 K) but also at given value of the q ($q = 0.5$) order parameter. Such a comparison will serve us to identify which part of the local structure is related to the properties described by q . Thirdly, three-dimensional plots of the complete $g_{ab}(\mathbf{r})$ reconstructed from the nine components computed in this work are given for comparison. Finally we present the behavior of the order parameter q as well as the average number of hydrogen bonding as a function of temperature and density.

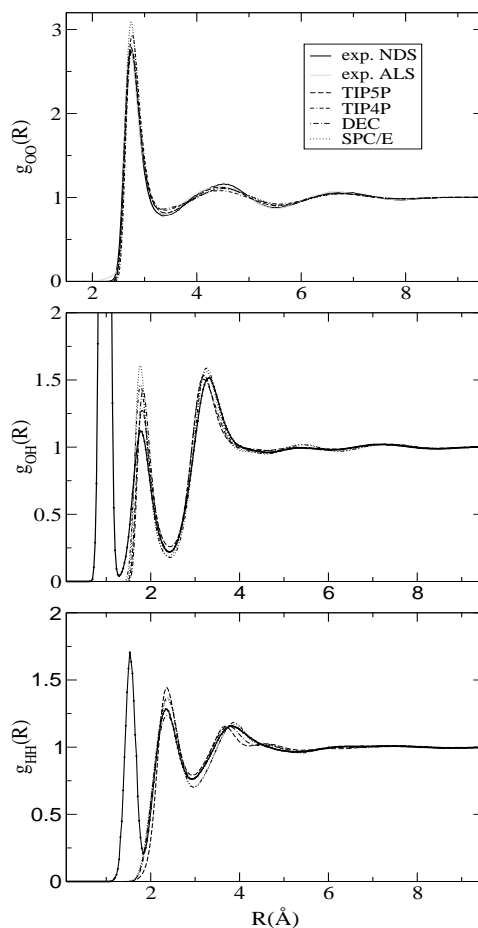


Figure 2.5. Comparison of the site-site distribution function of the four models with *NDS* (Soper, 2000) and *ALS* (Hura et al., 2000) (*ALS* data only for O-O) experiments at state 2 (298 K and $\rho = 0.995 \text{ g/cm}^3$). a) Oxygen-oxygen, b) oxygen-hydrogen and c) hydrogen-hydrogen pair distribution functions.

4.2.1 Site-site radial distribution function

On Figure 2.5 we compare $g_{OO}(r)$, $g_{OH}(r)$, and $g_{HH}(r)$ obtained by the different models as well as the experimental data at a temperature of 298 K and a density of 0.995 g/cm^3 (not, a) (The site-site radial distribution function $g_{ab}(r)$ corresponds to the component $g_{ab}^{00}(r)/\sqrt{4\pi}$).

The results obtained with the models and the experimental data show a good quantitative agreement, although several details should be further discussed.

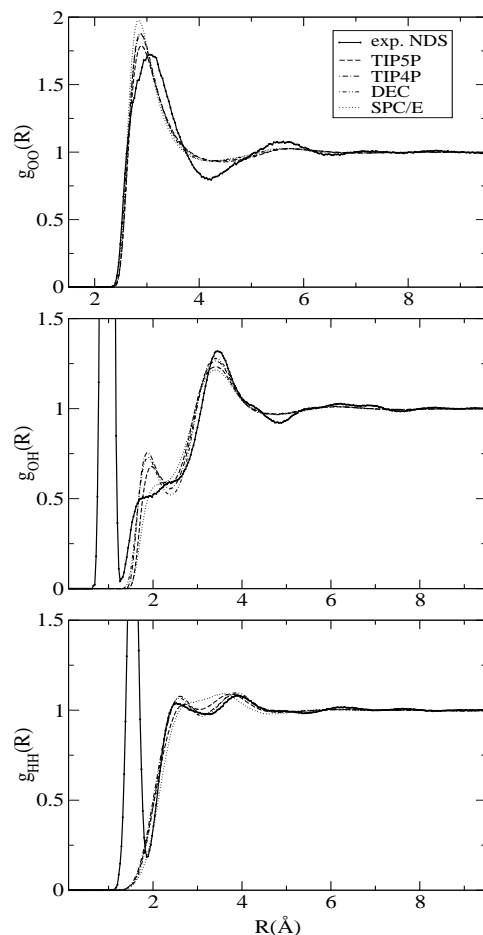


Figure 2.6. Comparison of the site-site distribution function of the four models with NDS (Soper, 2000) experiments at state 11 (673 K and $\rho = 0.66 \text{ g/cm}^3$). a) Oxygen-oxygen, b) oxygen-hydrogen and c) hydrogen-hydrogen pair distribution functions. Sharp inner peaks in the experimental data in plots b and c correspond to intra-molecular oxygen-hydrogen and hydrogen-hydrogen interactions.

In particular, the TIP5P is the model that better agrees with the most recent NDS experimental data (Soper, 2000, Hura et al., 2000, not, b) in Figure 2.5.a. Several detailed values of $g_{OO}(r)$ are presented in Table 2.3. From this table we can see that TIP5P presents improvement with respect to the TIP4P model. Similarly, the DEC model shows also an improvement with respect to the SPC/E model, especially in the height of the first peak. The agreement on the second peak is better for the TIP5P than for the other models. The position of the second peak is compatible with the presence of oxygen atoms in the second solvation

Table 2.3. Comparison of the remarkable details of the models studied and the experimental data. Information is listed as $r(\text{\AA}), g_{OO}(r)$.

Model	1 st Peak	1 st Minim.	2 nd Peak	2 nd Minim.
TIP4P	2.76, 2.93	3.41, 0.85	4.41, 1.08	5.59, 0.92
TIP5P	2.74, 2.78	3.38, 0.81	4.47, 1.13	5.52, 0.90
SPC/E	2.74, 3.08	3.33, 0.80	4.48, 1.11	5.64, 0.90
DEC	2.76, 2.75	3.33, 0.86	4.50, 1.10	5.58, 0.89
NDS ¹	2.73, 2.75	3.37, 0.78	4.50, 1.15	5.60, 0.87
ALS ²	2.73, 2.83	3.41, 0.79	4.44, 1.13	5.51, 0.86

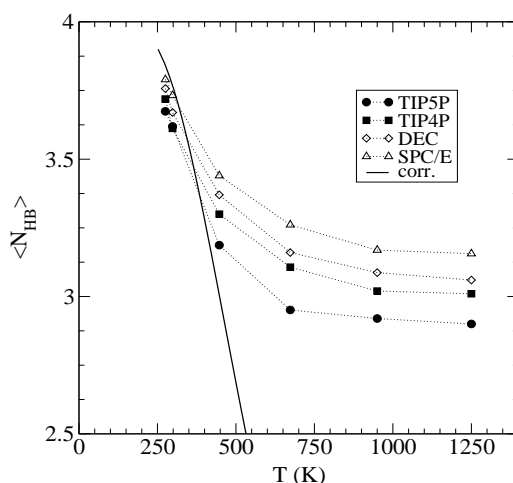


Figure 2.7. Comparison of the temperature evolution of the average number of hydrogen bond per molecule for the four models studied using the geometric definition with the theoretical correlation (Suresh and Naik, 2000) at constant density ($\rho = 0.995 \text{ g/cm}^3$).

shell, belonging to a hydrogen-bonded network, with an ice-like tetrahedral arrangement. Hence, the lower height of this second peak in the TIP4P and the DEC models would indicate that they reproduce a less long-ranged structured fluid.

As far as $g_{OH}(r)$ is concerned, all models overestimate the height of the first peak (Figure 2.5.b), which qualitatively results in an overestimation of the number of hydrogen bonds. In addition, all models present a slight shift in the position of the second peak towards lower distances than experimentally observed. In the case of the $g_{HH}(r)$ (Figure 2.5.c) the DEC model seems to reproduce, better than the others, the height of the first peak, and only TIP5P

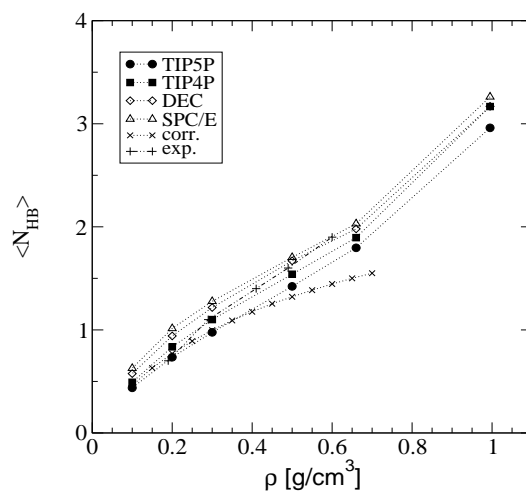


Figure 2.8. Density evolution of the average number of hydrogen bond per molecule at the supercritical 673 K isotherm. Experimental data com from reference (Matubayasi et al., 1997). The correlation is extra-poled at different densities at this temperature reference (Suresh and Naik, 2000).

fails to reproduce the position of the second peak. In general, the agreement between the simulated and experimental data is better for the $g_{OO}(r)$ than for the other radial distribution functions.

Figure 2.6 is analogous to Figure 2.5 but at supercritical conditions (673 K and $\rho = 0.66 \text{ g/cm}^3$ -state 11 of the Table 2.1-) which is representative of a high-density supercritical state. There are few experimental data at supercritical density (Soper, 2000). In Figure 2.6.a all four models display the same qualitative behavior, and an evident disagreement with experimental data. All the models predict a more structured first solvation shell than the experimental data, but underestimate the long range structure as seen experimentally in the $g_{OO}(r)$ at $\approx 5.8 \text{ \AA}$. However the position of the second peak suggests that the long-range structure does not correspond to a tetrahedral arrangement, since the position of the second peak is larger than 4.5 \AA . This discrepancy can be attributed to a too high electrostatic interaction due to the non-polarizable nature of the models studied here. Effectively, the dipole moment of these non-polarizable models corresponds to that of water at the ambient conditions, which is higher than that of less dense phases (the vapor at ambient conditions is 1.85 D). This would justify a much higher value of the first peak as well as a competition between the tetrahedral and dodecahedral structure resulting in absence of any secondary peak, contrary to the experimental data (Soper,

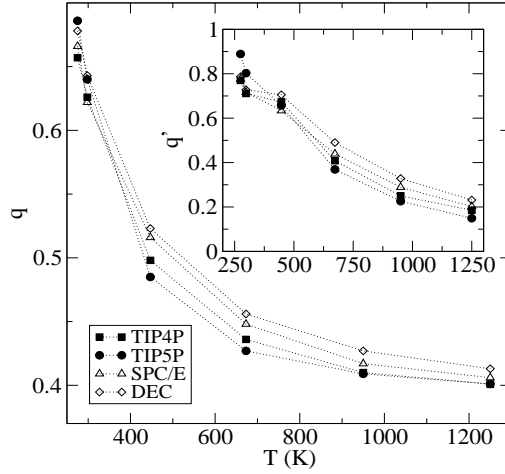


Figure 2.9. Temperature dependence of the two order parameter q and q' at constant density ($\rho = 0.995 \text{ g/cm}^3$).

Table 2.4. Average number of hydrogen bond per molecule computed by means of the geometrical criterion (sec II.D) for the four models studied here at $\rho = 0.995 \text{ g/cm}^3$

T[K]	TIP4P	TIP5P	SPC/E	DEC
275	3.72	3.67	3.79	3.76
298	3.61	3.62	3.73	3.67
447	3.30	3.19	3.44	3.37
673	3.11	2.95	3.26	3.16
950	3.02	2.92	3.17	3.09
1250	3.01	2.90	3.16	3.06

2000). For the case of the $g_{OH}(r)$ (Figure 2.6.b), the SPC/E presents a remarkable feature, the absence of the first peak, in agreement with the experimental data. Nevertheless, all models underestimate the high of the second peak. In the case of $g_{HH}(r)$ (Figure 2.6.c) DEC and TIP4P models reproduce very well the shoulder of this function at 3.3 \AA , contrary to SPC/E and TIP5P which reach a plateau.

4.2.2 HB analysis

Figure 2.7 shows the temperature dependence of $\langle N_{HB} \rangle$ as predicted by the four models in the 0.995 g/cm^3 isochore according to the criterion de-

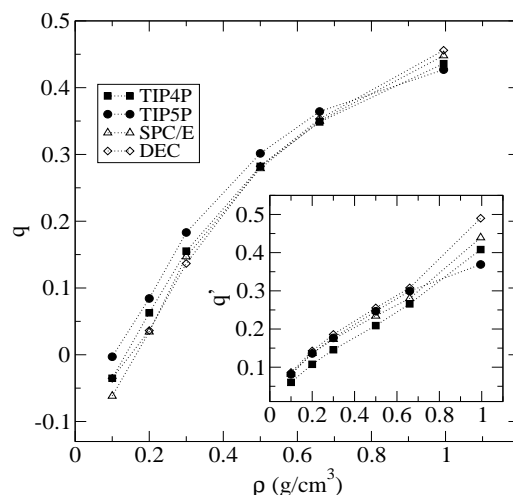


Figure 2.10. Density dependence of the two order parameter q and q' on the supercritical isotherm ($T=673$ K).

finied in chapter 2. The general trend is a decrease of $\langle N_{HB} \rangle$ with increasing temperature until a plateau is reached at temperatures greater than 600 K. At low temperature, the simulated data differ only by approximately 3.2% and they compare rather well with values obtained from dielectric relaxation data (Suresh and Naik, 2000) and neutron diffraction data (Soper, 2000) as shown in Table 2.4. However, in the high temperature range, the discrepancy between models becomes important and the observed plateau is believed to be an artifact due to the geometrical definition of hydrogen bond employed. Indeed, at such densities, two molecules may meet the criterion without necessarily form an HB if their relative energy is too high. It is important to notice that most of the previous HB analyses were carried out in regions close to the liquid-vapor saturation curve (Martí, 2000, Martí, 1999, Martí et al., 1996), or in a range of temperatures not so far from the ambient conditions. The 673 K supercritical isotherm was also extensively studied by MD (Kalinichev and Churakov, 1999), but only a few works (Yoshii et al., 1998) have been done in the dense 0.995 g/cm^3 isochore in a wide range of T , showing results compatible with those presented here. Additionally, we have evaluated the average number of hydrogen bonds as a function of the density, in the supercritical region in the 673 K isotherm. In Figure 2.8, the $\langle N_{HB} \rangle$ is presented for all models. The experimental results of reference (Matubayasi et al., 1997) show a reasonable agreement with the simulated data.

4.2.3 Order parameter

Another feature of water is its ability of forming tetrahedral arrangements giving rise to three-dimensional networks of hydrogen-bonded molecules under appropriate conditions. The parameter q introduced in eq. (1.14) is useful to quantify the degree of tetrahedral ordering around a given molecule (Errington and Debenedetti, 2001). In Figure 2.9 the temperature dependence of the order parameter q at a density of 0.995 g/cm^3 is presented. We observe the same qualitative behavior for all models. It is worth noticing that for all temperatures the value of q obtained by the DEC model is higher than that of the SPC/E, which, in turn, is higher than that of the TIP4P. However the TIP5P model predicts the highest value of q at 275 K, but the lowest value at 447 K and above. Therefore it seems that the four point charges of the TIP5P favor the tetrahedral arrangement at low temperatures (Mahoney and Jorgensen, 2000), due to the dominating effect of the electrostatic interactions. At higher temperatures, the excluded volume interactions between neighbors in the first solvation shell are dominant. This seems to favor the two models with an $\angle HOH$ angle close to the perfect tetrahedral arrangement, namely the SPC/E and the DEC models (for a perfect tetrahedral arrangement the angle between the center of the tetrahedron and the summits is $109,47$ degrees). In addition, q seems to reach a finite asymptotic value at higher temperatures, in agreement with the physical meaning of q . At very high temperatures all models would behave almost as spherical fluids and therefore the residual value of q is due to the excluded volume interactions of the particles in the first solvation shell (Tanaka, 1999). As far as the alternative order parameter q' (defined in eq. 1.15) is concerned, its dependence with temperature, also included in Figure 2.9, shows the same qualitative behavior as q . Hence, the TIP5P gives the highest value of q' at 275 K, to rapidly decrease to the lowest value at highest temperatures. Identically at each temperature analyzed, the sequence of values obtained for q' from the different models is the same as with q . Notice that q' tends to zero at high temperature. For completeness, we show in Figure 2.10 the density dependence of the q and q' parameters at the supercritical isotherm of $T=673 \text{ K}$ is given. As expected, the two parameters indicate an increase of the tetrahedral ordering as the density is increased, in this range.

In Figure 2.11 the relationship of q with the self-diffusion coefficient is presented at constant density ($\rho = 0.995 \text{ g/cm}^3$). It is remarkable that for q larger than 0.485, the predictions of the function $D(q)$ for all models seem to collapse in a single curve. The simulation results in this region correspond to temperatures below 447 K, and it is in agreement with the transition in the coordination number already commented on the dynamical analysis. For values of q lower than 0.485 (values of T larger than 447K) some disagreement appears. This behavior can be attributed to the fact that, below 447 K, self-diffusion is

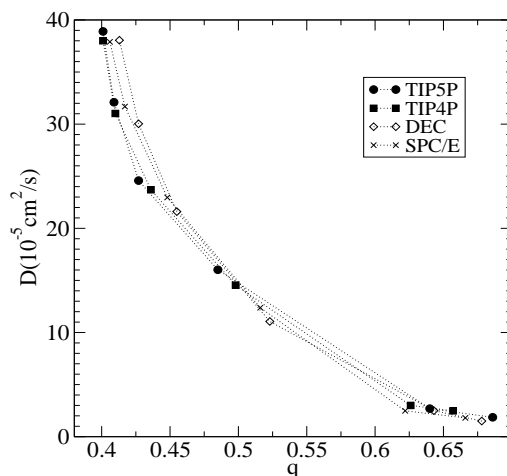


Figure 2.11. Relation between the self-diffusion coefficient and the q at constant density for the models studied ($\rho = 0.995 \text{ g/cm}^3$).

dominated by the time for a given molecule to escape from the cage formed by its hydrogen-bonded neighbors, belonging to a three-dimensional network. Other analyses (Jedlovsky et al., 1998) suggest that no such tetrahedral network exists at temperatures higher than 450 K so that, at fixed density, no direct relationship between D and q has to be observed above this temperature. On the other hand, no consistent behavior of D as a function of $\langle N_{HB} \rangle$ is seen in Figure 2.12. This fact is quite surprising and seems to reinforce the idea that the geometrical definition of $\langle N_{HB} \rangle$ given in chapter 1 is not adequate.

4.2.4 Spherical harmonic projections and 3D representation of $g_{ab}(r)$

To complete the analysis of the structural order in the system we present the spherical harmonic projection of the radial distribution function of each model at two different states: a) when the models have approximately the same value of $q \approx 0.5$ (i.e. when the oxygen atoms have the same local environment), and b) at the same temperature at $T=298\text{K}$.

We can see that the projected pair distribution functions for $l=0, 1, 2, 3$, and 4, and the corresponding values of m ($|m| \leq l$ even values of m do not contribute due to the symmetry of the molecule), at a density of 0.995 g/cm^3 and $q \approx 0.5$ correspond to values of temperatures of 434 K, 423 K, 447 K and 510 K for the models TIP4P, TIP5P, SPC/E and DEC respectively. The results of the four models are similar in the oxygen-oxygen radial distribution function

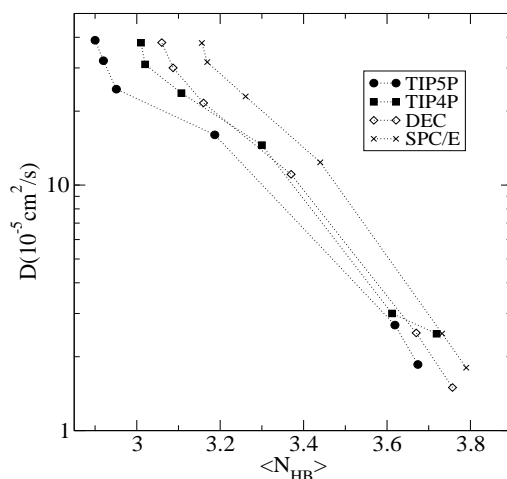


Figure 2.12. Relation between the self-diffusion coefficient and the $\langle N_{HB} \rangle$ at constant density for the models studied ($\rho = 0.995 \text{ g/cm}^3$).

(components $g_{OO}^{00}(r)$, $g_{OO}^{32}(r)$ and $g_{OO}^{40}(r)$). One can see that fixing the value of q leads to a similar three-dimensional structure of oxygen atoms (that can be taken as almost the whole water molecule) as can be seen in Figure 2.13 (corresponding to plots of the tree-dimensional representation of $g_{OO}(\mathbf{r})$).

In view of Figure 2.13 one can see that the differences between models become apparent in the distribution of hydrogen atoms around a given water molecule (see Figure 2.14). The peaks observed at different heights in Figure 2.13 correspond to water molecules (located) in a tetrahedral arrangement. Therefore, if the value of q is similar (at the intermediate conditions studied here) it is expected that the spatial arrangement of the oxygen atoms predicted by the models is also almost quantitatively similar. Only the SPC/E model shows a slightly higher peak at the plane $z = -2 \text{ \AA}$ than the other models.

However, the differences between models become apparent in the distribution of hydrogen atoms around a given water molecule. Figure 2.14, corresponds to plots of the tree-dimensional representation of $g_{OH}(\mathbf{r})$, at different planes orthogonal to the dipolar moment (the z -axis) of the reference molecule. The relative height of the peaks corresponding to TIP5P model indicates a major tendency of localizing the hydrogen atoms in more defined positions than the other models. The three-dimensional plots of $g_{OH}(\mathbf{r})$ shown in this figure also reveal the tetrahedral arrangement. However, the peaks in the upper plane $z = 1 \text{ \AA}$ are rather different. This deviation can be attributed to a change in the

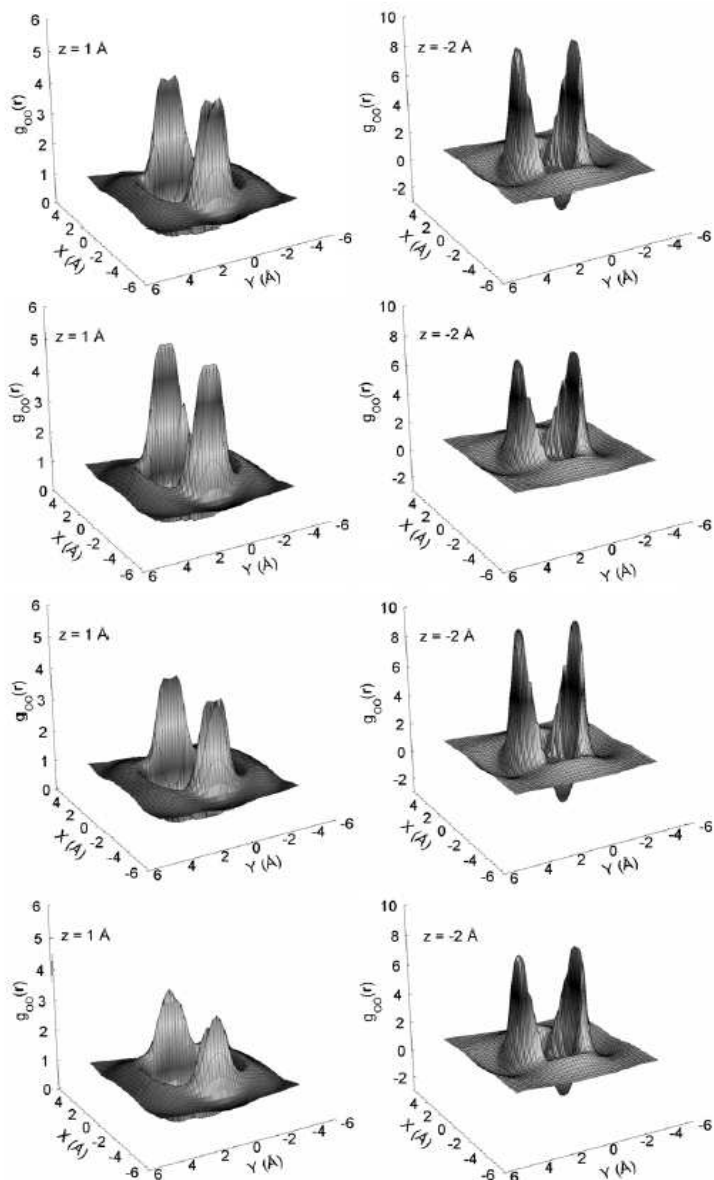


Figure 2.13. 3D oxygen-oxygen pair distribution function for the TIP4P, TIP5P, SPC/E and DEC (from top to bottom) at 434 K, 424 K, 447 K and 510 K respectively and the same orientational order parameter $q \approx 0.5$, at $\rho = 0.995 \text{ g/cm}^3$.

position of the maximum, rather than to a decrease of the capacity of localization of the hydrogen atoms by the different potentials. Notice, in addition, that the

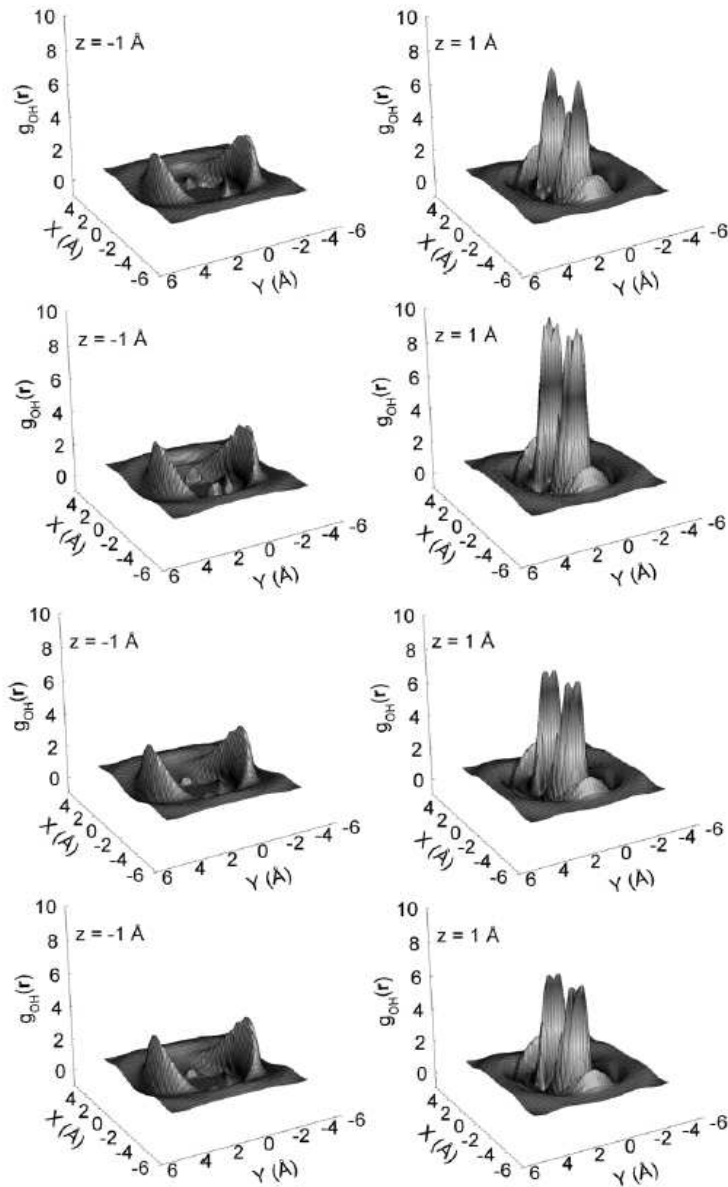


Figure 2.14. 3D oxygen-hydrogen pair distribution function for the TIP4P, TIP5P, SPC/E and DEC (from top to bottom) at 434 K, 424 K, 447 K and 510 K respectively and the same orientational order parameter $q \approx 0.5$, at $\rho = 0.995 \text{ g/cm}^3$.

two models TIP4P and TIP5P, have more localized hydrogen atoms in the plane $z = 1 \text{ \AA}$ than the other two models, whose positive point charge distribution is

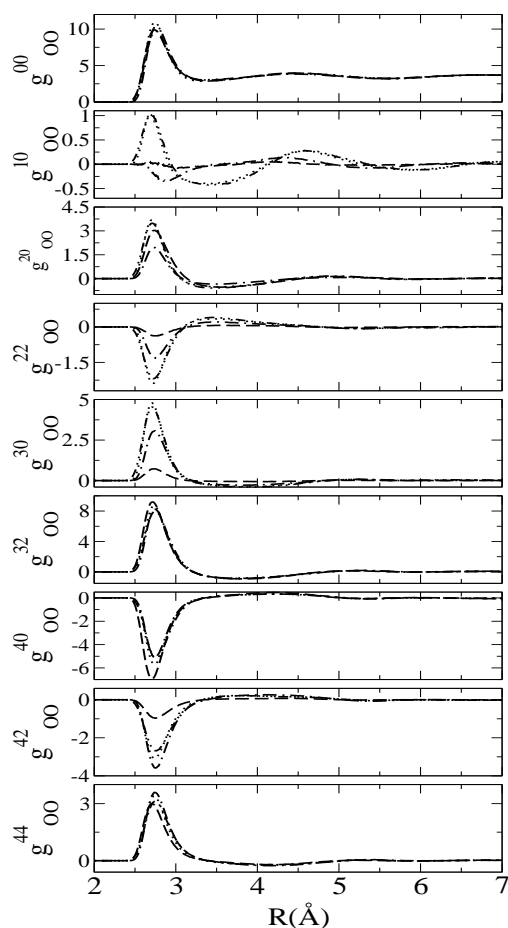


Figure 2.15. Comparison of oxygen-oxygen radial distribution function projected with spherical harmonics for the four models at the same temperature ($T=298$ K, at $\rho = 0.995$ g/cm^3). (---)TIP4P, (-.-)TIP5P, (---)DEC and (....)SPC/E.

different. This localization of hydrogen is more important in the TIP5P model due to the two negative charges in the position of the lone electron pairs.

In this work we have also analyzed the three-dimensional structure of water as predicted by the four models at a temperature of 298K, and at a density of 0.995 g/cm^3 , which are the conditions at which the models have been fitted (to better agree with experimentally measurable properties of water at ambient conditions).

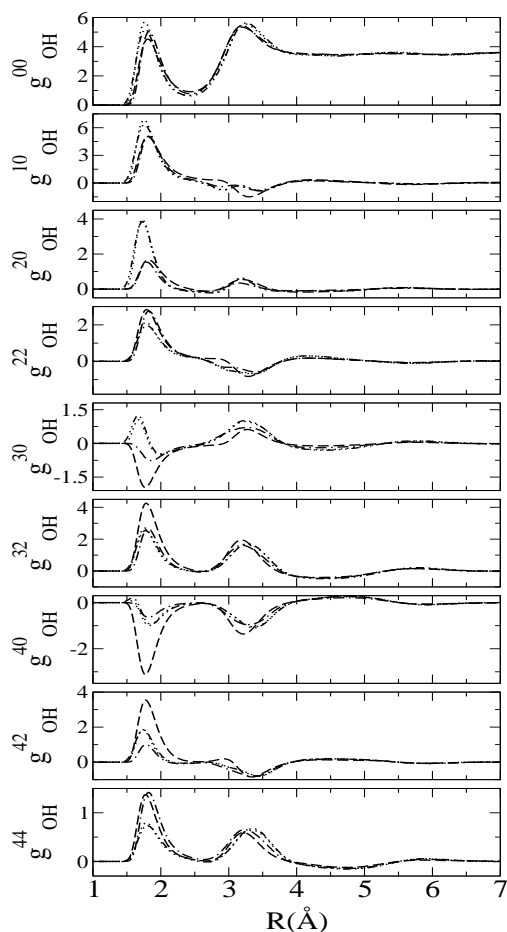


Figure 2.16. Comparison of oxygen-hydrogen radial distribution function projected with spherical harmonics for the four models at the same temperature ($T=298$ K, at $\rho = 0.995$ g/cm³). (· · ·)TIP4P, (- · - ·)TIP5P, (- - -)DEC and (—)SPC/E.

As could be expected, according to Figure 2.15, all models agree rather well as far as the radial distribution function (proportional to $g_{OO}^{00}(r)$) is concerned, where all models are compared at the same temperature ($T=298.15$ K). This is due to the fact that their parameters have been chosen in most of the cases just to reproduce experimental data on this function. Only a slight disagreement in the height of the first peaks is identifiable. Similar accord is also found in the second relevant component, $g_{OO}^{32}(r)$. However, significant differences can be found in components such as $g_{OO}^{20}(r)$, $g_{OO}^{22}(r)$, $g_{OO}^{30}(r)$ and $g_{OO}^{42}(r)$. As it was also observed in the comparison of the models at the same value

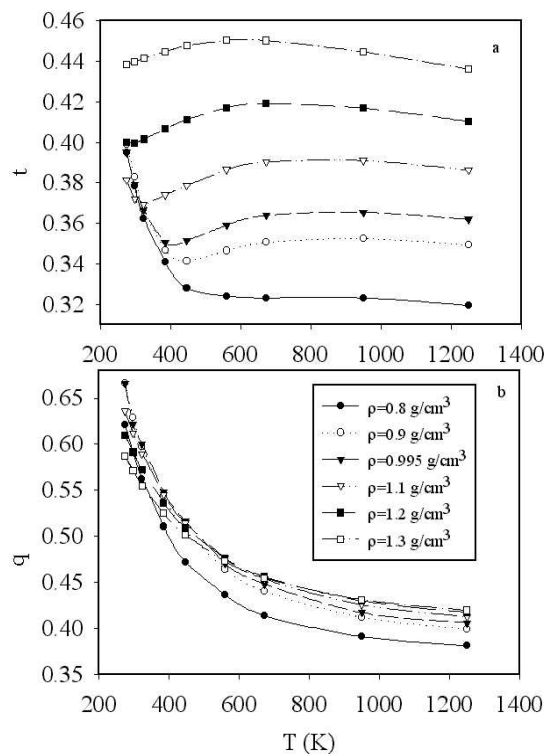


Figure 2.17. Comparison of the two order parameters for pure water (SPC/E model), at different densities and temperatures, a) translational order parameter and b) orientational order parameter.

of q , the TIP5P model is the one that displays the lower value in the first peak, as far as the latter four components mentioned are concerned. This fact indicates that the predictions of the three-dimensional structures of the system obtained from every model are significantly different, even at ambient temperature. The spherical harmonics projection of the oxygen-hydrogen pair distribution function (Figure 2.16) reflects these differences, where the peaks in the TIP5P model are higher than for the other models, showing that this model more strongly localizes the hydrogen atoms than the rest of the models.

The components shown in Figure 2.16 show major differences between the predictions of each model than in the case of the Oxygen-Oxygen pair distribution functions. It is noticeable that even in the $g_{OH}^{00}(\mathbf{r})$ component the height of the first peak, corresponding to the position of the closer hydrogen atom of the neighboring molecules, the models yield slightly different predictions. In the rest of the components the deviations are larger and even of different sign, as is the case of the $g_{OH}^{30}(\mathbf{r})$ component.

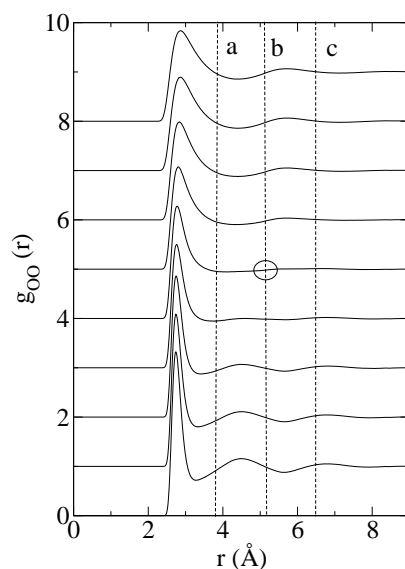


Figure 2.18. Temperature evolution of the $g_{OO}(r)$ at $\rho = 0.995 \text{ g/cm}^3$, from 275 K to 1250 K. The second peak lies between a and b only below $T=447$ K. At higher temperatures the second peak is shifted to larger radial distances, laying between lines b and c . Each $g_{OO}(r)$ are shifted by a factor of 1 from bottom to top.

In the case of the Oxygen-Hydrogen pair distribution function, the components shown in Figure 2.16 show major differences between the predictions of each model than in the case of the Oxygen-Oxygen pair distribution functions (Figure 2.15). It is noticeable that even in the $g_{OH}^{00}(r)$ component the height of the first peak, corresponding to the position of the closer hydrogen atom of the neighboring molecules, the models yield slightly different predictions. In the rest of the components the deviations are larger and even of different sign, as is the case of the $g_{OO}^{30}(r)$ component.

5. Second Part: Order transition in pure water

In the second part of the analysis we have computed the translational and the orientational order parameters for water at different conditions, given in Table 2.2. In Figure 2.17.b the temperature evolution of the orientational order parameter q is presented at different densities. This parameter decreases monotonically when temperature is increased, and, in general q increases with density. This property had been discussed previously (Figure 2.9) and no further discussion will be done here. On the other hand, Figure 2.17.a shows the

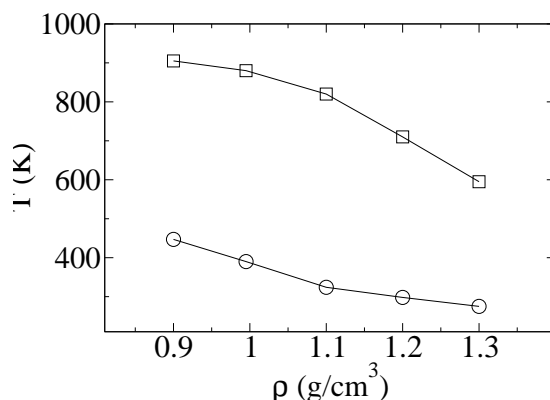


Figure 2.19. Loci of the maximum (squares) and minimum (circles) of the translational order parameter for pure water.

variation of the translational order parameter t in function of temperature at different densities. This parameter increases with density as can be expected. Even though, its temperature behavior presents remarkable aspects worth to be mentioned. At $\rho = 0.8 \text{ g/cm}^3$, t decreases monotonically, but, starting from $\rho = 0.9 \text{ g/cm}^3$ up to $\rho = 1.3 \text{ g/cm}^3$ the t parameter presents a clear minimum and a more spread maximum. The presence of the minimum has been reported by the work of Debenedetti *et. al.* (Errington and Debenedetti, 2001), but the presence of a maximum is reported for the first time in this work.

The physical meaning of the minimum on t is the transition suffered by the water structure at particular thermodynamic conditions when the second peak of the $g_{OO}(r)$ at almost $r \approx 4.5 \text{ \AA}$ disappears, as can be seen in Figure 2.18. When temperature is increased a second peak appears at large distances, giving a transition from tetrahedral to dodecahedral structures (see the analysis of Figure 2.3) and, hence, t increases until the temperature is high enough to reduce the height of the first as well as the second peak of $g_{OO}(r)$.

The loci of the minimum as well as the maximum of t is shifted to lower temperatures at higher densities as can be seen in Figure 2.19. As it was commented on the introduction of this chapter, the computation of any order parameter to account the percolating network requires a cluster analysis, even though, the loci of the line that separates the infinite cluster should lie between the lines of maximum and minimum of t , due to the fact that water also loses its tetrahedral structure and the degree of connectivity (through hydrogen bonds) between these lines.

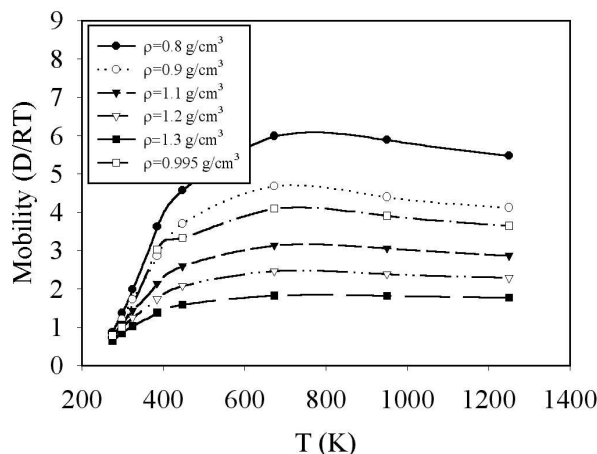


Figure 2.20. Mobility of pure water (FPC/E model), at different densities and temperatures.

Finally, Figure 2.20 shows the mobility ($D/k_B T$) of water molecules at different conditions. The general trend of this property is closely related with the temperature evolution of the self-diffusion of water at $\rho = 0.995 \text{ g/cm}^3$ discussed in Figure 2.2, however, in the case of the mobility the effect of the temperature produces a competition of two effects. First, the mobility increases when the rise of temperature produces a continuous destruction of the local order of water (see the relationship of D vs q in figure 2.11). This process persists until the effect of thermal agitation promotes a major frequency of collisions between molecules and consequently an increase of rebounds that affect the free path of molecules. Then, the maximum in the mobility is due to the competition of these two effects, and the loci of this maximum is also located in the region between the maximum and minimum of t presented in Figure 2.19.

6. Conclusions

In this work, classical Molecular Dynamics simulations have been undertaken aiming at a comparison of structural and dynamical properties of four rigid non-polarizable models of water (TIP4P, TIP5P, SPC/E and DEC). We have paid special attention to the 0.995 g/cm^3 isochore and the $T=673\text{K}$ supercritical isotherm.

We have found that the four models reproduce different three-dimensional patterns, as can be seen in the different components of the oxygen-oxygen, and oxygen-hydrogen pair distribution functions, in terms of a base of spherical harmonics. The differences are qualitatively the same in the two points analyzed (same value of q , and at 0.995 g/cm^3 and 298K . See Figure 2.13-2.16). Even

at ambient conditions, where the parameters of the model have been adjusted to give the best fit to certain structural as well as thermodynamic properties (radial distribution function, dielectric relaxation, etc.), the differences are significant. Therefore, the availability of experimental information of the detailed three-dimensional structure of water can be of crucial importance in the development of new simple models, reliable in high-density applications.

In the supercritical region $T=673\text{K}$ and $\rho = 0.66 \text{ g/cm}^3$, all models fail to reproduce the experimentally observed behavior of $g_{OO}(r)$ and $g_{OH}(r)$, in view of Figure 2.5. Effectively, the MD results reproduce a more structured first solvation shell, corresponding to a higher and narrower first peak than observed. However, they underestimate the long-range structure, as can be experimentally seen.

In the analysis of the average number of hydrogen bonds, $\langle N_{HB} \rangle$, reasonable good agreement was observed at low temperatures between models and experiments. On the other hand we observe that the geometrical definition leads to a plateau value of the average number of hydrogen bonds at high temperature, in the high-density region. Effectively, disregarding the energy of the bond in the definition of the hydrogen bonding interaction causes that, at high temperature, non-bonded particles are counted as hydrogen-bonded simply because they satisfy the geometrical criterion, although they are not effectively bonded if energy is taken into account.

The self-diffusion coefficient at high temperatures (above 450 K) in the 0.995 g/cm^3 isochore, shows important deviations from the experimental tendency in all the models analyzed. In view of the coincidence of the values found for the different models in this region, we have inferred that this fact can be a consequence of an inadequate repulsive interaction in the force field potentials. Furthermore, the major discrepancy between calculated diffusion coefficients occurs at temperatures around 450 K where a change in the structure of the first solvation shell (from tetrahedral to dodecahedral arrangements) takes place. Hence, we can argue that, as the temperature increases, the system passes from a diffusion dominated by the cage effect, due to hydrogen bonds (low temperature), to a diffusion dominated by collision effects (at high temperature), according to the change in the behavior of D in the region between 400 K and 500K.

From the tetrahedral order analysis through the q parameter, some important conclusions can be extracted. For instance, the TIP5P model presents a more structured system close to ambient conditions in comparison to the other three models. Above 298K and a density of 0.995 g/cm^3 , the DEC model seems to preserve the tetrahedral order more than the other models. The new definition of the order parameter q' permits to relate the analysis of the tetrahedral order

to a preferred axis (the dipolar moment, in our case, taken as the z-axis). Thus, with this definition one can discriminate between a general tetrahedral order in the first solvation shell (contained in q), and the order caused by directional hydrogen bonded interactions in water (described by q'). As a result, q' tends to zero at high temperature while q remains finite, since the excluded volume interactions in the particles in the first solvation shell manifest some degree of tetrahedral order if the density is high enough. The results obtained with both parameters in the four models analyzed indicate a decrease of the tetrahedral order with temperature (in the 0.995 g/cm^3 isochore), while q as well as q' increase with density (in the 673K isotherm), in the range studied, from 0.1 g/cm^3 to 1 g/cm^3 . This fact does not exclude the possibility of a decrease in the tetrahedral order at higher densities (Errington and Debenedetti, 2001). This analysis, however, lies beyond the scope of this part of the work.

Despite the fact that both TIP5P and DEC models represent an improvement over previous models (ST2 and SPC/E, respectively) in some properties as the local structure and the temperature of the maximum density (TMD) in the case of the TIP5P, and the correct value of the dielectric constant of water at practically any thermodynamic condition, for the DEC model, some other erroneous aspects remain when compared to older models. For instance: 1) at high temperatures, self-diffusion coefficient underestimates experimental data, for instance, at 0.995 g/cm^3 , 2) underestimation of bulk and shear viscosity (Smith and van Gunsteren, 1993, Guo and Zhang, 2001) at ambient conditions, and overestimation of the thermal conductivity (Bedrov and Smith, 2000) of pure water are some examples of the aspects that can be improved. One could think that there is no straightforward modification of this kind of models in a general point of view. In fact Glättli et al. (Glättli et al., 2002) have recently shown that general improvements in SPC-like models are not possible only with simple readjustment of charges, geometry or inclusion of LJ sites in the hydrogen atoms. But, improvements in some relative aspects are still mater of work, for example in dynamical properties. The results presented in this work are in the line to give useful tools to reach this goal.

Finally, in the second part of this chapter, even though the hypothesis of the presence of a second order phase transition can not be corroborated with the analysis carried out in this study, the information obtained in the complex behavior of the translational order parameter t , reinforce the arguments to proceed with a detailed cluster analysis to elucidate whether or not the infinite cluster is presented in water, and if this line separate the region where all anomalous behavior of water can be found.

Notes

1. reference (Soper, 2000)
2. reference (Hura et al., 2000)

Chapter 3

TRANSPORT PROPERTIES OF AQUEOUS SOLUTIONS

1. Introduction

The aqueous mixtures of associating fluids are systems whose equilibrium as well as dynamical properties presents non-ideal behavior that has motivated many experimental and theoretical studies. Many industrial processes involve the use of mixtures of this type, where great number of thermophysical properties is required to design and product industrial equipments. In all these cases, molecular simulation appears as a promising alternative way to determine properties relevant to prediction and design. Molecular models are based on a microscopic description that lies in the knowledge of the intermolecular forces and structures of molecules. Particularly, the Molecular Dynamic (MD) simulation technique is used to obtain equilibrium and transport properties of physical systems (Allen and Tildesley, 1989). This technique is based on the principle that atoms and molecules obey the laws of classical mechanics (Hansen and McDonald, 1991, Frenkel and Smith, 1996) and their motion is simulated in a computer. The main difference between the results obtained by this technique and those derived from phenomenological equations of state is that, in the former, the parameters are molecular in nature and do not depend on the thermodynamic conditions of the system, while, in the latter, the parameter often lack of physical meaning and depend usually on thermodynamic conditions such as temperature or pressure. In this way MD is analogous to real experiments because, after some interval of time, *measures* of physical macroscopic properties are obtained from averages involving velocities and positions of the particles. In addition, in many cases experimental measurements are expensive, and in some particular systems can be even dangerous (experiment

with inflammable or cancerous compounds, experiments at high temperature and pressure, etc).

Simulation methods require the use of accurate force fields. These force fields are parameterized on the basis of quantum mechanical calculations and/or experimental measurements. The accuracy of the predictions done with this models are ultimately determined by the accuracy of the force field and the extent to which the relevant phase space is sampled in the calculation, this is a characteristic common to all simulation studies. Consequently, extensive validation and testing are needed to ensure that the results are accurate (with respect to their agreement with experimental values for the property of interest) and reproducible (in the sense that that they represent converged values and are not artifacts of inadequate sampling or erroneous force field parameters). This chapter is devoted to both objectives, first of all to test the accuracy of the methodologies employed to reproduce experimental data of transport properties of aqueous solutions, and, secondly, to make some pure predictions on properties of systems where there is no experimental data at all. In the absence of the evaluation process, simulation methods can produce unreliable results, which would seriously affect their credibility and limit their use in industry (wor, 1999).

Then, to achieve this two main objectives we have decided to compute structural and transport properties of aqueous solutions of associating solutes, such as a) water+methanol, b) water+ethanol, c) water+DMSO (dimethyl sulfoxide) and d) water+acetone. Aqueous solutions of alcohol mixtures are quite well known and many works has been done to study thermodynamics (Benmore and Loh, 2000, Shevade and Gubbins, 2000) as well as transport properties (Matsumoto and Gubbins, 1990, Saiz et al., 1999, Slusher, 2000, Sesé and Palomar, 2001, Petravic and Delhommelle, 2002) of mixtures of this kind. Additionally, we decide to study the water+DMSO system due to its peculiar non-ideal properties. The dimethyl sulfoxide (DMSO) is a compound with applications in pharmacological industry, mainly to enhance skin absorption and, in general, biological membrane transport, which justifies the current interest on its properties. From a theoretical point of view, the peculiar structural and thermodynamic behavior of aqueous mixtures of DMSO has been studied during the last 10 years through Molecular Dynamics simulations (MD). One can mention studies of the molecular association between the species (Borin and Skaf, 1999), their hydrogen bond interaction (Luzar and Chandler, 1993), thermodynamic and dielectric properties of water-DMSO mixtures (Skaf, 1999, Laria and Skaf, 1999, Skaff, 1997a, Borin and Skaf, 1999, Liu et al., 1995) as well as solvation dynamics (Day and Patey, 1999) and electrolyte solutions (Adya et al., 2001), among others. Finally, the water+acetone mixture has been also selected for our analysis because this system also presents non-ideal behavior in the viscosity,

for instance. Several MD studies have been devoted to study the thermodynamic and transport properties of this mixture (Ferrario et al., 1990, Wheeler and Rowley, 1998, Venables and Schmuttenmaer, 2000).

The strong hydrogen bond association between water and associating solutes molecules is the main responsible for the strong non-ideal behavior of these types of mixtures, especially for molar fractions of water between 60% and 90%. At these particular compositions the shear viscosity of the mixture presents clear maximum. Additionally, the thermal conductivity of these systems is also a strong function of composition, particularly at high water concentrations. We are also interested on the possible connection of the dynamical behavior with local structural information of the local structure in these systems. For instance, for the water+DMSO mixture, neutron diffraction experiments (Soper and Luzar, 1992), as well as molecular simulations (Luzar and Chandler, 1993) studies support the evidence of the existence of some *aggregates* of the form 1DMSO:2 water in this particular concentration range. Such structures seem to be very stable, and their long relaxation times have been argued to be in close relation to the experimentally observed increment of the shear viscosity, in general to the slow dynamics of the collective modes of the mixture. Even though, the controversy about the existence of these structures is still alive and many aspects of the dynamical behavior of this system are still poorly understood. We are also interested in comparisons of the local structure of solutes that have similar and different hydrogen bond character (for instance DMSO and acetone are only *acceptors* of hydrogen bonds, while methanol and ethanol are both *donor* and *acceptors* of hydrogen bonds). Moreover, most of the previous works have focused on exploring only static and dynamic dielectric relaxations, and the structural properties of the mixture. Only a few works have been devoted to the analysis of the behavior of the transport properties of the water+associating solute systems.

In this chapter we have undertaken a series of equilibrium and non-equilibrium molecular dynamics simulations in order to investigate the shear viscosity and the thermal conductivity of water-associating solute mixtures in the whole range of compositions and at ambient conditions. We have also, to some extent, related the anomalies found in these properties with the variations of the local structure of the system together with the analysis of the survival probability of the water-water and water-solute hydrogen bond life times. With this purpose we have computed the tetrahedral order parameter q (Chau and Hardwick, 1998, Errington and Debenedetti, 2001) as a function of the molar fraction of water, as a description of the local three-dimensional arrangement around a given oxygen atom of a water molecule. Since q was originally introduced for pure systems, here we have proposed an extension to the kind of mixtures discussed in chapter 2. The lifetime of the H-bonds have revealed as one of the

properties more sensitive to composition and have strong influence in the transport coefficients and dynamical properties in general. The HB lifetimes have been analyzed through the study of the decay time of autocorrelation functions in a similar way of previous analysis (Guàrdia et al., 2002) of the hydrogen bond dynamics in associating liquids.

2. Fundamentals: Hydrogen bond lifetimes

Despite the fact that there is no unequivocal way to determine whether two molecules are Hydrogen Bonded or not, we assume a geometrical criterion (see chapter 1 and ref. (Martí, 2000)), which is sufficient for our purposes. The study of the temporal evolution of the Hydrogen bonds is not a straightforward issue due to the intermolecular vibrational motion inherent in the process of breaking and forming H-bonds. We decided to compute the survival probability or lifetime of the H-bonds from the long time decay of the autocorrelation functions (Guàrdia et al., 2002, Matsumoto and Gubbins, 1990)

$$C_{HB}(t) = \frac{\langle \eta_{ij}(t) \cdot \eta_{ij}(0) \rangle}{\langle \eta_{ij}(0)^2 \rangle} \cong \exp \left\{ -\frac{t}{\tau_{HB}} \right\} \quad (3.1)$$

where the variable $\eta_{ij}(t)$ takes the value 0 or 1 depending on the H-bond state of a given pair of oxygens. For instance, $\eta_{ij}(t) = 1$ if oxygens i and j are H bonded at times 0 and t and the bond has not been broken for any period longer than t^* , otherwise $\eta_{ij}(t) = 0$. We have investigated two limiting cases, $t^* = 0$ and $t^* = \infty$ which correspond to the continuous H-bond lifetime (τ_{HB}^C) and the intermittent H-bond (τ_{HB}^I) employed in previous works (Guàrdia et al., 2002).

3. Computational details

We have studied the transport properties of mixtures of water and four different associating solutes: a) water+methanol, b) water+ethanol, c) water+DMSO, and d) water+acetone. The molar fractions and the experimental density of the different mixtures are summarized in table 3.1. Different models have been used to compute transport properties of these mixtures. For each case we try to reproduce the experimental density of the mixture at ambient conditions to discriminate whether or not a particular set of models are appropriate for our purposes. For the water+alcohol simulations we decided to employ the Jorgensen *et al.* (Jorgensen, 1986) OPLS models for methanol and ethanol (systems *a* and *b*), and the TIP4P model for water (Jorgensen et al., 1983) with the mixing rule employed by Jorgensen (described in eq. (1.85) of chapter 1) in the development of the OPLS models for alcohols (Jorgensen, 1986). We decided

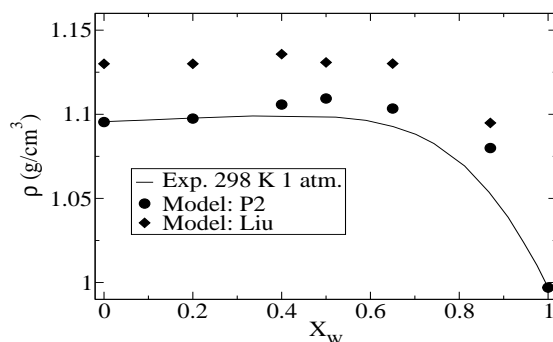


Figure 3.1. Comparison of the experimental density of the mixture of water+DMSO (Cowie and Toporowski, 1961) at 298 K and 1 atm with that obtained with the simulations at same conditions using the SPC/E (Berendsen et al., 1987) model for water and two models of DMSO, for instance, the P2 model (Luzar and Chandler, 1993) and the Liu *et al.* (Liu et al., 1995) model.

to employ these set of models because they are well known and has been employed in several studies of thermodynamics (Benmore and Loh, 2000, Shevade and Gubbins, 2000) as well as transport properties (Matsumoto and Gubbins, 1990, Saiz et al., 1999, Slusher, 2000, Sesé and Palomar, 2001, Petravac and Delhommelle, 2002) with adequate results for mixtures of this kind. In the case of the water+DMSO system (*c*) we have used the P2 model (where methyl groups were treated as united atoms) of Luzar and Chandler (Luzar and Chandler, 1993) for the DMSO, and the SPC/E (Berendsen et al., 1987) model to simulate water molecules. The use of these two models is supported by previous works (Borin and Skaf, 1999, Skaf, 1999) on self-diffusion and dielectric properties at ambient conditions, which find good agreement with experimental data. It is worth to point out that we have investigated the behavior of the more recent model for DMSO developed by Liu *et. al* (Liu et al., 1995), but we were unable to reproduce the density of the pure component at 298 K and 1 bar, reported in the original work. Our simulations of the density of the mixture at 298 K and 1 atm computed with the *NPT* ensemble are shown in Figure 3.1. The disagreement of the Liu's model is evident, failing to reproduce the experimental density of the mixture at the studied conditions and hence, it has been discarded ¹.

Therefore, we have focused on the P2 model, which correctly reproduces this property. Other works (Luzar and Chandler, 1993, Luzar, 1996, Skaff,

¹It is important to mention that a corrected version of the Liu's model was presented after this part of the work was performed (Bordat et al., 2002). In the new model the experimental density of pure DMSO at 298 K and 1 atm is well reproduced.

1997a, Skaff, 1997b), employing the P2 and SPC/E models, also report results that reasonably agree with experimental measurements on different properties. Finally, for the system water+acetone (system *c*) we have employed the SPC/E (Berendsen et al., 1987) model to simulate water molecules and the model of Wheeler *et al.* (Wheeler and Rowley, 1998) for the acetone molecules. Although Wheeler *et al.* reported that their model correctly reproduce the experimental density, being an improvement in comparison with previous models, we were unable to reproduce the density of pure acetone reported in the original work. For instance, the experimental density at 298 K and 1 atm is 0.785 g/cm^3 , and the density reported by the Wheeler's work was 0.783 g/cm^3 , we have obtained 0.767 g/cm^3 employing our code (see details on chapter 2, section 5.2, whit long-range corrections for energy and pressure and Reaction-Field methodology, to handle electrostatic interactions) and 0.769 g/cm^3 employing the code *mdgen* (mdg, 2003) with long-range corrections for energy and pressure and electrostatic interactions treated with the Ewald summation technique. Even though, we have decided to maintain this model to simulate acetone molecules. All models considered in this chapter has been treated as Lennard-Jones sites plus point charges according to,

$$U_{ij} = 4\epsilon_{ij} \left[\left(\frac{\sigma_{ij}}{r_{ij}} \right)^{12} - \left(\frac{\sigma_{ij}}{r_{ij}} \right)^6 \right] + \frac{q_i q_j}{4\pi\epsilon_0 r_{ij}} \quad (3.2)$$

where q_i is the partial charge on site i , ϵ_{ij} and σ_{ij} are the Lennard-Jones interactions between sites i and j on different molecules, being $r_{ij} = |\mathbf{r}_j - \mathbf{r}_i|$ is the separation distance between the corresponding sites. Crossed interactions were computed through Lorentz-Berthelot rules (eq. (1.83)) for the water+DMSO and water+acetone, while the geometric average (eq. (1.85)) has been employed for the water+alcohol systems. Details of the intermolecular potential parameters for water and solute molecules are given in Table 3.2.

We have performed different Molecular Dynamics simulations with three different ensembles. The viscosity coefficient was obtained using equilibrium molecular dynamic simulations in the *NVT* ensemble, using a weak coupling bath (Berendsen et al., 1984) (only a couple of simulations has been done in the *NPT* ensemble for the water+acetone system). The thermal conductivity coefficient was computed through constant temperature PeX (momentum exchange algorithm) non-equilibrium molecular dynamic scheme, details of the algorithm can be seen in chapter 1 and in Appendix E (Nieto-Draghi and Avalos, 2003). All simulations were carried out with 500 molecules except for the case of the water+ethanol system where 800 have been employed to improve

Table 3.1. Simulated thermodynamic states for the comparison analysis. All data at 298 K and 1 atm (water+methanol system at 313.15 K). (References for the experimental density: water+methanol (GOWProp-v5.1, 2002), water+ethanol (Bou-Ali, 1999), water+DMSO (Cowie and Toporowski, 1961) and water+acetone (Griffiths, 1952))

State	Mole Fractions					$\rho \text{ g/cm}^3$
	Water	Methanol	Ethanol	DMSO	Acetone	
1	1.0	0.0	-	-	-	0.98986
2	0.9	0.1	-	-	-	0.95457
3	0.772	0.228	-	-	-	0.91714
4	0.495	0.505	-	-	-	0.85190
5	0.36	0.64	-	-	-	0.82731
6	0.2	0.8	-	-	-	0.80164
7	0.0	1.0	-	-	-	0.77599
8	1.0	-	0.0	-	-	0.99750
9	0.95	-	0.05	-	-	0.97380
10	0.9	-	0.1	-	-	0.97141
11	0.8	-	0.2	-	-	0.933
12	0.0	-	1.0	-	-	0.78675
13	0.87	-	-	0.13	-	1.0537
14	0.65	-	-	0.35	-	1.0927
15	0.5	-	-	0.5	-	1.0989
16	0.4	-	-	0.6	-	1.0988
17	0.2	-	-	0.8	-	1.0977
18	0.0	-	-	1.0	-	1.0956
19	0.997	-	-	-	0.027	0.98730
20	0.806	-	-	-	0.194	0.92940
21	0.579	-	-	-	0.421	0.87000
22	0.310	-	-	-	0.690	0.82250
23	0.097	-	-	-	0.903	0.79680
24	0.0	-	-	-	1.0	0.78510

statistics. The size of the simulation box on each case has been adjusted to fit the experimental density of the mixture (see table 3.1). A cubic box was employed for the viscosity computation and a parallelepiped to determine the thermal conductivity coefficient via non-equilibrium simulations. In the latter, we have chosen $l_z = 2l_x = 2l_y$, with l_x, l_y, l_z being the dimensions of the box. The equations of motion were integrated through leapfrog (Allen and Tildesley, 1989) algorithm with a time step of 2 fs, meanwhile leapfrog implicit quaternions (Evans, 1997, Svanberg, 1997) were used to integrate the rotational part of the equations of motions (the *mdgen* code has been used for the water+ethanol system to handle the flexible model of ethanol with a 5th order Gear predictor-corrector integrator with Gaussian constraints to keep the geometry of the flexible molecule). All the simulations have been performed

Table 3.2. Potential parameters of the models employed. For more details about the models see ref.(Borin and Skaf, 1999) and ref.(Berendsen et al., 1987).

Site	σ [Å]	ϵ [KJ/mol]	Charge (e)
water (SPC/E) (Berendsen et al., 1987):			
<i>O</i>	3.165648	0.650167	-0.8476
<i>H</i>	0.0	0.0	0.4238
water (TIP4P) (Jorgensen et al., 1983):			
<i>O</i>	3.1535779	0.6486943	0.00
<i>H</i>	0.0	0.0	0.52
<i>M</i>	0.0	0.0	-1.04
Methanol (OPLS) (Jorgensen, 1986):			
<i>O</i> (<i>COH</i>)	3.07	0.711756	-0.700
<i>H</i>	0.0	0.0	0.435
<i>CH</i> ₃	3.775	1.230096	0.265
Ethanol (OPLS) (Jorgensen, 1986):			
<i>O</i> (<i>COH</i>)	3.07	0.711756	-0.700
<i>H</i>	0.0	0.0	0.435
<i>CH</i> ₂	3.905	0.493712	0.265
<i>CH</i> ₃	3.905	0.732200	0.0
DMSO (P2) (Luzar and Chandler, 1993):			
<i>S</i>	3.4	0.99741	0.139
<i>O</i>	2.8	0.29922	-0.459
<i>CH</i> ₃	3.8	1.230	0.160
Acetone (Wheeler and Rowley, 1998):			
<i>O</i>	3.01	0.70669	-0.540
<i>C</i>	3.78	0.41570	0.48
<i>CH</i> ₃	3.88	0.681748	0.03

with periodic boundary conditions and the *reaction field* methodology (Neuman, 1986b) with the choice $\epsilon_{RF} = \infty$, to account for the long-range electrostatic interactions. The reaction field and Lennard-Jones cut-off length is 10.26 Å, and a nearest neighbor list technique (Allen and Tildesley, 1989), with a cut-off radius of 11.1 Å, has been also employed. For the viscosity computations, an equilibration run of 100 ps has been done prior to each 10 ns production runs, to eliminate any memory of the initial conditions. On the other hand, at least 20 ns simulation was run for the thermal conductivity computations. In addition, to generate the thermal gradient in the NEMD calculations, we have chosen an exchange particle momentum frequency of 0.0025 fs⁻¹. An equilibration run of about 500 ps has been established to reach the suited linear temperature profile.

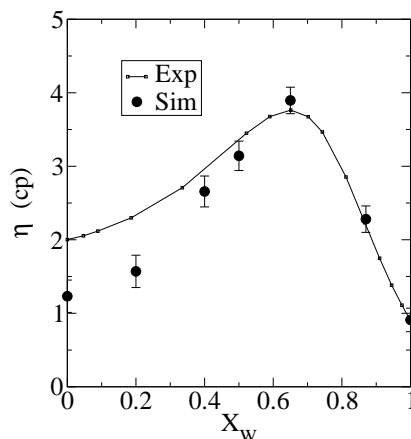


Figure 3.2. Shear viscosity of mixture of water+DMSO at 298 K and 1 atm. Experimental values are from ref.(Cowie and Toporowski, 1961).

4. Results and Discussion

In this section, the dynamic behavior of mixtures of a) water+methanol, b) water+ethanol, c) water+DMSO and d) water+acetone are presented. In particular, the shear viscosity as well as the thermal conductivity is calculated from our simulations and the results are compared with the available experimental data. In addition we discuss the possible relationship between the local structure of the three-dimensional network of the water molecules and the survival probability of hydrogen bonds with the non-ideal behavior displayed by the transport coefficients analyzed here.

4.1 Shear viscosity

The viscosity of mixtures of water and DMSO at 298 K as a function of the molar fraction of water is given in Figure 3.2. The general agreement between simulations and experimental measurements (Cowie and Toporowski, 1961) are good, except for the concentrated DMSO solutions, where significant deviations are found. Regarding the pure component behaviors, we have reproduced the value of 0.91 cp for the viscosity of SPC/E water model reported by Smith (Smith and van Gunsteren, 1993) *et. al.* at 300 K (obtained using the Einstein formula with a reaction field constant of $\epsilon_{RF} = \infty$). On the other hand, the viscosity predicted for pure DMSO by means of the P2 model is found to underestimate the corresponding experimental value ($1.23 \pm 0.14\text{ cp}$. vs. the experimental datum 2.003 cp). This fact is consistent with the observations of

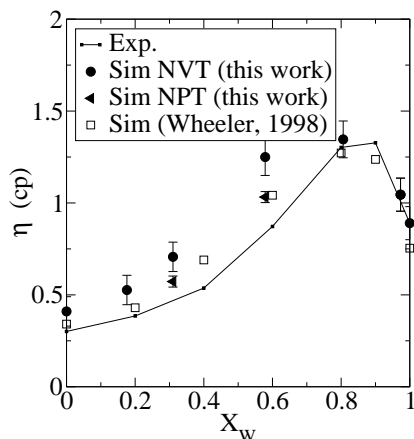


Figure 3.3. Shear viscosity of mixture of water+acetone. Our simulations were done at constant density at 298 K (*NVT*) and only two points were computed at constant pressure at 298 K and 1 atm (*NPT*). Our results are compared with the values obtained by Wheeler *et al.* (Wheeler and Rowley, 1998). Experimental values for the viscosity are from ref.(Noda *et al.*, 1982).

Borin *et al.* (Borin and Skaf, 1999), who reported a discrepancy of about the 67% between the experimental and computed self-diffusion coefficient of DMSO, for solutions of water in DMSO with $x_W < 0.5$. The self-diffusion coefficient predicted with the P2 model is higher than the experimentally obtained. Therefore, since our discrepancy of about 62% in the viscosity of pure DMSO, we can see that $D_{exp} \eta_{exp} \simeq D_{sim} \eta_{sim}$. We can then conclude that an exceeding mobility of the P2 model in a pure system would explain both discrepancies between the observed and calculated self-diffusion and viscosity coefficients at the same time.

Even though, the most remarkable characteristics of our results is that the simulations are capable of quantitatively reproducing the enhancement of the viscosity of the mixture, with a maximum around a molar fraction of $x_W = 0.65$ ($\eta_{sim} = 3.815 \pm 0.18$ cp, compared to $\eta_{exp} = 3.764$ cp). Since the simulation underestimates the viscosity of the pure component, this agreement between data would then imply that the crossed interactions in the mixture are overestimated for the models at these compositions, as it has already been pointed out by Borin (Borin and Skaf, 1999).

Other aqueous solutions also shown an enhancement of the viscosity of the mixture with respect to that of the pure components. This fact is particularly noticeable in the case of associating fluids like alcohols or substances that are hydrogen bond acceptors, such as ketones and sulfoxides, among others. The DMSO can be considered as a hydrogen bond *acceptor* since can only establish

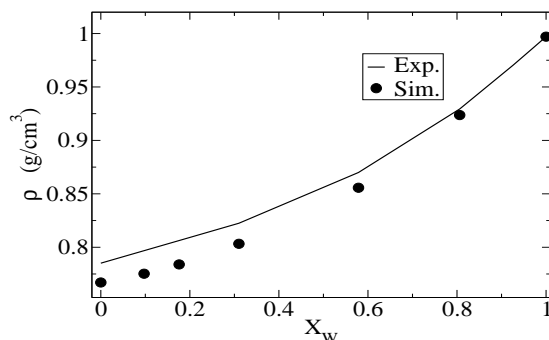


Figure 3.4. Comparison of the experimental density of the mixture of water+acetone (Griffiths, 1952) at 298 K and 1 atm with that obtained with the simulations at same condition using the SPC/E (Berendsen et al., 1987) model for water and the model of Wheeler *et al.* (Wheeler and Rowley, 1998) for acetone.

hydrogen bonds between the hydrogen atom of the water molecule and the oxygen atom of the sulfoxide group. Water and alcohols can form hydrogen bonds from both the hydrogen as well as the oxygen atom being, therefore, *donor* and *acceptor* at the same time. Mixtures of water and hydrogen bond acceptor substances show in general a good agreement between experimental and simulation data (Wheeler and Rowley, 1998, Slusher, 2000). In Figure 3.3 the variation of the viscosity of the mixture water+acetone at 298 K and 1 atm as a function of the molar fraction of water is observed. The agreement of our simulation at NVT is also good in comparison with the experimental data. However, the values reported by Wheeler *et al.*, obtained from non-equilibrium simulations with Lees-Edwards *sliding brick* boundary conditions in *NVT* ensemble, presents better agreement than our results at constant temperature. Even though, as it was commented in the computational details section, the Wheeler's model does not reproduce the experimental density (Griffiths, 1952) at 298K and 1 atm. This drawback of the model produces a too high pressure in the system if the experimental density is employed, giving an overestimation of the viscosity.

In addition, in Figure 3.3 we also compute the shear viscosity in *NPT* ensemble giving similar results as those of Wheeler, but we observe that the density of this two points are much lower than the experimental values (we obtain $0.803 g/cm^3$ and $0.856 g/cm^3$ for $x_w = 0.31$ and $x_w = 0.579$ that are lower than the corresponding experimental values of $0.8225 g/cm^3$ and $0.870 g/cm^3$ respectively). Also lower values than the data used by Wheeler *et al.* in their work. For instance, to show the differences in the density of the mixture predicted by the model, in Figure 3.4 we have computed the density of the mixture at 298 K and

1 atm at different compositions and compare our results with the experimental data. Important deviations can be observed at lower water concentrations.

Apart from the differences between our work and that of Wheeler, we have obtained good agreement on the viscosity of the mixture employing the Einstein's relation with equilibrium molecular dynamics simulations and, additionally, the enhancement of the viscosity at lower solute concentration is also well reproduced. Our results, despite the deficiencies of the employed models of DMSO and acetone, are in good agreement with the experimental data, following the observation that the viscosity of aqueous systems with solutes that are acceptors of HB are well reproduced in simulations. However, simulation data on binary mixtures where both species are simultaneously hydrogen bond *donors* and *acceptors* (water-alcohol, for instance) do not show such a good agreement when compared with experimental results in a wide range (Wheeler and Rowley, 1998, Slusher, 2000).

This enhancement of the viscosity has been attributed to changes in the three-dimensional structure of water occurred by the addition of a solute. For example, in the work of Wheeler *et. al.* (Wheeler and Rowley, 1998) in the case of acetone-water and methanol-water, basing their analysis on the work of Ferrario (Ferrario *et al.*, 1990) *et. al.*, the authors argue that the enhanced acceptor character of the methanol and acetone molecules disturb the tetrahedral coordination structure of water molecules. Such disturbed environment causes a decrease in the rotational relaxation time of the water molecules, yielding a higher rigidity of the system (Venables and Schmuttenmaer, 2000, Borin and Skaf, 1999). This argument would then be also valid for the case of water+DMSO.

Aiming at further exploring this hypothesis we have computed the variation of the tetrahedral order parameter q referred to the oxygen atoms around a given water molecule, as described in chapter 2. In Fig.3.5 the variation of q as a function of the molar fraction of water in methanol, DMSO and acetone mixtures are presented. In this figure, a maximum in the tetrahedrality is observed for pure water. The value of q decreases by the addition of any solute, up to a minimum, specific for each mixture. Such a minimum is, for instance, around $x_w \simeq 0.2$ for water+methanol, around $x_w \simeq 0.3$ for water+acetone, and at $x_w \simeq 0.4$ for water+DMSO. For smaller water molar fractions, q increases up to the residual value similar to that of a Lennard-Jones liquid like Argon (Nieto-Draghi *et al.*, 2003b), as it would be seen from one water molecule, except for the case of methanol, where small variation of this parameter is observed. Then, it is clear that methanol molecules introduce less perturbation on the local structure of water than the other two molecules. This effect can be related with two facts, first of all the size of methanol molecules is smaller than that of the other two, and second, methanol is a donor-acceptor solute

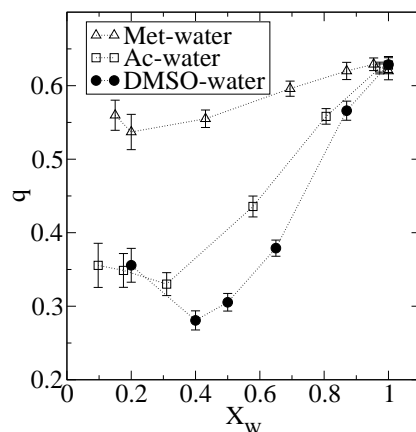


Figure 3.5. Variation of the tetrahedral order parameter q in function of the water concentration in the system at 298 K. Lines are only guides for the eyes.

and, hence, it can be inserted in the local network of water, contrary to DMSO and acetone which are merely acceptors of hydrogen bonds. From $x_w \simeq 0.65$ and down for the case of DMSO, the presence of aggregates with the structure 1DMSO:2water has been experimentally reported (Soper and Luzar, 1992). The formation of these aggregates strongly competes with the natural tetrahedral arrangement induced by the essential character of water. The formation of such complexes can then explain the minimum in q at molar fractions near the equimolar composition $x_w \simeq 0.5$. Notice, in addition, that this minimum is located near the composition at which the maximum in the density of the mixture is experimentally observed (Cowie and Toporowski, 1961). Similar analysis can be drawn for the acetone, but the differences in size with the DMSO (acetone is much smaller than DMSO) permits to acetone molecule a better insertion on the structure of the water network.

At first sight on Figures 3.2, 3.3 and 3.5 one could think that there is a relationship between the data obtained for the order parameter q and the viscosity coefficient η as a function of the water molar fraction of the mixtures. However, comparing the behavior of the system analyzed here, and sees that the location of the minimum in q and the maximum in η are not apparently correlated (the experimental viscosity of water+methanol (not shown) presents a maximum much spread than the other two systems, and its loci - $x_w \simeq 0.7$ - does not coincide with the minimum in the q parameter). Thus, the analysis of the results in the viscosity coefficient can be done as follows. The increase in the viscosity when $x_w \rightarrow 1$ is due to the effect of the hindrance introduced by the presence of solvent molecules whose volume is much larger than that of the water

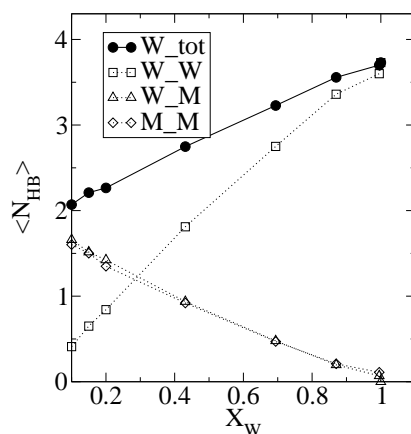


Figure 3.6. Variation of $\langle N_{HB} \rangle$ in function of the water concentration in the system water+Methanol at 298 K.

molecules, in analogy with the viscosity of colloidal suspensions. Fits of the concentration and temperature dependence given in ref. (Bulone et al., 1989) are consistent with this fact: the bigger the solvent molecule is, the larger is the rate of increase of the viscosity as the solute concentration increases. Aqueous mixtures of acetone or methanol have the same behavior, which is consistent with their relative volume (Wheeler and Rowley, 1998) (in addition with this effect, it is important to remember that methanol can form up to two HB and acetone is able to form only one, thus the association between methanol+water is higher than the water+acetone).

For instance, it is important to analyze the behavior of the average number of hydrogen bond $\langle N_{HB} \rangle$ per molecule in function of the molar fraction of water in the mixture for methanol (Figure 3.6), DMSO (Figure 3.7) and acetone (Figure 3.8) at 298 K and 1 atm. A direct analysis of these figures shows that methanol as well as DMSO tends to have in average two HB (taking into account self and cross association in the case of methanol) and, on the other hand, acetone has roughly only one HB per molecule. But the most remarkable aspect is the fact that water-water HB does not behave in a similar way for each mixture. In the case of water+methanol and water+DMSO a straight line is observed in the self-association of water molecules, but in the case of acetone an exponential behavior is observed. This implies that water prefer self-association in the case of acetone, which is a consequence of the fact that acetone are able to accept only one HB. This behavior was also reported by Venables *et al.* (Venables and Schmuttenmaer, 2000) where a detail balance of the different species H-bonded was carried out.

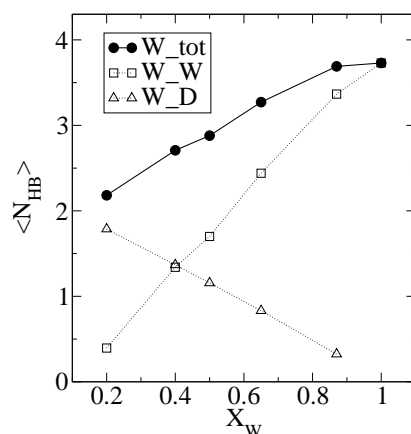


Figure 3.7. Variation of $\langle N_{HB} \rangle$ in function of the water concentration in the system water+DMSO at 298 K.

This difference in the average values of hydrogen bonds seems to have not a direct relation with the dynamical behavior. In fact we have shown (Nieto-Draghi et al., 2003b) in our analysis of chapter 2 that, for pure water that the differences in self-diffusion for the models analyzed are strongly correlated with the order of the local environment (some cage effect in Figure 2.11) and not with the average value of the hydrogen bonds in the system (Figure 2.12). Moreover, it is difficult to ensure something taking into account the arbitrariness of the HB definition employed (or any other one). Hence, the amount of HB that each species is able to form is not straight forwardly related with the relative values of the viscosity. In fact, water molecules have, in average $\langle N_{HB} \rangle \simeq 3.7$, much higher than the methanol molecule $\langle N_{HB} \rangle \simeq 1.98$ but, on the other hand, its viscosity is only 18 % higher. Additionally DMSO has no self-association and its viscosity is almost 2.3 times the viscosity of water.

Thus, the effect of the local structure and the $\langle N_{HB} \rangle$ cannot explain (alone), however, the continuous rise of the viscosity of the mixture up to solute molar fractions about 35% ($x_w \simeq 0.65$), as observed in the DMSO-water systems, or the increment observed at 10% ($x_w \simeq 0.90$) for the water+acetone mixture. It has been mentioned in previous paragraphs that the loss of local tetrahedral order can cause an increase of the local rigidity of the water molecules with respect to *more symmetrical* less rigid structures, even far from the perturbation caused by the solute. Venables *et al.* (Venables and Schmuttenmaer, 2000) suggest a possible mechanism, where water molecules in the solution start to adopt chain-like structures at different compositions and, then, long-lived HB slow down the dynamics of the system. Thus, an indirect mea-

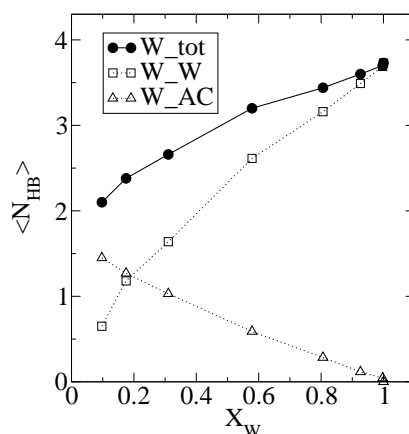


Figure 3.8. Variation of $\langle N_{HB} \rangle$ in function of the water concentration in the system water+Acetone at 298 K.

surement of this *rigidity* can be studied through the analysis of the dynamical behavior of the different HB present in the mixture, more than the average values of this property itself.

In Figure 3.9 we have computed the life-time of continuous hydrogen bonds formed in the mixture for a) water-water and b) water-solute interactions for the water+methanol, water+DMSO and water+acetone at 298 K and 1 atm as a function of the molar fraction of water in the system. On one hand, the strength of the hydrogen-bond interaction between water and any of the solutes (Figure 3.9.b), justifies the large lifetime observed by these cross bonds, when compared with those of water-water in the same system (Figure 3.9.a). On the other hand, the most interesting feature is the fact that water-water hydrogen bonds in any of the mixtures are indeed much long lived than the equivalent bonds in pure water (even at very high water concentrations), supporting the idea that the distortion of the environment of water molecules is related to the increase of the local rigidity. The existence of chains of water molecules with long-lived hydrogen bonds would then justify such an increase of the viscosity of the mixture (Venables and Schmuttenmaer, 2000). Moreover, separately analyzing each figure, several aspects are worth to be mentioned, for instance, in Figure 3.9.a the water+DMSO presents long-lived HB than the water+acetone and the water+methanol systems respectively. The presence of a maximum in this property for the water+DMSO is pronounced in comparison with that observed in the water+acetone, and the loci of this maximum corresponds with the minimum in q and the maximum in the density for the DMSO. The water+methanol system presents the shorter HB life-times of the systems analyzed here and, though no

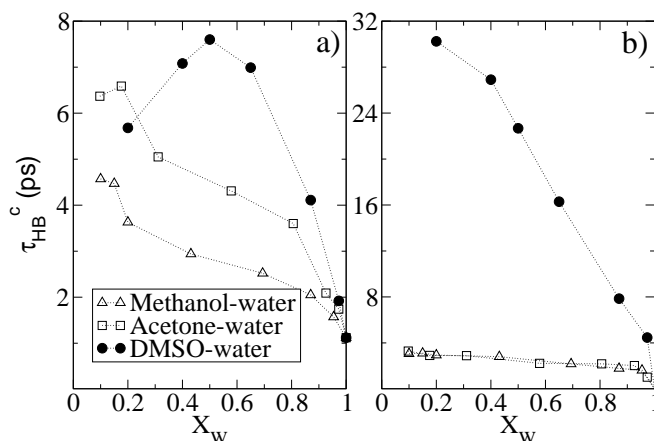


Figure 3.9. Variation of the life-times of continuous H-bond (τ_{HB}^c) with the molar fraction of water at 298 K, for a) Water-water and b) water-solute hydrogen bonds.

maximum is observed, there is a change in the tendency of this property when the minimum in q is observed for this mixture in Figure 3.5.

The behavior observed in Figure 3.9.b is completely different than in the case of water-water interactions. The cross interactions are much long lived for the water+DMSO in all concentrations. It seems that the water+acetone and water+methanol systems presents similar HB lifetimes. One aspect seems to be clear; the fact that the viscosity of the water+DMSO system is greater than the other two systems is clearly reflected in water-water and water-solute interactions. Additionally, the values of the viscosity of water+methanol and water+acetone are very close (at least at the thermodynamic conditions considered in this work -1 atm and 298 K-) and, hence, the water-solute HB lifetimes are also very similar for these systems. Additionally, the ability of the associating solute in inserting into those chains (formed by water+water molecules) or to terminate them, would determine the position of the maximum in the viscosity. Acetone, as a one-HB acceptor acts as a terminator of these *water chains*, while methanol (donor-acceptor) and the DMSO (twice-acceptor) can enter in these chains without breaking them. As a consequence, the maximum in the viscosity of acetone is located very close to $x_w \rightarrow 1$ (Wheeler and Rowley, 1998) while the other two mentioned compounds locate their maxima at about $x_w \rightarrow 0.65$. The differences observed in the value of the maxima of the viscosity can be related to the value of the viscosity for the pure components.

The comparison presented in Figure 3.10 is similar to that done in Figure 3.9 but in this case the intermittent HB are analyzed for the three systems at the same thermodynamic conditions. The relative values of τ_{HB}^i between the

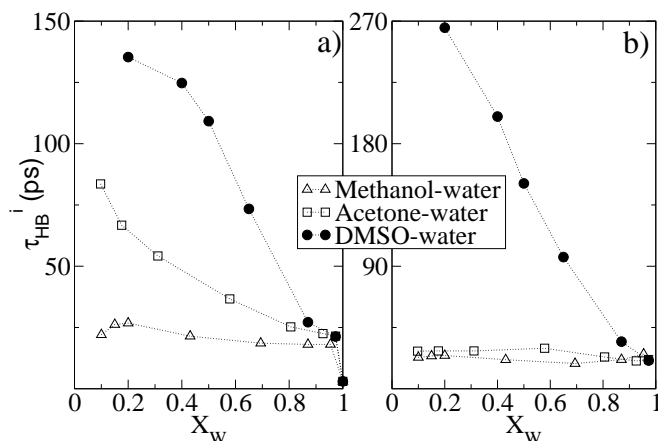


Figure 3.10. Variation of the life-times of intermittent H-bond (τ_{HB}^i) in function of the molar fraction of water at 298 K, for a) water-water and b) water-solute hydrogen bonds.

systems presented in Figure 3.10.a is very similar to that observed in the case of τ_{HB}^c , but different tendency is observed, for instance no maximum is observed for the water+DMSO and water+acetone systems and only a small maximum is observed for the water+acetone system. On the other hand, Figure 3.10.b presents almost the same shape of Figure 3.9.b and only the relative values of τ_{HB}^i makes the difference between them.

Finally, the decrease of the viscosity at lower values of x_w can be then attributed to the loss of this effect by pure stoichiometric requirements even though the life time of H-bonds of water molecules (both, water-water and water-solute) always increase. Although the information contained in q can be useful to understand the internal structure of these mixtures, it does not seem to have a direct relationship with the observed viscosity coefficients, probably because the overall mechanism of the increase of the viscosity is related to the cooperative effect of many molecules, while q only describes a rather local property. Even though, the variation of the life-times of HB bonds preserves the general picture observed in the viscosity of the mixture, *ie.* the greater the τ_{HB} is observed in the system, then, the greater the viscosity coefficients is obtained for the mixture.

4.2 Thermal conductivity

In this section the thermal conductivity of mixtures of water and associating fluids is presented and compared with the available experimental data. To the best of our knowledge the thermal conductivity of pure ethanol, methanol and

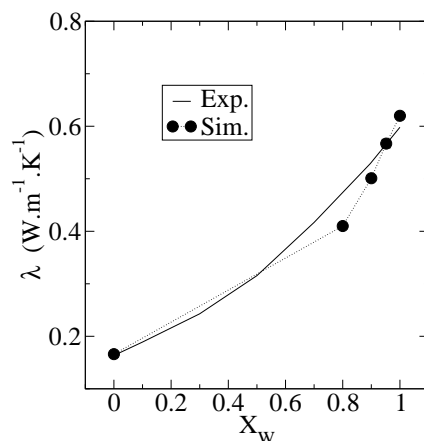


Figure 3.11. Comparison of experimental data of thermal conductivity (Qun-Fang et al., 1997) of water+ethanol at 298.15 K and 1 atm with simulations employing the TIP4P (Jorgensen et al., 1983) model of water and the OPLS (Jorgensen et al., 1984) model of ethanol.

acetone has not been reported before in simulations, and for the case of DMSO neither experimentally nor by simulations, at least under the conditions analyzed in this work. It is also worth to mention that the analysis of the thermal conductivity computed from simulations with aqueous solutions of associating fluids is reported here for the first time. Other analysis were done in ideal solutions employing equilibrium as well as non-equilibrium MD techniques, as was commented in the introduction of this chapter, but simulations of this property with realistic systems is scarce and most of them are dedicated to ideal liquids (Ar-Kr, or mixtures of hydrocarbons). We have computed the thermal conductivity of mixtures of a) water+ethanol, b) water+methanol, c) water+DMSO and d) water+acetone. In Figure 3.11 we present the variation of the simulation results of the thermal conductivity of water+ethanol at 298 K and 1 atm in function of the molar fraction of water and compared with the experimental data of Qun-Fang *et al.* (Qun-Fang et al., 1997). We have obtained a value of $\lambda = 0.166 W.m^{-1}.K^{-1}$ for pure ethanol, which is the same obtained in experiments ($\lambda = 0.1635 W.m^{-1}.K^{-1}$ (Qun-Fang et al., 1997)). On the other hand, in the water rich region some deviations are observed with respect to the experimental data for this property. Even though, the values predicted are very close to the experimental ones within an error of less than 10%. The difficulties presented in this system are the long simulation runs and a large size of the system box, required to have good statistics and to equilibrate the system.

The simulation results for the water+methanol system are shown in Figure 3.12 at 313 K and 1 atm and compared with the values of λ obtained from a

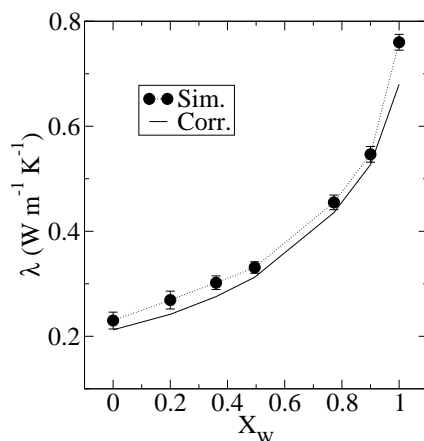


Figure 3.12. Comparison of thermal conductivity predicted with correlations (GOWProp-v5.1, 2002) of water+methanol at 313.15 K and 1 atm with simulations employing the TIP4P (Jorgensen et al., 1983) model of water and the OPLS (Jorgensen et al., 1984) model of methanol.

correlation of a commercial software (GOWProp-v5.1, 2002). These results present better agreement, in almost the whole range of water concentrations, than in the case of the water+ethanol system. We have obtained a value of $\lambda = 0.225 \text{ W.m}^{-1}.\text{K}^{-1}$ for pure methanol, very close to the value predicted in the correlation ($\lambda = 0.2122 \text{ W.m}^{-1}.\text{K}^{-1}$). The most important deviations come from the value of the thermal conductivity of pure water with the TIP4P model $\lambda = 0.76 \text{ W.m}^{-1}.\text{K}^{-1}$ which is known to produce a λ slightly higher than experiments (Bedrov and Smith, 2000). For the rest of compositions we have quantitative predictions for this property with deviations of less than 5%.

For the case of water+DMSO system, the thermal conductivity of the mixture at 298 K and 1 atm can be observed in Figure 3.13. The value obtained in our simulations for pure DMSO is $\lambda = 0.1957 \text{ W.m}^{-1}.\text{K}^{-1}$, which is in the range of that obtained for other similar organic solvents like acetone and acetonitrile ($0.1525 \text{ W.m}^{-1}.\text{K}^{-1}$ and $0.2034 \text{ W.m}^{-1}.\text{K}^{-1}$ (Qun-Fang et al., 1997), respectively). In addition we have further compared our results with the value of the thermal conductivity obtained from the correlation of Bridgman (Bridgman, 1923), which yields an estimate $\lambda = 0.2114 \text{ W.m}^{-1}.\text{K}^{-1}$ for the pure DMSO, which is close to the simulated value.

For the water-DMSO mixtures, due to the lack of experimental data, we have compared our simulation data with results obtained from the mixing rule of Li (Li, 1976), which that allows for an estimate of the thermal conductivity of mixtures of polar molecules at different molar fractions of water. The agreement between the correlation and simulation results is rather good. As a general

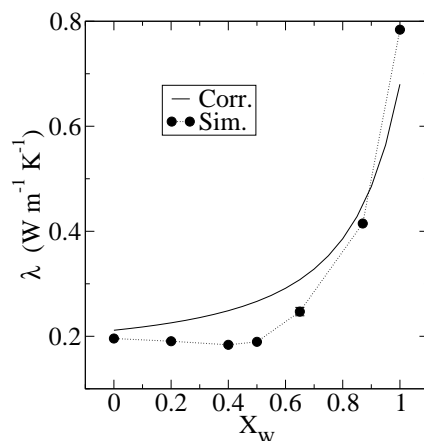


Figure 3.13. Comparison of thermal conductivity predicted with the correlation of Li (Li, 1976) (thermal conductivity estimated for DMSO using the correlation of Bridgman (Bridgman, 1923)) of mixture of water+DMSO at 298 K and 1 atm with simulations employing the SPC/E (Berendsen et al., 1987) model for water and the P2 (Luzar and Chandler, 1993) model of DMSO.

trend, the simulated values are systematically lower than the values obtained from the correlation, except for the case of pure water, where the SPC/E model is known to overestimate the experimental measurements (Bedrov and Smith, 2000). Moreover, it is very interesting to notice the minimum of the thermal conductivity, lying between $x_w = 0.4$ and $x_w = 0.5$, obtained. Mixtures with a minimum in the thermal conductivity have experimentally been reported in the literature (Li, 1976), in particular, for CCl_4 -Tert-butanol mixtures. The mixing rule used here, which also corresponds to this last reference, is a monotonous function of the volume fractions, thus being unable to predict such minimum in the thermal conductivity (Li, 1976). The fact that molecular simulations are model dependent does not allow us to be conclusive about the real existence of this minimum in the thermal conductivity, a matter that can only be experimentally elucidated. However, our results are still a very good estimate of the real value of the thermal conductivity of water-DMSO mixtures, never reported before.

Finally, in Figure 3.14 the variation of the thermal conductivity of the water+acetone with the molar fraction of water is presented at 298 K and 1 atm and compared with the correlation of Li (Li, 1976). We have used the most recent experimental values of this properties taken from the work of Qun-Fang *et al.* (Qun-Fang et al., 1997) at the same thermodynamic conditions. The values predicted in the simulations are in very good agreement with that of the correlation. For the case of pure acetone we have obtained a value of $\lambda = 0.17$

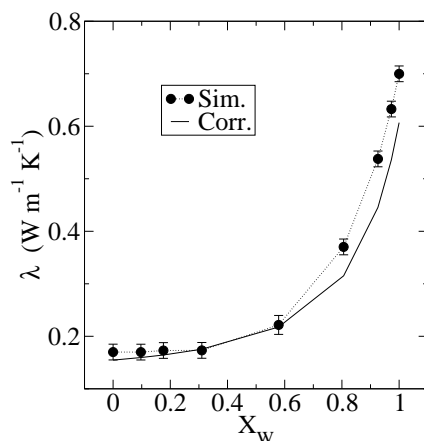


Figure 3.14. Comparison of the thermal conductivity predicted with the correlation of Li (Li, 1976) (and the experimental values of λ for acetone and water taken from ref. (Qun-Fang et al., 1997)) for the mixture of water+acetone at 298 K and 1 atm with our simulations employing the SPC/E (Berendsen et al., 1987) model of water and the model of Wheeler (Wheeler and Rowley, 1998) for acetone.

$W.m^{-1}.K^{-1}$, which is very close to that obtained in experiments at the same temperature ($0.154 W.m^{-1}.K^{-1}$ (Qun-Fang et al., 1997)). As it was comment for the previous simulations of this property the most important deviations are observed in the water rich region due to the deficiencies in the water models.

With regard to the possible relationship between the observed thermal conductivity of the mixture and the microscopic structure as described by q , only general indications can be given. It is firstly remarkable that for the case of water+DMSO the minimum in q is located around the same concentration at which the minimum in λ is seen. This would suggest a relationship between the formation of the aggregates and the loss of efficiency in the transport of energy by longitudinal vibrational modes in the mixture. On the other hand, no specific relationship is observed between λ and q for the other systems.

The increase of the local rigidity of the water does not have any strong effect in the thermal conductivity. However, the loss of the natural tetrahedral order of water by the presence of the solute seems to change the way with which the energy is transferred in the system, giving a major efficiency in the heat transport when the tetrahedral order in water is high. It is interesting to realize that the minimum of λ coincides with the region of larger density and minimum q for the water+DMSO system.

5. Conclusions

In this chapter we have presented a MD simulation study of transport properties of aqueous solutions of water+methanol, water+ethanol, water+DMSO and water+acetone over the entire concentration range. Our computations of the shear viscosity of the mixtures of water+DMSO and water+acetone at 298 K are in qualitative agreement with the experimental measurements, being able to reproduce the remarkable feature of the maximum of the viscosity at $x_W = 0.65$ for the water+DMSO and at $x_w \simeq 0.90$ for the water+acetone mixtures. From a quantitative point of view, we have found that the viscosity of pure DMSO is lower than experimentally found, for concentrations $x_W < 0.6$, although the agreement is very good for water-rich concentrations. This feature reinforces the idea that the P2 model for DMSO displays a relative high mobility that would also explain the calculated high self-diffusion coefficient of this substance at ambient conditions with respect to the experimental value (Borin and Skaf, 1999). Our computations of the viscosity of water+acetone system are in good agreement with the experimental data. However, some discrepancies have been observed with respect to the work of Wheeler *et al.* as far as the viscosity of this system is concerned. We attribute these differences to the fact that the model of acetone is not able to reproduce the experimental density of the mixture. Even though, we have proved that the computation of the shear viscosity of mixtures can be computed employing the Einstein relation in equilibrium MD with similar accuracy with that obtained with non-equilibrium MD (employing boundary driven methods).

As it was previously observed (Skaf, 1999), the behavior of water-DMSO mixtures is similar to that presented by acetonitrile-water and acetone-water in terms of the average number of hydrogen bonds and the general qualitative behavior of the shear viscosity of the mixture. In particular, our analysis of the tetrahedral order parameter q of water molecules indicates the presence of a minimum at different compositions for the case of the particular mixtures studied. For instance, for the water+DMSO the minimum of the tetrahedral order is located at equimolar compositions whose value is lower than the residual value corresponding to a Lennard-Jones liquid. This effect is probably caused by the presence of aggregates of the form 1DMSO:2water whose structure competes with the preferred tetrahedral arrangement of water molecules. This fact suggests that the fluid crosses over different structures that affect in different ways the local order of water molecules and their neighborhood. For the case of the water+acetone mixture, the variation of this parameter presents analogous behavior when the water concentration decreases in the mixture. However, the locus of the minimum is moved to lower molar fractions of water (Nieto-Draghi *et al.*, 2003b). Finally, for the water+methanol system, the variation of q is much less pronounced than in the two previous systems due to the different character

of the methanol molecule, being *donor* and *acceptor* of HB at the same time, but also because its size is smaller than that the other two solutes.

Moreover, we have computed the thermal conductivity of the four systems a) water+ethanol, b) water+methanol, c) water-DMSO and d) water+acetone, and we have observed good agreement when the simulations results are compared with the available experimental data. Some aspects of the quality of the models are reflected in the case of water+ethanol system, where a slightly different slope is observed in λ at low alcohol concentrations. In any case, however, the agreement is within 10 %. For the water+methanol and water+acetone system a quantitative prediction of this property is given, and for the case of water+DMSO, a clear minimum in this property is found at about $x_W = 0.6$ is observed. This kind of minimum in the thermal conductivity has been experimentally observed in other mixtures of associating fluids. The lack of experimental data on the thermal conductivity of water-DMSO mixtures and the fact that the available correlations cannot predict the complex behavior of associating fluids make our simulation results valuable data to estimate the properties of this system.

Finally, together with the obvious interest of the prediction of transport coefficients of fluids of high-applied interest, our work is also intended as a small contribution to the general understanding of the complex structural and dynamic behavior of systems with directional bonds like the hydrogen-bond interactions. In this direction, many questions remain open. For instance, one can mention, on one hand, the need for a clear explanation of the increase of the rigidity of the system when the tetrahedral transient network of water molecules is disturbed by the presence of solute, as it is indicated by the increase of the lifetime of the water-water hydrogen bonds with the increase of the solute molecules. On the other hand, the effect of long-range correlations of hydrogen-bonded molecules in dynamic properties such as the viscosity of the mixture, as well as the ability of the solute to continue or to terminate such chains or clusters of hydrogen-bonded molecules.

The intrinsic difficulties presented in the non-ideal character of these type of mixtures (the effect of the association) and the inconveniences encountered in the computation of the microscopic expression of the heat flux make predictions in this type of systems very difficult. Apart from the technical difficulties of the simulations (already mentioned in the descriptions of the methodologies and coefficients in chapter 1), there is also the problem of a lack of experimental data for this property for the water+DMSO mixtures. Even though, the general behavior of the predictions made suggest that quantitative estimations of transport properties can be achieved by means of molecular simulation employing the different methodologies described in the chapter 2 of this work. This fact

renders molecular simulations as a powerful tool, from an engineering point of view, to make predictions on different properties of systems in the absence of experimental data. The case of the thermal conductivity of the water+DMSO system is a clear example.

Chapter 4

SORET EFFECT IN ASSOCIATING FLUIDS

1. Introduction

The Soret effect is an irreversible process taking place in a mixture of two or more components in a thermal gradient. This effect was first described by Ludwig (1856) (Ludwig, 1856), who observed small differences in the concentration profile of aqueous solutions of Sodium sulphate, which was in a glass heated from below. Independently, Soret (Soret, 1879a) published the first work of thermal diffusion. Later, in 1880 he presents the first systematic analysis of the effect in ionic aqueous solutions (Soret, 1879b, Soret, 1880). Some years before in 1872, Dufour (Dufour, 1872a, Dufour, 1872b) described the inverse process, in which a temperature gradient is observed when a mixture of two gases interdiffuse. The thermal diffusion is usually known as the Soret Effect or Ludwig-Soret effect. With respect to thermal conduction and diffusion the Soret effect is a crossed effect in the sense that it involves a composition gradient as a result of a heat flux. The first attempt to provide a physical explanation of this process was in 1910 from the kinetic theory of gases developed by Chapman and Enskog. This theory was successful in predicting the thermal diffusion observed in dilute gases with differences in their molar masses. The Kinetic theory opened the door for new technologies, which were applied in separation of isotopic mixtures. For instance, the development of thermo-gravitational devices played an important role in the development of the nuclear energy. This technique allowed the study of the Soret effect in mixtures of gases and liquids but, unfortunately, the kinetic theory of gases fails at the limit of dense phases and, consequently, does not predict the behavior of this phenomenon in most of the common liquid solutions.

In 1930 Onsager *et. al* (Onsager et al., 1939) state a phenomenological description of the thermal diffusion process, being this description known as the *Onsager reciprocity relations*. In this theory it was assumed that the corresponding *fluxes* (mass or energy currents) can be expressed as linear combinations of the *gradients* of the local affinities (see eq. 1.43). Additionally, in 1943 the PhD thesis of S. R. de Groot (de Groot et al., 1943, de Groot, 1945) and later in 1948 in the work of Wirtz (Wirtz, 1948), present a physical explanation of the process, considering the Soret effect through an activated diffusion process. It is also remarkable the so-called *forgotten effect* or the initial instability of the Soret effect at short times in which an inversion of the sign of the composition gradient is found at the beginning of the experiments. Later, in 1950 Prigogine *et. al* measured the Soret coefficient in binary liquid mixtures (Prigogine et al., 1950a). These authors also remarked the fact that the Soret coefficient presents a change in its sign for mixtures of cyclohexanol+cyclohexane (Prigogine et al., 1950b), explaining the process through a simple model of active solvent and inert solvent based on the work of Wirtz. This remarkable characteristic in the migration mechanism of the constituents, changing the direction according to the composition, it is only observed in associating fluids. Tichacek *et. al* (Tichacek et al., 1955) also observed a change in the sign of the Soret coefficient for water+methanol mixtures. Later, in 1988 Kolodner *et. al* (Kolodner et al., 1988) published a detailed experimental work on the thermal diffusion of water+ethanol mixtures, using a laser-beam-deflection technique. He observed that the change in the sign of the coefficient was always independent of the average temperature of the experiments (it always occur at approx. $x_{et} = 0.26$). In addition, Piazza *et. al* recently published a set of experiments employing also a laser-beam-deflection technique, where charged colloids present a strong concentration as well as temperature dependence of the Soret coefficient. Here, the sign of S_T can be tuned by varying the Debye-Huckel screening length (Piazza and Guarino, 2002, Piazza, 2003, Iacopini and Piazza, 2003) by changing the ion concentration of NaCl in the solution. Similarly, Wiegand and collaborators employed a Thermal Diffusion Raleigh Scattering (TDRS) technique to solutions of water+ethanol with colloidal particles or poly(ethylene oxide) (Leppla and Wiegand, 2003, de Gans et al., 2003a, de Gans et al., 2003b), finding that the migration of colloidal particles are attached to the migration of the best solvent in the solution. These new and accurate experimental data motivate the interest to understand the process of thermal diffusion from a theoretical point of view and also because a microscopic scope of the process was not clear at all.

The first simulation to determine the Soret coefficient was performed by MacGowan and Evans in 1986 (MacGowan and Evans, 1986a, MacGowan and Evans, 1987) employing NEMD of Lennard-Jones like particles. Their results

were confirmed by Paolini and Ciccotti (Paolini and Ciccotti, 1987). Even on these preliminary studies, the problem of the appropriate definition of the heat flux arisen as one of the cornerstones of the accuracy of the results obtained in simulations. For instance, Vogelsang *et. al* (Vogelsang et al., 1987, Vogelsang and Hoheisel, 1988) employing EMD as well as NEMD, stated the importance of a rigorous definition of the heat flow in multicomponent systems. For instance, in equilibrium molecular dynamics simulations partial molar enthalpies play an important role in the computation of the phenomenological coefficient required determining the Soret coefficient (see the discussion about this point in the methodological part chapter 2, also see appendix E). Although EMD calculations presents the inconvenient that partial molar enthalpies should be introduced in the microscopic expression of the heat flux, in the case of almost ideal solutions, these quantities can be computed through an ideal approximation (Paolini and Ciccotti, 1987). There have been only a few attempts to compute the Soret coefficient in molecular liquids using molecular dynamics. The work of Hoheisel *et. al* (Schaink et al., 1993) on Cyclohexane-benzene mixtures, and $CF_4 - CH_4$ mixtures were the first attempts to compute the Soret coefficient of real systems, but their simulations were not sufficiently large to have a good estimation of the S_T (their correlation function does not converge to zero). Simon and collaborators (Simon et al., 1998, Simon et al., 1999) present the first systematic comparison of simulation and experimental data in alkane binary mixtures, and Perronace *et. al* (Perronace et al., 2002a, Perronace et al., 2002b) make the same comparison for new experimental data of Ar-Kr mixtures and also for n-pentane-n-decane mixtures. In the last case, equilibrium as well as non-equilibrium MD was employed with good agreement with the experimental data.

All these previous works have been done only on ideal (or quasi ideal) solutions. However, there is no single simulation results on associating mixtures, and hence there is no a microscopic study of the role played by the association on the change in the sign of the Soret coefficient, for non-ideal solutions. In this chapter, we have computed the Soret coefficient of non-ideal aqueous solutions of associating mixtures through direct NEMD simulations, to avoid any computation of partial molar enthalpies of the components in the mixture. We have studied mixtures of water plus methanol, ethanol, acetone and dimethyl sulfoxide (DMSO). We have reproduced quantitatively the experimental data (Tichacek et al., 1955, Bou-Ali, 1999, Kolodner et al., 1988, Zhang et al., 1996) of the Soret coefficient for the alcohols solutions, but the most remarkable aspect is that our simulations were able to reproduce the concentration where the change in the sign of the coefficient is experimentally observed. Unfortunately, for the other two systems there is no experimental data available for this transport property and, therefore, our simulations are predictions of the stud-

ied property. Together with the computation of the Soret coefficient we try to provide some qualitative explanation of the behavior of S_T for this type of systems. A reasonable explanation of the change in the sign of the Soret coefficient is given in the theoretical works of Kempers (Kempers, 2001), Haase (Haase et al., 1971), Dougherty and Drickamer (Dougherty and Drickamer, 1955), and Shukla *et. al* (Shukla and Firoozabadi, 1998) that can be generalized to other systems presenting similar phenomenology. In order to support our qualitative picture we have modeled a two dimensional lattice for mixtures of particles through a non-equilibrium Monte Carlo technique, to show that the change in the sign of the Soret coefficient is strongly connected to the nature of cross interactions with respect of those of the pure component. If cross interactions are greater than that of the two pure component interactions, for instance, then a change in the sign will be observed for the Soret coefficient. This fact suggests that mass and volume effects do not determine the value of the sign of the Soret coefficient.

2. Computational details

We have studied the Soret coefficient of aqueous mixtures of methanol, ethanol, DMSO and acetone. In all cases the molar fractions and the size of the simulation box was adjusted to fix the experimental densities of the mixtures, which are summarized in table 3.1 of the chapter 3. The models employed in our simulations were also discussed in the previous chapter and their potential parameters are given in table 3.2.

All models for the molecules considered in this chapter have been treated as composed of several Lennard-Jones sites plus point charges, according to

$$U_{ij} = 4\epsilon_{ij} \left[\left(\frac{\sigma_{ij}}{r_{ij}} \right)^{12} - \left(\frac{\sigma_{ij}}{r_{ij}} \right)^6 \right] + \frac{q_i q_j}{4\pi\epsilon_0 r_{ij}} \quad (4.1)$$

where q_i is the partial charge on site i , ϵ_{ij} and σ_{ij} are the Lennard-Jones interactions between sites i and j on different molecules, being $r_{ij} = |\mathbf{r}_j - \mathbf{r}_i|$ the separation distance between the corresponding sites. Crossed interactions were computed through Lorentz-Berthelot rules (eq. (1.83)) for the water+DMSO and water+acetone, while geometric average (eq. (1.85)) has been employed for the water+alcohol systems.

We have performed all Molecular Dynamics simulations with the constant temperature PeX (momentum exchange algorithm) nonequilibrium molecular dynamic scheme. Details of the algorithm have been given in chapter 1 (addi-

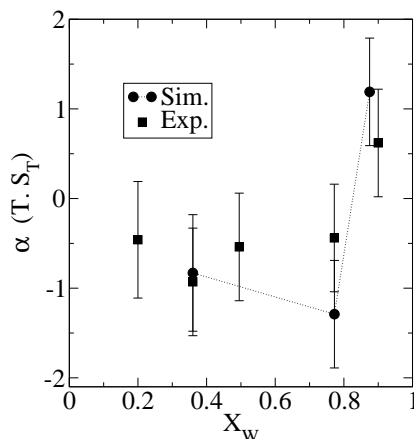


Figure 4.1. Comparison of the thermal diffusion factor α for the mixture water+methanol at 313 K and 1 atm with the experimental data of (Tichacek et al., 1955).

tional information can be obtained in Appendix E (Nieto-Draghi and Avalos, 2003)). Simulations were carried out with 500 molecules for the water+DMSO and water+acetone systems, whereas 800 molecules have been employed for the case of the water+methanol and water+ethanol systems to improve statistics. A parallelepiped box was employed to determine the Soret coefficient via non-equilibrium simulations. We have chosen $l_z = 2l_x = 2l_y$, with l_x, l_y, l_z being the dimensions of the box. The alcohol water systems were simulated employing the *mdgen* code (mdg, 2003) (which can handle the flexible molecules of ethanol), while our code has been employed for the other two mixtures. The equations of motion were integrated with a time step of 2 fs. All the simulations have been performed with periodic boundary conditions and the *reaction field* methodology (Neuman, 1986b) with the choice $\epsilon_{RF} = \infty$, to account for the long-range electrostatic interactions. The reaction field and Lennard-Jones cut-off length is 10.26 Å, and a nearest neighbor list technique (Allen and Tildesley, 1989), with a cut-off radius of 11.1 Å, has been also employed. At least 25 ns simulation was run for the computation of the Soret coefficient for each mixture. In addition, to generate the thermal gradient in the NEMD calculations, we have chosen an exchange particle momentum frequency of 0.0025 fs^{-1} . An equilibration run of about 500 ps has been performed to reach the suited linear temperature profile.

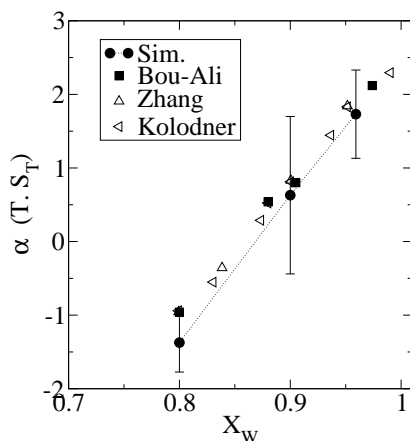


Figure 4.2. Comparison of the thermal diffusion factor α for the mixture water+ethanol at 298 K and 1 atm with the experimental data of Bou-Ali (Bou-Ali, 1999), Kolodner (Kolodner et al., 1988) and Zhang (Zhang et al., 1996).

3. Results and Discussion

In this section we present the simulation results for the thermal diffusion factors (as defined in chapter 1) of the four mixtures analyzed. Our results are compared with the available experimental data for the water+alcohol systems. Unfortunately, there is no experimental data for the other two systems, however, because they belong to the case of associating fluids, we believe that they should behave as water-alcohol mixtures. Additionally, we present the simulation of the lattice model of mixtures of particles computed with the non-equilibrium MC discussed in the fundamental section of this chapter.

In Figure 4.1 we present the variation of the thermal diffusion factor for the mixture water+methanol as a function of the molar fraction of water at 313 K and 1 atm. Our simulations are compared with the experimental data of Tichacek *et. al* (Tichacek et al., 1955) at the same thermodynamic conditions. Despite the fact that our simulations suffered large fluctuations (also found in previous calculations of the Soret coefficient in other mixtures (Simon et al., 1998, Simon et al., 1999, Perronace et al., 2002a)) of about 30%, our simulation results agree with the experimental data within the error of both quantities. Moreover, taking into account the difficulties associated with the computation of the Soret coefficient using molecular dynamics, we consider that there is a remarkable agreement between experimental and simulation results. The change in the sign of the Soret coefficient is observed between 80% and 95% of molar concentration of water for both, experiments and simulations. Contrary to

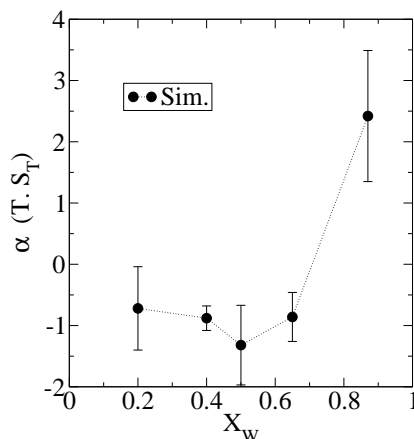


Figure 4.3. Prediction of the thermal diffusion factor α for the mixture water+DMSO at 298 K and 1 atm.

mixtures of non-associating fluids, where a weak concentration dependence of thermal diffusion is observed (for example, mixtures of *n*-pentane and *n*-decane (Perronace et al., 2002a)), in this case the variation of α at water rich regions changes substantially. It is important also to show that α remains negative and almost constant at $x_w < 0.8$. This fact implies that there is no substantial change in the degree of separation of the constituents when the concentration of water decreases. It is remarkable that our simulations are able to reproduce this particular behavior.

Since the difference in size between methanol and ethanol are small, we expect that their thermal diffusion factors in water solutions will be also similar. Effectively, on Figure 4.2 we present the variation of the thermal diffusion factor for the mixture of water+ethanol in function of the molar fraction of water at 298 K and 1 atm. Our simulation results are compared with the experimental data taken from the PhD thesis of Bou-Ali (Bou-Ali, 1999) and previous works (Kolodner et al., 1988, Zhang et al., 1996) at the same thermodynamic conditions. In this case the agreement with the experimental data is even better than in the previous mixture, and the region where the change in the sign of α is observed is also well reproduced. Contrary to the Tichacek's data, which was published in 1956 (Tichacek et al., 1955), the experiment for ethanol are more recent (1999) and the technique employed in the last case was successfully tested (Bou-Ali et al., 1998). The change in the sign of the Soret takes place between 80% and 90% of molar fraction of water. Unfortunately, the long simulation times required to have linear concentration profiles for the water+ethanol system was one of the main difficulties to compute more simulation points;

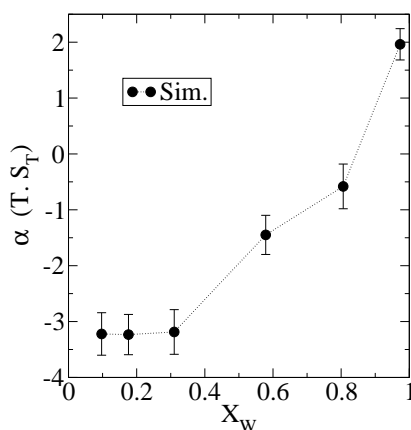


Figure 4.4. Prediction of the thermal diffusion factor α for the mixture water+acetone at 298 K and 1 atm.

even though, we consider that our results for this mixture are very good. In view of Figure 4.1 and Figure 4.2, we can observe that the values of α obtained in both cases are quite similar, though the water+ethanol system presents large separations in comparison to the water+methanol system. Additionally, the concentration where the change in the sign of the Soret coefficient is observed is within the same low solute concentration range in both cases.

In Figure 4.3 we present the prediction of the variation of the thermal diffusion factor for the mixture of water+DMSO in function of the molar fraction of water at 298 K and 1 atm. Unfortunately, there is no experimental data of thermal diffusion for this mixture, but taking into account the accuracy of the methodology employed in the two previous mixtures we consider that our predictions are good approximations of the real ones. It would be interesting to have experimental measurements of the Soret effect for this mixture, particularly if one takes into account the non-ideal behavior observed for this mixture for other transport properties discussed in chapter 3.

We can further compare our simulation results with the values obtained with the previous two components. The change in the sign is observed between 70% and 80% of water, slightly less concentrated in water than in the two previous cases. But, in general, the results are very similar to the values obtained for water+methanol and water+ethanol. For example, the value of the thermal diffusion factor also remains constant for water concentrations lower than 65%, as it was observed for the case of the water+methanol mixture.

Finally, in Figure 4.4 we have computed the thermal diffusion factor for the mixture of water+acetone in function of the molar fraction of water at 298 K and 1 atm. In this case we were also unable to find experimental data of thermal diffusion for this mixture to compare with our simulation results. However, some aspects are worth to be mentioned. The change in the sign of the Soret coefficient is observed at the same range as in the water+alcohol mixtures, *i.e.* between 80% and 90%. On the other hand, there are some differences between these two mixures. In particular, the value of α in the water diluted zone is higher than all of the previous cases, being almost three times larger. Apart from this numeric difference; the value of the coefficient also reaches a constant value in the region of low water concentration. It would be interesting to also have experimental data of this mixture to compare with the predictions done here for this mixture.

3.1 Lattice model of a mixture of particles

We consider a simple two-dimensional lattice model of an incompressible binary mixture of two species, 1 and 2. Each lattice position is either occupied by molecules of the type 1 or 2, and the total number of molecules $N_{tot} = N_1 + N_2$ are equal to the total number of available positions in the lattice M (no vacancy places are allowed so no thermal dilatation effects are described). Furthermore, it is important to realize that N_1 and N_2 are constant during the process. The size of the lattice is fixed by $M = l_x l_y$, being l_x and l_y the number of positions in the x and y direction. In the model only adjacent molecules interact via pair energies, ϵ_{11} , ϵ_{22} for pure components, and for cross interactions a Lorentz-Berthelot like combining rule is employed,

$$\epsilon_{12} = c_1(\epsilon_{11} \cdot \epsilon_{22})^{1/2} \quad (4.2)$$

where c_1 is a positive constant (c_1 should be positive to avoid phase separation) employed to tune the strength of crossed interactions. We can define the Hamiltonian of the system according to

$$H = \frac{1}{2} \sum_{i,j \in (nn)} \sigma_i \cdot \vec{J} \cdot \sigma_j \quad (4.3)$$

where σ_i is a vector which describes whether a site is occupied by a particle of type 1, $\sigma_1 = (1, 0)$, or type 2, $\sigma_2 = (0, 1)$, and $i, j \in (nn)$ means that the sum

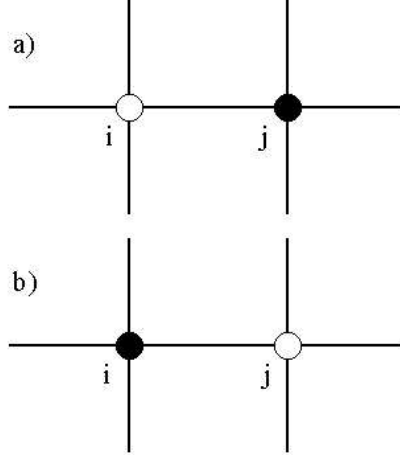


Figure 4.5. Schematic representation of two particles chosen to be interchanged in the lattice. a) The state A before the switch process and b) the state B after the switch process.

is done over the nearest neighbors. The interaction matrix $\bar{\mathbf{J}}$ defines all possible particle-particle interactions

$$\bar{\mathbf{J}} = \begin{pmatrix} \epsilon_{11} & \epsilon_{12} \\ \epsilon_{21} & \epsilon_{22} \end{pmatrix} \quad (4.4)$$

with $\epsilon_{12} = \epsilon_{21}$. The interactions are restricted to nearest neighbors, and we will use a square lattice for now on. In order to avoid phase separation the restriction $\epsilon_{11} + \epsilon_{22} < 2\epsilon_{12}$ is imposed. For normal fluids crossed interactions follows the rule $\epsilon_{11} < \epsilon_{12} < \epsilon_{22}$ but, for our purposes the choice of appropriate values of the constant c_1 in eq. (4.2) ensures that $\epsilon_{11} < \epsilon_{12}$ and $\epsilon_{22} < \epsilon_{12}$. With this particular strong-crossed interaction it is possible to mimic the role played by the hydrogen bonds in aqueous mixtures of alcohols, ketones and sulfoxides.

To introduce a non-equilibrium situation, the simplest choice is to set a given temperature at each site, according to a linear law of the form

$$T(i) = \frac{T_{hot} - T_{cold}}{l_x} \cdot x(i) + T_{cold} \quad (4.5)$$

where T_{hot} and T_{cold} are the hot and cold temperatures at the boundaries in x direction. $T(i)$ is the temperature at site i , located at the space point $(x(i), y(i))$. Once the temperature on each point in the lattice is defined and the energetic interaction between particles is established, the movements of particles are done

by simple switch between neighboring particles. For instance, in Figure 4.5.a we observe a schematic representation of the system in a hypothetical state A , before the switching process, and in Figure 4.5.b, the system is in the state B , after the interchange. The detailed balance condition states that, in equilibrium,

$$P_{eq}(A) \cdot W(A \rightarrow B) = P_{eq}(B) \cdot W(B \rightarrow A) \quad (4.6)$$

where $P_{eq}(A)$ and $P_{eq}(B)$ are the equilibrium probabilities of the system to be on the overall state A or B represented by a realization of all the vectors σ_i . $W(A \rightarrow B)$ is the transition probability of the forward process in the system passing from state A to state B , in a given Δt while $W(B \rightarrow A)$ is the opposite backward transition probability. The equilibrium probability of the state A at temperature T is given by

$$P_{eq}(A) \propto e^{-H(A)/kT} \quad (4.7)$$

where $H(A)$ is given by eq. (4.3). According to this, in equilibrium the transition probabilities have to satisfy the relation

$$\begin{aligned} \frac{W(A \rightarrow B)}{W(B \rightarrow A)} &= \frac{P_{eq}(B)}{P_{eq}(A)} = \frac{e^{-H(B)/kT}}{e^{-H(A)/kT}} \\ &= e^{-(H(B)-H(A))/kT} \end{aligned} \quad (4.8)$$

according to eq. (4.6). Notice that the exponent express the difference in energy by a switch between stated A and B . Therefore,

$$H(B) - H(A) = (E_i(B) - E_i(A)) + (E_j(B) - E_j(A)) \quad (4.9)$$

where, i and j are the particles that are switched in the process, $E_i(A)$ being

$$E_i(A) = \sum_{k \in (nm)} \sigma_i(A) \cdot \bar{\mathbf{J}} \cdot \sigma_k(A) \quad (4.10)$$

The transitions probabilities in the non-equilibrium situation is chosen to be

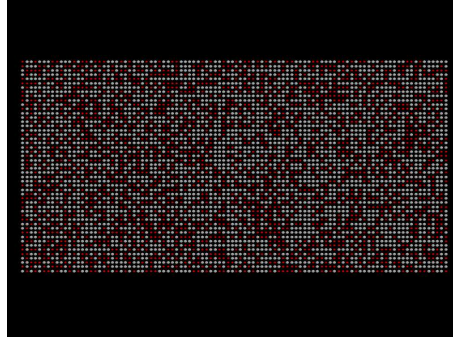


Figure 4.6. Schematic representation of the lattice simulation of a equimolar mixture of 5000 particles computed with Non-equilibrium MC.

$$W(A \rightarrow B) = \min \left[e^{-((E_i(B)-E_i(A))/kT_i+(E_j(B)-E_j(A))/kT_j)}, 1 \right] \quad (4.11)$$

The Metropolis rule (Frenkel and Smith, 1996) can be employed to accept or reject any attempt of switching particles in the lattice. Firstly, a particle in the lattice is selected randomly, and then one of its four neighbors is randomly selected for the switch. To accept the movement, a random number ζ is generated uniformly on the interval $(0, 1)$. The random number is compared with $W(A \rightarrow B)$, and if $\zeta < W(A \rightarrow B)$ then the switch is accepted, otherwise the attempt of interchange is refused. A schematic representation of the lattice can be seen in Figure 4.6

For all simulations with the lattice model, we have used 5000 particles of the two types (1 and 2) with a temperature gradient of 100 K with 300 K of average temperature. We have performed 1×10^4 MC steps to have linear concentration profiles and 5×10^7 steps to compute the appropriate averages. Finally, after an equilibration period, a concentration profile is observed in the lattice in the x direction. In all cases eq.(1.49) has been employed to compute the Soret coefficient, with the molar fraction here defined as $x_1 = N_1/N_{tot}$.

In Figure 4.7 we show the variation of the thermal diffusion factor with the molar fraction of particles of type 2. In this figure we have tuned crossed interactions through varying the constant c_1 of eq. (4.2) which modifies the cross interactions, with different values 0.707, 1.0, 1.414 and 1.8. The normal Lorentz-Berthelot rule is obtained with $c_1 = 1.0$. It is clear from Figure 4.7 that changing the cross interaction the thermal diffusion factor suffer a strong variation. Particularly, the change in the sign is possible if $c_1 > 1.414$ (for the particular case of $\epsilon_{11} = -2000$ J/mol and $\epsilon_{22} = -1000$ J/mol, but the argument is valid for any other set of parameters). This means that whenever the cross

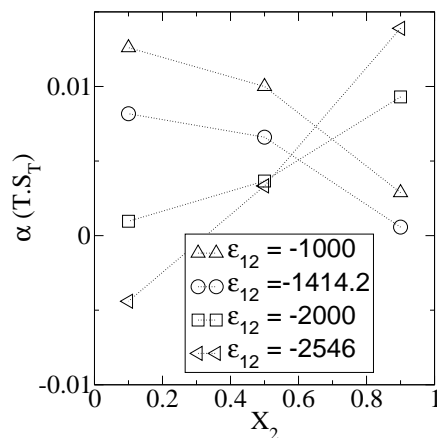


Figure 4.7. Thermal diffusion factor α for the mixture of particles in function of the molar fraction of one component varying the cross interactions. The pure component interactions are $\epsilon_{11} = -2000$ and $\epsilon_{22} = -1000$, the mixture interactions are computed through $\epsilon_{12} = c_1(\epsilon_{11} \cdot \epsilon_{22})^{1/2}$.

interactions are larger than pure interactions, for instance ϵ_{11} and ϵ_{22} , then a change in the sign in the thermal diffusion will be observed. The change in the sign of the slope of α versus x_2 is negative when $\epsilon_{12} < (\epsilon_{11} + \epsilon_{22})/2$ and positive in the opposite case.

This behavior can be understood in the following way. If crossed interactions are stronger than pure interactions, the minor component, for example 1, will tend to concentrate in the cold region due to the fact that this will lower the total energy of the system. Due to the dilute character on the solution on component 1, only cross interaction ϵ_{12} will compete with the pure interaction of the other constituent ϵ_{22} . On the other hand, if the concentration of 1 increases at the point to be the majority, then the constituent 2 will also tend to concentrate in the cold region for the same energetic considerations. In this case, the thermal diffusion factor changes its sign when the concentration of the mixture is changed between these two limiting cases. It is important to remark the fact that there is no mass effect at all in these computations. We want to insist on the point that the sign inversion of the Soret coefficient is not possible if there are only mass or volume differences between the components in the mixture. Differences in mass and volume between the molecules in the mixture have been exhaustively discussed in previous works (Reith and Muller-Plathe, 2000), and hence no further discussion about this point will be done here.

The role played by the strong cross interaction in the lattice model is definitely similar to the role played by the hydrogen bonds in aqueous solutions of

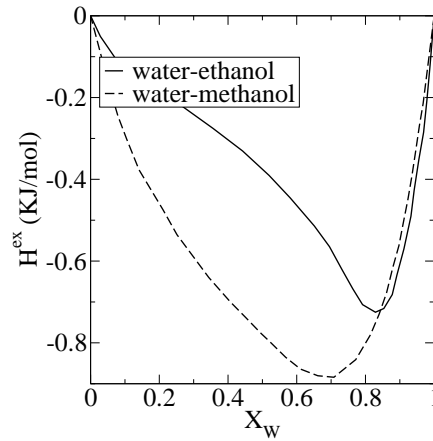


Figure 4.8. Excess enthalpy of mixing for the systems water+methanol and water+ethanol at 298 K and 1 atm. Experiments come from reference (Ness, 1989, Raddzio and Tomaszkiwicz, 1986)

associating fluids. This is an expected result since hydrogen bonds introduce non-ideality in the mixtures. For example, in figure 4.8 the excess enthalpy of mixing for the water+methanol and water+ethanol is given at 298 K and 1 atm. It is clear from the figure that the strong non-ideality of the mixture is reflected in the high negative excess enthalpy of mixing. Notice, in addition, that the concentrations where the minimum in H^{ex} is observed for both systems is similar to the concentrations where the thermal diffusion factor changes its sign. It is worth mentioning that the slope of the excess enthalpy of mixing dH^{ex}/dx_w is related with the difference of the partial molar enthalpies $\bar{h}_w - \bar{h}_{et,met}$. It seems rather likely that the sign of $\bar{h}_w^{ex} - \bar{h}_{et,met}^{ex}$ is strongly related to the sign of the sorlet coefficient. Several theories attempt to predict the value of α employing this kind of thermodynamic quantities (see for instance references (Kempers, 2001, Haase et al., 1971, Dougherty and Drickamer, 1955, Shukla and Firoozabadi, 1998)).

Additionally, in Figure 4.9 we have computed the thermal diffusion factor for the lattice model of the mixtures of particles with cross interaction greater than self-interactions. The ratio between $\epsilon_{22}/\epsilon_{11}$ has been tuned in this case. It is observed that the concentration where the inversion takes place is proportional to the ratio of self-interactions of pure components. For instance, if $\epsilon_{22} > \epsilon_{11}$, then the change in the sign will occur at the higher concentrations of component 2.

A direct connection with the behavior observed on the true systems, presented in Figures 4.1, 4.2, 4.3 and 4.4, can be done. Associating fluids, consequently,

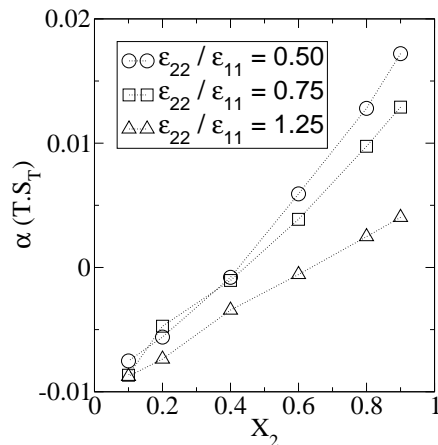


Figure 4.9. Thermal diffusion factor α for the mixture of particles in function of the molar fraction of one component varying the relation of the strength interaction between pure components. Here $\epsilon_{11} = -2000$ and $\epsilon_{12} = -3000$.

presents stronger cross association than self-association. This point was indirectly observed in the fact that cross HB between water and any of the solutes studied here (Figure 3.9.b) are longer lived than water-water HB (showed in Figure 3.9.a, Chapter 3). Consequently, we can clearly state that the strength of the interactions is the main responsible of the change in the sign of the Soret coefficient for the mixtures presented in this work. Additionally, we can also state that the concentrations at which the change in the sign was observed, for the four mixtures analyzed here to the light of the lattice model, implies that water-water interaction is stronger than the solute-solute interaction, something that is, in fact, the case.

4. Conclusions

We have computed in this chapter the thermal diffusion coefficients for aqueous mixtures of methanol, ethanol, DMSO, and acetone through non-equilibrium molecular dynamics simulations. For the case of the alcohol mixtures, we have observed a good agreement between our simulation results and the available experimental data, even quantitatively. For the other two systems we were unable to find experimental data to confirm our predictions of the Soret coefficient. However, we believe that the simulations performed in this work are good estimations of this property for these mixtures at the thermodynamic conditions studied here. It would be of great interest to have a set of experimental data for these two systems to corroborate our results. After a careful

analysis of the results presented in the previous section of this chapter, some important conclusion arises from the discussion.

Simulations of the thermal diffusion factor for the mixture of water+methanol at 298 K and 1 atm has been compared with the experimental data of Tichacek *et. al* (Tichacek et al., 1955) in Figure 4.1 obtaining a good agreement. Our simulations were able to reproduce qualitatively this property, but, the most remarkable aspect is that the concentration where the change in the sign is experimentally observed (between 80% and 95% of molar concentration of water) was also reproduced by our simulations. Additionally, the fact that α remains almost constant at lower molar fractions of water is also observed in our simulations.

In a similar way, simulation results for the mixtures of water+ethanol at 298 K and 1 atm were also compared with the experimental data (Bou-Ali, 1999, Kolodner et al., 1988, Zhang et al., 1996) in Figure 4.2 obtaining an excellent agreement. This agreement is remarkable taking into account the difficulties involved in the computations of this kind of crossed effects. For this system similar concentration range for the change in sign was observed in our simulations (and in agreement with the experiments) between 80% and 90% of molar fraction of water.

For the case of water+DMSO computed at 298 K and 1 atm and showed in Figure 4.3 we can observe a similar qualitative behavior than in the water+alcohols systems. A change in the sign of α is observed between 70% and 80% of water, slightly less concentrated in water than in the other two previous cases. Additionally, the fact that the thermal diffusion factor is almost constant at lower water concentration is also present in this system. Finally, for the case of the mixture of water+acetone at 298 K and 1 atm, the change in the sign of the Soret coefficient is observed at the same range than the previous mixtures, between 80% and 90%. On the other hand there are some differences in this particular case, the value of α in the water diluted zone is higher than all of the previous cases, being almost three times greater.

In general, we can summarize some remarkable aspects of the behavior of the four mixtures presented in this chapter. First of all, the change in the sign of the thermal diffusion factor always occurs at water rich concentrations ($x_W \rightarrow 1$). Second, the value of α approaches to a constant negative value at high solute concentrations. Third, the thermal diffusion factors for the four systems analyzed are independent on the associating character of each solute. Hence, the differences between *acceptor* (acetone and DMSO) or *donor-acceptor* (alcohols) character of the solutes play no role in this transport property, contrary to what is observed in the viscosity coefficient presented in the previous chapter. Additionally, it seems that the differences in the molar masses between all of

the solutes play a secondary role in the final value of the Soret coefficient (note, for instance that the mass of DMSO is 78 g/mol , more than twice the mass of the methanol molecule 32 g/mol), contrary to what it is observed for normal non-associating liquid mixtures.

In order to have a more insight in the comprehension of the Soret effect a non-equilibrium Monte Carlo method has been applied to a lattice model of a mixture of two species 1 and 2, that differ only in their interaction energies. From the analysis of the simulations of this model some important conclusions can be drawn about the important parameters that govern the process of thermal diffusion.

For this lattice model we have obtained a change in the sign of the thermal diffusion factor if crossed interaction are larger than pure interactions. This fact confirms the hypothesis that the role played by the hydrogen bonds in associating fluids, is the main responsible for the change in the sign of α in this kind of systems. In this case, the species in minor concentrations will tend to concentrate in the cold region in order to lower the total energy of the system. We have observed that tuning the cross interaction parameters in the model we were able to mimic the hydrogen bond effect present in associating fluids, changing the sign of the coefficient. Moreover, we have corroborated this hypothesis in a mixture of Lennard-Jones particles ($T = 120 \text{ K}$ and $\rho = 1.3079 \text{ g/m}^3$) with the same masses, sizes and different interaction energies ($\epsilon_{11} = 1.0$ and $\epsilon_{22} = 1.39$), together with an enhanced crossed interaction (employing eq. 4.2 with $c_1 = 2.0$). In this case, we have obtained values of $\alpha(x_2 = 0.1) = -1.97$, $\alpha(x_2 = 0.5) = -0.187$ and $\alpha(x_2 = 0.9) = 1.679$, where a clear change in the sign of the Soret effect is observed, and, in addition, the values of the thermal diffusion factor are in the same order of magnitude compared with the values observed in alcohol-water mixtures. In previous analysis of the thermal diffusion effect in Lennard-Jones mixtures this fact has remained unnoticed and it was not emphasized the important role played by an enhanced crossed interaction in the change of the sign of this transport property (Reith and Muller-Plathe, 2000).

Additionally, we have observed that changing the ratio of the strength of the interactions of both species in the system it is possible to modify the concentration where the change in the sign is observed. This fact is a consequence of the competition between pure and crossed interaction energies. Making the analogy with real systems, water-water interaction is indeed stronger than any of the solute-solute interactions of the components studied.

Considering the numbers of attempts to provide a reliable and general theory in the literature for the Soret Coefficient, we have provided a set of comparisons of simulation results that are capable to reproduce the experimental data

available for the systems studied. Additionally, with the implementation of a simple lattice model, and simple Lennar-Jones mixture simulations, we were also able to identify the most important variables that govern the behavior of the Soret coefficient in associating fluids, particularly focused in the change of sign of this effect. In any case, there is still lacking a simple theory that would be able to predict the Soret coefficient for different systems at the same time, non-associating and associating, for instance.

Chapter 5

DYNAMICAL AND STRUCTURAL PROPERTIES OF BENZENE IN SUPERCRITICAL WATER

1. Introduction

The supercritical states of a mixtures can be defined as a state at which the temperature and the pressure are above of the critical values, say, T_c (critical temperature) and P_c (critical pressure) of the mixture. For instance, water at such supercritical conditions of pressure and temperature is a powerful solvating agent for separation purposes and a medium for chemical reaction, due to the fact that the density of water can be tuned from gas-like to liquid-like by just adjusting the pressure (Shaw et al., 1991, Katrizky et al., 1996, Savage et al., 1995). Supercritical Water (SCW) can solvate non-polar substances and precipitates common ions, contrary to what is observed under ambient conditions. This change in the solvation capability of water is explained by a relaxation of the three-dimensional structure of the hydrogen bond network (Yao and Okada, 1998) followed by a reduction of the dielectric constant of water. This fact favors the solvation of nonpolar solutes like hydrocarbons and aromatic compounds. Additionally, the viscosity of water at these supercritical conditions and at densities between the critical ρ_c and $2\rho_c$ is of the order of one tenth of the liquid viscosity at ambient conditions (Haar et al., 1984, Dudziak and Franck, 1966, Todheide, 1972). Consequently, the diffusion coefficient is inversely higher, being this fact important for diffusion-controlled chemical reactions. In view of these advantages, industrial process at such high pressure and high temperature conditions are of particular interest. For example, supercritical water oxidation (SCWO) and supercritical extraction, among others. For instance, (SCWO) becomes one of the most important application because provides a reliable way to destroy biochemical and pharmacological hazardous wastes from industrial process (Modell et al., 1982, Thomason et al., 1990, Thomason and

Modell, 1984, Tester et al., 1991, Killilea et al., 1992). For example, degradation of steam currents with aromatic compounds can be easily achieved through (SCWO). Although SCW chemistry promises to be a common industrial application, there are fundamental and technological challenges to be overcome. Problems like the highly corrosive environment (Mitton et al., 1991), able to destroy the reactor chamber, or the oxidation of all species, avoiding the production of intermediate desirable compounds, are some of the disadvantages of this technique.

The development of industrial applications, like those previously mentioned, therefore requires the knowledge of different thermodynamic, as well as transport properties of these mixtures, often not available. It is known that obtaining experimental data at these extreme conditions is difficult due to the severe conditions of oxidation and corrosion presented in SCW. Additionally, most of the equipment required is expensive. In view of these problems, molecular simulation techniques represent a reliable alternative to provide data for many of these properties; in particular, molecular dynamics simulations can be employed to obtain information about different transport properties as well as the different solute-solvent interactions at a microscopic and macroscopic level. Aiming at providing insights on the behavior of aromatic compounds in SCW, we have decided to explore mixtures of water and benzene at several molar fractions and at different temperatures and pressures, in the supercritical region of the mixture. For instance, we have computed the self and mutual diffusion coefficient, the shear viscosity, the dielectric constant and the relaxation dynamics of the hydrogen bonds of the water molecules. Recent works (Furataka and Ikawa, 1998b) experimentally studied this mixture at supercritical conditions. Particularly, Infrared Spectra experiments (Furataka and Ikawa, 1998a) suggest the presence of water-benzene complexes at 2676 cm^{-1} and 3649 cm^{-1} absorption bands, where water is able to form hydrogen bonds with the electron cloud of the benzenic ring. NMR spectra experiments (Furataka and Ikawa, 2000) found that the rotational lifetimes of the hydrogen bonds of water are of the order of 2×10^{-13} s. These values are in perfect agreement with our simulation results, where hydrogen bonds lifetimes of about $1.9 - 2.0 \times 10^{-13}$ s has been found. We have employed, a new Anisotropic United Atom (AUA) model for benzene that reproduces the total quadrupolar moment of the benzene molecule through the inclusion of point charges (Nieto-Draghi et al., 2003a). We have seen that the inclusion of these point charges in the model of benzene is required if benzene is intended to be mixed with water at supercritical conditions. In fact, a previous version of this model without taking into account these types of interactions fails to reproduce the phase diagram of the mixture (Contreras, 2002). Additionally, the inclusion of these charges in the benzene molecule allows the possibility of forming weak hydrogen bonds with water.

In this chapter we will present our simulation results of the analysis of these mixtures, employing a charged model of benzene.

2. Fundamentals

In order to explore the behavior of water+benzene mixtures at supercritical states we have computed different properties such as self-diffusion, mutual diffusion, shear viscosity, order orientation, hydrogen bond dynamics, and dielectric properties. Some of these properties have been discussed in previous chapters; thus, we pay attention here to the description of the dielectric behavior of a mixture of dipolar and quadrupolar liquids. Additionally, an extension of the orientational parameter q , described by equation (1.14), is done in order to study its radial variation in mixtures of water with other solutes.

2.1 Dielectric response of a mixture of dipolar and quadrupolar interactions

Consider the electrostatic potential Φ created by a distribution of charges, represented by an expansion in multi-poles. For instance,

$$\Phi(\mathbf{r}) = \frac{1}{4\pi\epsilon_0} \int_V d\mathbf{r}' \frac{1}{|\mathbf{r} - \mathbf{r}'|} \left[\rho(\mathbf{r}') - \nabla' \cdot \mathbf{P}(\mathbf{r}') + \nabla\nabla' : \bar{\bar{\mathbf{Q}}}(\mathbf{r}') + \dots \right] \quad (5.1)$$

where ϵ_0 is the vacuum dielectric permittivity constant, $\rho(\mathbf{r}')$ is the density distribution of net charges in the system, $\mathbf{P}(\mathbf{r}')$ is the electric dipolar moment, while ρ represents the free charge, \mathbf{P} and $\bar{\bar{\mathbf{Q}}}$ describe the charge distribution at a molecular level. Thus, the term between brackets stands for the total charge responsible for the electric field. According to this, Poisson equation allows us to write

$$\nabla \cdot \mathbf{E} = \frac{1}{\epsilon_0} \left[\rho - \nabla \cdot \mathbf{P} + \nabla\nabla : \bar{\bar{\mathbf{Q}}} + \dots \right] \quad (5.2)$$

thus,

$$\epsilon_0 \nabla \cdot \mathbf{E} + \nabla \cdot \mathbf{P} - \nabla\nabla : \bar{\bar{\mathbf{Q}}} + \dots = \rho \quad (5.3)$$

where the right hand side only contains the free charge. This equation allow us to define the electric displacement vector \mathbf{D} which, in components reads

$$D_i = \varepsilon_0 E_i + P_i - \sum_j \frac{\partial Q_{ij}}{\partial x_j} + \dots, \quad (5.4)$$

so that $\nabla \cdot \mathbf{D} = \rho$. In this last equation, i stands for the three Cartesian coordinates. In a isotropic homogeneous material, in the absence of an externally applied electric field, \mathbf{P} and $\bar{\mathbf{Q}}$ and all the other multipoles vanish by symmetry requirements. Thus, when applying an external field \mathbf{E} , we can write

$$\mathbf{P} = \varepsilon_0 \chi_e \mathbf{E} \quad (5.5)$$

here χ_e is the electric susceptibility of the fluid and $\mathbf{P} \parallel \mathbf{E}$ since, due to the isotropy of the system, \mathbf{E} is the only vector. The quadrupolar tensor $\bar{\mathbf{Q}}$ and the electric field are also related. Effectively, since \mathbf{E} is the only vector in the system, we can construct a second-rank irreducible tensor from \mathbf{E} . In fact, the only way to express $\bar{\mathbf{Q}}$ in function o the electric field is therefore through

$$Q_{ij} = \chi_q \left(\hat{E}_i \hat{E}_j - \frac{\delta_{ij}}{3} \right) \cdot |\mathbf{E}| \quad (5.6)$$

where \hat{E} is $\mathbf{E}/|\mathbf{E}|$ and δ_{ij} is the Kronecker symbol. The constant χ_q is similar to χ_e for the quadrupolar interactions in the fluid and express the susceptibility of the system to produce macroscopic quadrupolar moments upon the application of an external electric field. In view of eq. (5.6) and eq. (5.4) we can see that quadrupoles do not contribute to the dielectric response of the system if \mathbf{E} is homogeneous ($\mathbf{k} \rightarrow 0$), since their contribution to \mathbf{D} is in the form

$$\frac{\partial Q_{ij}}{\partial x_i} \propto \frac{\partial}{\partial x_i} \left(\hat{E}_i \hat{E}_j - \frac{\delta_{ij}}{3} \right) \cdot |\mathbf{E}| \quad (5.7)$$

vanishing in a uniform field. It is important to mention that at finite wavelenghts we can have a contribution from eq. (5.6), and the effects of the quadrupoles should be taken into account. Finally, the response of the system at cero frequency only comes from eq. (5.5), where the electric susceptibility of the fluid can be expressed as

$$\chi_e = 1 - \frac{\epsilon(0)}{\epsilon_0} \quad (5.8)$$

here $\epsilon(0)$ is the dielectric constant or the permittivity of the continuous medium. We can conclude that the quadrupolar moment of a molecule in a fluid does not directly contribute to the dielectric constant at zero wavelength. However, the addition of quadrupolar molecules to a dipolar fluid like water can affect its dipolar dielectric response through the local coupling between the dipole and the quadrupole, due to the strong inhomogeneity in the local electric field (see ref. (Nymand et al., 2001), for instance). In the case of our study we have two types of molecules, water with permanent dipole moment μ and benzene with a quadrupole moment tensor \mathbf{Q}_{ij} . The models employed to simulate both species do not include any polarizability. Consequently, the value of the dielectric constant $\epsilon(0)$ is only affected by the presence of the permanent dipole moment of the water molecules in the mixture.

Once we have established that nonpolarizable molecules with permanent quadrupolar moment do not directly contribute to the dielectric constant of the mixture, the static dielectric constant depends only on the magnitude of the dipole moment of the particles, the number of dipoles in the system, and on the coupling between dipoles and quadrupoles. Additionally, the relation between the dielectric constant and the fluctuations of the total dipole moment of the system in simulations depends on the way that long-range electrostatic forces are treated. Consequently, for a simulated system composed of polar molecules (water) with periodic boundary conditions and long range electrostatic interactions treated by a Reaction Field methodology with conducting boundary conditions ($\epsilon_{RF} \rightarrow \infty$), the dielectric constant $\epsilon(0)$ is given by (Neuman, 1986b)

$$\lim_{\epsilon_{RF} \rightarrow \infty} \frac{(\epsilon(0) - 1)(\epsilon_{RF} + 1)}{3(2\epsilon_{RF} + \epsilon(0))} = \frac{\epsilon(0) - 1}{3} = yG_k \quad (5.9)$$

here G_k is the finite system g-factor

$$G_k = \frac{\langle \mathbf{M}^2 \rangle}{N\mu^2} \quad (5.10)$$

which measures the equilibrium fluctuation of the total dipole moment of the system, $\mathbf{M} = \sum_{i=1}^N \mu_i$. This coefficient depends strongly on the boundary conditions and the shape of the simulation box. The factor y in eq. (5.9) takes into account the effect of the temperature and density

$$y = \frac{4\pi\rho\mu^2}{9k_B T} \quad (5.11)$$

Here, ρ and T are the number density and temperature of the system, k_B is the Boltzmann's constant and $\mu = \sum_{i=1}^{N_{esp}} x_i \mu_i$ is the average permanent dipolar moment of the mixture, x_i is the molar fraction of the i th specie and N_{esp} is total number of species in the mixture. G_k is measured during the simulation and it is related with the experimentally accessible Kirkwood g-factor g_k according to

$$g_k y = \frac{(\epsilon(0) - 1)(2\epsilon(0) + 1)}{9\epsilon(0)} \quad (5.12)$$

The Kirkwood g-factor accounts for the corrections of reorientation of polar molecules at equilibrium. In fact, it is possible to have information about the reorientation of the dipole vectors in the system monitoring a radial decomposition of G_k , consequently we propose in this work a simple function that account for this information, according to

$$g_{\mu_i \mu_j}(r) = \left\langle \frac{1}{N\mu^2} \sum_{i=1}^N \left[\sum_{j=1, j \neq i}^N \frac{\mu_i \cdot \mu_j}{n(r)} \right] \right\rangle \quad (5.13)$$

where N is the total number of molecules in the system, $r = |\mathbf{r}_j - \mathbf{r}_i|$ and $n(r)$ is the number of molecules located at a distance \mathbf{r} . There are several manners to study dipole-dipole orientational distribution functions, for example employing Fourier-Hankel transforms of the dipolar symmetry projections of pair correlation functions (see reference (Skaf and Ladanyi, 1995)). However, the simple approximation done in eq. (5.13) is enough for our purposes.

Additionally, it is possible to monitor the reorientational relaxation times of the permanent dipole moment vector of water molecules μ (see Figure 5.1.a) and a hypothetical vector normal to the plane of the benzene molecule (see Figure 5.1.b). Hence, we compute reorientational correlation functions of these two vectors according to

$$C_\mu(t) = \left\langle P_2[\hat{e}_i^w \cdot \hat{e}_j^w] \right\rangle \quad (5.14)$$

$$C_Q(t) = \left\langle P_2[\hat{e}_i^B \cdot \hat{e}_j^B] \right\rangle \quad (5.15)$$

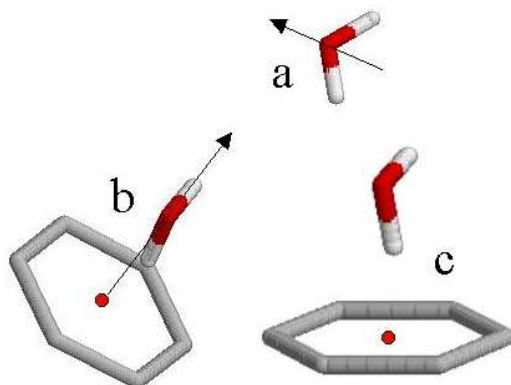


Figure 5.1. Representation of the dipole moment vector μ of the water molecule (a), a vector normal to the plane of the benzene molecules \mathbf{Q} (b) and a schematic representation of a possible HB between water and the center of the electron cloud of the benzene molecule (c).

where P_2 is the second Legendre polynomial, \hat{e}_i^w and \hat{e}_i^B are the unit vectors defined in Figures 5.1.a and 5.1.b. Assuming an exponential decay of $C_\mu(t)$ and $C_Q(t)$, it is possible to obtain the dipole moment reorientational relaxation times τ_μ and its equivalent for the benzene molecule τ_Q . These functions will be used in the result section to explore the reorientation of the molecules in the system.

2.2 Tetrahedral structure of water around benzene molecules

In chapter 1 we have introduced the orientational order parameter q according to eq. (1.14) to study the local tetrahedral structure of water molecules in pure water (chapter 2) and in mixtures (chapter 3). Here, we are interested in the influence of the degree of distortion that benzene molecules (which is a non-polarizable molecule with a planar geometry) generate in the local structure of water. In chapter 3 we have discussed the average values of q for different water models at different temperatures, and particularly at supercritical conditions (673 K and densities varying from 0.1 to 0.995 g/cm³). Here we implement the same parameter q , but from a different point of view: we want to map the variation of q in the surroundings of a benzene molecule. With this purpose a tetrahedral order radial function $q(r)$ is introduced

Table 5.1. Potential parameters of the models employed. For more details about the models see the cited reference.

Site	σ [Å]	ϵ [KJ/mol]	Charge(e)	δ_{LJ} [Å]	δ_{charge} [Å]
water (SPC/E) (Berendsen et al., 1987):					
<i>O</i>	3.165648	0.650167	-0.8476	0	0
<i>H</i>	0.0	0.0	0.4238	0	0
benzene (AUA) (Nieto-Draghi et al., 2003a):					
<i>CH</i>	3.2499	0.7424402	0.0637	0.45506	1.08
<i>center</i>	0.0	0.0	-0.3822	0	0
distance $C - C = 1.4$ Å					

$$q(r) \equiv \left\langle \frac{1}{N_B} \sum_{i=1}^{N_B} \left[\sum_{j=1}^{N_w} \frac{q_j}{n(r)} \right] \right\rangle \quad (5.16)$$

where N_B and N_w are the total number of benzene and water molecules, q_j is the value of the tetrahedral order parameter of the water molecule j at a distance $r = |\mathbf{r}_j - \mathbf{r}_i|$ from a benzene molecule i , and $n(r)$ is the number of water molecules contained in a spherical shell at r . The brackets account for a time average during the simulation. In this way $q(r)$ is zero close to any benzene molecule and tends to the average value of q of the mixture at $r \rightarrow \infty$.

Finally, we have also computed the average number of hydrogen bonds $\langle N_{HB} \rangle$ for water-water, and for water-benzene if the geometrical criteria defined in chapter 1 is fulfilled, between the center of the electron cloud of the benzene molecule and the hydrogen atom of a water molecule as illustrated in Figure 5.1.c. Additionally, we compute the hydrogen bond life times of these two types of interactions through eq. 3.1 defined in chapter 3.

Another way to collect information about the local structure is through the computation of the coordination number of the arrangement of water molecules around each benzene molecule,

$$n_{cord} = 4\pi\rho \int_0^{r_{cm_w,cm_B}^{min}} g_{cm_w,cm_B}(r) r^2 dr \quad (5.17)$$

here ρ is the number density of the mixture, g_{cm_w,cm_B} is the center of mass to center of mass radial distribution function between water and benzene molecules, and r_{cm_w,cm_B}^{min} is the first minimum of this function. This coordination number n_{cord} give us information about the degree of solvation of benzene molecules in the system.

Table 5.2. Simulated thermodynamic states for the benzene+water mixture.

State	X_B	T(K)	P[bar]	ρ [g/cm^3]
1	$\rightarrow 0$	573	329	0.84805
2	0.1	573	320	0.78574
3	0.21	573	324.6	0.725
4	$\rightarrow 0$	673	123.62	0.300
5	0.16	673	177.68	0.300
6	0.21	673	206.38	0.300
7	$\rightarrow 0$	673	238.1	0.660
8	0.1	673	559.2	0.660
9	0.21	673	824.62	0.660
10	$\rightarrow 0$	673	5493.05	0.995
11	0.1	673	6861.13	0.995
12	0.21	673	7929.4	0.995

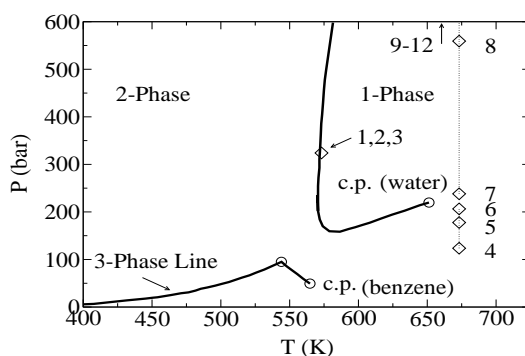


Figure 5.2. Phase diagram for water-benzene mixtures. The thick solid lines: one -phase critical curve and liquid-liquid-gas three phase curve; c.p is the critical points and the diamond symbols are the different thermodynamic states presented in table 5.2. Experimental data taken from the literature (Alwani and G. M. Schneider, 1967, Tsonopoulos and Wilson, 1983).

3. Computational details

We have computed different structural and transport properties of mixtures of benzene in water at three different molar fractions $x_B \rightarrow 0$, $x_B = 0.1$ and $x_B = 0.21$ through Molecular Dynamics simulations. We have employed the SPC/E (Berendsen et al., 1987) model to simulate water molecules and, originally, we have employed a AUA (Anisotropic United Atom) model for benzene (Contreras, 2002). However, this model of benzene was unable to reproduce the phase diagram of the mixture with water at supercritical conditions (we always observe a phase separation independently of the pressure). A second

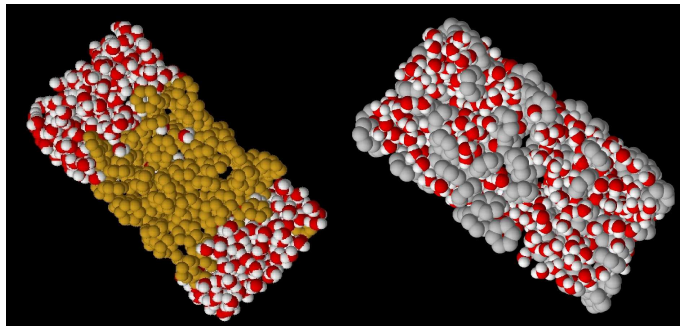


Figure 5.3. Snapshot of the mixture Water+Benzene at $x_B = 0.21$, at 573 K and 329 bar for two AUA models of benzene. Without point charged (left) and with the inclusion of point charges (right).

version of this AUA model, where the inclusion of point charges was added to the intermolecular potential in order to mimic the quadrupolar moment of this molecule (Nieto-Draghi et al., 2003a), allows us to reproduce the one phase supercritical region of the mixture. The second AUA model for benzene was obtained by considering seven electrostatic point charges respecting molecular symmetry (one at the molecular center and six on the C-H axis). The amplitude and location of these charges were determined by fitting the ab initio electrostatic potential on a grid of reference points around the benzene molecule. Then the Lennard-Jones parameters were recalibrated to match the liquid-vapor coexistence curve of benzene, using the same procedure as in reference (Contreras, 2002). A snap shot representation of the simulation of water+benzene at $x_B = 0.21$, at 573 K and 329 bar is observed in Figure 5.3. The figure on the left side shows the old AUA model for benzene without point charges, where the formation of two phases is clear. The figure on the right side shows the new AUA model modified including point charges to mimic the quadrupole moment of benzene, in this case there is only one phase as it is observed in experiments (Furataka and Ikawa, 2000). Moreover, the coordination number of water molecules around benzene molecules is almost zero in the case of the old model, whereas $n_{cord} = 12.66$ for the case of the new model (this point will be discussed later in the next section, particularly in Figure 5.10). Finally, the potential parameters of the SPC/E and AUA model for benzene are summarized in table 5.1.

We have studied two different supercritical regions of the phase diagram of the mixture, the first one at 573 K and 324 bar and the second at 673 K and at three different densities 0.300, 0.660 and 0.995 g/cm³, all conditions are

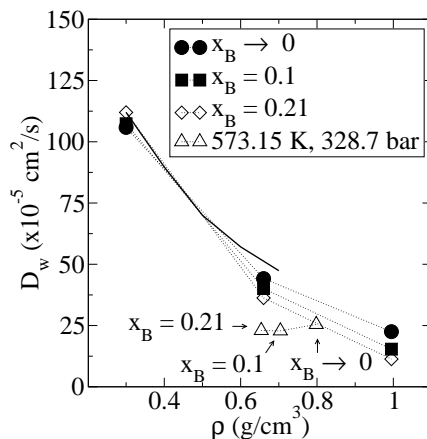


Figure 5.4. Density variation of the self-diffusion coefficient of water in the mixture water+benzene at the supercritical isotherm ($T=673$ K). Additionally, the self-diffusion of water at 573 K and 329 bar is included at three concentrations. The experimental data (Lamb et al., 1981) of self-diffusion of pure water (continuous line) is presented for comparison.

summarized in table (5.2) and shown in the phase diagram of the mixture in Figure 5.2¹.

In this case we have computed the density of the mixture for states 1 to 3 through NPT simulations with long-range correction for pressure and energy (see eq. (1.81) and (1.82)). These densities have been used for NVT simulations to compute different transport and structural properties of the mixtures.

All simulations were carried out with 256 molecules and the size of the simulation box on each case has been adjusted to fit the desired density of the mixture (see table 5.2) employing a cubic box. The equations of motion were integrated with a time step of 2 fs. All simulations have been performed with periodic boundary conditions and the *reaction field* methodology (Neuman, 1986b) with the choice $\epsilon_{RF} = \infty$, to account for the long-range electrostatic interactions. The reaction field and Lennard-Jones cut-off length was 9.26 Å, and a nearest neighbor list technique (Allen and Tildesley, 1989), with a cut-off radius of 10.1 Å, has been also employed. An equilibration run of 300 ps has been done prior to each 5 ns production runs, to eliminate any memory of the initial conditions.

¹In the present experimental results the water concentration in this region is almost independent of pressure, meaning that the density of the mixture changes little along the vertical line in the phase diagram at least in the region between 100 – 300 bar (Furataka and Ikawa, 2000).

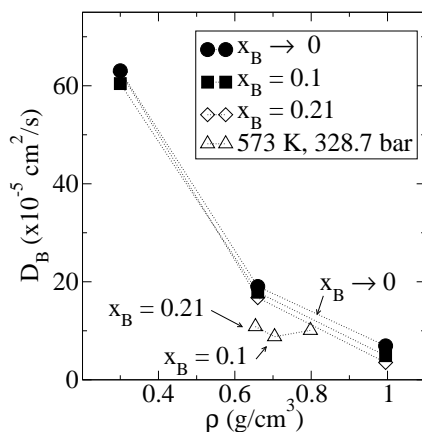


Figure 5.5. Density variation of the Self-diffusion coefficient of benzene in the mixture water+benzene at the supercritical isotherm ($T=673$ K). Additionally, the self-diffusion of benzene at 573 K and 329 bar is included at three concentrations.

4. Results and discussion

In this section we present the results obtained in our simulations of mixtures of water+benzene at supercritical conditions. In some cases we were able to compare with the available experimental data, however, the lack of experimental data for other properties does not permit the comparison of some of the results obtained. In some cases industrial correlations, based on experimental data, are available and hence we have employed them for comparison and discussion. This section is organized as follows, first the dynamical behavior of the systems is presented; for instance, the variation of the self and mutual diffusion of the mixture, at different thermodynamic conditions, are presented followed by the corresponding shear viscosity on each state. Later, the local structure of the mixture is explored through the analysis of the variation of q and $q(r)$ together with the average number of hydrogen bonds $\langle N_{HB} \rangle$ and their life times. The different dielectric properties of the mixture are finally discussed at the end of this section.

In Figure 5.4 the variation of the self-diffusion of water molecules in the mixture of water+benzene is presented for states 1 to 12 and at different densities. Our simulation results show a strong density dependence of the self-diffusion coefficient of water with a small influence of the molar fraction of benzene in the mixture, at least for states 4 to 12 of table 5.2. Moreover, if we compare this results with the experimental data (Lamb et al., 1981) on self-diffusion of pure water at the 673 K supercritical isotherm (see Figure 2.4), we observe almost the same general behavior at least at the lower densities. At low densities,

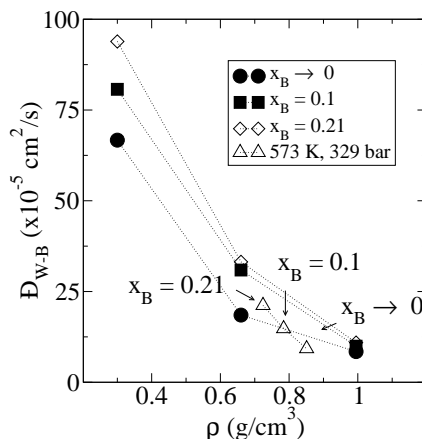


Figure 5.6. Density variation of the Maxwell-Stefan mutual diffusion coefficient of the mixture water+benzene at the supercritical isotherm ($T=673$ K). Additionally, the mutual-diffusion of the mixture at 573 K and 329 bar is included at three concentrations.

($\rho = 0.3$ g/cm³) our data shows that increasing the molar fraction of benzene slightly increases the water self-diffusion coefficient. This fact is inverted at higher densities ($\rho = 0.995$ g/cm³). Surprisingly, this property remains almost constant for systems 1 to 3 (573 K and ~ 324 bar) where the mobility of water molecules are not affected by the concentration of benzene. Furthermore, the D_w decreases when the density increases.

In Figure 5.5 we present the self-diffusion of benzene molecules in the mixture for all of the thermodynamic conditions presented in this chapter. The behavior of D_B with the density is similar to that observed for D_w , but in this case benzene molecules present almost a 60% lower values of self-diffusion than water. Additionally, it seems that D_B is even less dependent of the concentration of benzene than water. This fact is not surprising since we are dealing with relatively small concentrations of benzene. However, one aspect that is worth to be mentioned is that at the state 2 (573 K, ~ 324 bar and $x_B = 0.1$) the self-diffusion of benzene presents a small minimum. This minimum is something unexpected and we have not a clear physical explanation for this behavior.

On Figure 5.6 the density variation of the Maxwell-Stefan (MS) mutual diffusion coefficient is presented for the mixture. Contrary to the previous cases, here strong concentration dependence is observed, apart of the relation with the density. Additionally, the mutual diffusion coefficient increase when the concentration of benzene is incremented, but this behavior is only observed at low and medium densities. On the other hand, at $\rho = 0.995$ g/cm³ \overline{D}_{w-B} is

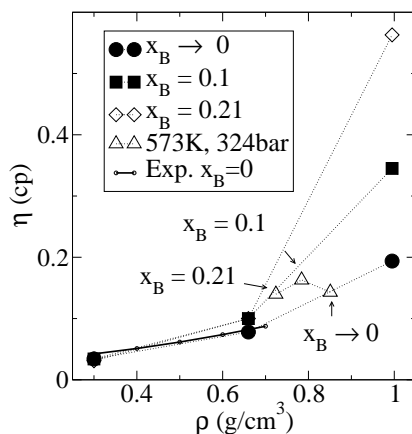


Figure 5.7. Density variation of the shear viscosity coefficient of the mixture water+benzene at the supercritical isotherm ($T=673$ K). Additionally, the viscosity at 573 K and 329 bar is included at three concentrations. Here we also include the experimental data of Lamb (Lamb et al., 1981) for pure water.

almost independent of x_B . Similar behavior is observed for this coefficient for states 1 to 3, where an increment on the MS mutual diffusion is observed when the concentration of benzene increases. In addition to this effect, we should also consider the effect of the different densities between these states. The MS mutual diffusion coefficient is a cross effect due to the fact that involve the relative diffusion of particles of one type respect of the particles of the other type. However, the behavior of \bar{D} does not substantially differ from that exhibited by the self-diffusion coefficients for both, water and benzene. Thus, MS diffusion coefficient is, under the thermodynamic conditions considered, a good approximation of the diffusion coefficient. Effectively, the thermodynamic factor Q in eq. (1.31) is approximately 1 for low density and high temperature if the mixture behaves nearly ideally.

In Figure 5.7 the density variation of the shear viscosity is observed for the mixture water+benzene. This property follows the inverse behavior of the diffusion coefficient, as it is expected. In general, the values obtained for η are much smaller (between 25 times less at low densities and 1.6 times less at high densities) than the values of viscosity for pure water at ambient conditions. We find, for instance, 0.91 cp for the SPC/E water model at 300 K (experimental viscosity of water is 0.89 cp at ambient temperature and pressure). Our results of η present the general trend experimentally observed for pure water at supercritical conditions (Haar et al., 1984, Dudziak and Franck, 1966, Todheide, 1972), particularly, here we compare our simulations results with

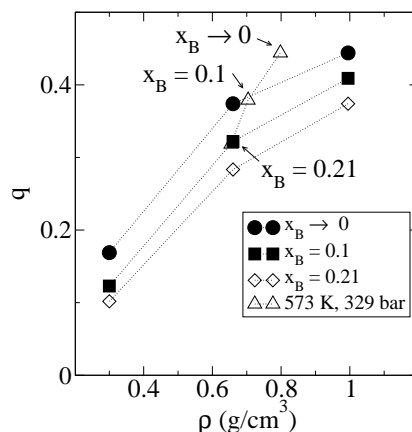


Figure 5.8. Variation of the local tetrahedral order parameter q of the mixture water+benzene at 673 K. Additionally, the same parameter at 573 K and 329 bar is included at three concentrations.

the experimental data of Lamb (Lamb et al., 1981) for pure water, where a perfect agreement is observed. The possibility of changing the density and, consequently, the viscosity of the mixture, by just adjusting the pressure in the system, makes SCW an appropriate chemical reaction medium. Notice, for instance, that the viscosity at $\rho = 0.995 \text{ g/cm}^3$ is almost 17 times larger than the viscosity at $\rho = 0.300 \text{ g/cm}^3$ at the lower molar fractions of benzene. On the other hand, η remains almost constant when the pressure of the system is kept constant as between states 1 and 3 (independently of the amount of benzene in the system). In addition, Figure 5.7 shows that η is not too affected by the concentration of benzene at lower and medium densities. However, the shear viscosity is strongly affected by the presence of the solute at densities greater than 0.660 g/cm^3 . For instance, the viscosity at $\rho = 0.995 \text{ g/cm}^3$ and $x_B = 0.21$ is three times larger than the viscosity at $x_B \rightarrow 0$.

Since we were unable to find experimental data for the shear viscosity of the mixture at the thermodynamic conditions of our study, we have used an empirical correlation (Woerlee, 2001) for the product $\bar{D}_{ij} \cdot \eta$, applicable for supercritical fluids, where \bar{D}_{ij} is the Maxwell-Stefan mutual diffusion in a binary mixture and η the viscosity. The correlation is based on the kinetic gas theory and an activation energy theory using a Boltzmann factor. This activation energy theory is similar to the Eyring theory of absolute reaction rates (Glasstone et al., 1941). For the state 4 (673 K and $\rho = 0.300 \text{ g/cm}^3$) we have a value of $\bar{D}_{WB} \cdot \eta = 2.27 \times 10^{-12} \text{ Pa.m}^2$, which is almost the same number obtained with the correlation ($\bar{D}_{WB} \cdot \eta = 2.2 \times 10^{-12} \text{ Pa.m}^2$ employing eq. (13) in reference (Woerlee, 2001)). This agreement does not

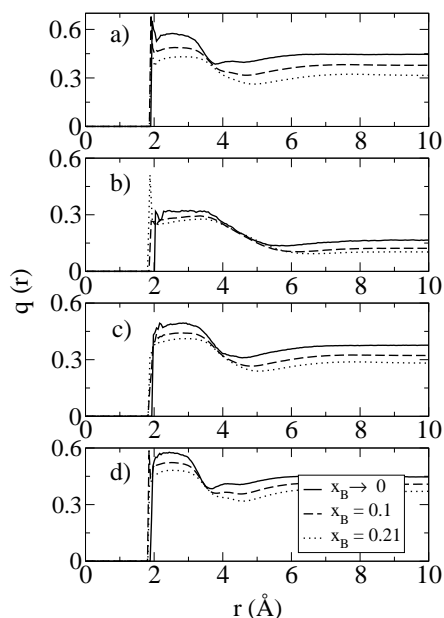


Figure 5.9. Radial variation of the local tetrahedral order parameter q of the mixture water+benzene at three concentrations. From top to bottom, a) 573 K and 329 bar, b) 673 K and $\rho = 0.3 \text{ g/cm}^3$, c) 673 K and $\rho = 0.66 \text{ g/cm}^3$ and d) 673 K and $\rho = 0.995 \text{ g/cm}^3$.

imply that we have got correct values of \bar{D}_{WB} and η separately, but ensures that there is a concordance between the properties obtained in our simulations, or in other words, that the activation energies involved for diffusion and viscous process are equal at least for small and medium densities.

Since the approximate error for the viscosity in our simulation ranges from 10% to 18%, we cannot be conclusive about the existence of a maximum in the viscosity observed at $x_B = 0.1$ in state 2. Experimental data of viscosity at these conditions may shed some light about the observed behavior.

We have presented the dynamic properties of different mixtures by means of the self and mutual diffusion coefficients and shear viscosity. Now we pay attention to the local structure of the water molecules in the mixture, and how the variation of the molar fraction of benzene influences such structure. In figure 5.8 the density variation of the local tetrahedral order parameter q of water molecules in the mixture is presented at different concentrations of benzene. For the case of the 673 K isotherm we observe that q increases when ρ increases. At the same density, q decreases with an increasing molar fraction of benzene. Both facts are expected: on one hand, the tetrahedral order parameter increases

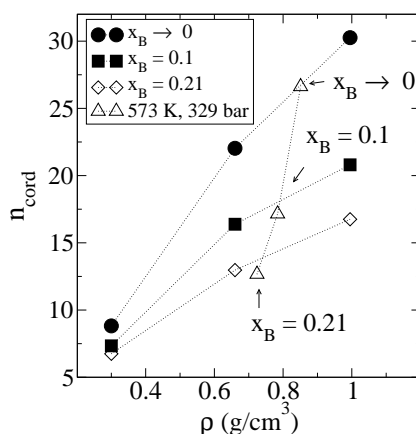


Figure 5.10. Variation of the coordination number of water molecules in the first solvation shell around benzene molecules with the density and composition of benzene in the supercritical isotherm of 673 K, and at 573 K and 324 bar.

with density due to the fact that the interaction with the neighbors is an ordering effect. This is the case for water up to densities of the order of 1 g/cm^3 . Due to the directional interactions, a high density is achieved in water through a sacrifice of tetrahedral order. However, in the conditions showed here, the increase of the density only plays an ordering effect (as it was observed in Figure 2.10). On the other hand the insertion of a non-associating solute in the mixture tends to decrease the values of q perturbing the local structure of water. Similarly, we observe that the presence of more benzene reduces the value of this parameter at states 1 to 3. However, this tendency is more pronounced here than in the previous cases, due to the differences in the density between these three states, and also because the differences in temperature (states 1, 2 and 3 have 100 K lower temperature than the rest of the points).

In figure 5.9 we observe the radial variation of the tetrahedral order parameter q for the mixture of water+benzene at three compositions. From top to bottom, a) 573 K and 329 bar, b) 673 K and $\rho = 0.3 \text{ g/cm}^3$, c) 673 K and $\rho = 0.66 \text{ g/cm}^3$ and d) 673 K and $\rho = 0.995 \text{ g/cm}^3$. Each figure represents the variation of the tetrahedral order parameter q of water molecules with respect to the separation of this molecules to any benzene. In other words, it measures the evolution of the degree of distortion generated by a benzene molecule in the structure of water. In contrast, Figure (5.8) only shows the average value of q . Consequently, $q(r)$ is zero at short distances (the average radius of the benzene molecule) and goes to the average value of q when r is large.

We observe a first broad peak close to the benzene molecule, this peak is generated by the presence of the benzene, creating a solvation shell of water molecules that presents an enhanced structure in comparison to other water molecules that are at further distances from the solute. Another important aspect of this figure is the fact that the average size of the distortion generated by benzene molecules are about 6 to 7 Å, for medium and high densities, and greater than 7 Å for the lower density. The height of the peak is in general a strong function of the density and molar fraction of benzene. The lower the x_B the higher the peak. The width of the peak is also proportional to the density, and hence we observe that the degree of distortion is greater when the density is lower (Figure 5.9.b). This radial decomposition of the parameter q represents an interesting tool that can provide more information about the effect that different types of solutes have in the local structure of water.

As was mentioned before, one of the most important characteristics of the new AUA model of benzene employed, is the ability of forming hydrogen bonds with water molecules. This association allows water to solvate the benzene molecules. In order to explore this solvation we have computed the coordination number of water molecules in the first solvation shell around each benzene molecule in Figure 5.10 at the different conditions of this study. From this figure it is clear that the amount of water molecules around each benzene molecule increases with the density of the mixture and decreases with the amount of benzene in the system.

Additionally, in Figure 5.11 we observe the center of mass to center of mass radial distribution functions between benzene and water molecules at the different thermodynamic conditions studied. From this figure it is clear the presence of a first peak, at approximately 2.5 Å, where water molecules are hydrogen bonded with the center of the benzenic ring. The radial position of this first peak is quite similar to the distance where the first peak of the g_{OO} is observed for pure water at approximately 2.75 Å (see Figure 2.5 and Figure 2.6 in Chapter 2). The second, and more pronounced, peak is located at larger radial distance at about 4.85 Å showing the hydration of water molecules in the first solvation shell. At the higher density on Figure 5.11.d it is possible to observe a third small peak as expected in a high-density liquid-order. In general, the height of each peak increases with the density and, is quite affected by the presence of the amount of benzene molecules. For instance, the first peak presents a small increment with the benzene concentration, due to the fact that the presence of this molecule disturbs the local structure of water, favoring the cross association between the two species. This fact will be commented later in the analysis of the hydrogen bond life times (see, for instance, Figure 5.13).

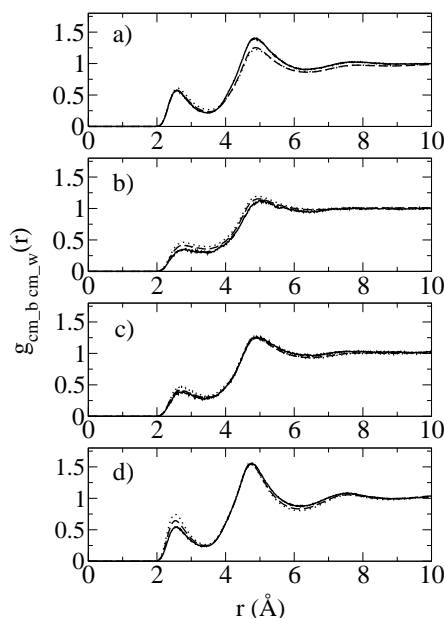


Figure 5.11. Center of mass to center of mass radial distribution function between benzene and water molecules at $x_B \rightarrow 0$ (continuous line), $x_B = 0.1$ (dashed line) and $x_B = 0.21$ (dotted line). From top to bottom, a) 573 K and 329 bar, b) 673 K and $\rho = 0.3 \text{ g/cm}^3$, c) 673 K and $\rho = 0.66 \text{ g/cm}^3$ and d) 673 K and $\rho = 0.995 \text{ g/cm}^3$.

Consequently with the presence of the small first peaks in Figure 5.11, in Figure 5.12 we observe the density variation of the average number of hydrogen bonds $\langle N_{HB} \rangle$ for the mixture. The number of HB increases with the density for states 4 to 12, and in general $\langle N_{HB} \rangle$ decreases with the addition of benzene molecules. This behavior is expected, since the inclusion of a solute (with a different associating character in comparison with water) in the system reduces the capability of water to form HB with itself (closed symbols in the figure). The most remarkable feature of this figure is the presence of cross HB between water and benzene molecules (open symbols in the figure). The presence of this type of interaction, between the hydrogen atoms of water molecules and the electron clouds of the benzenic ring has been suggested by infrared spectra experiments (Furataka and Ikawa, 1998a) at 2676 cm^{-1} and 3649 cm^{-1} absorption bands. At lower densities crossed HB are rare, but at $\rho = 0.995 \text{ g/cm}^3$ almost each benzene molecule has between 0.8 and 1 HB. Though the geometrical criteria employed to discriminate when two molecules have a HB presents its limitations (see, for instance the discussion done about this point chapter 2), the values presented here are a qualitative picture of the real behavior of this property in the mixture as suggested by the experiments

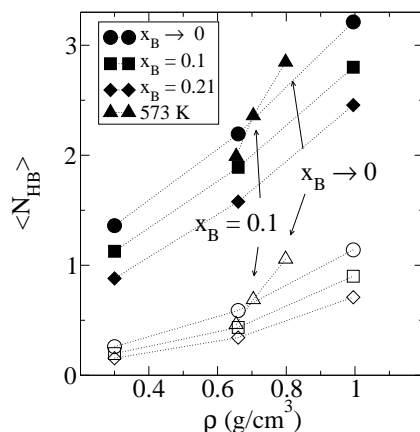


Figure 5.12. Density variation of the average number of hydrogen bonds $\langle N_{HB} \rangle$ of the mixture water+benzene at the supercritical isotherm ($T=673\text{ K}$). Additionally, $\langle N_{HB} \rangle$ at 573 K and 329 bar is included at three concentrations. Full symbols are w-w HB and empty symbols are benzene-water HB.

(Furataka and Ikawa, 1998b). States 1 to 3 reinforce the fact that this property is strongly affected by the presence of the solute where the $\langle N_{HB} \rangle$ decreases rapidly with the molar fraction of benzene for water-water and water-benzene HB.

Another characteristic of the hydrogen bond behavior is the lifetime presented for water-water interactions as well as for water-benzene. In Figure 5.13 the density variation of life times of continuous HB τ_{HB}^c for the mixture water+benzene at supercritical conditions is observed. Full symbols represent water-water HB while open symbols account for water-benzene HB. This property shows a complex behavior with respect to the density and composition, but we can find some general trends. For instance, cross HB are longer lived than water-water HB, and the addition of benzene molecules also increase the values of τ_{HB}^c for both, crossed and pure water interactions. This fact is not surprising since the benzene molecules have slow rotational dynamics and, therefore water molecules attached to them also reduce its dynamics. Additionally, as was commented in the analysis of the center-to-center radial distribution function, between water and benzene presented in Figure 5.11, the increment in the values of the first peak of this function with the addition of benzene is in perfect agreement with the increment of the lifetime of crossed HB. However, there is a remarkable aspect in the behavior of crossed HB at $x_B \rightarrow 0$ and 673 K (empty circle), where a complete different behavior is observed for this property, in comparison with the other two molar fractions of benzene. Effectively, a clear maximum is observed at $\rho = 0.660\text{ g/m}^3$, being the value of τ_{HB}^c at

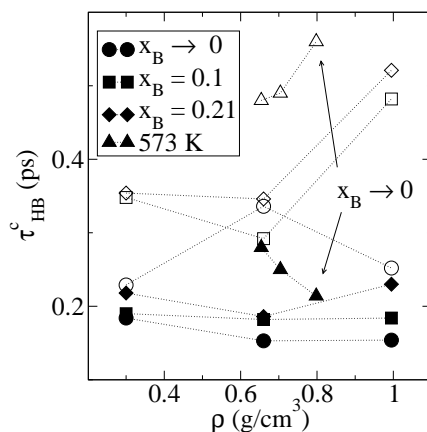


Figure 5.13. Density variation of life times of continuous HB for the mixture water+benzene at the supercritical isotherm ($T=673$ K). Additionally, τ_{HB}^c at 573 K and 329 bar is included at three concentrations. Full symbols are w-w HB and empty symbols are water-benzene HB.

this point greater than the corresponding value at $x_B = 0.1$, and, on the other hand, the value of τ_{HB}^c is surprisingly low at the highest density for $x_B \rightarrow 0$. Additionally, NMR spectra experiments (Furataka and Ikawa, 2000) found that the rotational lifetimes of the hydrogen bonds (that can be taken as an approximation of the values of the hydrogen bond life times) of water is of the order of 0.2 ps, which is in perfect agreement with our simulations results, where water-water hydrogen bonds life-times are between 0.18 – 0.27 ps.

Figure 5.14 is similar to Figure 5.13 but for intermittent HB. As a rule, intermittent HB presents a long decay time in comparison to the continuous hydrogen bonds, as it was previously discussed in chapter 3 for mixtures of different associating molecules with water. The value of τ_{HB}^i increases with density and with the molar fraction of benzene in a similar manner than the continuous HB. However, in this case the difference between crossed hydrogen bonds and those for water-water are much smaller, being in some cases identical. Additionally, the lifetime of HB for water molecules suffer a strong variation from state 1 to state 2 with the addition of 10% of benzene.

In Figure 5.15 the Normalized reorientational correlation function of the dipole moment vector of water molecules is presented at different states a) 573 K and 329 bar, b) 673 K and $\rho = 0.3$ g/cm³, c) 673 K and $\rho = 0.66$ g/cm³ and d) 673 K and $\rho = 0.995$ g/cm³. Since it is difficult to interpret the reorientational correlation functions by it selves (the decay time associated is more illustrative), we can remark some interesting aspects. For $C_\mu(t)$ a strong initial non-exponential decay is observed. A complex dependence of

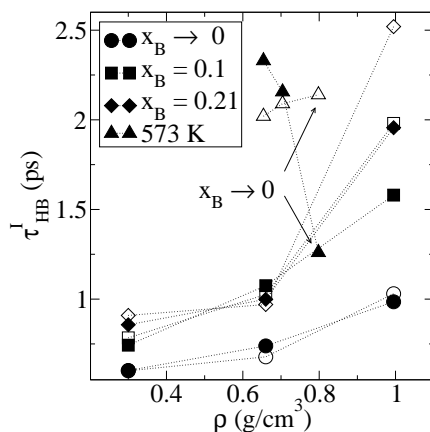


Figure 5.14. Density variation of life times of intermittent HB for the mixture water+benzene at the supercritical isotherm ($T=673$ K). Additionally, τ_{HB}^I at 573 K and 329 bar is included at three concentrations. Full symbols are w-w HB and empty symbols are water-benzene HB.

this function with the molar fraction of benzene is appreciated. On the other hand, the function $C_Q(t)$ (defined in eq. (5.15)) of the hypothetical quadrupolar vector of benzene molecules (not shown) is almost insensitive to the amount of benzene in the mixture, and presents an exponential decay with almost the same qualitative behavior for all the states studied.

The density variation of reorientational time of the dipole vector τ_μ (full symbols) of water molecules and the reorientational time of quadrupolar vector τ_Q (empty symbols) of benzene molecules for the mixture water+benzene at the supercritical conditions are shown in Figure 5.16. In general, both τ_μ and τ_Q increase with the density, being the second one much larger than the first one. This difference is logical due to the fact that benzene molecules reorients more slowly than water molecules because their larger size. This argument also explains the fact that more concentrated solutions present larger values of reorientational times. However, an opposite behavior is observed for states 1, 2 and 3, in which the effect of composition is less important than the effect of the density. For this case, τ_μ and τ_Q are larger for the infinite diluted solutions than for the other compositions. Dipolar orientational correlation functions can be experimentally obtained from optical measurements such as Raman scattering, fluorescence depolarization and Kerr relaxation experiments (Rothschild, 1984, Berne and Pecora, 1976, Fleming, 1986), however experiments at supercritical condition are scarce (Lamb et al., 1981, Lamb and Jonas, 1981). Unfortunately we were unable to find data for our particular system at these supercritical conditions.

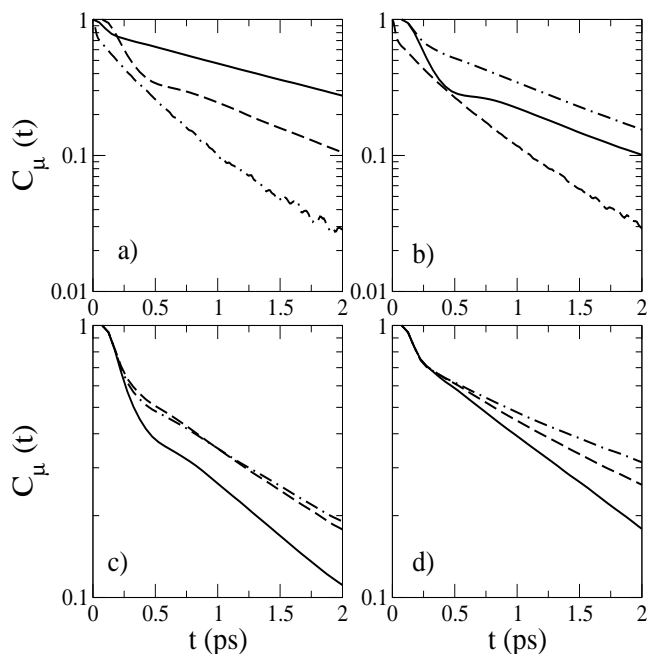


Figure 5.15. Normalized time-correlation function of the dipole moment vector of water molecules for $x_B \rightarrow 0$ (line), $x_B = 0.1$ (dashed line) and $x_B = 0.21$ (dashed dotted line) at a) 573 K and 329 bar, b) 673 K and $\rho = 0.3 \text{ g/cm}^3$, c) 673 K and $\rho = 0.66 \text{ g/cm}^3$ and d) 673 K and $\rho = 0.995 \text{ g/cm}^3$.

The capability of SCW of solvating nonpolar systems is due to the fact that water molecules suffer a strong relaxation of its dielectric constant. Many works have been devoted to the study of the solvation dynamics and dielectric properties of common ions in SCW through Molecular Dynamics Simulations (Balbuena et al., 1996, Chialvo et al., 1995, Chialvo et al., 2002, Cummings and Chialvo, 1996, Chialvo et al., 1996), but only a few studies have been devoted to the dielectric properties of non-ionic solutes in SCW (Re and Laria, 1997). This lack of information, particularly on systems with hydrocarbons or aromatic compounds, does not permit a direct comparison with our simulation results, however we speculate that the estimations presented here may capture the qualitative behavior of the dielectric of the mixture.

In Figure 5.17 the density variation of the dielectric constant $\epsilon(0)$ of the mixture water+benzene at the supercritical conditions is presented. We observe an increment of the dielectric constant with the density. The presence of the benzene molecules reduces considerably the dielectric constant of the mixture as expected since this constituent does not contribute to the value of $\epsilon(0)$. It is

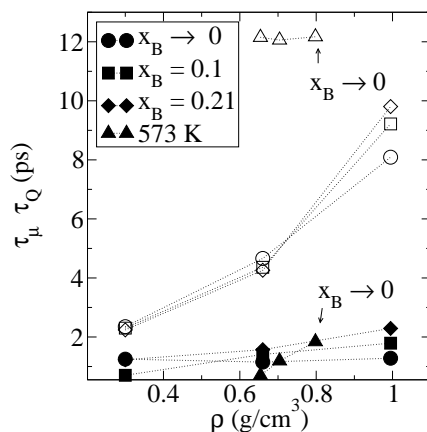


Figure 5.16. Density variation of decay time of the dipole vector τ_μ (full symbols) of water molecules and the decay time of quadrupolar vector τ_Q (empty symbols) of benzene molecules for the mixture water+benzene at the supercritical isotherm ($T=673$ K). Additionally, both quantities are included at 573 K and 329 bar at three concentrations.

important to remark that even with a polarizable model of benzene (in this case we would have a contribution to the dipolar moment of the mixture) its contribution to $\epsilon(0)$ would be several times smaller than the contribution provided by the dipole moment of water. For this reason we believe that the predictions done here are not affected by this point. Our results are compared with the values provided by Skaf *et al.* (Skaf and Laria, 2000) and the experimental data of Uematsu (Uematsu and Franck, 1980) for pure water at the supercritical region at slightly lower temperature of 650 K. Both, simulations and experimental data, are in agreement with the values obtained for the lower concentration of benzene $x_B \rightarrow 0$. In general, $\epsilon(0)$ presents almost a linear dependence with the density. For states 1 to 3 we observe the same qualitative behavior but, in this case, the dielectric constant is more affected by the presence of benzene. We want to remark that other works have been devoted to the study of the dielectric response of aqueous mixtures of methanol through molecular dynamic simulations (Skaf and Ladanyi, 1995, Ladanyi and Skaf, 1996) and experiments (Petong *et al.*, 2000), as well as for mixtures of DMSO+water (Skaf, 1999) but, to the best of our knowledge, there is no a systematic study of the dielectric response neither for mixtures at supercritical conditions nor for the system water+benzene.

In addition, it is known that non-polarizable models of water underestimate the dielectric constant of water at liquid like densities, precisely because at these conditions the polarizability plays an important role in the dielectric response of the system. For instance we have obtained a value of $\epsilon(0) = 65.6$ F/m for the dielectric constant of pure water at 298 K and 1 bar employing $\epsilon_{RF} \rightarrow \infty$, which

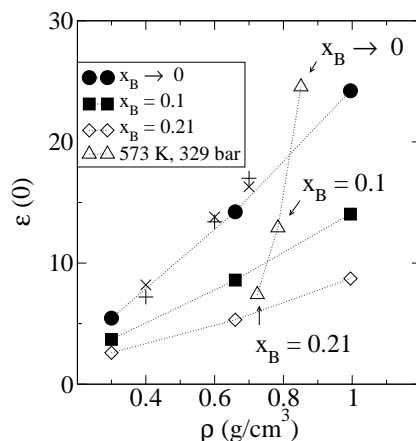


Figure 5.17. Density variation of the dielectric constant $\epsilon(0)$ (in F/m) of the mixture water+benzene at the supercritical isotherm ($T=673$ K). Additionally, $\epsilon(0)$ is included at 573 K and 329 bar at three concentrations. Simulation results of Skaf *et al.* (Skaf and Laria, 2000) (cross symbols) and the experimental data of Uemata (Uematsu and Franck, 1980) (plus symbols) of pure water at 650 k are also included for comparison.

is in agreement with other values reported for the SPC/E model in the literature (Glattli *et al.*, 2002, Skaf, 1999). There is some dispersion in the reported values of $\epsilon(0)$ due to the fact that the different possible alternatives of treat the long-range electrostatic interactions affect the final values of $\epsilon(0)$, yielding values between 7 – 8%. In any case, all values reported are considerably smaller than the value experimentally observed, $\epsilon(0) = 78.5$ F/m.

Unfortunately, the limitations of the non-polarizable character of the model employed to simulated benzene molecules does not permit the computation of the dielectric constant of this compound (the experimental value for benzene is $\epsilon(0) = 2.3$ F/m). However, it seems that at supercritical conditions and at medium densities the values obtained with non-polarizable models for water reproduce well the dielectric constant of water (Skaf and Laria, 2000).

In order to have more information about the reorientation of the dipole vectors in the system, we compute a radial decomposition of G_k . In Figure 5.18 the radial variation of the product of the dipole vector of water molecules $\mu_i \cdot \mu_j$ in the mixture is presented. In this figure, $g_{\mu_i \mu_j}(r)$ (defined in eq. (5.13)) shows several peaks which are related to the relative orientation of the water molecules at different radial shells. Positive peaks represents the parallel orientations generated by the influence of the hydrogen bond interactions between water molecules, on the other hand, small negative values indicate a deviation of this behavior with slight anti-parallel orientations. The first pronounced peak

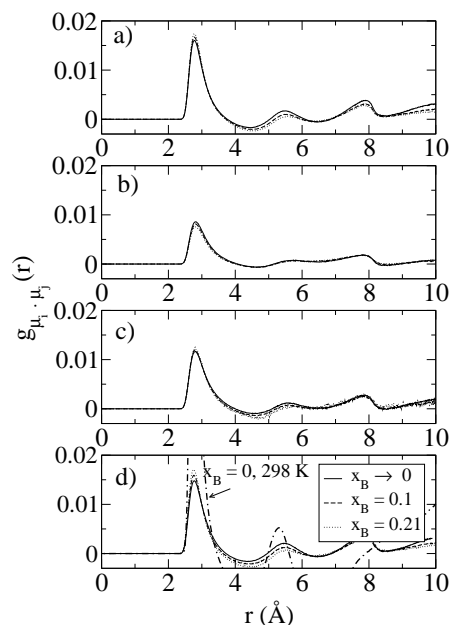


Figure 5.18. Radial variation of the product of the dipole vector of water molecules $\mu_i \cdot \mu_j$ in the mixture at for $x_B \rightarrow 0$ (line), $x_B = 0.1$ (dashed line) and $x_B = 0.21$ (dashed dotted line) for (from top to bottom) a) 573 K and 329 bar, b) 673 K and $\rho = 0.3 \text{ g/cm}^3$, c) 673 K and $\rho = 0.66 \text{ g/cm}^3$ and d) 673 K and $\rho = 0.995 \text{ g/cm}^3$.

observed in all plots represents the presence of water molecules in the first nearest neighbor shell whose dipoles moment strongly correlated with that of the test particle. The successive small peaks tell us that the correlated of orientations at large distances are progressively lost to finally reach $g_{\mu_i \mu_j}(r) \rightarrow 0$ when $r \rightarrow \infty$. The relative orientation between molecules is in close relation with the density. Consequently, the first peak of this function also increases when the density is increased as seen from Figure 5.18.b to Figure 5.18.c. Additionally, in the last figure we also include the value of $g_{\mu_i \mu_j}(r)$ of pure water at 298 K and 1 bar for comparison.

The temperature of the system also influences the value of the peaks (see the differences between Figure 5.18.a at 573 K and the others at 673 K) due to the fact that more rotational kinetic energy destroys the relative orientation of the dipoles and hence the dielectric constant of the fluid decreases. Surprisingly, $g_{\mu_i \mu_j}(r)$ seems to be unaffected by the increment of the molar fraction of benzene, probably because this molecule does not interact in any particular orientation with water molecules, remember that even with the possible HB between water and benzene molecules this bond is not oriented in any partic-

ular direction. Other works (Skaf, 1999, Skaf and Ladanyi, 1995) devoted to the analysis of the dielectric response of aqueous solutions of associating fluids such as methanol and DMSO, employ Fourier-Hankel transformation of the dipolar symmetry projections of pair correlations functions to analyze the orientation of dipoles but, since only water molecules present dipolar interactions we consider that the information given by $g_{\mu_i\mu_j}(r)$ is a good description of the reorientational distributions of dipoles in the mixture.

5. Conclusions

We have presented in this chapter a MD simulation study of transport and dielectric properties of aqueous solutions of benzene at supercritical conditions. We have explored two regions of the phase diagram of the mixture (see table 5.2), a) the supercritical 673 K isotherm at three different densities and b) the region of constant temperature 573 K and constant pressure around 324 bar. The lack of experimental data on the studied properties forces a comparison of our MD data with correlation and properties of pure components, to have a framework of reference. One of the first aspects to be mentioned is the capability of the new AUA (Nieto-Draghi et al., 2003a)(Anisotropic United Atom) model of benzene to reproduce the condition of one phase at the thermodynamic conditions of our study. The inclusion of point charges in the force field parameters of the benzene, reproducing the quadrupolar moment of the molecule, is an essential requirement to have an adequate interaction with water molecules. We have also demonstrated that this kind of non-polarizable model with permanent quadrupolar moments do not contribute directly to the value of the dielectric constant. Though some assumptions and simplifications can be done to compute the dielectric constant of the benzene molecule with non-polarizable models (Nymand et al., 2001), formally a degree of polarizability should be included in any model of benzene in order to compute the dielectric constant in a consistent way.

The self-diffusion of water (Figure 5.4) and benzene (Figure 5.5) present a strong density dependence, and we observe that the values of D_i are smaller when the density is increased. The increment of the molar fraction of benzene tends to decrease the value of this constant for both species, being the effect more pronounced at higher densities. Maxwell-Stefan mutual diffusion (Figure 5.6) presents the same density dependence, but in this case the effect of the amount of benzene is more pronounced at low densities. The behavior of the shear viscosity (Figure 5.7) is in close relation with that observed for the diffusion coefficient. In general η increases with density at supercritical conditions and the increment of x_B also produces a rapid growth in the value of this property. We employed an empirical correlation (Woerlee, 2001) for the product $\bar{D}_{ij} \cdot \eta$

applicable for supercritical fluids and a good agreement was found between our simulations and the values predicted by the correlation.

We have analyzed the local structure of the mixture through the computation of the orientational tetrahedral parameter q and we found that this property increases with the density and decreases with the addition of benzene molecules at all points of the supercritical 673 K isotherm. This behavior is more pronounced at states 1 to 3 at 573 K and ~ 324 bar. In addition of this parameter we have also analyzed the radial variation of the local tetrahedral order parameter q of the mixture, centered in the solute molecule. We have observed a first broad peak, which is a direct consequence of the presence of the solute that creates a solvation shell of water molecules with enhanced structure in comparison to other water molecules that are at distances further from benzene molecules. This behavior was observed in all the states analyzed in this chapter. In addition to this structural property, the average number of hydrogen bonds per molecule is also strongly influenced by the density, in a similar way as the q parameter. We also studied the presence of crossed HB between the hydrogen atom of water molecules and the electron ring of the benzene molecule. A considerable number of this kind of conformations fulfilled the geometrical requirements employed in this work to account for hydrogen bond interactions. These crossed HB are in qualitative agreement with the experimental observation of the formations of water-benzene aggregates ((Furataka and Ikawa, 1998b)). We have observed a considerable number of hydrogen bonds between water and benzene molecules at higher densities, with life times that are larger than the water-water hydrogen bonds present in the fluid. Additionally, we found good agreement between our simulations for water-water hydrogen bond lifetimes and NMR spectra experiments (Furataka and Ikawa, 2000) for reorientational hydrogen bond lifetimes. We continue the analysis done in this part of the work with the computation of the reorientational dynamics for the dipolar moment of water molecules and a vector defined on the benzene. A similar qualitative behavior between the two species was observed.

We closed the analysis done in this chapter with the computation of the dielectric response of the mixture determining the dielectric constant. We found that $\epsilon(0)$ decreases with the addition of benzene molecules. In addition the dielectric constant is directly affected by the density of the system, being this effect more pronounced at low molar fractions of benzene. The limitations of the model of benzene, without polarizability, will not affect the validity of the results obtained for this property since the contribution of this molecule should be of second order of importance in comparison to the high compared with the high dipole moment of water. Therefore, our results will be valid in mixtures non-diluted in water. The introduction of a radial decomposition of the dipolar moment product reflects the high orientational character of water molecules in

the first solvation shell, even at high temperatures and pressures. The presence of benzene does not affect in a significant way the orientation of the dipoles in the system, since benzene molecule does not have any preferential orientation.

Chapter 6

CONCLUSIONS AND PERSPECTIVES

We have employed Molecular Dynamics Simulations to study the intrinsic relationship existing between the structure and the dynamics of pure water, and the influence that mixtures with other organic solvents (such as alcohols, ketones, sulfoxides and benzene) may have in these structures. Since the relevant conclusion of the results have been discussed in detail on each chapter, here we only want to make emphasis on the most important considerations arisen in the discussion of the present manuscript.

We have computed transport and structural properties of water employing four rigid non-polarizable models of water (TIP4P, TIP5P, SPC/E and DEC). The self-diffusion coefficient observed is in good agreement with experimental data at 0.995 g/cm^3 up to $\sim 447 \text{ K}$, above this temperature a great deviation was observed. The dynamical behavior of pure water at this high density is strongly affected by the tetrahedral structure caused by the presence of the three dimensional network of hydrogen bonded molecules. In this way, a direct relationship between the self-diffusion coefficient and an order parameter, that accounts for this tetrahedral structure, was found up to $\sim 447 \text{ K}$, at the density studied. We have shown that this fact is model independent, something that emphasizes the general relationship. The order transition suffered in the local structure of water at temperatures above $\sim 345 \text{ K}$, from high to very high densities (0.9 to 1.3 g/cm^3), suggests the possibility of some kind of crossover between two regimes. The comparison done between different models of water, together with the different tools to analyze the structure of water, are our main contribution for the development of more accurate and reliable models of water.

The mixtures of water with organic associating fluids (methanol, ethanol, acetone and dimethyl sulfoxide) shows that local structure of water is affected

in a different manner according to the associating character of the solute, for instance, acceptor or donor-acceptor of hydrogen bonds. The increment and the maximum of the shear viscosity observed at particular concentrations of this kind of solutions is mainly caused by the loss of the tetrahedral order (symmetry) in the water molecules, created by the presence of the solute molecules (through crossed hydrogen bonds). This loss of the symmetry suffered by the water molecules promotes the formation of chain-like structures with long-lived hydrogen bonds with respect to those observed in pure water. The computation of the thermal conductivity of these kind of mixtures, and the improvements done in the NEMD algorithm proposed (see appendix E), are other two important contribution of this part of the work.

The study of the thermal diffusion of aqueous solutions of associating solutes shows that this effect can be obtained by non-equilibrium molecular dynamics simulations and can reproduce, even quantitatively, the experimental data, at least for the case of the two alcohols employed. We believe that the change in the sign of the thermal diffusion factor will appear in all cases where the energy of the crossed interaction between different species are more negative than the interaction energies between pure components. Even though, this argument should be supported by a consistent theory able to predict the change in the sign of this coefficient, something that, for the moment has not been done.

Supercritical water, employing the SPC/E model, is able to solvate benzene molecules if a consistent model of this compound is used. Such a model should include point charges in order to reproduce the quadrupolar moment of benzene. We show that the use of a non-polarizable model of benzene does not contribute directly to the computation of the dielectric constant of the mixture at zero wave vector \mathbf{k} . In this way, we obtain an important reduction of the dielectric constant of the mixture with the increment of the amount of benzene molecules, at least at medium and high densities. Our study qualitatively captures the experimental observation that some degree of association through hydrogen bonds is observed between the hydrogen atom of water molecules and the electron clouds of the benzenic ring. We also observe that these bonds are longer lived than the corresponding hydrogen bonds between water molecules. The Maxwell-Stefan mutual diffusion coefficient, and the shear viscosity of the mixture are also strongly affected by the presence of the benzene molecules at supercritical conditions.

We have made an effort in the present work for the development of new theoretical and methodological tools, from a molecular modeling point of view (Nieto-Draghi and Avalos, 2003), to improve the comprehension of the properties studied. We believe that these tools can be useful for a better understanding of the observed behavior of the different liquid systems.

After the main conclusion presented above we can mention some aspects that could be natural continuation of this work:

- Optimization of a water model to improve its predictive capabilities. In order to do this, for example the set of radial distribution functions projected with spherical harmonics for the different atom-atom interactions given in chapter 2, can be compared with similar data obtained from Neutron Diffraction Scattering experiments recently available. With this set of functions it is possible to apply some kind of Reverse Monte Carlo technique, in order to better reproduce the experimental microscopic structure.
- From the analysis of the crossover observed in water above ~ 345 K, from high to very high densities (0.9 to 1.3 g/cm³), it would be interesting to make a cluster analysis to quantify the size and topology of the hydrogen bonded cluster water molecules.
- For the case of the observed enhancement of the shear viscosity and the relationship observed with the formation of hydrogen bonded chains, it would be of great interest to determine the size and topology of these chains, aiming at a better picture of the microscopic process involved and its relationship with the nature of the solute.
- The formulation of a consistent theory, able to predict the sign and the value of the Soret coefficient is required. The behavior observed in the simple lattice model proposed in this work may help on the achievement of this goal.
- The observed behavior of benzene molecules at supercritical water seems to capture the experimental observation of the formation of aggregates between water and benzene. The analysis done here can be extended to more complex molecules with particular industrial interest.

Appendix A

Spherical Harmonics expansion of the RDF

Pair distribution function can be expanded in term of spherical harmonics, as it was previously mentioned in chapter 1. In this work, several spherical harmonics have been chosen to explore the surrounded space of a central molecule, thus eq. 1.10 is partially expanded according to,

$$\begin{aligned}
 g(\mathbf{r}) = g(r, \theta, \phi) = & \frac{1}{\sqrt{4\pi}} \cdot g_{ab}^{00}(r) \\
 & + \sqrt{\frac{3}{4\pi}} \cdot \cos(\theta) \cdot g_{ab}^{10}(r) \\
 & + \sqrt{\frac{5}{4\pi}} \cdot \left(\frac{3}{2} \cos^2(\theta) - \frac{1}{2} \right) \cdot g_{ab}^{20}(r) \\
 & + 2\sqrt{\frac{5}{96\pi}} \cdot 3 \sin^2(\theta) \cdot \cos(2\phi) \cdot g_{ab}^{22}(r) \\
 & + \sqrt{\frac{7}{16\pi}} \cdot (5 \cos^3(\theta) - 3 \cos(\theta)) \cdot g_{ab}^{30}(r) \\
 & + \frac{15}{2} \sqrt{\frac{7}{30\pi}} \cos(\theta) \cdot \sin^2(\theta) \cdot \cos(2\phi) \cdot g_{ab}^{32}(r) \\
 & + \frac{3}{16\sqrt{\pi}} (35 \cos^4(\theta) - 30 \cos^2(\theta) + 3) \cdot g_{ab}^{40}(r) \\
 & + \frac{15}{4\sqrt{10\pi}} \cdot (7 \cos^2(\theta) - 1) \cdot \sin^2(\theta) \cdot \cos(2\phi) \cdot g_{ab}^{42}(r) \\
 & + \frac{105}{8\sqrt{70\pi}} \cdot \sin^4(\theta) \cos(4\phi) \cdot g_{ab}^{44}(r)
 \end{aligned} \tag{A.1}$$

where r , θ and ϕ are defined in Figure 1.2, and

$$\cos(\theta) = \hat{r} \cdot \hat{k} \tag{A.2}$$

$$\cos(\phi) = -\hat{j} \cdot \frac{\hat{r} \times \hat{k}}{|\hat{r} \times \hat{k}|} \quad (\text{A.3})$$

$$\cos(2\phi) = 2 \cos^2(\phi) - 1 \quad (\text{A.4})$$

$$\cos(4\phi) = 8 (\cos^4(\phi) - \cos^2(\phi)) + 1 \quad (\text{A.5})$$

being \hat{r} a unitary vector in the direction of the two sites of interest and \hat{j} and \hat{k} are unitary vectors in the directions of y axis and z axis respectively.

Appendix B

Quaternion formalism for rotational dynamics

It is possible to transform an arbitrary vector e from a space-fixed (s) frame to a body-fixed (b) frame through a rotational matrix A , thus

$$\mathbf{e}^b = \bar{A} \cdot \mathbf{e}^s \quad (\text{B.1})$$

$$\bar{A} = \begin{pmatrix} q_0^2 + q_1^2 - q_2^2 - q_3^2 & 2(q_1q_2 + q_0q_3) & 2(q_1q_3 + q_0q_2) \\ 2(q_1q_2 - q_0q_3) & q_0^2 - q_1^2 + q_2^2 - q_3^2 & 2(q_2q_3 + q_0q_1) \\ 2(q_1q_3 + q_0q_2) & 2(q_1q_3 - q_0q_1) & q_0^2 - q_1^2 - q_2^2 + q_3^2 \end{pmatrix} = A(Q) \quad (\text{B.2})$$

where,

$$q_0 = \cos\left(\frac{1}{2}\theta\right) \cdot \cos\left(\frac{1}{2}(\phi + \psi)\right) \quad (\text{B.3})$$

$$q_1 = \sin\left(\frac{1}{2}\theta\right) \cdot \cos\left(\frac{1}{2}(\phi - \psi)\right) \quad (\text{B.4})$$

$$q_2 = \sin\left(\frac{1}{2}\theta\right) \cdot \sin\left(\frac{1}{2}(\phi - \psi)\right) \quad (\text{B.5})$$

$$q_3 = \cos\left(\frac{1}{2}\theta\right) \cdot \sin\left(\frac{1}{2}(\phi + \psi)\right) \quad (\text{B.6})$$

are the quaternions with the constrain $q_0^2 + q_1^2 + q_2^2 + q_3^2 = 1$, being θ , ϕ and ψ Euler angles.

Now, it is possible to find an expression to advance in time the quaternions,

$$\dot{\mathbf{Q}} = B \cdot \mathbf{W}^b \quad (\text{B.7})$$

where $\mathbf{W}^b = (0, w_x^b, w_y^b, w_z^b)$ is an extended angular velocity vector. This vector can be determined by,

$$\mathbf{w} = I^{-1} \cdot \mathbf{J} \quad (\text{B.8})$$

here I^{-1} is the inverse of the principal momentum inertia tensor (diagonal), and \mathbf{J} is the angular momentum vector. Consequently, the torque then determines the evolution of the angular momentum, according to

$$\dot{\mathbf{J}} = \mathbf{T} \quad (\text{B.9})$$

Finally, the rotational motion can be formulated through a leap-frog type algorithm. Thus the angular momentum and the quaternions are then propagated according to,

$$\mathbf{J}(t + \Delta t/2) = \mathbf{J}(t - \Delta t/2) + \Delta t \cdot \mathbf{T}(t) \quad (\text{B.10})$$

$$\mathbf{Q}(t + \Delta t) = \mathbf{Q}(t) + \Delta t \cdot \dot{\mathbf{Q}}(t + \Delta t/2) \quad (\text{B.11})$$

However, in this case the complication arises that $\dot{\mathbf{Q}} = \dot{\mathbf{Q}}(\mathbf{J}, \dot{\mathbf{Q}})$. Then this problem can be overcome through the use of an auxiliary equation that calculate the angular momentum at time t by taking half step in eq. (B.10) and eq. (B.11).

$$\mathbf{J}(t) = \mathbf{J}(t - \Delta t/2) + \Delta t/2 \cdot \mathbf{T}(t) \quad (\text{B.12})$$

Since $\mathbf{Q}(t)$ is known, it is possible to apply eq. (B.1), eq. (B.7) and eq. (B.8) to convert $\mathbf{J}(t)$ to $\dot{\mathbf{Q}}(t)$, which is then used to estimate $\mathbf{Q}(t + \Delta t/2)$:

$$\mathbf{Q}(t + \Delta t/2) = \mathbf{Q}(t) + \Delta t/2 \cdot \dot{\mathbf{Q}}(t) \quad (\text{B.13})$$

When $\mathbf{Q}(t + \Delta t/2)$ has been estimated, one apply eq. (B.1), eq. (B.7) and eq. (B.8) to convert from $\mathbf{J}(t + \Delta t/2)$ to the corresponding value of $\dot{\mathbf{Q}}(t + \Delta t/2)$. Then, eq. (B.11) can be evaluated.

Appendix C

Error function and complementary error function

The error function is defined according to,

$$\operatorname{erf}(x) = \frac{2}{\sqrt{\pi}} \int_0^x e^{-u^2} du \quad (\text{C.1})$$

with the following properties,

$$\operatorname{erf}(-x) = -\operatorname{erf}(x) \quad (\text{C.2})$$

$$\operatorname{erf}(0) = 0 \quad (\text{C.3})$$

$$\operatorname{erf}(\infty) = 1 \quad (\text{C.4})$$

The complementary error function is defined according to,

$$\operatorname{erfc}(x) = 1 - \operatorname{erf}(x) = \frac{2}{\sqrt{\pi}} \int_x^\infty e^{-u^2} du \quad (\text{C.5})$$

$$\operatorname{erfc}(0) = 1 \quad (\text{C.6})$$

$$\operatorname{erfc}(\infty) = 0 \quad (\text{C.7})$$

Appendix D

Adaptation of the DEC model parameters for the use of reaction field methodology

Rewriting equations 1.87 through 1.92 with the reaction field methodology we have,

$$u_{qq} = \frac{1}{2} \sum_{i,j} \frac{q_i q_j}{4\pi\epsilon_0 r_{ij}} \cdot \left[1 + \frac{\epsilon_{RF} - 1}{2\epsilon_{RF} + 1} \frac{r_{ab}^3}{r_c^3} \right] \quad (D.1)$$

$$u_{q^d q^d} = \frac{1}{2} \sum_{i,j} \frac{q_i^d q_j^d}{4\pi\epsilon_0 r_{ij}} \cdot \text{erf} \left(\frac{r_{ij}}{2\xi} \right) \cdot \left[1 + \frac{\epsilon_{RF} - 1}{2\epsilon_{RF} + 1} \frac{r_{ab}^3}{r_c^3} \right] \quad (D.2)$$

$$u_{q q^d} = \sum_{i,j} \frac{q_i q_j^d}{4\pi\epsilon_0 r_{ij}} \cdot \text{erf} \left(\frac{r_{ij}}{\sqrt{2}\xi} \right) \cdot \left[1 + \frac{\epsilon_{RF} - 1}{2\epsilon_{RF} + 1} \frac{r_{ab}^3}{r_c^3} \right] \quad (D.3)$$

$$u_{q^d q} = \sum_{i,j} \frac{q_i^d q_j}{4\pi\epsilon_0 r_{ij}} \cdot \text{erf} \left(\frac{r_{ij}}{\sqrt{2}\xi} \right) \cdot \left[1 + \frac{\epsilon_{RF} - 1}{2\epsilon_{RF} + 1} \frac{r_{ab}^3}{r_c^3} \right] \quad (D.4)$$

$$u_{rep} = A_{rep} \frac{\text{erfc}(z)}{z} \left(z = \frac{r_{oo}}{2\xi_r} \right) \quad (D.5)$$

$$u_{disp} = -\frac{C_6}{r_{oo}^6} \quad (D.6)$$

And the corresponding forces on each side are given by

$$\mathbf{F}_{qq} = \frac{q_i q_j}{4\pi\epsilon_0} \left[\frac{1}{r_{ij}^3} - \frac{\epsilon_{RF} - 1}{2\epsilon_{RF} + 1} \frac{2}{r_c^3} \right] \cdot \mathbf{r}_{ij} \quad (\text{D.7})$$

$$\mathbf{F}_{q^d q^d} = -\frac{q_i^d q_j^d}{4\pi\epsilon_0} \left[\frac{1}{r_{ij}} \frac{1}{\sqrt{\pi\xi}} e^{-\frac{r_{ij}^2}{4\xi^2}} \left(\frac{1}{r_{ij}} + \frac{\epsilon_{RF} - 1}{2\epsilon_{RF} + 1} \frac{r_{ij}^2}{r_c^3} \right) + \frac{1}{r_{ij}} \operatorname{erf} \left(\frac{r_{ij}}{2\xi} \right) \left(\frac{-1}{r_{ij}^2} + \frac{\epsilon_{RF} - 1}{2\epsilon_{RF} + 1} \frac{2r_{ij}}{r_c^3} \right) \right] \cdot \mathbf{r}_{ij} \quad (\text{D.8})$$

$$\mathbf{F}_{qq^d} = -\frac{q_i q_j^d}{4\pi\epsilon_0} \left[\frac{1}{r_{ij}} \frac{2}{\sqrt{2\pi\xi}} e^{-\frac{r_{ij}^2}{2\xi^2}} \left(\frac{1}{r_{ij}} + \frac{\epsilon_{RF} - 1}{2\epsilon_{RF} + 1} \frac{r_{ij}^2}{r_c^3} \right) + \frac{1}{r_{ij}} \operatorname{erf} \left(\frac{r_{ij}}{\sqrt{2}\xi} \right) \left(\frac{-1}{r_{ij}^2} + \frac{\epsilon_{RF} - 1}{2\epsilon_{RF} + 1} \frac{2r_{ij}}{r_c^3} \right) \right] \cdot \mathbf{r}_{ij} \quad (\text{D.9})$$

$$\mathbf{F}_{q^d q} = -\frac{q_i^d q_j}{4\pi\epsilon_0} \left[\frac{1}{r_{ij}} \frac{2}{\sqrt{2\pi\xi}} e^{-\frac{r_{ij}^2}{2\xi^2}} \left(\frac{1}{r_{ij}} + \frac{\epsilon_{RF} - 1}{2\epsilon_{RF} + 1} \frac{r_{ij}^2}{r_c^3} \right) + \frac{1}{r_{ij}} \operatorname{erf} \left(\frac{r_{ij}}{\sqrt{2}\xi} \right) \left(\frac{-1}{r_{ij}^2} + \frac{\epsilon_{RF} - 1}{2\epsilon_{RF} + 1} \frac{2r_{ij}}{r_c^3} \right) \right] \cdot \mathbf{r}_{ij} \quad (\text{D.10})$$

$$\mathbf{F}_{rep} = -\frac{A_{rep}}{r_{ij}} \left[\frac{-1}{r_{ij}} \frac{2}{\sqrt{\pi}} e^{-\frac{r_{ij}^2}{4\xi_r^2}} - \frac{1}{r_{ij}^2} 2\xi_r \operatorname{erfc} \left(\frac{r_{ij}}{2\xi_r} \right) \right] \cdot \mathbf{r}_{ij} \quad r_{ij} = r_{oo}^{ij} \quad (\text{D.11})$$

$$\mathbf{F}_{dis} = -6 \frac{C_6}{r_{ij}^8} \cdot \mathbf{r}_{ij} \quad r_{ij} = r_{oo}^{ij} \quad (\text{D.12})$$

where $\mathbf{r}_{ij} = (x_{ij}\hat{x}, y_{ij}\hat{y}, z_{ij}\hat{z})$, and the parameters are the same that in Table 1.1 and Table 1.2.

Appendix E

NEMD algorithm to generate heat flux

Due to the increase of the computational power, the calculation of physical properties of fluids with industrial interest from molecular simulations has attracted considerable attention. However, calculations of transport properties of mixtures by means of molecular simulations are still rather scarce when compared with the effort devoted to calculations of equilibrium thermodynamic properties, such as phase equilibria diagrams, for instance. Molecular dynamics simulations have been widely used to determine transport properties due to the fact that the method essentially reproduces the microscopic dynamics of the particles through the integration of the equations of motion provided suitable intermolecular potentials. Transport properties can be obtained from systems in thermal equilibrium by the use appropriate *Green-Kubo* formulae, which involve the integration of correlation functions of the proper microscopic *current*, depending on the property studied (Hansen and McDonald, 1991). There also exist non-equilibrium methods, in which the so-called thermodynamic forces (or, equivalently, the currents) are externally imposed on the system, and its response is thus calculated (Evans and Morris, 1990). In this research note we will focus our attention to an improvement of the non-equilibrium PEX algorithm of Müller-Plathe (Muller-Plathe, 1997, Reith and Muller-Plathe, 2000), aiming at its application to the calculation of thermal conductivity of mixtures.

There are several difficulties in the use of the Green-Kubo formalism for the calculation of the thermal conductivity of mixtures. The most important one is the presence of a contribution in the form of differences of *partial molar enthalpies* of the species in the microscopic expression of the heat flux density (de Groot and Mazur, 1984, Hoheisel, 1999, Vogelsang et al., 1987, Dysthe et al., 1999b). Partial molar properties are difficult to obtain in simulations with a fixed number of particles. Hence, in general, it is not known an efficient way to obtain these magnitudes in the course of the same simulations that lead to the determination of the thermal conductivity, without its separate evaluation. Only in the case of ideal mixtures, nevertheless, the contribution arisen from the partial molar enthalpies can be disregarded in a Green-Kubo formalism (Dysthe et al., 1999b). In the case of very non-ideal solutions, this simplification is no longer valid. Therefore, there is an evident interest in developing non-equilibrium schemes suitable for the determination of the thermal conductivity in non-ideal mixtures.

Among others, the non-equilibrium algorithm presented by Müller-Plathe in ref. (Muller-Plathe, 1997) is especially appropriate. Effectively, in the process of externally maintaining a

heat flux, the total momentum and total energy of the system are kept constants. In addition, the algorithm is simple and efficient. Another advantage of the PeX-like algorithms is that they can also be employed in the calculation of cross effects like the Soret coefficient (Reith and Muller-Plathe, 2000). The original work was addressed to the analysis of pure systems, which was later extended to mixtures and molecular fluids (Reith and Muller-Plathe, 2000, Bedrov and Smith, 2000). The application of PeX to mixtures however has some limitations, which we will comment on later. In this short note we present a simple scheme to impose a heat flux in multicomponent systems, which is a generalization of the constant temperature PeX (momentum exchange) algorithm developed by Müller-Plathe *et. al.* (Muller-Plathe, 1997) and overcomes the limitations of the original method.

In the PeX scheme, the simulation box has periodic boundary conditions in the three directions of the space. In the z -direction, one considers two slabs of a given thickness, large enough to contain many particles in average, but much smaller than the length of the box in this direction. To maintain a heat flux, with a given frequency ν the fastest particle in so-called *cold* slab is selected to exchange its velocity with the slowest particle in the *hot* slab. Due to the selection procedure the induced energy exchange between the chosen particles effectively leads to an energy flow *pumped* back from the cold to the hot slab, which maintains a given temperature gradient, related to the selected frequency of exchange. For molecular systems, the exchanged velocities are those of the respective centers of mass of the molecules participating in the exchange. Hence, the new and old velocities after and before the exchange are related according to

$$\mathbf{v}_c^{new} = \mathbf{v}_h^{old} \text{ and } \mathbf{v}_h^{new} = \mathbf{v}_c^{old} \quad (\text{E.1})$$

where the subscripts c and h denote a particle in the cold or hot slab, respectively. Notice that the algorithm given in this equation eq. (E.1) the exchange is restricted to particles of the same mass, since it is the only way in which the total momentum as well as total energy of the system are invariant under this process. This simple algorithm has been generalized to mixtures (Reith and Muller-Plathe, 2000) by proposing the same exchange given by eq. (E.1) for every species present in the system at every time. Therefore, if one species is very diluted in a given slab, it can occur that the process cannot be continued without paying the price of heating the species not in an equivalent way.

Aiming at a generalization to multicomponent systems independently of the compositions, we propose the following algorithm. First, we select the molecule whose kinetic energy is the largest (instead of the faster molecule) in the cold region, together with that of the lower kinetic energy (instead of the slowest) in the hot region, independently of the molecular species present in each slab. The idea behind the new scheme is to consider an energy and momentum exchange between cold and hot slabs as if a hypothetical *elastic collision* between these two selected molecules would take place. Obviously such exchange keeps constant the total energy as well as the total momentum of the overall system. Therefore, after such a virtual collision, the new velocity of the molecule for the cold region can be expressed as (Goldstein, 1996)

$$\mathbf{v}_c^{new} = -\mathbf{v}_c^{old} + 2 \frac{m_c \mathbf{v}_c^{old} + m_h \mathbf{v}_h^{old}}{m_c + m_h} \quad (\text{E.2})$$

while, for the hot region,

$$\mathbf{v}_h^{new} = -\mathbf{v}_h^{old} + 2 \frac{m_c \mathbf{v}_c^{old} + m_h \mathbf{v}_h^{old}}{m_c + m_h} \quad (\text{E.3})$$

where m_c and m_h are the respective masses of the particles selected in the cold and hot slabs. Furthermore, notice that eqs. (E.2) and (E.3) reduce to the old algorithm as expressed in eq. (E.1) if the masses of the particles entering in the exchange are the same. Finally, for molecular systems, the velocities entering in our algorithm are the center of mass velocities of both species, exchanging their energy and momentum. Therefore, the system can also describe polymeric systems, for instance, if required.

The energy exchange induced by the virtual collision is added to the value of the accumulated energy exchanged by the two slabs. As a consequence, the heat flow induced in steady state by this method of exchange can be obtained indistinctly from the variation of energy in one of the slabs, either the *hot* or the *cold*, according to the expression

$$\langle J_z(t) \rangle = \frac{1}{2At} \sum_{transfers(t)} \frac{1}{2} m_h ((\mathbf{v}_h^{new})^2 - (\mathbf{v}_h^{old})^2) \quad (\text{E.4})$$

Here, the sum is done over all the transfers occurred since an initial time (after the steady state is reached), and t is the time interval since this origin. The factor 2 comes from the fact that we consider a thick hot slab in the center of the simulation box while two half the thickness cold slabs are placed at the edges. Hence, the system described is in fact of double size. In this expression, A is the cross-sectional area and $\langle J_z(t) \rangle$ is the heat flow density in the z direction (i.e. the direction of the imposed temperature gradient), since in steady state in a system macroscopically at rest the heat flow has to equate the energy per unit of time pumped back by the procedure. Eq. (E.4) should not be confused with a microscopic expression for the heat current (Hansen and McDonald, 1991), but a result of the steady state energy balance after the system has been driven out of equilibrium by the energy exchange procedure previously discussed. As such, no need of partial molar enthalpies is required for its evaluation. In addition, it is obvious that $\langle J_z(t) \rangle$ corresponds to the macroscopic heat flow measured in the experiments (MacGowan and Evans, 1986a, Evans and MacGowan, 1987, de Groot and Mazur, 1984).

We want to insist that in the PeX algorithm, in its original formulation for mixtures (Reith and Muller-Plathe, 2000), the momentum exchange should be done only between particles of the *same* species. Hence, it is required that the number of particles in both slabs is sufficiently large, on one hand, to be sure that it is always possible to find particles of each species to exchange their energy. On the other hand, it is also desirable that the collisions inside the slabs properly thermalize the velocity distribution before a new exchange is done, to avoid different non-equilibrium temperatures in each species. These requirements are fulfilled on relatively dense phases, such as liquid densities, but would fail for very diluted gaseous mixtures or for systems that phase separate and hence some species are unlikely to be found in some of the slabs. In the new scheme these restrictions are not present. Our method, not distinguishing between species is not affected by such a restriction.

Finally, once the thermal gradient is stabilized and the process is stationary, the thermal conductivity can be obtained from

$$\lambda = \lim_{dT/dz \rightarrow 0} \lim_{t \rightarrow \infty} \frac{\langle J_z(t) \rangle}{dT/dz} \quad (\text{E.5})$$

where $\langle dT/dz \rangle$ is the resulting temperature gradient in the z direction (Bedrov and Smith, 2000). The requirement of $dT/dz \rightarrow 0$ is formally demanded to guarantee that the linear regime is achieved and the classical linear non-equilibrium thermodynamics apply. Certainly, eq. (E.5) is the simulation counterpart of the experimental determination of the thermal conductivity, and can be directly compared with experimental data obtained from the ratio between heat flux and temperature gradient. This point of view is the same as that adopted in ref. (MacGowan and Evans, 1987, Evans and MacGowan, 1987) in which the effect of the composition gradients, induced by the temperature gradient, is absorbed into the value of λ , in this way directly accessible experimentally. It is a matter of taste to separate the observed heat flux into different contributions, *i. e.* that due to the thermal gradient plus that due to the composition gradients. This is the choice expressed in the classical monograph of the de Groot and Mazur. As a consequence, what they name *thermal conductivity* is not directly given by the ratio expressed in eq. (E.5). The thermal diffusion coefficient has to be introduced to cancel the effect of the induced composition gradients. As a consequence, the λ defined in this last reference cannot be obtained directly from experiments. Finally, it is worth mentioning that the difference in the values of λ obtained from both prescriptions only differ by a few percent, which in many cases is less than the error made in its determination.

Appendix F Correlations

1. Correlation for Self-diffusion coefficient of water

From the work of I. Svishchev *et al.* (Svishchev and Zassetsky, 2000) a fitted equation was taken in order to estimate the self-diffusion coefficient at constant density ($\rho = 0.995 \text{ g/cm}^3$) in ranges outside of the experimental data available. For instance we readjust slightly one of the parameters to exactly reproduce this experimental values.

$$D = D_0 T^{\frac{1}{2}} \left(\frac{T}{T_s} - 1 \right)^\gamma \quad (\text{F.1})$$

where γ , D_0 , and T_s are fitting parameters. The original values of the fitted parameters are $D_0 = 6.24 \times 10^{-6} \text{ cm}^2/(\text{s.K}^{1/2})$, $\gamma = 1.62$, $T_s = 218 \text{ K}$. Thus, readjusting $D_0 = 6.759 \times 10^{-6} \text{ cm}^2/(\text{s.K}^{1/2})$ is possible to reproduce $D = 2.3 \times 10^{-5} \text{ cm}^2/\text{s}$ at $T = 298 \text{ K}$ in agreement with the experimental data of Krynicki *et al.* (Krynicki et al., 1980).

2. Average number of Hydrogen bond in function of Temperature

From the work presented Suresh *et al.* (Suresh and Naik, 2000), is possible to extract a theoretical equation that relates the density and temperature of the system with the average number of hydrogen bond per molecule. Thus, from eq. (8) of this article,

$$P = \frac{K}{1 + K} \quad (\text{F.2})$$

and

$$\langle N_{HB} \rangle = 4P = \frac{4(\sqrt{1+8\rho K} - 1)}{(\sqrt{1+8\rho K} + 1)} \quad (\text{F.3})$$

where P is the probability that a given association site on a central water molecule, is bonded at a certain instant of time, thus $\langle N_{HB} \rangle$ is the average number of hydrogen bonds per molecule, and $K = e^{\frac{-(H-TS)}{k_B T}}$ is the equilibrium bond formation. Rearranging eq. (F.3) and introducing this expression we have,

$$T(\langle N_{HB} \rangle) = \frac{H}{S - k_b \ln \left[\frac{1}{8\rho} \left[\frac{(\langle N_{HB} \rangle + 4)^2}{(4 - \langle N_{HB} \rangle)^2} - 1 \right] \right]} \quad (\text{F.4})$$

where H = -5.58 kcal/mol of H-bond is the enthalpy of formation of a Hydrogen bond, S = -8.89 cal/K mol of H-bond is the entropy of formation of a Hydrogen bond, ρ is the system density in g/cm^3 and k_b the Boltzman constant.

Finally, introducing eq. (F.3) into eq. (F.4) its possible to have an expression of $D=D(\langle N_{HB} \rangle)$.

Appendix G

Physical properties

1. Properties of the different models to simulate water

Table 1 Some of the calculated physical properties of the water models (Chapling, 2003).

All the data is at 25°C and 1 atm, except ^a at 20°C.

Many of the data values given in table 1 vary significantly between different workers. As can be deduced from the data given (and other data), although such simple models are of great utility, no universally applicable model can be identified at this time. It should also be noted that many simulations are performed with just a few hundred water molecules within rectangular periodic boxes no more than 2.5 nm along each edge for times equivalent to a few picoseconds; conditions that reduce discovery of long-range effects. (Chapling, 2003)

Model	μ	$\epsilon(0)$	$D, 10^{-5} \text{ cm}^2/\text{s}$	$U_{av}, \text{ kJ/mol}$	$\rho_{max} \text{ }^\circ\text{C}$	Exp. coeff. $10^{-4} \text{ }^\circ\text{C}^{-1}$
SPC	2.27	65	3.85	-41.0		
SPC/E	2.35	71	2.49	-41.5	-38	
PPC	2.52	77	2.6	-43.2	+4	
TIP3P	2.35	82	5.19	-41.1	-13	9.2
TIP4P	2.18	53 ^a	3.29	-41.8	-25	4.4
TIP4P-FQ	2.64	79	1.93	-41.4	+7	
SWFLEX-AI	2.69		3.66	-41.7		
TIP5P	2.29	81.5	2.62	-41.3	+4	6.3
Expt.	2.65,3.0	78.4	2.30	-41.5	+3.984	2.53

References

- [not, a] Notice that sharp peaks in the NDS experimental data at low distances correspond to intra-molecular correlations and therefore are not described by the radial distribution function defined here, which correspond to inter-molecular correlations.
- [not, b] In ref. 10, results issued by the TIP5P were compared to data obtained from ALS X-RAY technique, with the same degree of agreement as with the NDS data.
- [wor, 1999] (1999). Workshop on Predicting the Thermophysical Properties of Fluids by Molecular Simulation. Web address <http://www.ctcms.nist.gov/fstart/ptpfms/statement.html>.
- [mdg, 2003] (2003). Molecular Dynamics Genral code developped by Bernard Rousseau at the Laboratoire de Chimie Physique, Univerite de Paris Sud-XI.
- [Adya et al., 2001] Adya, A. K., Kalugin, O. N., Volobuev, M. N., and Kolesnik, Y. V. (2001). *Mol. Phys.*, 99:835.
- [Allen and Tildesley, 1989] Allen, M. P. and Tildesley, D. J. (1989). *Computer Simulation of Liquids*. Clarendon Press Oxford, Oxford, Great Britain, first edition.
- [Alwani and G. M. Schneider, 1967] Alwani, Z. and G. M. Schneider, B. B. (1967). *Phys. Chem.*, 71:633.
- [Andersen, 1980] Andersen, H. C. (1980). *J. Chem. Phys.*, 72:2384.
- [Andersen, 1983] Andersen, H. C. (1983). *J. Comp. Phys.*, 52:24.
- [Arfken, 1981] Arfken, G. (1981). *Mathematical Methods for Physics*. Academic Press, New York, USA, first edition.
- [Badyal et al., 2000] Badyal, Y., Saboungi, M., Price, D., Shastri, S., Haeffner, D., and Soper, A. K. (2000). *J. Chem. Phys.*, 112:9206.
- [Balbuena et al., 1996] Balbuena, P. B., Johnston, K. P., and Rosicky, P. J. (1996). *J. Phys. Chem.*, 100:2706.
- [Barrat and Hansen, 2003] Barrat, J. L. and Hansen, J. P. (2003). *Basic concepts for simple and complex liquids*. Cambridge University Press, Cambridge, UK, first edition.

- [Bedrov and Smith, 2000] Bedrov, D. and Smith, G. D. (2000). *J. Chem. Phys.*, 113:8080.
- [Benmore and Loh, 2000] Benmore, C. and Loh, Y. L. (2000). *J. Phys. Chem.*, 112:5877.
- [Berendsen et al., 1987] Berendsen, H. J. C., Grigera, J. R., and Straasma, T. P. (1987). *J. Phys. Chem.*, 91:6269.
- [Berendsen et al., 1984] Berendsen, H. J. C., Postma, J. P. M., van Gunsteden, W. F., DiNola, A., and Haak, J. R. (1984). *J. Phys. Chem.*, 81:3684.
- [Berne and Pecora, 1976] Berne, B. J. and Pecora, R. (1976). *Dynamic Light Scattering*. Wiley, New York, USA.
- [Bluhm et al., 2002] Bluhm, H., Ogletree, D. F., C. S. Fadley, Z. H., and Salmeron, M. (2002). *J. of Phys.: Cond. Matt.*, 14:L227.
- [Bordat et al., 2002] Bordat, P., Sacristan, J., Reith, D., Girard, S., Glattli, A., and Muller-Plathe, F. (2002). *J. Am. Chem. Soc. (Submitted)*.
- [Borin and Skaf, 1999] Borin, I. A. and Skaf, M. S. (1999). *J. Chem. Phys.*, 110:6412.
- [Bou-Ali, 1999] Bou-Ali, M. M. (1999). *Determinacion termogravitacional del coeficiente Soret en mezclas liquidas binarias. Influencia del numero de Grashof sobre la estabilidad convectiva en columnas de difusion termica*. PhD thesis, Universidad del Pais Vasco.
- [Bou-Ali et al., 1998] Bou-Ali, M. M., Encenarro, O., Madariaga, J. A., Santamaria, C. M., and Valencia, J. J. (1998). *J. Phys.: Condens. Matt.*, 10:3321.
- [Bridgman, 1923] Bridgman, P. W. (1923). *Proc. Am. Acad. Arts. Sci.*, 59:141.
- [Bulone et al., 1989] Bulone, D., Spinnato, C., Madonia, F., and Palma, U. (1989). *J. Chem. Phys.*, 91:408.
- [Carey and Korenowski, 1998] Carey, D. M. and Korenowski, G. M. (1998). *J. Chem. Phys.*, 108.
- [Chapling, 2003] Chapling, M. (2003). *Water Structure Behavior, Review* (<http://www.sbu.ac.uk/water/>).
- [Chau and Hardwick, 1998] Chau, P. L. and Hardwick, A. J. (1998). *Mol. Phys.*, 93:511.
- [Chialvo and Cummings, 1996a] Chialvo, A. and Cummings, P. (1996a). *J. Phys. Chem.*, 100:1309.
- [Chialvo et al., 1996] Chialvo, A. A., Cummings, P., and Cochran, H. D. (1996). *Int. J. of Therm.*, 17:147.
- [Chialvo et al., 1995] Chialvo, A. A., Cummings, P., Cochran, H. D., Simonson, J. M., and Mesmer, R. E. (1995). *J. Chem. Phys.*, 103:9379.
- [Chialvo and Cummings, 1996b] Chialvo, A. A. and Cummings, P. T. (1996b). *J. Phys.: Condens. Matter*, 8:9281.
- [Chialvo et al., 2002] Chialvo, A. A., Ho, P., Palmer, D. A., Gruszkiewicz, M. S., Cummings, P., and Simonson, J. M. (2002). *J. Phys. Chem.*, 106:2041.

- [Contreras, 2002] Contreras, R. O. (2002). *Determinacion del equilibrio Liquido-Vapor de agua, aromaticos y sus mezclas mediante simulacion molecular*. PhD thesis, Universitat Rovira i Virgili.
- [Cowie and Toporowski, 1961] Cowie, J. M. G. and Toporowski, P. M. (1961). *Can. J. Chem.*, 39:2240.
- [Cummings and Chialvo, 1996] Cummings, P. T. and Chialvo, A. A. (1996). *J. Phys.: Condens. Matter*, 8:9281.
- [Day and Patey, 1999] Day, T. J. F. and Patey, G. N. (1999). *J. Chem. Phys.*, 110:10937.
- [de Gans et al., 2003a] de Gans, B., R. Kita, B. M., and Wiegand, S. (2003a). *J. Chem. Phys.*, submitted.
- [de Gans et al., 2003b] de Gans, B., Wiegand, S., and Luettmmer-Strathman, J. (2003b). *Phys. Rev. Lett.*, submitted.
- [de Groot, 1945] de Groot, S. R. (1945). *L'effect Soret*. PhD thesis, Amsterdam.
- [de Groot et al., 1943] de Groot, S. R., Gorter, C. J., and Hoogenstraaten, W. (1943). *Physica*, 10:81.
- [de Groot and Mazur, 1984] de Groot, S. R. and Mazur, P. (1984). *Non-equilibrium thermodynamics*. Dover Publications, INC., New York, USA.
- [de ven Lucassen et al., 1998] de ven Lucassen, I. V., T. J. H. Vlugt, A. J. J. V. d. Z., and Kerkhof, P. J. A. M. (1998). *Mol. Phys.*, 94:495.
- [DNA, 2001] DNA (2001). *Molecular Page: Water and Ice Structure* (http://cwis.nyu.edu/pages/mathomol/modules/water/info_water.htm).
- [Dougherty and Drickamer, 1955] Dougherty, E. L. and Drickamer, H. G. (1955). *J. Phys. Chem.*, 59:443.
- [Dudziak and Franck, 1966] Dudziak, K. H. and Franck, E. U. (1966). *Ber. Bunsenges. Phys. Chem.*, 70:1120.
- [Dufour, 1872a] Dufour, L. (1872a). *Arch. Sci. phys. nat.*, 45:9.
- [Dufour, 1872b] Dufour, L. (1872b). *Ann. Phys.*, 28(5):490.
- [Dysthe et al., 1999a] Dysthe, D. K., Fuchs, A. H., and Rousseau, B. (1999a). *J. Chem. Phys.*, 110:4047.
- [Dysthe et al., 1999b] Dysthe, D. K., Fuchs, A. H., Rousseau, B., and Durandean, M. (1999b). *J. Chem. Phys.*, 110:4060.
- [Errington and Debenedetti, 2001] Errington, J. R. and Debenedetti, P. (2001). *Nature*, 409:318.
- [Evans and Morris, 1990] Evans, D. and Morris, G. (1990). *Statistical Mechanics of Nonequilibrium Liquids*. Academic Press, San Diego, CA, USA.
- [Evans, 1997] Evans, D. J. (1997). *Mol. Phys.*, 34:317.
- [Evans and MacGowan, 1987] Evans, D. J. and MacGowan, D. (1987). *Phys. Rev. A*, 36:948.

- [Ferrario et al., 1990] Ferrario, M., Haughney, M., McDonald, I. R., and Klein, M. L. (1990). *J. Chem. Phys.*, 93:5156.
- [Fleming, 1986] Fleming, G. R. (1986). *Chemical Application of Ultrafast Spectroscopy*. Oxford University Press, New York, USA.
- [Franck and Roth, 1992] Franck, E. and Roth, K. (1992). *Faraday Dis. Chem. Soc.*, 43.
- [Frank, 1952] Frank, F. C. (1952). *Proc. R. Soc. London, Ser. A*, 215:43.
- [Franks, 2000] Franks, F. (2000). *Water: 2nd Edition A matrix of life*. Royal Society of Chemistry, Cambridge, UK.
- [Franzese et al., 2001a] Franzese, G., Malescio, G., Skibinsky, A., Buldyrev, S. V., and Stanley, H. E. (2001a). *Nature*, 409:692.
- [Franzese et al., 2001b] Franzese, G., Malescio, G., Skibinsky, A., Buldyrev, S. V., and Stanley, H. E. (2001b). *arXiv:cond-mat/0102029 v1*.
- [Franzese et al., 2001c] Franzese, G., Malescio, G., Skibinsky, A., Buldyrev, S. V., and Stanley, H. E. (2001c). *arXiv:cond-mat/0111239 v1*.
- [Franzese et al., 2001d] Franzese, G., Margués, M., and Stanley, H. E. (2001d). *arXiv:cond-mat/0112341 v1*.
- [Frenkel and Smith, 1996] Frenkel, D. and Smith, B. (1996). *Understanding Molecular Simulation, from Algorithms to Applications*. Academic Press, San Diego, CA, second edition.
- [Furataka and Ikawa, 1998a] Furataka, S. and Ikawa, S. (1998a). *J. Chem. Phys.*, 108:1347.
- [Furataka and Ikawa, 1998b] Furataka, S. and Ikawa, S. (1998b). *J. Chem. Phys.*, 108:5159.
- [Furataka and Ikawa, 2000] Furataka, S. and Ikawa, S. (2000). *J. Chem. Phys.*, 113:1942.
- [Glasstone et al., 1941] Glasstone, S. N., Laidler, K., and Eyring, H. (1941). *The theory of Rate Process*. McGraw-Hill, New York, USA.
- [Glattli et al., 2002] Glattli, A., Daura, X., and van Gunsteren, W. F. (2002). *J. Chem. Phys.*, 116:9811.
- [Goldstein, 1996] Goldstein, H. (1996). *Classical Mechanics*. Addison-Wesley Publishing Company, Massachusetts, USA.
- [GOWProp-v5.1, 2002] GOWProp-v5.1 (2002). *Norcraft Software*.
- [Griffiths, 1952] Griffiths, V. S. (1952). *J. Chem. Soc.*, page 1326.
- [Guàrdia et al., 2002] Guàrdia, E., Martí, J., Padró, J., and Komolkin, A. V. (2002). *J. Mol. Liq.*, 96:3.
- [Guillot and Guissani, 2001] Guillot, B. and Guissani, Y. (2001). *J. Chem. Phys.*, 114:6720.
- [Guo and Zhang, 2001] Guo, G. and Zhang, Y. (2001). *Mol. Phys.*, 99:283.
- [Haar et al., 1984] Haar, L., Gallager, J. S., and Kell, G. S. (1984). *NBS/NCR Steam Tables: Thermodynamic and Transport Properties and Computer Programs for Vapor and Liquids States of Water in SI Units*. National Standard Reference Data System, USA.

- [Haase et al., 1971] Haase, R., Borgmann, H.-W., Ducker, K.-H., and Lee, W.-P. (1971). *Z. Naturforsch. A*, 26:1224.
- [Haile, 1997] Haile, J. M. (1997). *Molecular Dynamics Simulation, Elementary Methods*. John Wiley and Sons, INC., New York, USA.
- [Hansen and McDonald, 1991] Hansen, J. P. and McDonald, I. R. (1991). *Theory of Simple Liquids*. Academic Press, London NW1 7DX, second edition.
- [Heide, 1984] Heide, H. G. (1984). *Ultramicroscopy*, 14:271.
- [Hoheisel, 1999] Hoheisel, C. (1999). *Transport Properties of Fluids: Their Correlation, Prediction and Estimation*, volume 1. edited by J. Millat, J. H. Dymond and C. A. Nieto de Castro, (Cambridge University Press, New York), New York, USA, first edition.
- [Hunenberger and van Gunsteren, 1998] Hunenberger, P. H. and van Gunsteren, W. F. (1998). *J. Chem. Phys.*, 108:6117.
- [Hura et al., 2000] Hura, G., Sorenson, J., Glaeser, R., and Head-Gordon, T. (2000). *J. Chem. Phys.*, 113:9140.
- [Iacopini and Piazza, 2003] Iacopini, S. and Piazza, R. (2003). *Europhys. Lett.*, submitted.
- [Isaacs et al., 2000] Isaacs, E. D., Shukla, A., Platzman, P. M., Hamann, D. R., and Barbiellini, B. (2000). *J. Phys. Chem. Sol.*, 61:403.
- [Jedlovsky et al., 1998] Jedlovsky, P., Broholt, J. P., Bruni, F., Ricci, M. A., and Soper, A. K. (1998). *J. Chem. Phys.*, 108:8540.
- [Jorgensen, 1986] Jorgensen, W. (1986). *J. Phys. Chem.*, 90:1276.
- [Jorgensen et al., 1983] Jorgensen, W., Chandrasekhar, J., Madura, J. D., Impey, R. W., and Klein, M. (1983). *J. Chem. Phys.*, 79:926.
- [Jorgensen et al., 1984] Jorgensen, W. J., Madura, J. D., and Swenson, C. J. (1984). *J. Am. Chem. Soc.*, 106:6638.
- [Kalinichev and Churakov, 1999] Kalinichev, A. G. and Churakov, S. V. (1999). *Chem. Phys. Lett.*, 302:411.
- [Katrizky et al., 1996] Katrizky, A. R., Allin, S. M., and Siskin, M. (1996). *Acc. in Chem. Res.*, 29:399.
- [Kempers, 2001] Kempers, L. J. T. M. (2001). *J. Chem. Phys.*, 115:6330.
- [Killilea et al., 1992] Killilea, W. R., Swallow, K. C., and Hong, G. T. (1992). *J. Sup. Flu.*, 5:72.
- [Kleman and Sadoc, 1979] Kleman, M. and Sadoc, J. F. (1979). *J. Physique Lett.*, 40:L569.
- [Kolodner et al., 1988] Kolodner, P., Williams, H., and Moe, C. (1988). *J. Chem. Phys.*, 88:6512.
- [Kropman and Bakker, 2001] Kropman, M. F. and Bakker, H. J. (2001). *Science*, 291:2118.
- [Krynicky et al., 1980] Krynicky, K., Green, C. D., and Sawyer, D. W. (1980). *Farad. Disc. of Chem. Soc.*, 66:199.

- [Ladanyi and Skaf, 1996] Ladanyi, B. and Skaf, M. (1996). *J. Phys. Chem.*, 100:1368.
- [Lamb et al., 1981] Lamb, W. J., Hoffman, G. A., and Jonas, J. (1981). *J. Chem. Phys.*, 74:6875.
- [Lamb and Jonas, 1981] Lamb, W. J. and Jonas, J. (1981). *J. Chem. Phys.*, 74:913.
- [Laria and Skaf, 1999] Laria, D. and Skaf, M. S. (1999). *J. Chem. Phys.*, 111:300.
- [Leppla and Wiegand, 2003] Leppla, C. and Wiegand, S. (2003). *Phi. Mag.*, *accepted*.
- [Li, 1976] Li, C. C. (1976). *Am. Inst. Chem. Eng. J.*, 22:927.
- [Liu et al., 1995] Liu, H., Muller-Plathe, F., and van Gunsteren, W. (1995). *Am. Chem. Soc.*, 117:4363.
- [Ludwig, 1856] Ludwig, C. (1856). *Math. Naturwiss*, 20:539.
- [Luzar, 1996] Luzar, A. (1996). *Faraday Discuss.*, 103:29.
- [Luzar and Chandler, 1993] Luzar, A. and Chandler, D. (1993). *J. Chem. Phys.*, 98:8160.
- [MacGowan and Evans, 1986a] MacGowan, D. and Evans, D. (1986a). *Phys. Rev. A*, 34:2133.
- [MacGowan and Evans, 1987] MacGowan, D. and Evans, D. (1987). *Phys. Rev. A*, 36:948.
- [MacGowan and Evans, 1986b] MacGowan, D. and Evans, D. J. (1986b). *Phys. Rev. A*, 34:2133.
- [Mahoney and Jorgensen, 2000] Mahoney, M. W. and Jorgensen, W. L. (2000). *J. Chem. Phys.*, 112:8910.
- [Marrion, 1992] Marrion, J. B. (1992). *Classical Dynamics of Particles and Systems*. Academic Press, London, UK, 2nd edition.
- [Marrone et al., 1998] Marrone, P. A., Arias, T. A., Peters, W. A., and Tester, J. W. (1998). *arXiv:cond-mat/9807215*.
- [Martí, 1999] Martí, J. (1999). *J. Chem. Phys.*, 110:6876.
- [Martí, 2000] Martí, J. (2000). *Phys. Rev. E*, 61:449.
- [Martí et al., 1996] Martí, J., Padró, J., and Guàrdia, E. (1996). *J. Chem. Phys.*, 105:639.
- [Matsumoto and Gubbins, 1990] Matsumoto, M. and Gubbins, K. E. (1990). *J. Chem. Phys.*, 93:1981.
- [Matubayasi et al., 1997] Matubayasi, N., Wakai, C., and Nakahara, M. (1997). *J. Chem. Phys.*, 107:9133.
- [Mayanovic et al., 2001] Mayanovic, R. A., A. J. Anderson, W. A. B., and Chou, I.-M. (2001). *Chem. Phys. Lett.*, 336:212.
- [Mishima and Stanley, 1984] Mishima, O. and Stanley, H. E. (1984). *Nature(London)*, 396:329.
- [Mishima and Stanley, 1998] Mishima, O. and Stanley, H. E. (1998). *Nature*, 396:329.
- [Mitton et al., 1991] Mitton, D. B., Orzalli, J. C., and Latanision, R. M. (1991). *Corrosion in Supercritical Water Oxidation Systems. In Physical Chemistry Systems: Meeting the Needs*

- of Industry*. H. J. White, J. V. Sengers, D. B. Neumann and J. C. Bellows, Ed.; Begel House, New York, USA.
- [Modell et al., 1982] Modell, M., Gaudet, G. G., Simson, M., Hong, G. T., and Biemann, K. (1982). *Sol. Wast. Manag.*, 25:26.
- [Muller-Plathe, 1997] Muller-Plathe, F. (1997). *J. Chem. Phys.*, 106:6082.
- [Nelson, 1983] Nelson, D. R. (1983). *Phys. Rev. B*, 28:5515.
- [Ness, 1989] Ness, S. V. (1989). *Termodinámica en Ingeniería Química*. Mac Graw Hill, Mexico, DF, cuarta edition.
- [Netz et al., 2002a] Netz, P. A., Starr, F. W., Barbosa, M. C., and Stanley, H. E. (2002a). *arXiv:cond-mat/0201138 v1*.
- [Netz et al., 2002b] Netz, P. A., Starr, F. W., and H. E. Stanley, M. C. B. (2002b). *arXiv:cond-mat/0201130 v1*.
- [Neuman, 1986a] Neuman, M. (1986a). *J. Chem. Phys.*, 82:5663.
- [Neuman, 1986b] Neuman, M. (1986b). *J. Chem. Phys.*, 85:1567.
- [Nieto-Draghi and Avalos, 2003] Nieto-Draghi, C. and Avalos, J. B. (2003). *Mol. Phys.*, 101:2303.
- [Nieto-Draghi et al., 2003a] Nieto-Draghi, C., Avalos, J. B., Contreras, R., Ridard, J., and Ungerer, P. (2003a). *J. Phys. Chem. B*. (Submitted).
- [Nieto-Draghi et al., 2003b] Nieto-Draghi, C., Bonet, J., and Rousseau, B. (2003b). *J. Chem. Phys.*, 118:7954.
- [NIST, 2001] NIST (2001). *National Institute of Standards and Technology* (<http://webbook.nist.gov>).
- [Noda et al., 1982] Noda, K., Ohashi, M., and Ishida, K. (1982). *J. Chem. Eng. Data*, 27:326.
- [Nosé, 1984a] Nosé, S. (1984a). *J. Chem. Phys.*, 81:511.
- [Nosé, 1984b] Nosé, S. (1984b). *Mol. Phys.*, 52:268.
- [Nymand and Linse, 2000] Nymand, T. and Linse, P. (2000). *J. Chem. Phys.*, 112:6152.
- [Nymand et al., 2001] Nymand, T., Ronne, C., and Keiding, S. R. (2001). *J. Chem. Phys.*, 114:5246.
- [Onsager et al., 1939] Onsager, L., Furry, W. H., and Jones, R. C. (1939). *Phys. Rev.*, 73:141.
- [Paolini and Ciccotti, 1987] Paolini, G. V. and Ciccotti, G. (1987). *Phys. Rev. A*, 35:5156.
- [Perronace et al., 2002a] Perronace, A., Ciccotti, G., Leroy, F., Fuchs, A. H., and Rousseau, B. (2002a). *Phys. Rev. E*, 66:031201.
- [Perronace et al., 2002b] Perronace, A., Leppla, C., Leroy, F., Rousseau, B., and Wiegand, S. (2002b). *J. Chem. Phys.*, 116:3718.

- [Petong et al., 2000] Petong, P., Pottel, R., and Kaatze, U. (2000). *J. Phys. Chem.*, 104:7420.
- [Petrvac, 2000] Petrvac, J. (2000). *Prédiction de la Viscosité dans des Mélanges Multi-constituants par Dynamique Moléculaire*. PhD thesis, Laboratoire de Chimie Physique, Université Paris-Sud.
- [Petrvac and Delhommelle, 2002] Petrvac, J. and Delhommelle, J. (2002). *J. Phys. Chem.* (submitted).
- [Piazza, 2003] Piazza, R. (2003). *Phi. Mag.*, submitted.
- [Piazza and Guarino, 2002] Piazza, R. and Guarino, A. (2002). *Phys. Rev. Lett.*, 88:208302–1.
- [Polikhronidi et al., 2001] Polikhronidi, N. G., Abdulagatov, I. M., Magee, J. W., and Stepanov, G. V. (2001). *Int. J. of Therm.*, 22:189.
- [Poole et al., 1992] Poole, P. H., Sciortino, F., Essmann, U., and Stanley, H. E. (1992). *Nature*, 360:324.
- [Prigogine et al., 1950a] Prigogine, I., Brouckere, L. D., and Amand, R. (1950a). *Physica XVI*, 7:577.
- [Prigogine et al., 1950b] Prigogine, I., Brouckere, L. D., and Amand, R. (1950b). *Physica XVI*, 11:851.
- [Qun-Fang et al., 1997] Qun-Fang, L., Rui-Sen, L., and Dan-Yan, N. (1997). *J. Chem. Eng. Data*, 42:971.
- [Raddzio and Tomaszewicz, 1986] Raddzio, S. L. and Tomaszewicz, I. (1986). *Thermodyn. Acta*, 103:257.
- [Re and Laria, 1997] Re, M. and Laria, D. (1997). *J. Phys. Chem. B*, 101:10494.
- [Reith and Muller-Plathe, 2000] Reith, D. and Muller-Plathe, F. (2000). *J. Chem. Phys.*, 112:2436.
- [Ricci et al., 1998] Ricci, M. A., Nardone, M., Fontana, A., Andreani, C., and Hahn, W. (1998). *J. Chem. Phys.*, 108.
- [Rondot et al., 2002] Rondot, S., Aaboubi, O., P. Baudart, D. Erre, E. M., and Patat, J. M. (2002). *Eur. Phys. J. A.P.*, 17:75.
- [Rothschild, 1984] Rothschild, W. G. (1984). *Dynamics of Molecular Liquids*. Wiley, New York, USA.
- [Saiz et al., 1999] Saiz, L., Padró, J. A., and Guàrdia, E. (1999). *Mol. Phys.*, 97:897.
- [Savage et al., 1995] Savage, P. E., Golapan, S., Mizan, T. I., Martino, C. J., and Brock, E. E. (1995). *AICHE*, 41:1723.
- [Scala et al., 2000a] Scala, A., Starr, F. W., Nave, E. L., Sciortino, F., and Stanley, H. E. (2000a). *Nature*, 406:166.
- [Scala et al., 2000b] Scala, A., Starr, F. W., Nave, E. L., Stanley, H. E., and Sciortino, F. (2000b). *arXiv:cond-mat/0007488 v1*.

- [Schaink et al., 1993] Schaink, M., Luo, H., and Hoheisel, C. (1993). *J. Chem. Phys.*, 12:9912.
- [Sesé and Palomar, 2001] Sesé, G. and Palomar, R. (2001). *J. Phys. Chem.*, 114:9975.
- [Shaw et al., 1991] Shaw, W. R., Brill, T. B., Clifford, A. A., Eckert, C. A., and Frank, E. U. (1991). *Chem. and Eng. News*, 51:26.
- [Shevade and Gubbins, 2000] Shevade, A. and Gubbins, K. E. (2000). *J. Phys. Chem.*, 113:6933.
- [Shukla and Firoozabadi, 1998] Shukla, K. and Firoozabadi, A. (1998). *Ind. Eng. Chem. Res.*, 37:3331.
- [Simon et al., 1998] Simon, J., Dysthe, D., Fuchs, A. H., and Rousseau, B. (1998). *Flu. Phase Equi.*, 150:151.
- [Simon et al., 1999] Simon, J., Rousseau, B., Dysthe, D., and Hafskjold, B. (1999). *Etropie*, 217:29.
- [Skaf, 1999] Skaf, M. S. (1999). *J. Phys. Chem. A*, 103:10719.
- [Skaf and Ladanyi, 1995] Skaf, M. S. and Ladanyi, B. M. (1995). *J. Chem. Phys.*, 102:6542.
- [Skaf and Laria, 2000] Skaf, M. S. and Laria, D. (2000). *J. Chem. Phys.*, 113:3499.
- [Skaff, 1997a] Skaff, M. S. (1997a). *Mol. Phys.*, 90:25.
- [Skaff, 1997b] Skaff, M. S. (1997b). *J. Chem. Phys.*, 107:7996.
- [Slusher, 2000] Slusher, J. T. (2000). *Mol. Phys.*, 98:287.
- [Smith and van Gunsteren, 1993] Smith, P. E. and van Gunsteren, W. F. (1993). *Chem. Phys. Lett.*, 215:315.
- [Soper, 2000] Soper, A. K. (2000). *Chem. Phys.*, 258:121.
- [Soper et al., 1997] Soper, A. K., Bruni, F., and Ricci, M. A. (1997). *J. Chem. Phys.*, 106:247.
- [Soper and Luzar, 1992] Soper, A. K. and Luzar, A. (1992). *J. Chem. Phys.*, 97:1320.
- [Soret, 1879a] Soret, C. (1879a). *Arch. Sci. phys. nat.*, 2:48.
- [Soret, 1879b] Soret, C. (1879b). *Comptes Rendus Acad. Sci.*, 91:279.
- [Soret, 1880] Soret, C. (1880). *Arch. Sci. phys. nat.*, 4:209.
- [Speedy, 1982] Speedy, R. J. (1982). *J. Phys. Chem.*, 86:982.
- [Stanley et al., 2002a] Stanley, H., Barbosa, M., Mossa, S., Netz, P., Sciortino, F., Starr, F., and Yamada, M. (2002a). *arXiv:cond-mat/0206542*.
- [Stanley et al., 2002b] Stanley, H. E., Barbosa, M. C., Mossa, S., Netz, P. A., Sciortino, F., Starr, F. W., and Yamada, M. (2002b). *arXiv:cond-mat/0206542 v1*.
- [Stanley and Teixeira, 1980] Stanley, H. E. and Teixeira, J. (1980). *J. Chem. Phys.*, 73:3404.

- [Starr et al., 2000] Starr, F. W., Sastry, S., Sciortino, F., and Stanley, H. E. (2000). *arXiv:cond-mat/0001296 v1*.
- [Stillinger and Rahman, 1974] Stillinger, F. and Rahman, A. (1974). *J. Chem. Phys.*, 60:1545.
- [Suresh and Naik, 2000] Suresh, S. J. and Naik, V. M. (2000). *J. Chem. Phys.*, 113:9727.
- [Svanberg, 1997] Svanberg, M. (1997). *Mol. Phys.*, 92:1085.
- [Svishchev and Zassetsky, 2000] Svishchev, I. M. and Zassetsky, A. Y. (2000). *J. Chem. Phys.*, 113:7432.
- [Tanaka, 1999] Tanaka, H. (1999). *J. Phys.: Condens. Matter*, 11:L159.
- [Tassaing and Bellissent-Funel, 2000] Tassaing, T. and Bellissent-Funel, M. C. (2000). *J. Chem. Phys.*, 113:3332.
- [Taylor and Krishna, 1993] Taylor, R. and Krishna, R. (1993). *Multicomponent mass transfer*. John Wiley and Sons, INC., New York, USA.
- [Tester et al., 1991] Tester, J. W., Holgate, H. R., Armellini, F. J., Webley, P. A., Killilea, W. R., Hong, G. T., and Barner, H. E. (1991). *Supercritical Water Oxidation Technology: Process Development and Fundamental Research. In Emerging Technologies in Hazardous Waste Management III*. D. W. Tedder and F. G. Pholand, Ed.; American Chemical Society, Washington, D.C., USA.
- [Thomason et al., 1990] Thomason, T. B., Hong, G. T., Swallow, K. C., and Killilea, W. R. (1990). *Thermal Process*, 1:31.
- [Thomason and Modell, 1984] Thomason, T. B. and Modell, M. (1984). *Haz. Wastes*, 1:453.
- [Tichacek et al., 1955] Tichacek, L. J., Kmak, W. S., and Drickamer, H. G. (1955). *J. Phys. Chem.*, 60:660.
- [Tironi et al., 1997] Tironi, I., Luty, B. A., and van Gunsteren, W. F. (1997). *J. Chem. Phys.*, 106:6068.
- [Todheide, 1972] Todheide, K. (1972). *In: F. Franks(ed.), Water, a Comprehensive Treatise*. Plenum Press, New York, USA.
- [Tsonopoulos and Wilson, 1983] Tsonopoulos, C. and Wilson, G. M. (1983). *AICHE J.*, 29:990.
- [Uematsu and Franck, 1980] Uematsu, M. and Franck, E. (1980). *J. Phys. Chem. Ref. Data*, 9:1291.
- [van der Spoel et al., 1998] van der Spoel, D., van Maaren, P. J., and Berendsen, H. J. C. (1998). *J. Chem. Phys.*, 108:10220.
- [Venables and Schmuttenmaer, 2000] Venables, D. S. and Schmuttenmaer, C. A. (2000). *J. Chem. Phys.*, 113:11222.
- [Vogelsang and Hoheisel, 1988] Vogelsang, R. and Hoheisel, C. (1988). *J. Chem. Phys.*, 89:1588.
- [Vogelsang et al., 1987] Vogelsang, R., Hoheisel, C., Paolini, G. V., and Ciccotti, G. (1987). *Phys. Rev. A*, 36:3964.

- [Wheeler and Rowley, 1998] Wheeler, D. R. and Rowley, R. L. (1998). *Mol. Phys.*, 94:555.
- [Wirtz, 1948] Wirtz, K. Z. (1948). *Naturforschung*, 3a:672.
- [Woerlee, 2001] Woerlee, G. F. (2001). *Ind. Eng. Chem. Res.*, 40:465.
- [Yamada et al., 2002] Yamada, M., Mossa, S., Stanley, H., and Sciortino, F. (2002). *arXiv:cond-mat/0202094*.
- [Yao and Okada, 1998] Yao, M. and Okada, K. (1998). *J. Phys.: Condens. Matter*, 10:11495.
- [Yoshii et al., 1998] Yoshii, N., Yoshie, H., Miura, S., and Okazaki, S. (1998). *J. Chem. Phys.*, 109:4873.
- [Zhang et al., 1996] Zhang, K. J., Briggs, M. E., Gammon, R. W., and Sengers, J. V. (1996). *J. Chem. Phys.*, 104:6881.
- [Zhou and Miller, 1996] Zhou, Y. and Miller, G. H. (1996). *J. Chem. Phys.*, 100:5516.

Resumen de la Tesis

Las técnicas de Modelado Molecular han sido utilizadas para estudiar sistemas de interés industrial prácticamente desde el surgimiento de los ordenadores como herramientas de cálculo. Las simulaciones por ordenador se han convertido en una fuente relevante y fiable de datos y propiedades físicas de compuestos, cuando las condiciones de temperatura y presión hacen imposible el uso de las ecuaciones de estado tradicionales. Estas ecuaciones de estado presentan parámetros ajustables que, en muchos casos, dependen de las condiciones termodinámicas del sistema como son la presión o la temperatura. Llevar a cabo experimentos en estas condiciones extremas implica la utilización de costosos equipos y sofisticados instrumentos de medición capaces de soportar altas presiones y temperaturas. En estos casos las técnicas de simulación molecular se presentan como una buena alternativa para la obtención de propiedades y datos de compuestos requeridos para el diseño y construcción de equipos industriales (wor, 1999). Por otro lado el modelado molecular ha sido utilizado en los últimos años como una herramienta indispensable para el desarrollo de teorías y la comprensión de muchos procesos físicos en todos los ámbitos de la ciencia y la ingeniería (Barrat and Hansen, 2003). Estas técnicas de simulación requieren de la utilización de modelos que representen los átomos y las moléculas de las sustancias reales. Estos modelos representan el punto central para una correcta descripción microscópica de cualquier fluido (Allen and Tildesley, 1989).

La simulación Dinámica Molecular (MD, por sus siglas en inglés) es una de las técnicas empleadas en la obtención de propiedades de transporte y de equilibrio de sistemas reales (Hansen and McDonald, 1991). Esta técnica se basa en el principio físico de que los átomos y las moléculas de un fluido obedecen las leyes de la mecánica clásica (Goldstein, 1996), por lo que el comportamiento dinámico de las partículas puede ser descrito por medio de ecuaciones, siendo éstas fácilmente integrables por medio de un ordenador de cálculo. La diferen-

cia principal existente entre los resultados obtenidos por medio de ésta técnica y los obtenidos por las ecuaciones fenomenológicas de estado es, que en el primer caso, los parámetros utilizados son moleculares por naturaleza y por tanto no dependen de las condiciones termodinámicas del sistema en estudio, mientras que en el segundo caso estos parámetros si dependen de las condiciones del sistema y, generalmente, carecen de un significado físico real. En este sentido, la simulación dinámica molecular es análoga a los experimentos reales, donde luego de un intervalo de tiempo, es posible obtener medir propiedades físicas macroscópicas del sistema a través de la utilización promedios temporales de propiedades microscópicas, como, por ejemplo, posiciones y velocidades de las partículas.

El estudio de sistemas con interés desde un punto de vista industrial o biológico a incrementado el interés de en el mejoramiento de los modelos moleculares que pueden ser utilizados en las simulaciones. Adicionalmente, el incremento en el poder de cálculo de los ordenadores actuales ha motivado la aplicación de estas técnicas sobre sistemas reales con un alto grado de complejidad, principalmente en los casos de sistemas biológicos (DNA, 2001) donde el agua juega un papel importante como solvente. Aún cuando la molécula de agua puede considerarse como “simple”, el comportamiento colectivo de muchas moléculas de agua juntas dista mucho de la simplicidad. En este sentido el agua es un fluido fascinante, con muchas propiedades particulares a diferentes condiciones termodinámicas, en comparación con muchas otras sustancias (Chapling, 2003). La mayor parte de las propiedades peculiares del agua pueden ser explicadas por la presencia de los puentes de hidrógeno entre diferentes moléculas de agua. Dichos puentes de hidrógeno ocasionan la formación de redes tridimensionales complejas de moléculas interconectadas (Franks, 2000, NIST, 2001). Por ejemplo, el agua se expande al ser enfriada a presión atmosférica y a temperaturas por debajo de los 4 C, además, es posible observar la presencia de una línea de máxima densidad en fase líquida al cambiar la temperatura (Heide, 1984, Mishima and Stanley, 1984). A temperaturas mas bajas (por debajo del punto de congelación del agua a 0 C), el agua cristaliza de tal manera que el hielo es menos denso que el agua líquida y la relación existente entre la estructura del hielo y el movimiento de las moléculas esta lejos de ser trivial (Stanley et al., 2002b, Netz et al., 2002b, Netz et al., 2002a, Scala et al., 2000a, Starr et al., 2000). De la misma manera, las mezclas acuosas con otras sustancias pueden presentar también un comportamiento complejo, particularmente si estas sustancias son capaces de compartir puentes de hidrógeno con las moléculas de agua (Matsumoto and Gubbins, 1990, Saiz et al., 1999, Slusher, 2000, Sesé and Palomar, 2001). Muchas propiedades físicas de mezcla de este tipo de fluidos asociantes en agua tienen un comportamiento no ideal, como por ejemplo entalpías de exceso negativas (Ness,

1989, Raddzio and Tomaszkiwicz, 1986), altas energías de vaporización, incremento de la viscosidad de la mezcla en comparación con los componentes puros (Ferrario et al., 1990, Wheeler and Rowley, 1998, Venables and Schmuttenmaer, 2000), mínimos en la conductividad térmica de la mezcla (Li, 1976) y cambios en el signo del coeficiente de Soret (Kolodner et al., 1988, de Gans et al., 2003a, de Gans et al., 2003b). En muchos de estos casos, existe un vacío en la comprensión de la naturaleza de los procesos físicos que generan estos comportamientos anómalos.

Por otro lado, el agua en condiciones supercríticas (cuando la temperatura y la presión están por encima de los valores críticos), ha ganado un gran interés por parte de la comunidad científica e industrial debido a las particulares características del agua en estas condiciones (Chialvo and Cummings, 1996b, Shaw et al., 1991, Katrizky et al., 1996). Una de las mayores motivaciones existentes en estudiar el agua supercrítica es, de acuerdo con los resultados experimentales, que existe una relajación en la estructura de los puentes de hidrógeno del agua, hecho que genera una importante disminución de la constante dieléctrica de este fluido (Skaf and Laria, 2000, Yao and Okada, 1998, Jedlovsky et al., 1998). Este hecho permite que el agua supercrítica pueda disolver compuestos no polares u orgánicos y precipite sales comunes, algo que el agua en condiciones normales es incapaz de hacer. Mas aún, el hecho de que la densidad del agua supercrítica pueda ser ajustada mediante un cambio en la presión del sistema, permite que el agua pueda ser utilizada como un medio de separación o de reacción química. Esta variación en la densidad tiene una influencia directa en el coeficiente de viscosidad y por tanto en la manera como se difunden las moléculas (Haar et al., 1984), hecho que es de vital importancia para reacciones controladas por la difusión. La extracción supercrítica, la oxidación seca de compuestos orgánicos de desecho, el tratamiento de aguas residuales y de servicios en procesos industriales son ejemplos de aplicaciones del agua supercrítica (Modell et al., 1982, Thomason et al., 1990, Thomason and Modell, 1984, Tester et al., 1991, Killilea et al., 1992).

El comportamiento peculiar observado por el agua a diferentes condiciones termodinámicas y en presencia de otras sustancias, el conocimiento y entendimiento de las propiedades de este tipo de sistemas son una de las principales motivaciones de este trabajo. Nosotros hemos realizado un extenso estudio de las relaciones intrínsecas existentes entre la estructura local del sistema, desde un punto de vista microscópico, y las propiedades dinámicas de transporte, tanto en el caso del agua pura como en el caso de mezclas acuosas de solventes orgánicos (como alcoholes, cetonas, sulfóxidos y benceno) por medio de la simulación dinámica molecular. En este trabajo se han desarrollado nuevas herramientas analíticas y algoritmos de simulación destinados a brindar una mejor

descripción y comprensión de los procesos físicos microscópicos involucrados en las diferentes propiedades estudiadas.

En primer lugar, se ha realizado un análisis de la relación existente entre la estructura local de puentes de hidrógeno presente en el agua pura en condiciones sub y supercríticas. Para ello se realizó una comparación entre cuatro diferentes modelos comúnmente utilizados en la literatura (van der Spoel et al., 1998, Mahoney and Jorgensen, 2000, Berendsen et al., 1987, Guillot and Guisani, 2001). Los resultados obtenidos nos han permitido relacionar de una manera directa la estructura tetraédrica local de las moléculas de agua (Errington and Debenedetti, 2001, Chau and Hardwick, 1998), creada por la presencia de los puentes de hidrógeno y el valor que alcanza el coeficiente de auto-difusión en condiciones de densidad de líquido. Adicionalmente, se ha prestado especial atención a la transición estructural en el orden local del agua al pasar de regiones sub críticas por encima de 345 K, a supercríticas y a diferentes densidades (desde 0.9 a 1.3 g/cm³). Este hecho podría sugerir la transición de un fluido formado por agregados infinitos de moléculas enlazadas con puentes de hidrógeno a agregados finitos de moléculas. Por otro lado, la comparación de las propiedades predichas por los diferentes modelos de agua escogidos esta en la línea de proporcionar información para el desarrollo de nuevos y mejores modelos de agua.

La fuerte interacción debida a los puentes de hidrógeno presente en las moléculas de agua juega un rol central en el comportamiento de soluciones acuosas, particularmente cuando estos solutos son también capaces de formar puentes de hidrógeno. En este trabajo se han estudiado mezclas acuosas de fluidos asociantes, como metanol, etanol, acetona y sulfóxido de dimetilo (DMSO por sus siglas en inglés). Se han escogido estas sustancias en particular, debido a que son solventes orgánicos conocidos cuyas propiedades están a disposición, además de que son comúnmente utilizados en muchos procesos industriales. El análisis de los resultados de simulación muestra que la presencia de diferentes tipos de soluto (con diferentes características de asociación, pudiendo ser moléculas capaces de donar y recibir o solamente recibir puentes de hidrógeno) perturban de una manera diferente la estructura tetraédrica local del agua. Esta pérdida en la estructura tetraédrica del agua origina un incremento en la rigidez de las moléculas de agua, con respecto a otras, más simétricas y menos rígidas presentes en el agua pura. En otras palabras, la ruptura de la simetría tiene como consecuencia un incremento del tiempo de vida de los puentes de hidrógeno presentes en la mezcla, favoreciendo la formación de estructuras de tipo cadena, hecho que justifica el aumento observado en la viscosidad de la mezcla. Por otro lado, se han realizado simulaciones para calcular la conductividad térmica de la mezcla obteniendo resultados que presentan un acuerdo excelente con los datos experimentales en las condiciones termodinámicas estudiadas.

El efecto Ludwig-Soret (Ludwig, 1856, Soret, 1879a) es otra de las propiedades analizadas en este trabajo. Este efecto cruzado macroscópico consiste en un proceso difusivo causado por la presencia de un gradiente de temperatura en sistemas multicomponentes. El grado de la separación observada, así como el signo de la separación (la dirección en la que migra cada especie) está cuantificado por el coeficiente de Soret o el factor de difusión térmica. En muchos casos, cuando no existe asociación entre las especies presentes en la solución, este coeficiente es positivo en todo el rango de concentración. Esto significa que el componente más pesado tenderá a acumularse en la región más fría del sistema, mientras que el proceso contrario ocurrirá para el componente más ligero (Prigogine et al., 1950a). El valor del coeficiente de Soret depende, en mayor grado, de la diferencia en el peso molecular y en el volumen molar entre los componentes de la mezcla para el caso de soluciones ideales (Simon et al., 1998, Simon et al., 1999, Bedrov and Smith, 2000). Sin embargo, para el caso de fluidos asociantes, el signo de este coeficiente puede cambiar de signo a una concentración particular (Tichacek et al., 1955). En este caso el componente más ligero migrará a la región fría del sistema. Este efecto ha sido estudiado por más de cien años y muchas teorías han sido propuestas para explicar este fenómeno (Kempers, 2001, Haase et al., 1971, Dougherty and Drickamer, 1955). Sin embargo, en el caso de mezclas asociantes, parece que ninguna de las teorías existentes proporciona una explicación satisfactoria para el comportamiento observado por este tipo de soluciones. En vista de esta situación se ha calculado el coeficiente de Soret para soluciones acuosas de los compuestos orgánicos antes mencionados, con el fin de proporcionar una explicación cualitativa que pueda contribuir a un mejor entendimiento de este fenómeno. Nuestras simulaciones reproducen el cambio de signo observado en estos sistemas obteniendo un acuerdo cuantitativo excelente con los datos experimentales (Tichacek et al., 1955, Bou-Ali, 1999) y, de acuerdo a nuestro conocimiento en el tema, esta es la primera vez que dichos resultados en este tipo de sistemas son presentados empleando simulación dinámica molecular. Adicionalmente, la utilización de un modelo simple de red nos ha permitido observar que el cambio de signo en el coeficiente aparece siempre que la energía de interacción cruzada, entre las moléculas de diferentes especies, es más negativa que las energías de interacción entre los componentes puros.

Finalmente, la última parte de este trabajo se ha dedicado al estudio de las propiedades estructurales, dieléctricas y de transporte de mezclas acuosas de benceno en condiciones supercríticas. La molécula de benceno ha sido seleccionada por ser el aromático más sencillo y por que los resultados obtenidos pueden ser de importancia en el estudio de algunos procesos industriales como la oxidación acuosa supercrítica. En nuestras simulaciones se ha utilizado un nuevo modelo anisotrópico de átomo unificado (AUA por sus siglas en inglés)

que es capaz de reproducir el momento cuadrupolar del benceno mediante la incorporación de puntos de carga (Contreras, 2002). En este sentido, se ha podido demostrar que, para poder disolver el benceno en agua supercrítica, la inclusión de este tipo de cargas es un requisito indispensable. Se han calculado varias propiedades de la mezcla como coeficientes de auto difusión y difusión de Maxwell-Stefan y coeficiente de viscosidad en condiciones supercríticas. En este caso se ha podido observar una fuerte dependencia de estos coeficientes con la densidad de la solución y la concentración de benceno. Adicionalmente, datos experimentales recientes han mostrado la presencia de ciertos grupos de moléculas de benceno y agua (Furataka and Ikawa, 1998a). Este tipo de agregados sugiere la presencia de puentes de hidrógeno entre el hidrógeno del agua y la nube de electrones π presentes en el anillo bencénico (Furataka and Ikawa, 2000). Nuestros resultados de simulación están cualitativamente de acuerdo con este hecho, debido a que se ha encontrado que al menos la mitad de las moléculas de benceno poseen un puente de hidrógeno con una molécula de agua. De hecho, también se ha podido observar que este tipo de puentes de hidrógeno cruzados tienen un tiempo de vida medio mayor que los observados entre las moléculas de agua. Por otro lado, se ha podido observar que existe una importante reducción de la constante dieléctrica de la mezcla al disminuir la densidad o aumentar la concentración de benceno en la mezcla, al menos a concentraciones altas y medias. El conocimiento de la respuesta dieléctrica de la mezcla es de vital importancia en agua supercrítica, particularmente para los casos de reacciones químicas en presencia de radicales libres e iones (Marrone et al., 1998).

Publication list

Dynamical and structural behavior of aqueous solutions

- C. Nieto-Draghi, B. Rousseau, J. Bonet Avalos (2003), Dynamical and structural properties of four rigid non-polarizable models of water, *J. Chem. Phys.* 118 (17), 7954–7964.
- C. Nieto-Draghi, J. Bonet Avalos (2003) Non-equilibrium momentum exchange algorithm for molecular dynamics simulation of heat flow in multi-component systems, *Mol. Phys.* 101, 2303.
- C. Nieto-Draghi, B. Rousseau, J. Bonet Avalos (2003), Transport properties of dimethyl sulfoxide aqueous solutions, *J. Chem. Phys.* 119, 4782.
- B. Rousseau, C. Nieto-Draghi, J. Bonet Avalos (2003) Thermal diffusion in aqueous solutions: what can we learn from molecular simulations?, *Phys. Rev. Lett.* (submitted).
- C. Nieto-Draghi, O. Contreras, P. Ungerer, J. Ridard, J. Bonet Avalos, Dynamical and structural properties of benzene in supercritical water, *J. Phys. Chem. B* (submitted).
- C. Nieto-Draghi, B. Rousseau, J. Bonet Avalos, Effect of the hydrogen bonding in the dynamical and structural properties of aqueous solutions of associating fluids, *Mol. Liq.* (submitted).